RSC Applied Interfaces

ROYAL SOCIETY OF CHEMISTRY

REVIEW

View Article Online
View Journal | View Issue

Cite this: *RSC Appl. Interfaces*, 2024, 1, 340

Recent advances in removal of pharmaceutical pollutants in wastewater using metal oxides and carbonaceous materials as photocatalysts: a review†

Suneel Kumar Srivastava

The pharmaceuticals industry has played an important role in developing medicines for improving health and quality of life in treating humans and animals around the world. But it is also considered to be one of the sources of pollutants entering deliberately or accidentally into global water bodies causing toxicity that eventually threatens human health, aquatic organisms and environments even at low concentrations. These contaminants are non-biodegradable and cannot be completely removed from various water matrices following conventional treatment methods. In this regard, photodegradation techniques involving modified/unmodified semiconducting materials have attracted a lot of attention as a promising solution in achieving complete antibiotic degradation with the generation of non-toxic by-products. In view of this, the present review article summarizes current research progress in the removal of several emerging contaminants, such as acetaminophen, amoxicillin, sulfamethoxazole, norfloxacin, ibuprofen, ciprofloxacin, tetracycline, diclofenac and atenolol in water. Considerable emphasis has been placed on metal oxides and carbon-based photocatalysts following their modification through doping with metals and non-metals, metal loading, the formation of composites, immobilization and heterostructure/heterojunction approaches. Finally, the review ends with future prospects for nanomaterial-based heterogeneous photocatalysts in the removal of pharmaceutical contaminants from water.

Received 22nd August 2023,
Accepted 14th December 2023

DOI: 10.1039/d3lf00142c

rsc.li/RSCApplInter

1 Introduction

Water plays an essential role in sustaining a cherished healthy life for living organisms as well as ecosystems. Therefore, the purity of water remains of utmost concern for the survival of human beings, plants, animals and several other living species in the world. A report presented by UNESCO at the UN 2023 Water Conference revealed the non-availability of safe drinking water for 26% of the global population.[1] This problem is also compounded by the presence of several pollutants in water bodies. This contributes to the depletion of fresh water, resulting in an overall water crisis worldwide.[2] This adversely affects human health, several other living organisms and sustainable social development. According to an estimate, about 80% of wastewater is discharged globally into the environment without any prior treatment, jeopardizing human health, the ecosystem, and the environment.[3] In this regard, dye effluents, heavy metals and pesticides discharged as wastewater from different industries contribute significantly to water pollution.[4–12]

In addition, the wide application of pharmaceuticals in daily life for the treatment of complex diseases is also the major contributor of emerging contaminants, with potential adverse effects on humans and the aquatic environment.[13–22] The presence of these pharmaceutical pollutants could lead to cancers, severe bleeding, organ damage, birth defects, reproductive disorders, endocrine disorders, and mild to severe toxic effects in human beings in the global population.[14] The toxic effects are also threats to mammals, other organisms, and the ecosystem. Fig. 1 shows the effect of pharmaceuticals in reducing the quality of water.[14] The presence of these pharmaceutical pollutants in water through improper disposal, irrigation of crops, and consumption by agriculture, humans, and animals seriously affects the ecosystem.

Further, the accumulation of antibiotic drugs in water can result in the development of antibiotic-resistant bacteria and the dissemination of antibiotic-resistant genes in humans and other living organisms.[15,16] According to a recent report, urban wastewater treatment plants are

Department of Chemistry, Indian Institute of Technology, Kharagpur-721302, India. E-mail: suneel@chem.iitkgp.ac.in, suneelchemkgp@gmail.com

† Electronic supplementary information (ESI) available. See DOI: https://doi.org/10.1039/d3lf00142c

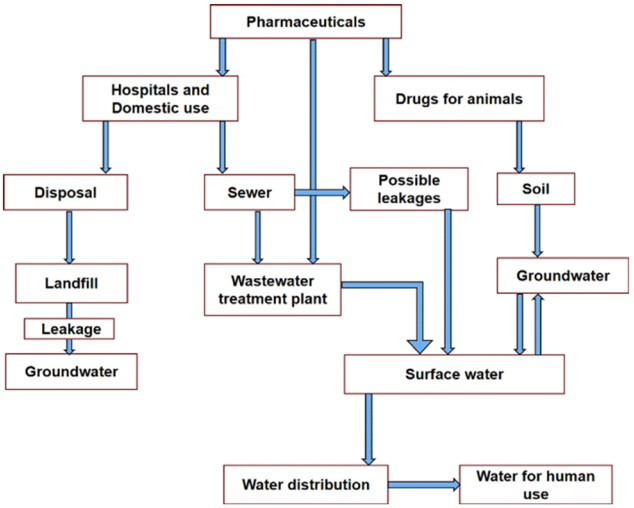

Fig. 1 Routes of pharmaceutical contaminants (PCs). Reproduced from ref. 14 with permission from Elsevier (2022).

recognized sources for the dissemination of antibiotic resistance in the environment.[17] In view of the rising effects of this antibiotic resistance on the global population, the removal of these bioactive molecules from the environment is important to slow down the growth of resistant microorganisms. In addition, antibiotic residues absorbed by plants could interfere with physiological processes, leading to potential ecotoxicological effects.[18] These contaminants cannot be completely removed from various water matrices by conventional chemical, physical, flocculation, reverse osmosis or a few other processes, due to the formation of secondary pollutants, high cost, and operational time.[19] Therefore, the development of cost-effective, eco-friendly, economical, and effective technologies is urgently needed to remove these emerging contaminants, due to the rising effects of antibiotic resistance in aquatic environments.

Design of the surface and interface plays a promising role in the performance of photocatalysts through maximizing the efficacy of catalysts. Therefore, heterogeneous photocatalysis has been receiving considerable attention as one of the most attractive, low-cost, efficient and outstanding approaches in the degradation of pharmaceutical pollutants.[19–55] In this regard, a considerable amount of research interest has focused mostly on TiO_2 and to some extent on other semiconducting materials and transition metal oxides as photocatalysts in the degradation of pharmaceutical pollutants in water.[23–39] The choice of semiconducting metal oxides as photocatalysts is motivated by the availability of a renewable energy source (solar energy) and the generation of non-toxic degradation products (chemicals and gases). They can be commonly prepared by sol–gel, hydrothermal, solvo-thermal, microwave heating, wet chemical, physical vapour deposition and chemical vapour deposition methods.[30] However, the potential of TiO_2 and other semiconducting metal oxides could not be harnessed due to the higher rate of recombination of electron–hole pairs and its limited photocatalytic activity under visible light exposure.

Recently, carbonaceous materials have also been reported as promising materials for use in the photocatalytic degradation of antibiotics in water.[40–50] This is facilitated by combining these carbon-based materials with other semiconductors, which is considered to be an outstanding approach to enhancing photocatalytic performance. In order to facilitate this, carbonaceous materials with different structures and properties are used as additives in semiconductor materials. This invariably results in enhanced charge separation and visible light activity and is considered the best solution. In addition, semiconducting metal oxides and carbonaceous materials are subjected to doping with metals, non-metals, metal oxides, coupling with noble metal nanoparticles and the formation of composites.[36,39,49] Other approaches involving immobilization and the formation of a heterojunction are reported as imperative alternative strategies for achieving enhanced photocatalytic efficiency for these photocatalysts in water treatment.[51]

According to the available literature, several reviews have been published focusing on metal oxides,[23–30] TiO_2,[31–33] ZnO-based photocatalysts,[34] semiconductors,[35] doped TiO_2,[36] hybrids,[37] TiO_2–carbon dot nanocomposites,[38] plasmonic metal–TiO_2 composites,[39] carbonaceous/carbon-based materials,[40,41] g-C_3N_4,[42] MWCNT,[43] carbon dots,[38,44] activated carbon,[45] graphene-based composites,[46–48] graphene–TiO_2 and doped graphene–TiO_2 nanocomposites,[49] graphene-based materials,[50] and nanomaterial-based heterogeneous photocatalysts[51] as photocatalysts for the

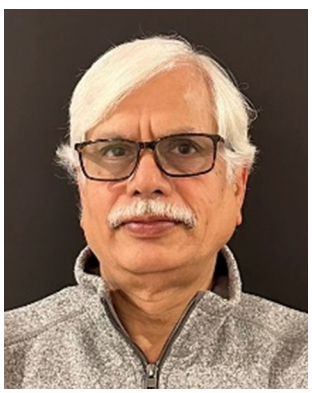

Suneel Kumar Srivastava

Suneel Kumar Srivastava received his Ph.D degree from the Indian Institute of Technology, Kharagpur in 1984. He is a former Professor in the Department of Chemistry of the same Institute, serving from 1986 to 2021. Dr Srivastava carried out his post-doctoral work as a DAAD Fellow in the Technical University, Karlsruhe (1988–89, 2002, 2006), University of Siegen (1994, 1999), Technical University, Munchen (2009), Leibniz Institute of Polymer Research, Dresden (2013) Germany, and University of Nantes, France (2003, 2007). His research interests are in the field of nondimensional nanomaterials for their application in the fields of energy, environments and polymer nanocomposites. Dr Srivastava has guided 23 Ph.Ds, published about 200 research papers in referred journals, contributed to 16 chapters in books and edited 2 books.

Table 1 Structure and uses of different pharmaceutical pollutants. Adopted from PubChem[55]

Pollutant (formula)	Structure	Uses
Acetaminophen ($C_8H_9NO_2$)	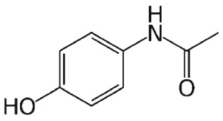	Nonprescription analgesic and antipyretic medication for mild-to-moderate pain and fever
Amoxicillin ($C_{16}H_{19}N_3O_5S$)	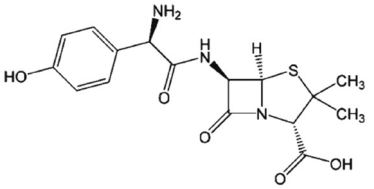	Bacterial infections, and dental abscesses
Sulfamethoxazole ($C_{10}H_{11}N_3O_3S$)	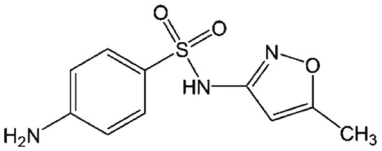	Used in treatment of a variety of bacterial infections, including those of the urinary, respiratory, and gastrointestinal tracts
Ibuprofen ($C_{13}H_{18}O_2$)	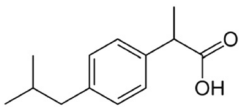	Anti-inflammatory; analgesic; antipyretic
Norfloxacin ($C_{16}H_{18}FN_3O_3$)	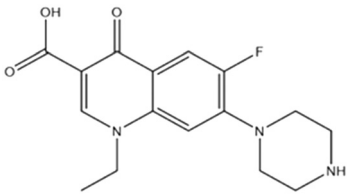	In treatment of urinary tract infections and prostatitis
Ciprofloxacin ($C_{17}H_{18}FN_3O_3$)	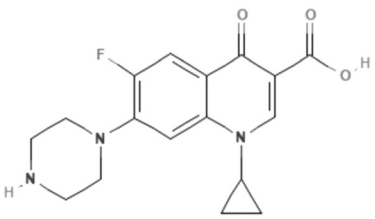	Therapy of mild-to-moderate urinary and respiratory tract infections caused by susceptible organisms
Tetracycline ($C_{22}H_{24}N_2O_8$)	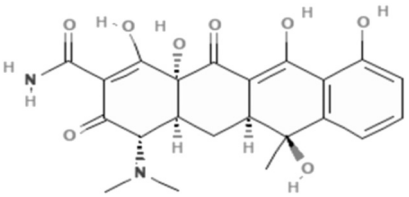	Role as an antimicrobial agent, an antibacterial drug, an antiprotozoal drug, a protein synthesis inhibitor and an *Escherichia coli* metabolite
Diclofenac ($C_{14}H_{11}Cl_2NO_2$)	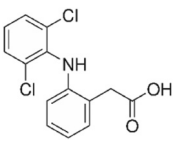	Therapy of chronic forms of arthritis and mild-to-moderate acute pain
Atenolol ($C_{14}H_{22}N_2O_3$)	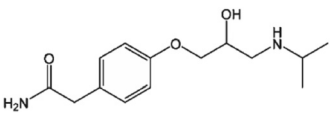	As a cardioselective beta-blocker that is widely used in the treatment of hypertension and angina pectoris

treatment of wastewater containing pharmaceuticals. Alternatively, several review articles have reported on the photodegradation of antibiotic contaminants in water, such as amoxicillin,[21] ibuprofen,[22] tetracycline,[52,54] ciprofloxacin,[53,54] and norfloxacin[54] antibiotics in wastewater and several others, which are referred to in section 3. However, there is still a need for an extensive review article in this field, covering in a single window a larger number of pharmaceutical pollutant photocatalysts for their photocatalytic performance.

The present review is focused primarily on the photocatalytic degradation of acetaminophen, amoxicillin, sulfamethoxazole, ibuprofen, norfloxacin, ciprofloxacin, tetracycline, diclofenac, *etc.* The structure and uses as well as the solubility of these antibiotics in water are provided in Table 1 (ref. 55) and ESI,† respectively. In view of this, the article describes the fundamental properties of semiconducting materials as photocatalysts as well as role of metal oxides, carbon-based materials, and heterojunctions and the immobilization approaches employed and the mechanisms involved in the removal of these pharmaceutical pollutants. Subsequently, the article deals with the removal of the above-mentioned drugs from contaminated water using semiconducting TiO_2, ZnO, and many other oxides, their combination with graphitic-carbon nitride (g-C_3N_4), carbon nanotubes (CNTs), activated carbon (AC), graphene oxide, graphene and graphene quantum dots, doping with metals and nonmetals, the formation of composites, semiconducting materials deposited on certain supports as photocatalysts and a heterojunction approach. It is anticipated that, in the light of this, the current review could be of immense help in identifying cost-effective and efficient photocatalytic methods for the remediation of these pharmaceutical pollutants. In addition, various research gaps, their possible solutions and several future prospects are also provided at the end of this article for the possible enhancement of environmental conservation.

2 Important photocatalysts and their role in the removal of pharmaceutical pollutants

The primary mechanism for the degradation of organic pollutants by a semiconducting material involves irradiating it with light energy in the form of photons ($h\nu$) sufficiently greater than the band gap energy of the photocatalyst (Fig. 2 (ref. 37)). Holes (h_{VB}^+) and electrons (e_{CB}^-) are generated in this manner in the valence band (VB) and the conduction band (CB), respectively. The separated holes reacts with hydroxyl ions (OH^-) or water molecules (H_2O) to produce hydroxyl radicals (·OH). In addition, the separated electrons reacts with dissolved O_2 in water to produce superoxide radicals ($\cdot O_2^-$), which upon further reaction, produce ·OH.[37,51] Subsequently, the active species generated in this manner react with pharmaceutical pollutants on the surface of the semiconductor catalyst to give H_2O, CO_2 and other by-products.

$$\text{Semiconductor} + h\nu \rightarrow h_{VB}^+ + e_{CB}^-$$

$$h_{VB}^+ + H_2O \rightarrow H^+ + \cdot OH$$

$$e_{CB}^- + O_2 \rightarrow \cdot O_2^-$$

$$\cdot O_2^- + H^+ \rightarrow HO_2\cdot$$

$$HO_2\cdot + HO_2\cdot \rightarrow H_2O_2 + O_2$$

$$H_2O_2 + \cdot O_2^- \rightarrow \cdot OH + OH^- + O_2$$

$$H_2O + h_{VB}^+ \rightarrow \cdot OH + H^+$$

$$h_{VB}^+ + OH^- \rightarrow \cdot OH$$

It should be mentioned that the efficiency of a photocatalytic reaction depends on the capability of the photocatalyst to generate longer-lived e^- and h^+ that lead to the formation of reactive free radicals. In addition, photodegradation efficiency also depends on catalyst loading, contaminant concentration, pH, the presence of ions in the water, hydrogen peroxide, ultrasound irradiation, bubbling of O_2 and N_2 into the solution and irradiation time.[13,26,34]

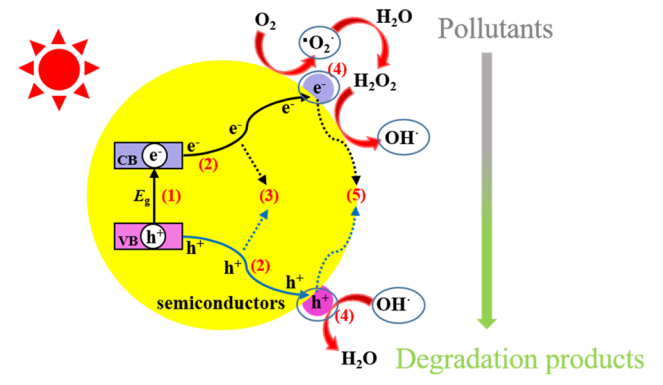

Fig. 2 Photocatalytic processes over a heterogeneous photocatalyst. Reproduced from ref. 37 with permission from MDPI (2021).

2.1 Metal oxides

Several semiconductor metal oxides have been used as photocatalysts in the abatement of aqueous pollution due to organic pollutants. From this point of view, TiO_2 has received a considerable amount of attention and its choice is mainly guided by its superior photocatalytic degradation efficiency, low processing cost, high environmental stability, nontoxicity, chemical stability, and high oxidizing ability.[31–33] However, its wide band gap (~3–3.2 eV),[32] and the fast e^-–h^+ recombination rate of photogenerated electron–hole pairs in TiO_2 limit its applications. Semiconducting ZnO (band gap: 3.37 eV) has been used as another photocatalyst in water treatment as an alternative to TiO_2.[56] Several other metal oxides (ZrO_2, Fe_2O_3, γ-Fe_3O_4, SnO_2, Mn_2O_3, WO_3, CeO_2, CuO,

and NiO) have also been investigated as alternatives to TiO_2 and ZnO.[26] Nano-engineered metal-oxide-based photocatalysts have also attracted a lot of attention in wastewater treatment.[57] However, metal oxide catalysts experience similar drawbacks to TiO_2. As a consequence, significant developments have taken place in recent years in tailoring these metal oxide photocatalysts. This is achieved by reducing their band gap by the addition of dopants that include both metals and non-metals, such as iron, copper, carbon, nitrogen, platinum and sulfur. In addition, metal sulfides,[58] metal ferrites,[59] and oxychlorides[60] have also been explored as emerging photocatalysts for the removal of pharmaceutical pollutants.

Photocatalytic studies have been reported on the performance of semiconductor–metal composites in the removal of several pollutants from water. In this regard, plasmonic composites in combination with various semiconducting photocatalysts have been widely studied for enhancing overall photocatalytic performance.[61,62] The improved photocatalytic efficiency is attributed to the surface plasmon resonance effect. In addition, metal nanoparticles can decrease the recombination rate of the photo-induced e^-–h^+ pairs of the semiconductor material by effective electron trapping in the conduction band. Metal oxide nanocomposites derived from a mixture of two or more oxides or between these oxides and other functional semiconductor materials have also been found to be efficient, economical, and environmentally friendly photocatalysts in water pollutant remediation.[63,64]

2.2 Carbonaceous materials

The photocatalytic performance of various carbonaceous materials has been receiving more attention for antibiotic removal owing to their intriguing properties and good stability.[40,41] The choice of these carbonaceous materials in removing antibiotics is mainly guided by simple and cost-effective synthesis methods, the easy availability of raw materials and their unique physiochemical properties, such as the presence of micropores, mesopores, and macropores, the large number of oxygen-functional groups, high porosity, and high surface area, coupled with good visible-light adsorption ability, chemical stability, excellent electrical conductivity and high intrinsic electron mobility.[40] The carbonaceous materials explored for this purpose include carbon dots,[38] g-C_3N_4,[42,65] activated carbon[45,66] and carbon nanotubes (CNTs).[67] Graphene is another carbon-based material composed of a one-atom-thick layer of carbon atoms arranged in a hexagonal lattice.[68] It is a semimetal with a small degree of overlap between the valency band and the conduction band.[69] This makes graphene a promising candidate for application in photocatalysis. However, the photocatalytic performances and practical applications of carbon-based materials have not been encouraging, due to poor solar-light absorption and the rapid recombination of photogenerated electron–hole pairs.[41] Interestingly, combinations of these carbon-based materials with other semiconductor metal oxides have been utilized as promising photocatalysts owing to their notable properties like stability, conductivity, durability and high absorptivity. In addition, carbon-based materials–metal oxide nanocomposites have also enhanced the degradation efficiency of pharmaceuticals by improving the generation of radical species, through improved surface area and light absorption, and reducing the recombination of generated charge carriers.[48,69]

2.3 Heterojunction nanocomposites as photocatalysts

A heterojunction is defined as the interface between two layers or regions of different semiconductors with unequal band structures that can result in band alignments. Based on this concept, semiconductor–semiconductor-based heterojunction composites showed excellent improvements in photocatalytic efficiency. This is ascribed to minimized charge carrier recombination, the interface of the heterojunction, superior charge transfer, prolonged charge carrier lifetime, separate active sites, and extended light absorbance characteristics.[51] These semiconductor heterojunction photocatalysts are classified into several types: *i.e.*, conventional heterojunctions (type-I, type-II, and type-III), p–n heterojunctions, direct Z-scheme heterojunctions, and S-scheme heterojunctions.[70–73] The schematic separation of charges *via* electron migration from one semiconductor to another in various heterojunction mechanisms is represented in Fig. 3.[51] Among these, in a type-I heterojunction, the VB and CB of semiconductor-1 are respectively lower and higher than those of semiconductor-2 (Fig. 3(a)). The photogenerated holes migrate from the VB of semiconductor-1 to the VB of semiconductor-2 accompanied by the transfer of photoelectrons from the CB of semiconductor-1 to the CB of semiconductor-2.[52] However, this type-I heterojunction cannot spatially separate e^-–h^+ pairs and this leads to the accumulation of charge carriers and their accelerated recombination rate. A type-II heterojunction (Fig. 3(b)) involves the transfer of photogenerated holes generated in semiconductor-2 to semiconductor-1, considering the VB of semiconductor-1 to be lower than that of semiconductor-2 on irradiating with light.[52] In contrast, photogenerated electrons in the CB of semiconductor-1 can migrate to that of semiconductor-2, if the level of the CB in semiconductor-1 is higher than that of semiconductor-2. It should be noted that the spatial separation of electron–hole pairs can occur in a type-II heterojunction. Furthermore, the structure of a type-III heterojunction is similar to that of a type-II heterojunction; however, charge-carrier separation cannot occur in a type-III heterojunction because the band gaps of both semiconductors do not overlap, since the levels of the VB and CB of both semiconductors are very far apart (Fig. 3(c)). When p-type and n-type semiconductors are combined, a p–n heterojunction can be formed. A space-charge region could be formed at the interface before light irradiation due to diffusion of the majority of charge carriers,

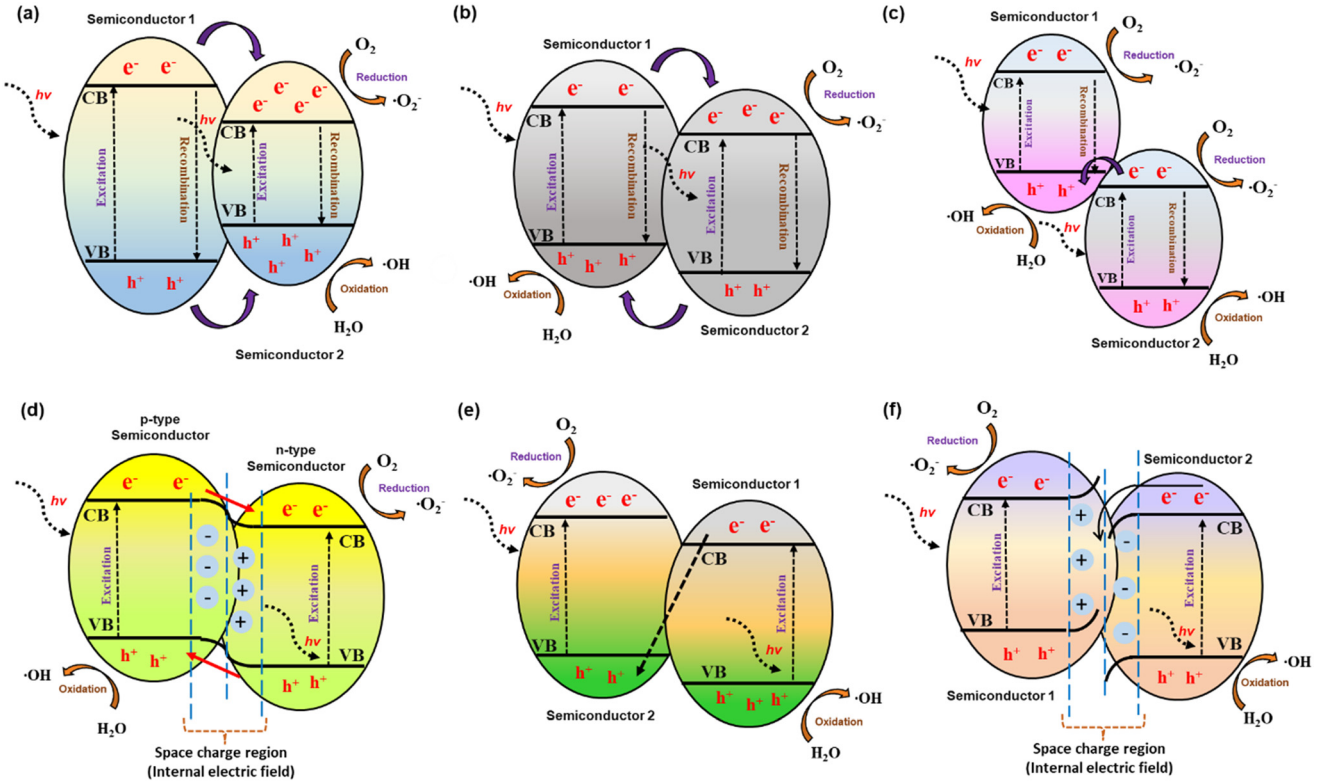

Fig. 3 Schematic illustration of various types of heterojunction: (a) straddling bandgap (type I), (b) staggered bandgap (type II), (c) broken bandgap (type III), (d) p–n type, (e) direct Z-scheme, and (f) S-scheme. Reproduced from ref. 51 with permission from Amer Sci Publ (2023).

leading to a built-in electric field, as shown in Fig. 3(d). In the Z-scheme heterojunction system, the band structure is quite analogous to that of a type-II heterojunction, but the direction of charge transfer is the opposite. The photogenerated electrons from the second semiconductor migrate aggressively to the VB of the first semiconductor and occupy the available holes, while the strongly oxidative holes in the VB of the second semiconductor and strongly reductive electrons in the CB of the first semiconductor take part in the redox reaction (Fig. 3(e)). In a step-scheme (S-scheme) heterojunction, two n-type semiconductors are combined with a staggered band structure similar to a type-II heterojunction (Fig. 3(f)).

2.4 Immobilized photocatalysts

The immobilization of photocatalysts on supports (Fig. 4)[51] can maximize the activity of semiconductors by offering a greater number of active sites. The high photocatalytic activity of such immobilized semiconductor photocatalysts is guided by the properties of their semiconductor-active species and the kind of support employed.[51] The high catalytic performance of these immobilized photocatalysts originates from impeding the rate of electron–hole pair recombination. The recovery, reusability, and stability issues of a photocatalyst remain challenging after several reaction runs. In this regard, the immobilization of a catalyst on a support facilitates the rapid separation and efficient recycling of the catalyst. This reduces production costs as well as minimizing waste generation, especially in industrial applications compared to conventional pure photocatalysts.[74]

3 Removal of pharmaceutical components using different Photocatalysts

In this review article, we present the use of photocatalysts based on bare metal oxides (TiO_2, ZnO and other oxides) and carbon-based materials (graphitic carbon nitride, g-C_3N_4, carbon nanotubes CNTs, activated carbon AC, and graphene) in the removal of pharmaceutical pollutants from water. In addition, several modification approaches are also highlighted and those involving metal loading, doping with metals and nonmetals, the formation of composites, immobilization and the formation of heterojunctions for this purpose are described below for pharmaceutical pollutants.

3.1 Acetaminophen

Acetaminophen (ACT), also known as paracetamol is commonly used all over the world as a painkilling, anti-inflammatory, analgesic, and antipyretic drug.[75–78] It is available both as a single-entity formulation and in combination with other medications. The presence of acetaminophen in wastewater, surface water and groundwater can have an adverse effect on living organisms

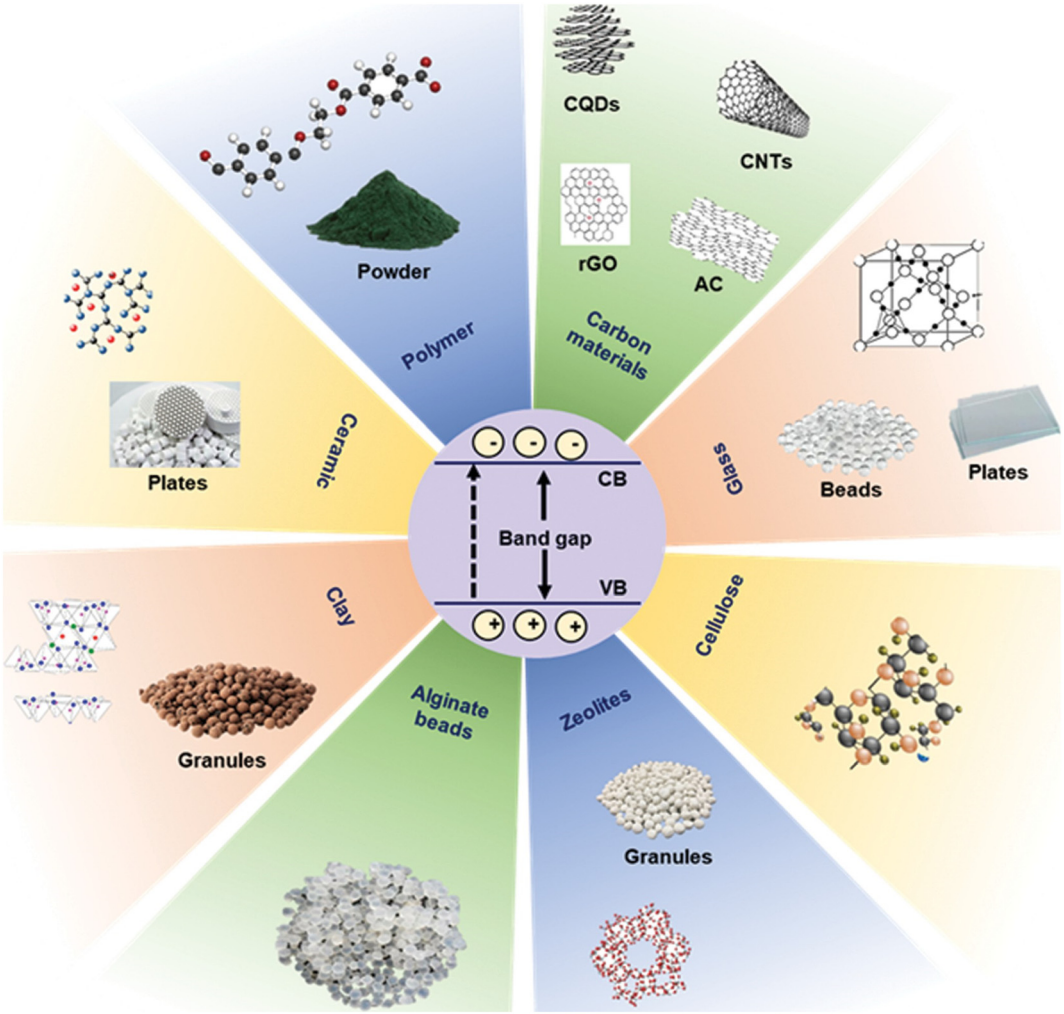

Fig. 4 Supporting materials used for the immobilization of photocatalysts. Reproduced from ref. 51 with permission from Amer Sci Publ (2023).

and environmental ecology owing to its oxidative transformation to toxic *N*-acetyl-*p*-benzoquinone imine. The stable chemical structure of acetaminophen remains one of the major constraints to its removal through conventional wastewater treatment. Therefore, attention has focused on its removal from aqueous media following a photocatalysis approach, as described below.[79–147]

3.1.1 Metal oxides. Two titania photocatalysts prepared by a sol–gel method showed higher photocatalytic activity than commercial TiO_2–P25 when tested for the photodegradation of paracetamol in aqueous solution.[79] Marizcal-Barba *et al.*[80] studied the photocatalytic degradation of acetaminophen in the presence of TiO_2 synthesized by a sol–gel method and observed its 99% degradation of acetaminophen corresponding to a pH of 10, acetaminophen concentration of 35 mg L^{-1} and a catalyst dose of 0.15 g of TiO_2. Hollow mesoporous TiO_2 microspheres have also been investigated as a photocatalyst to study the degradation of acetaminophen in water owing to its large surface area and the possibility of efficient light harvesting capability.[81] These findings showed an increase in the conversion fraction of the drug to 94% in 60 min following a 25% increase in the initial reaction rate and good photodegradation activity even after 10 repeated runs.

Zhang *et al.*[82] reported about 95% photocatalytic degradation of acetaminophen in an aqueous solution of TiO_2 (1.0 g L^{-1}) after 100 min of irradiation under a 250 W metal halide lamp. This is attributed to direct hole (h^+) oxidation and ipso-substitution comprising the main initial steps in the degradation. The photodegradation of paracetamol (20 mg L^{-1}) has been investigated in the presence of nanostructured TiO_2 catalysts with a nanotube-type morphology using ultraviolet radiation (λ: 254 nm) and the removal efficiency was found to be 99% after 100 min.[83] The photocatalytic degradation of acetaminophen in water has also been reported using ZnO,[84] faceted-TiO_2[85] and molecularly imprinted ZnO nanonuts.[86]

3.1.2 Metal-incorporated metal oxides. The introduction of metal species into TiO_2 and other metal oxides could modify their structural, electronic, optical and morphological properties. In view of this, several studies have been reported on the photodegradation of pharmaceutical pollutants in

metal-loaded metal oxides. Jiménez-Salcedo *et al.*[87] applied an organometallic approach for the preparation of Au–TiO_2 nanohybrids and studied the degradation of paracetamol (0.3 mg L^{-1}) under UVA light. These studies revealed 100% degradation of paracetamol in 30 min for Au–TiO_2 photocatalysts compared to TiO_2 (40 min). The kinetic studies also supported these findings as being inevitable from the higher rate constant of Au–TiO_2 photocatalysts (0.14 min^{-1}) compared to TiO_2 photocatalysts (0.12 min^{-1}) in the degradation of paracetamol. In addition, Ag-, Au- and Pt-loaded TiO_2 (Ag/TiO_2, Au/TiO_2 and Pt/TiO_2) have shown significant enhancement in the photocatalytic degradation (>90%) of acetaminophen in water over a wide pH range (4.2–8.0) under solar light.[88]

Pd-decorated CuO nanostructured thin film showed enhanced visible-light degradation of acetaminophen.[89] The influence of radical trappers revealed no role for ·OH, $\cdot O_2^-$ (or $^1O_2$) radicals on the photocatalytic degradation of acetaminophen. The photocatalyst possessed good stability, as indicated by the observed insignificant change in photodegradation even after 5 cycles. According to the available literature, $ZnFe_2O_4$ (bandgap: 1.9 eV) is non-toxic and exhibits good photostability.[90] Its photocatalytic behaviour is guided by several factors, such as its preparative method, morphology, and the presence of impurities. In view of this, Huerta-Aguilar *et al.*[91] reported the efficient degradation of paracetamol during water treatment using Au nanoparticles grown on $ZnFe_2O_4$ as a visible light (200 W halogen lamp, C-type R7s, $\lambda > 400$ nm) assisted photocatalyst. TiO_2/BN/Pd nanofibers showed significantly enhanced degradation of ACT (>90%), compared to pure TiO_2 (20%) after 4 h under visible-light irradiation.[92] This was explained on the basis of the good dispersion of Pd nanoparticles on TiO_2–BN nanofibers to facilitate the transfer of photoexcited hole carriers and a decrease in photogenerated electron–charge recombination. Reusability studies and recycling tests on the TiO_2/BN/Pd photocatalyst indicated its good stability over 5 cycles under UV and visible light.

3.1.3 Doped metal oxides. C,N-co-doped TiO_2 (20 mg) degraded 69.31% paracetamol (4 mg L^{-1}) under UV light and 70.39% under solar light in 120 min.[93] According to Shaban and Fallata,[94] carbon-doped TiO_2 nanoparticles (2.0 g L^{-1}) successfully photocatalytically degraded acetaminophen (2 ppm) in aqueous solution, seawater, and real polluted seawater on irradiation with UV and natural sunlight. This enhancement could be attributed to the lowering of its bandgap as a result of carbon doping in TiO_2. In addition, Mg-doped TiO_2 has also been reported in the photodegradation of paracetamol.[95] Accordingly, 25 wt% Mg-doped TiO_2 produced 60% and 48.3% degradation of paracetamol under UV and visible light, respectively. In all likelihood, the Mg dopant in TiO_2 acts as a photosensitizer for photocatalysts and hinders the recombination of electron–hole pairs. In another study, TiO_2 and Ta-doped TiO_2 nanomaterials showed 70–80% degradation of paracetamol in 2 h in UV-irradiated aqueous suspensions, which was attributed to surface acidity as a key parameter.[96] Mn-doped TiO_2 exhibited 53% degradation of an aqueous solution of acetaminophen in 3 h under ultrasound and UV irradiation owing to the reduced band gap (1.6 eV) and the high surface area (158 m^2 g^{-1}).[97] Fe-doped TiO_2,[98] $KAl(SO_4)_2$ and $NaAlO_2$-doped TiO_2,[99] N-doped halloysite (HNT)/TiO_2,[100] carbon-self-doped TiO_2,[101] Bi^{3+}-doped TiO_2[102] and $Ba_{0.95}$-$Bi_{0.05}Fe_{0.95}Cu_{0.05}O_3$[103] have also been prepared and examined for the photocatalytic degradation of acetaminophen and paracetamol.

The degradation of acetaminophen and its reaction mechanism have been investigated in presence of Ag–ZnO[104] and La-doped ZnO[105] photocatalysts under visible-light

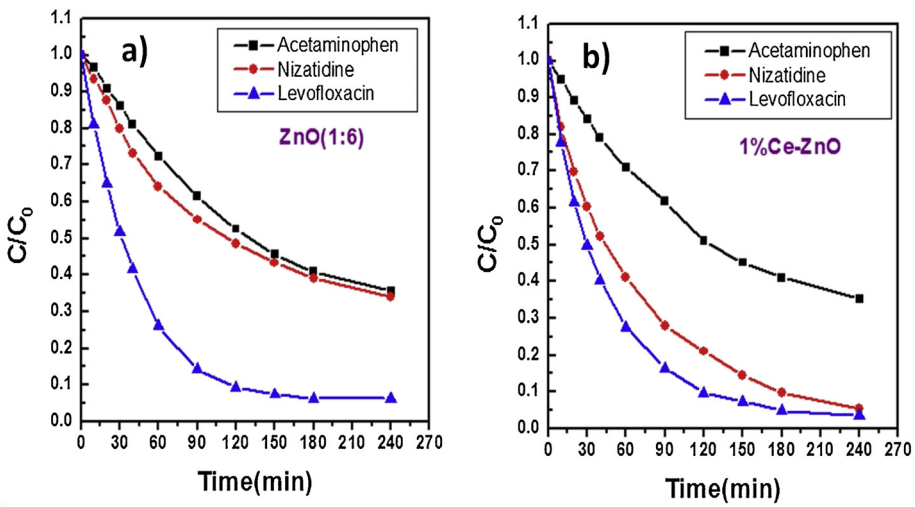

Fig. 5 (a) Photocatalytic degradation of pharmaceuticals over (a) ZnO (1 : 6) and (b) 1% Ce–ZnO nanostructured photocatalysts [experimental conditions: catalyst dosage: 1 mg mL^{-1}; concentration of pharmaceutical: 5 mg L^{-1}]. Reproduced from ref. 106 with permission from Elsevier (2019).

irradiation. Abri *et al.*[106] studied the photocatalytic degradation of nizatidine, acetaminophen and levofloxacin over ZnO (1 : 6) nanostructured photocatalysts under UVB light for 240 min and the findings are displayed in Fig. 5(a). Similar studies on using 1% Ce-doped ZnO produced almost no change in the degradation of acetaminophen and levofloxacin compared to that observed for nizatidine (~95%), as evidenced from Fig. 5(b). Such different photocatalytic degradation of these pharmaceuticals in the presence of ZnO and 1% Ce–ZnO photocatalysts could be attributed to their chemical structures.

Kumar *et al.*[107] investigated the photocatalytic degradation of acetophenone by irradiating nitrogen-implanted ZnO nanorod arrays (NRAs) with visible light. It should be noted that an N ion (1×10^{16} ions per cm^2) doped ZnO NRA sample (referred to as N–ZnO_4) showed maximum degradation efficiency (98.46%) of acetaminophen (20 ppm) in the presence of sunlight under 120 minute duration. The linear variation in $\ln(C_0/C)$ *versus* irradiation time followed pseudo-first-order degradation kinetics for acetaminophen. Furthermore, the superior photocatalytic activity of the N–ZnO_4 catalyst was inevitable from the high value of its rate constant (0.038 min^{-1}) compared to pristine ZnO NRAs (0.0045 min^{-1}). In addition, further investigations also revealed a more or less unaltered degradation efficiency (98.46% to 97.63%) of N–ZnO_4 after five repeated cycles. The findings of the effect of scavengers on the photocatalytic degradation of acetaminophen in the presence of N–ZnO_4 showed a decrease in degradation efficiency for acetaminophen (98.4%) in the presence of benzoquinone (BQ 28.52%), EDTA (65.6%) and methanol (98.4%) due to the major role played by O_2. The mechanism of acetaminophen degradation on subjecting N-ion-implanted ZnO NRAs to visible light suggested a shifting of the band gap to the visible region.

3.1.4 Metal oxide composites. Nanosized Fe_2O_3–TiO_2 nanocomposites exhibited higher degradation (95.85%) of acetaminophen compared to bare TiO_2 under stimulated solar radiation (optimal conditions: initial concentration of ACT: 30 mg L^{-1}; catalyst loading: 1.25 g L^{-1}; initial pH: 11).[108] Khasawneh *et al.*[109] synthesized a hematite (α-Fe_2O_3)-doped TiO_2 nanocomposite *via* a sol–gel method and investigated the role of UV light on the degradation of paracetamol. The photocatalytic degradation of acetaminophen has also been

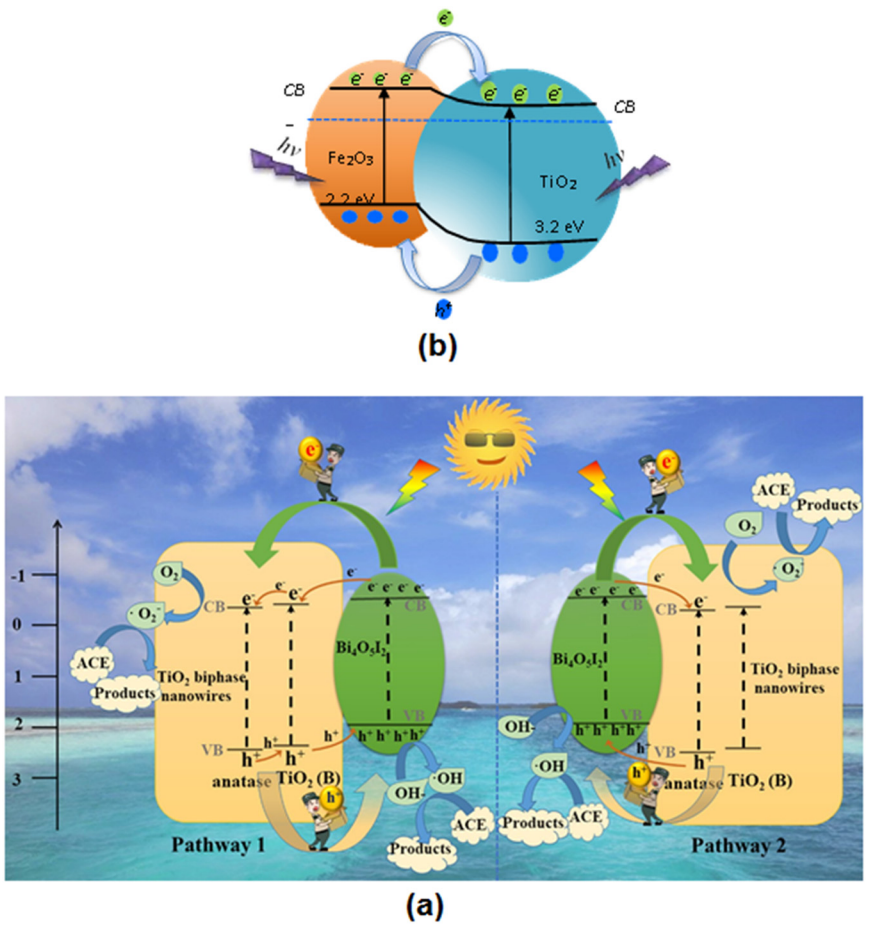

Fig. 6 (a) Schematic of the possible charge separation and photocatalytic mechanism of TiO_2–$Bi_4O_5I_2$ composite under visible-light irradiation. Reproduced from ref. 114 with permission from Elsevier (2020). (b) Schematic diagram of charge transfer in the photoexcited TiO_2/Fe_2O_3 core–shell photocatalyst. Reproduced from ref. 117 with permission from Elsevier (2017).

investigated using montmorillonite nanosheets modified with TiO_2 under UV radiation.[110] These findings revealed 100% removal efficiency for acetaminophen in aqueous solution corresponding to pH 7, catalyst dose of 0.75 g L^{-1}, acetaminophen concentration of 2 mg L^{-1} and contact time within 120 min.

Magnetic TiO_2/Fe_3O_4 (1.16 g L^{-1}) and $TiO_2/SiO_2/Fe_3O_4$ (1.34 g L^{-1}) nanoparticles degraded acetaminophen, antipyrine, caffeine, and metoprolol pharmaceuticals on illuminating its aqueous solution (pH: 7, ACT concentration: 30 mg L^{-1}).[111] $TiO_2/SiO_2/Fe_3O_4$ nanoparticles also showed good reusability, as evidenced within four repeated experiments. Czech and Tyszczuk-Rotko[112] explored the visible-light (centered at 500–550 nm) driven photocatalytic removal of acetaminophen from water using MWCNT (1.72 wt%)–TiO_2–SiO_2 nanocomposites and observed ~82% efficiency due to the key role played by photogenerated holes. In another study, Fernandes *et al.*[113] selected combinations of Fe_2O_3 and Fe_3O_4 nanoparticles due to their easy availability and used them in the photodegradation of acetaminophen under UV-vis irradiation. The total acetaminophen (and caffeine) degradation (20 ppm/150 mL) took place by means of 0.13 g catalyst L^{-1} solution in 45 min (and 60 min) and it remained almost unaltered over five cycles. A ternary heterogeneous anatase-TiO_2 (B) biphasic nanowires/$Bi_4O_5I_2$ composite exhibited 95% degradation of acetaminophen in 6 min under visible-light irradiation.[114] This is ascribed to the multiphase structure, including the synergistic effect of anatase TiO_2 and $Bi_4O_5I_2$. A schematic of the possible charge separation and photocatalytic mechanism of the TiO_2–$Bi_4O_5I_2$ composite under visible-light irradiation is displayed in Fig. 6(a).

Chau *et al.*[115] synthesized a $Cu_2O/WO_3/TiO_2$ ternary composite in view of the narrow band gaps of Cu_2O (2.20 eV) and 2.70 eV (WO_3) guided by their low cost, nontoxicity, chemical stability and strong absorption ability towards visible light. The composite fabricated in this manner produced 92.50% photodegradation of ACT (1 mg L^{-1}) compared to pure TiO_2 under 60 min of solar irradiation. This is attributed to the effective separation and low recombination rate of the charge carriers. The produced composite exhibited high reusability for photodegradation with 83% at the fifth cycle of ACT photodegradation. Nanostructured titania supported on activated carbon (AC) has been used to study the effects of photocatalyst dosage, initial solution pH and irradiation (UV) time on the photocatalytic degradation of aqueous acetaminophen.[116] Abdel-Wahab *et al.*[117] prepared flower-like core–shell TiO_2/Fe_2O_3 photocatalysts instead of TiO_2/Fe_3O_4 due to the photostability of Fe_2O_3 compared to Fe_3O_4 and investigated its activity in the degradation of paracetamol in aqueous solution using a medium-pressure mercury lamp (450 W). These findings indicated increases in the photocatalytic degradation of paracetamol (52.5%) to 87.8% for 50% content of TiO_2. This is ascribed to the separation of the photogenerated electron–hole pairs accomplished by coupling the narrow band gap with the wide band gaps of Fe_2O_3 and TiO_2, respectively. A schematic diagram of charge transfer in the photoexcited TiO_2/Fe_2O_3 core–shell photocatalyst is displayed in Fig. 6(b). Jallouli *et al.*[118] used TiO_2 nanoparticles and TiO_2/cellulosic fiber to carry out the photocatalytic degradation of paracetamol under UV and sunlight irradiation. $WO_3/TiO_2/SiO_2$[119] and TiO_2/ZSM-5 (ref. 120) also exhibited enhanced photocatalytic degradation of acetaminophen in contaminated wastewater.

TiO_2 immobilized on glass spheres (sunlight)[121] and ZnO–polystyrene (UV-LED)[122] photocatalysts effectively removed acetaminophen and paracetamol, respectively. The photodegradation of acetaminophen is also reported with zeolite-supported TiO_2 and ZnO under UV and sunlight,[123] bi-modified titanate nanomaterials (visible light),[124] $BaTiO_3$/TiO_2 composite (UV-vis),[125] and Ag/AgCl@ZIF-8 (visible light).[126]

3.1.5 C_3N_4 and C-dot-based composites. The rapid photocatalytic degradation of acetaminophen (and levofloxacin) targeted by modifying g-C_3N_4 bulk material to g-C_3N_4 nanosheets under solar-light irradiation reached 99% in 60 min compared to bulk g-C_3N_4 (38% in 240 min).[127] Such performance of g-C_3N_4 nanosheets could be assigned to multiple contributions, such as smaller particle size, rich carbon surface and lower band gap. Contemporary studies on exfoliated g-C_3N_4 have also been reported for the degradation of paracetamol (and ibuprofen) in an aqueous environment under visible light.[128] A ZnO/Ph–g-C_3N_4 nanocomposite acted as an efficient visible-light-active catalyst for the photodegradation of paracetamol in aqueous suspension.[129] The findings revealed hydroxyl and superoxide radical anions to be responsible for the degradation process.

Heterostructures comprising α-Fe_2O_3/g-C_3N_4[130] have been examined for the photocatalytic degradation of acetaminophen. The photocatalytic activity of g-C_3N_4 combined with UiO-66-NH_2 in different proportions (25%-g-C_3N_4/UiO-66-NH_2, 50%-g-C_3N_4/UiO-66-NH_2, 75%-g-C_3N_4/UiO-66-NH_2) was tested for the removal of acetaminophen from an aqueous solution under given experimental conditions ([ACT]: 5 mg L^{-1}, [Cat]: 0.5 g L^{-1}, V: 350 mL).[131] The corresponding findings on the temporal evolution of acetaminophen with the different samples and their pseudo-first-order rate constants (k_{obs}) are displayed in Fig. 7(a) and (b). These findings depict complete removal of acetaminophens by the 75%-g-C_3N_4/UiO-66-NH_2 heterostructure in 120 min with a pseudo-first-order rate constant of 2 h^{-1}. It is suggested that incorporation of UiO-66-NH_2 in g-C_3N_4 enhanced the separation of the photogenerated charges. Silica–carbon quantum dots (1 wt%) decorated TiO_2 as a sunlight-driven photocatalyst completely removed acetaminophen 33.3% faster than pure TiO_2.[75] Gupta *et al.*[132] studied the augmented photocatalytic degradation of acetaminophen using hydrothermally treated g-C_3N_4 and persulfate under LED irradiation.

3.1.6 Graphene and its composites. Khavar *et al.*[133] observed the complete degradation of acetaminophen (pH

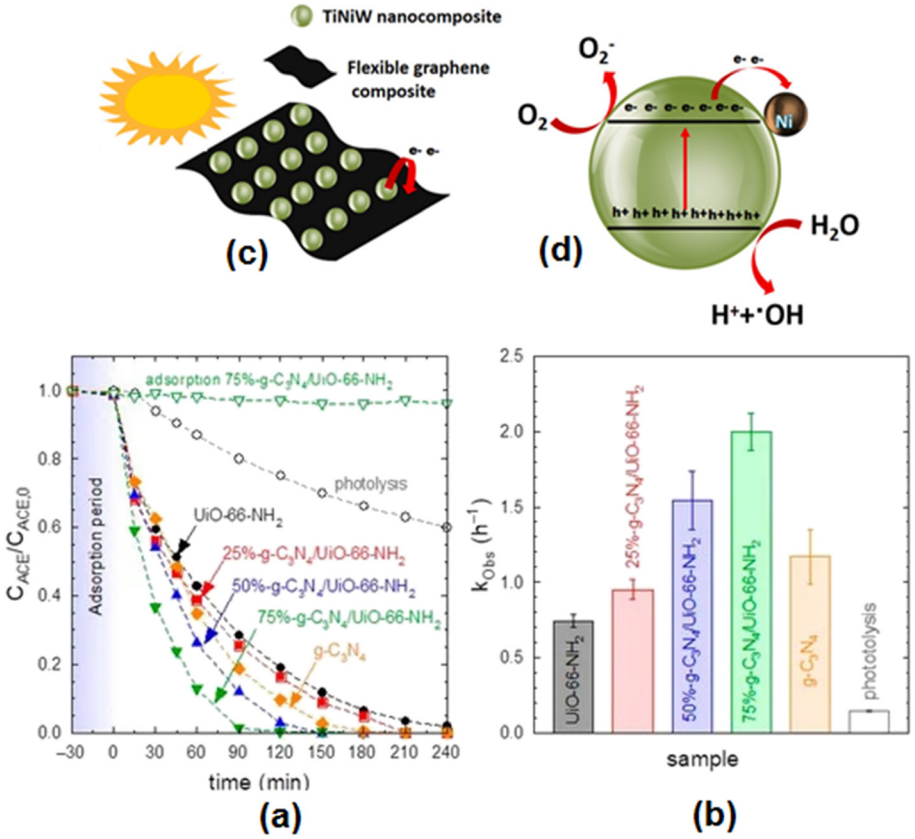

Fig. 7 (a) Photocatalytic degradation of acetaminophen with different g-C_3N_4/UiO-66-NH_2 samples. (b) Pseudo-first-order rate constant (k_{obs}) of different g-C_3N_4/UiO-66-NH_2 samples. Experimental conditions: V = 350 mL; T = 20 °C, C_{ACE} = 5 mg L^{-1}; C_{CAT} = 0.5 g L^{-1}. Reproduced from ref. 131 with permission from MDPI (2022). (c) Schematic illustration of the TiNiW NPs decorating the surface of the graphene composites and (d) TiNiW nanoparticle showing the possible chemical reactions for the formation of reactive oxygen species that degrade the ACT contaminant. Reproduced from ref. 138 with permission from Elsevier (2021).

5.4) for 3 wt% rGO@TiO_2 under visible UVA-LED irradiation within 50 min. A graphene-oxide-supported bioinspired CuO photocatalyst (50 wt%) showed 96.2% acetaminophen degradation.[134] A calcined ZnFe-layered double hydroxide (CLDH)/rGO (for initial wt. of GO: 30 mg) exhibited the highest degradation of about 95% of paracetamol in 420 min, owing to the synergistic effect between Zn–Fe calcined LDH and rGO.[135] Tao *et al.*[136] synthesized nanocomposites comprising 5% graphene/TiO_2 nanotubes by a hydrothermal method and observed a 96% degradation rate for acetaminophen (5 mg L^{-1}) under UV-light irradiation for 3 h. Further investigations indicated holes to be the main oxidation species in the photocatalytic process. According to Umejuru *et al.*,[137] coal fly ash (CFA) decorated with graphene oxide nanorods with Pb^{2+}-ion-loaded spent adsorbent exhibited 93% degradation of acetaminophen on subjection to photocatalysis. Ni@TiO_2:W nanoparticles (TiNiW) and TiNiW immobilized on the surface of a flexible graphene (FG) composite on subjection to natural solar irradiation (3 h) achieved acetaminophen degradation efficiencies of 100% and 86%, respectively.[138] Subsequent findings suggested that acetaminophen degradation was mainly caused by reactive oxygen species, such as ·OH radicals and h^+. Reusability experiments confirmed the stability of TiNiW and FG/TiNiW composite for the degradation of acetaminophen. Fig. 7(c) schematically represents the TiNiW nanoparticles decorated on the flexible graphene support and a proposed use in the mechanism of acetaminophen degradation. It is suggested that on subjecting it to solar excitation, photogenerated electrons could be rapidly trapped by the graphene layers, as evident through the scheme displayed in Fig. 7(d). Core/shell rGO/BiOBr[139] and vitamin-C-assisted synthesis of rGO–Ag/PANI[140] have also been reported to successfully achieve the improved photocatalytic degradation of acetaminophen.

3.1.7 Heterojunctions and Z-scheme-based photocatalysts. Recently, Parida *et al.*[20] fabricated a Bi_2O_3/MnO_2 Z-scheme heterojunction and achieved 94.3% photocatalytic degradation efficiency (0.0202 min^{-1}) for acetaminophen in 120 min. This was found to be about 3.5 and 3.8 times higher than MnO_2 and Bi_2O_3, respectively, in deionized water. Their studies on real water systems further revealed relatively inferior degradation efficiency in tapwater (88.7%), municipal (75.5%), hospital (63.6%) and pharmaceutical industry (55.4%) wastewater compared to that in deionized water (94.3%). The assembly of Sr@TiO_2 with UiO-66-NH_2 in different ratios was used to construct Sr@TiO_2/UiO-66-NH_2

Table 2 Performance data on removal of acetaminophen in water using variety of photocatalysts

Photocatalyst	Preparative method	ACT	Catalyst dose	pH	Light source	Degradation and time	Rate constant
TiO_2-rutile[76]	Precipitation	20 ppm	0.1 g (50 mL)	9	Tungsten halogen lamp (400 W), 0.0146 W cm^{-2}	68% (60 min)	—
TiO_2-anatase[76]	Thermal precipitation method	20 ppm	0.1 g (50 mL)	9	Tungsten halogen lamp (400 W), 0.0146 W cm^{-2}	60% (60 min)	—
ZnO[76]	Thermal precipitation method	20 ppm	0.1 g (50 mL)	9	Tungsten halogen lamp (400 W), (0.0146 W cm^{-2})	~100% (60 min) in 1 h	—
TiO_2: 80% anatase + 20% rutile (Degussa P25)[77]	Commercial	40 mg L^{-1} (250 mL)	2 g L^{-1}	—	UV lamp (15 W)	97% (300 min)	—
TiO_2/Ag (5%)[78]	Photodeposition method	20 μg L^{-1} (O_2: 100 cm^3 min^{-1})	1 g L^{-1}	—	UV radiation (365 nm)	94.50% (240 min)	—
TiO_2[79]	Sol–gel method	50 ppm (750 mL)	1.33 g L^{-1}	—	TQ159-ZO lamp (150 W)	~50% (180 min)	0.0056 min^{-1}
TiO_2[80]	Sol–gel method	35 mg L^{-1}	0.15 g	10	UV lamp with a wavelength of 256 nm, 1 mW cm^{-2}	99% (180 min)	—
Solid TiO_2 spheres[81]	Template-free solvothermal route	50 mg L^{-1}	0.1 g L^{-1}	—	Mercury lamp (500 W)	90% (60 min)	0.075 min^{-1}
Mesoporous TiO_2 microspheres[81]	Template-free solvothermal route	50 mg L^{-1}	0.1 g L^{-1}	—	Mercury lamp (500 W)	94% (60 min)	0.043 min^{-1}
TiO_2 (High Techn. Nano co. Ltd)[82]	Commercial	50 μM	1.0 g L^{-1}	9	Metal halide lamp (250 W), $\lambda \geq 365$ nm	~95% (100 min)	—
ZnO powders (Fluka)[84]	Commercial (thermally calcined at 100 °C)	50 mg L^{-1}	0.25 g (0.25 L)	—	UV-lamp (315–400 nm), P.D: 0.66 mW cm^{-2}	~97% (240 min)	0.0136 min^{-1}
ZnO nanonuts[86]	Chemical method	5×10^{-5} M	~1.0 mg	7.2	UV lamp: 4 mW cm^{-2}, 368 nm	~92% (180 min)	1.32×10^{-2} min^{-1}
TiO_2 (Degussa P25)[87]	Commercial	0.3 mg L^{-1}	40.5 mg (70 mL)	Neutral	LED lamp – UVA light (15 W), 365 nm	100% (40 min)	0.12 min^{-1}
Au–TiO_2[87]	Mixing tempered colloidal solution of au and TiO_2 in water	0.3 mg L^{-1}	40.5 mg (70 mL)	Neutral	LED lamp – UVA light (15 W), 365 nm	100% (32 min)	0.14 min^{-1}
Au–g-C_3N_4[87]	Reflex method	0.3 mg L^{-1}	40.5 mg (70 mL)	5.9	Visible light	100% (25 min)	0.17 min^{-1}
Ag(1 wt%)/TiO_2[88]	Sonicating mixture of TiO_2 and aqueous $AgNO_3$, stirring and irradiating with 450-W ACE lamp for 1 h	20 mg L^{-1}	0.4 g L^{-1}	6.3	Simulated solar light xenon lamp (1000 W), 50.0 mW cm^{-2}	~98% (180 min)	0.019 min^{-1}
Au(1 wt%)/TiO_2[88]	Sonicating mixture of TiO_2 and aqueous H_2AuCl_6, stirring and irradiating with 450 W ACE lamp for 1 h	20 mg L^{-1}	0.4 g L^{-1}	6.3	Simulated solar light xenon lamp (1000 W), 50.0 mW cm^{-2}	~93% (180 min)	0.016 min^{-1}
Pt(1 wt%)//TiO_2[88]	Sonicating mixture of TiO_2 and aqueous H_2AuCl_6, stirring and irradiating with 450 W ACE lamp for 1 h	20 mg L^{-1}	0.4 g L^{-1}	4.2	Simulated solar light xenon lamp (1000 W), 50.0 mW cm^{-2}	~100% (180 min)	0.020 min^{-1}
Pd/CuO[89]	Deposition and sputtering	10 mg L^{-1} (20 mL)	15 (l) × 15 (w) × 1 (t) mm film	—	Xenon arc lamp: 150 W, $\lambda > 420$ nm	~90% (240 min)	0.796 h^{-1}
TiO_2/BN/Pd[92]	Electrospinning and atomic layer deposition	1 mg L^{-1} (250 mL)	0.5 g L^{-1}	6.8	Medium-pressure metal halide UV lamp (400 W)	100% (10 min)	0.019 min^{-1}
TiO_2/BN100/Pd100[92]	Electrospinning and atomic layer deposition	1 mg L^{-1} (250 mL)	0.5 g L^{-1}	6.8	400 W halogen linear lamp (visible irradiation)	98% (180 min)	0.28 min^{-1}
C,N-co-doped TiO_2[93]	Peroxo–gel method	4 mg L^{-1}	20 mg	—	UV-light (10 W), λ: 365 nm	69.31% (120 min)	—
C-doped TiO_2[94]	Sol–gel method	2.0 ppm	2.0 g L^{-1}	7	Low UV lamp pressure (15 W), 365 nm, 65 W m^{-2}	100% (90 min)	0.0817 min^{-1}
Supported titania-based catalysts (25 wt% mg	Industrial petrochemical (source)	20 mg L^{-1}	0.7 g L^{-1} (25 mL)	4.3	UV lamp: 365 nm, 30 W m^{-2}	60% (60 min)	—

Table 2 *(continued)*

Photocatalyst	Preparative method	ACT	Catalyst dose	pH	Light source	Degradation and time	Rate constant
doping)[95]					Mercury vapour lamp (125 W), (202 W m^{-2})	48.3% (60 min)	—
TiO_2[96]	Hydrolysis of Ti isopropoxide (sol–gel method)	35 mg L^{-1}	0.5 g L^{-1}	5.5	UV irradiation: HG500 lamp (30 mW cm^{-2})	~84% (120 min)	12.4 ± 0.2 × 10^{-3} min^{-1}
Ta-doped TiO_2 (Ti/Ta molar ratio: 1%)[96]	Hydrolysis of Ti isopropoxide (sol–gel method) followed by Ta doping through impregnation method	35 mg L^{-1}	0.5 g L^{-1}	5.5	UV irradiation: HG500 lamp (30 mW cm^{-2})	~70% (120 min)	9.4 ± 0.1 × 10^{-3} min^{-1}
TiO_2[96]	Hydrolysis of Ti isopropoxide in presence of CH_3COOH	35 mg L^{-1}	0.5 g L^{-1}	5.5	UV irradiation: HG500 lamp (30 mW cm^{-2})	~70% (120 min)	9.3 ± 0.1 × 10^{-3} min^{-1}
Ta-doped TiO_2 (Ti/Ta molar ratio: 1%)[96]	Hydrolysis of Ti isopropoxide in presence of CH_3COOH followed by ta doping through impregnation method	35 mg L^{-1}	0.5 g L^{-1}	5.5	UV irradiation: HG500 lamp (30 mW cm^{-2})	~73% (60 min)	10.4 ± 0.1 × 10^{3} min^{-1}
Mesoporous MnO_x–TiO_2[97]	Sol–gel method	25 ppm (150 mL)	0.1 g L^{-1}	—	Continuous sonication (20 W) and UVA radiation (160 W m^{-2})	26% (180 min)	—
IL-Fe-doped TiO_2 with Fe to Ti molar ratios (%): 2[98]	Sol–gel method	10 mg L^{-1} (200 mL)	0.65 g L^{-1}	7	UV lamps	90.35% (90 min)	0.25 min^{-1}
Synthetic TiO_2 doped with $(KAl(SO_4)_2)$[99]	Sol–gel method	0.10 mM	1.0 g L^{-1}	6.9	Visible light: source (light emitting diodes) with $\lambda > 440$ nm	95% (540 min)	5.20 × 10^{-3} min^{-1}
Carbon-self-doped TiO_2[101]	Sol–gel method (product calcined at 300 °C)	0.1 mM (500 mL)	1.0 g L^{-1}	6.9	LEDs ($\lambda > 440$ nm)	~96% (540 min)	5.0 × 10^{-3} min^{-1}
Bi^{3+}(10%)-doped anatase TiO_2[102]	Hydrolysis method	10^4 M (100 mL)	0.1 g L^{-1}	5	Source: UV-vis, (4 W cm^{-2})	~100% (240 min)	0.97 h^{-1}
$Ba_{1-x}BiFe_{1-x}Cu_xO_3$ ($x = 0.05$)[103]	Pechini method	50 mg L^{-1}	0.75 g L^{-1}	9	Metal halide efficacy lamp	98.1% (120 min)	—
Ag/ZnO[104]	Chemical method	5 mg L^{-1} (500 mL)	1 g L^{-1}	8.5	Tungsten halogen lamp (300 W)	90.8% (120 min)	0.020 min^{-1}
1.0 wt% La-doped ZnO[105]	Precipitation method	100 mg L^{-1} (500 mL)	0.1 g	—	Compact fluorescent lamps: 20 W	99% (3 h)	—
1% Ce-doped ZnO[106]	Hydrothermal method	5 mg L^{-1}	1 mg mL^{-1}	6.8	UV-B mercury lamp (8 W)	68% (240 min)	0.0058 min^{-1}
N-Implanted ZnO nanorod array (NRA)[107]	ZnO NRAs by two-step process followed by N implantation by low energy ion beam	20 ppm (5 mL)	10 × 10 mm aligned ZnO NRA	—	Visible-light irradiation	98.46% (120 min)	0.038 min^{-1}
$TiO_2/SiO_2/Fe_3O_4$[111]	Ultrasonic-assisted sol–gel method	30 mg L^{-1} (400 mL)	1.34 g L^{-1}	7	Low-pressure mercury lamp: λ: 254 nm, 3.8×10^{-6} Ein L^{-1} s^{-1}	~97% (300 min)	1.7 × 10^9 M^{-1} s^{-1}
MWCNT (1.72 wt%) TiO_2–SiO_2[112]	Sol–gel method	10 mg L^{-1}	—	Nearly neutral	High-pressure mercury lamp, 500–550 nm, 7.31–7.53 mW m^{-2}	81.6% (60 min)	0.0113 min^{-1}
Magnetite–hematite[113]	Hydrothermal	20 mg	0.13 g L^{-1}	—	Medium-pressure hg vapour lamp (400 W)	~100% (45 min)	—
TiO_2 (438 mg)–$Bi_4O_5I_2$[114]	*In situ* calcination method	3 ppm	25 mg	—	Xenon lamp with a light filter of 400 nm	~95% (6 min)	0.425 min^{-1}
$Cu_2O/WO_3/TiO_2$[115]	Hydrothermal	1 mg L^{-1} (80 mL)	20 mg	9	Solar-light irradiation (source)	92.5% (60 mL)	4.42 × 10^{-2} min^{-1}
Flower-like 50% TiO_2/Fe_2O_3[117]	Modified ultrasonic assisted sol–gel method	50 mg L^{-1} (50 mL)	0.1 g L^{-1}	—	Medium-pressure Hg lamp (450 W)	87.8% (90 min)	0.0219 min^{-1}
3% $WO_3/TiO_2/SiO_2$[119]	Solution method	10 mg L^{-1}	1.0 g L^{-1}	9	Xenon lamp (500 W) without cut-off filter 800 nm cut-off filter (800 nm > λ > 200 nm)	88% (240 min)	0.70 h^{-1}

Table 2 *(continued)*

Photocatalyst	Preparative method	ACT	Catalyst dose	pH	Light source	Degradation and time	Rate constant
TiO_2 (40 wt%) /ZSM-5[120]	Sol–gel method	15 mg L^{-1} (500 mL)	1.0 g L^{-1}	6.8	UV lamp (14 W), 254 nm, 0.97 mW cm^{-2}	96.6% (180 min)	—
1.1% ZnO/polystyrene[122]	Solvent casting method	12.5 mg L^{-1}	25 g (50 mL)	6.5	UV light (13 W m^{-2})	77% (240 min)	—
Bi modified titanate[124]	Hydrothermal method	0.7 mg L^{-1}	1.0 g L^{-1}	7	Metal halogen lamp with UV and IR cut-off filters	88% (180 min)	12.61 × 10^{-3} min^{-1}
$BaTiO_3/TiO_2$ ratio of 3 : 1 (w/w)[125]	Grounding followed by drying and calcination	5 mg L^{-1}	1 g L^{-1}	7	Xenon lamp: 500 W (200 nm < λ < 800 nm)	95% (240 min)	0.5529 h^{-1}
Ag/AgCl@ZiF-8[126]	Stirring method	1 mg L^{-1}	0.5 g L^{-1}	5	Metal halogen lamp (500 W) combined with UV and IR cut-off wave length	99% (90 min)	0.0579 min^{-1}
g-C_3N_4[127]	Thermal oxidation etching process	5 mg L^{-1}	0.1 g (250 mL)	—	Solar irradiation (source)	99% (60 min)	—
Exfoliated g-C_3N_4[128]	Thermal synthesis	25 g dm^{-3}	0.9 g	—	UVA lamp: 368 nm, 0.96 mW cm^{-2}	41% (120 min)	4.5 × 10^{-3} Mol dm^{-3} min^{-1}
Exfoliated g-C_3N_4[128]	Thermal synthesis	25 g dm^{-3}	0.9 g	—	Visible light lamp (446 nm), an intensity of 8.5 mW cm^{-2}	54% (120 min)	—
0.05% ZnO/Ph–g-C_3N_4[129]	Single-step calcination and combustion process	20 mg L^{-1}	1 g L^{-1}	—	Halogen lamp (500 W)	90.8% (120 min)	—
α-Fe_2O_3/g-C_3N_4[130]	Dispersion under sonication followed by heating in air	2.0 mg L^{-1} (H_2O_2: 5.0 mM)	0.1 g L^{-1}	5.0	Xenon lamp: 35.0 W (λ > 420 nm)	100% (25 min)	0.134 min^{-1}
g-C_3N_4(75%)/UiO-66-NH_2[131]	Hydrothermal method	5 mg L^{-1} (350 mL)	0.5 g L^{-1}	4–5	9 W lamps, 365 nm	100% (120 min)	2.0 h^{-1}
Bi_2O_3/MnO_2[20]	Room temperature solution phase synthesis	5 mg L^{-1}	1 g L^{-1}	6.8	200 W LED strip (λ > 420 nm)	94.3% (120 min)	0.0202 min^{-1}
TiO_2@rGO prepared by using 3 wt% GO[133]	Sol–gel method	50 mg L^{-1} (25 mL)	2.0 g L^{-1}	5.4	LED lamps (18 no.) and each of l3 W, λ: 365 nm, 95 μW cm^{-2}	100% (50 min)	0.061 min^{-1}
Calcined ZnFe-LDH/rGO (using 30 mg of GO)[135]	Hydrothermal calcined method (using 30 mg GO)	5 mg L^{-1} (50 mL)	25 mg	—	Xenon lamp (500 W), 300 nm cut-off filter	95% (420 min)	0.00737 min^{-1}
5% graphene/TiO_2 nanotubes[136]	Hydrothermal	5 mg L^{-1} (500 mL)	0.1 g L^{-1}	7	UV lamp (14 W), 254 nm	96% (180 min)	00197 min^{-1}
Coal fly ash (CFA)/GO/WO_3 NRs[137]	Hydrothermal	5 mg L^{-1}	100 mg	—	250 HW lamp	86% (180 min)	−0.0116 min^{-1}
Ni@TiO_2:W[138]	Hydrothermal treatment immobilizing	25 mg L^{-1}	30 mg (100 mL)	7	Solar natural irradiation (754 ± 13 W m^{-2})	100% (180 min)	10.7 × 10^{-3} min^{-1}
Flexible graphene/Ni@TiO_2:W[138]	TiNiW grown on the surface of graphene	25 mg L^{-1}	30 mg (100 mL)	7	Solar natural irradiation (754 ± 13 W m^{-2})	86% (180 min)	8.8 × 10^{-3} min^{-1}
1% rGO/BiOBr core/shell[139]	Hydrothermal	5 mg L^{-1} (30 mL)	—	5.5–9.5	Hg/xenon lamp (visible light irradiated with 400 nm cut-off filter), 20 mW cm^{-2}	93% (105 min)	0.006 min^{-1}
rGO–Ag/PANI[140]	Mixing reduced GO with polyaniline $AgNO_3$ by vitamin C	25 mg L^{-1}	50 mg	5	Visible light	99.6% (100 min)	—
Sr@TiO_2 with UiO-66-NH_2[141]	By carrying out growth of UiO-66-NH_2 on $SrTiO_3$	5 mg L^{-1}	250 mg L^{-1} (150 mL)	—	Xenon lamp: 600 W m^{-2} (λ cut-off filter: 320 nm)	~94% (240 min)	0.67 h^{-1}
15 wt%CeO_2/IK–g-C_3N_4[142]	Mixing method	10 mg L^{-1} (20 mL)	2.0 g L^{-1}	9	Visible light lamps (8 W), 465 ± 40 nm	98% (90 min)	0.0386 min^{-1}
5% g-C_3N_4/TiO_2/persulfate[143]	Ultrasonic mixing	5 mg L^{-1} (100 mL) and PS: 2 mM	0.331 g L^{-1}	7	Xenon lamp (300 W) with 400 nm cut-off filter	99.3% (30 min)	0.181 min^{-1}

Table 2 *(continued)*

Photocatalyst	Preparative method	ACT	Catalyst dose	pH	Light source	Degradation and time	Rate constant
CdO–ZnO (0.1 : 0.2 mole ratio)[144]	Homogeneous co-precipitation	12 ppm	1 g L^{-1}	6.15	Halogen lamp (500 W)	96% (160 min)	0.05 min^{-1}
Magnetic mesoporous carbon[146]	*In situ* chemical co-precipitation method	20 mg L^{-1}, PMS: 0.6 mM	0.12 g L^{-1}	6	UVC lamp – Philips (6 W) with 254 nm cut-off filter	97.4% (40 min)	—
TiO_2/graphene/g-C_3N_4 (60 : 10 : 30)[147]	Hydrothermal method	50 mg L^{-1}	0.6 g L^{-1}	9	Xenon lamp (SSL irradiation): 300 W, λ cut-off filter: 420 nm	100% (120 min)	2.7 × 10^{-2} min^{-1}

heterostructures and achieved more than 90% conversion of acetaminophen under solar light.[141] A visible-light-driven 15 wt% CeO_2/I,K-co-doped C_3N_4 heterojunction photocatalyst removed about 98% acetaminophen from aqueous solution after 120 min of irradiation compared to pure g-C_3N_4 (47%) and doped IK-C_3N_4 (75%).[142] In another study, a g-C_3N_4/TiO_2 (weight ratio: 5%)–persulfate (PS) photocatalytic system showed almost complete photodegradation ability and stability for acetaminophen under visible-light irradiation.[143] Visible-light-mediated CdO–ZnO demonstrated efficient photocatalytic performance as a heterogeneous photocatalyst in the decomposition of paracetamol in an aqueous solution.[144] Radical scavenger tests established the dominance of ·OH and h^+ for this photocatalytic process.

A heterojunction magnetic ternary g-C_3N_4/TiO_2–$MnFe_2O_4$ halloysite photocatalyst showed about 79.1% removal of acetaminophen (10 ppm) within 90 min under visible light.[145] The ternary photocatalyst could be easily recovered by applying an external magnetic field and reused several times without any significant reduction in its catalytic activity. The removal efficiency for acetaminophen under optimum conditions in the presence of a magnetic carbon heterojunction coupled with UV light and peroxymonosulfate was insignificantly reduced from 97.4% even after five consecutive cycles.[146] Moradi *et al.*[147] used 0.6 g L^{-1} of TiO_2/graphene/g-C_3N_4 (60 : 10 : 30) Z-type photocatalyst and observed complete degradation of acetaminophen (50 mg L^{-1}) at a pH of 9.0 in 120 min due to a synergistic effect. Their investigations also showed HO· and O_2·$^-$ radicals to be the dominant species in the degradation of acetaminophen.

Table 2 records the performance data of different photocatalysts on the removal of acetaminophen from wastewater.

3.2 Amoxicillin

Amoxicillin (AMX) is a widely used semi-synthetic β-lactam and broad-spectrum antibiotic in the treatment of different types of infection for treating both human and animal diseases.[148] Therefore, it is possible to find traces of this drug or its degradation products in various aquatic environments in the treated discharge from wastewater treatment plants. Its presence in aquatic animals and humans contributes to toxic effects though the aquatic system due to its structure, high polarity, and water solubility. However, amoxicillin in water is not easy to remove by conventional wastewater treatment processes due to its resistance to biodegradation. Hence, it is necessary to conduct a large amount of research on the treatment and removal of amoxicillin from wastewater using a variety of photocatalysts before discharging it into the natural aquatic environment.[149–216]

3.2.1 Metal oxides

3.2.1.1 TiO_2. Radosavljević *et al.*[149] applied TiO_2 in a nanocrystalline form and compared it with commercial TiO_2 to study the photocatalytic degradation of amoxicillin using an Osram Ultra-Vitalux® lamp as the light source. Their findings indicated almost complete degradation of AMX after 210 min for catalyst and AMX concentrations of 2 g dm^{-3} and 100 mg dm^{-3}, respectively. The UV-mediated photocatalytic degradation of amoxicillin was found to be low (27.6%) in the presence of TiO_2 (10–25 nm) compared to cephalexin (63.5%) and tetracycline (100%) under optimal conditions.[150] Pereira *et al.*[151] used photoreactors and studied the degradation of amoxicillin in aqueous solution (pH: 7.5) by subjecting it to a solar-driven TiO_2 (0.5 g L^{-1}) assisted photocatalytic process. According to this, TiO_2/solar UV radiation was able to reduce the antibiotic concentration from 40 to 3.1 mg L^{-1} after 4.6 kJ_{UV} of UV accumulated energy per liter of solution.

The degradation of amoxicillin (10 mg L^{-1}) was also examined under UV and visible irradiation (15 min) and found to be nearly 100% for TiO_2 and ZnO (both 0.01 g), respectively.[152] Amoxicillin (104 mg L^{-1}) in aqueous solution (pH ~ 5) was completely degraded under TiO_2/UVA (365 nm) in 30 min in the presence of H_2O_2 (100 mg L^{-1}).[153] TiO_2-catalyzed photodegradation of amoxicillin (10 mg L^{-1}) was found to be ~100% under UV irradiation of 30 min duration.[154] According to Klauson *et al.*,[155] Degussa P25 TiO_2 showed about 83% degradation of AMX (pH: 6.0) after 2 h under solar radiation. Moosavi and Tavakoli[156] studied amoxicillin degradation in contaminated water using TiO_2 in solar photocatalysis, considering variations in pH, catalyst dose and initial concentration of amoxicillin. These studies showed 84.12% degradation of amoxicillin after 240 min under optimum conditions of pH 9.5, catalyst dose of 1.5 g L^{-1}

and initial concentration of amoxicillin of 17 mg L^{-1} under 240 min of solar irradiation due to a synergistic effect. In addition, several other studies have also been reported using TiO_2,[157–159] and supported TiO_2[160] on the photocatalytic remediation of amoxicillin.

3.2.1.2 ZnO and other metal oxides. The effect of operating variables has been studied on the degradation of amoxicillin (104 mg L^{-1}) in aqueous solution driven by a UV/ZnO photocatalyst prepared by a microwave-assisted gel combustion method, which achieved complete degradation corresponding to a zinc oxide concentration of 0.5 g L^{-1}, irradiation time of 180 min and pH 11.[161] The photocatalytic reactions followed pseudo-first-order kinetics with a rate constant of 0.018 min^{-1}. In another study, the photocatalytic removal of amoxicillin (and sulfamethoxazole) was achieved in 6 h from aqueous solutions using ZnO nanoparticles irradiated with UVC irradiation.[162] Al-zobai *et al.*[163] reported the recovery of 72.3%, 85.3%, and 100% of amoxicillin under optimum conditions using UV/TiO_2, UV/ZnO/TiO_2 and UV/ZnO.[163] Bi_2O_3/Fe (3 wt%), successfully synthesized by a microwave-assisted precipitation method, exhibited a degradation efficiency of 76.34% and a degradation rate for amoxicillin of 0.0079 min^{-1}.[164]

The effect of AMX concentration, WO_3 dosage, and pH was studied for the photocatalytic degradation of amoxicillin by solar-driven simulated irradiation.[165] These findings revealed the complete removal of AMX under optimal conditions corresponding to an initial AMX concentration of 1.0 μM, catalyst dosage of 0.104 g L^{-1} and pH 4. Sol–gel-synthesized nano-NiO under optimal conditions efficiently degraded 96% of amoxicillin from pharmaceutical wastewater.[166] The photodegradation process was found to follow pseudo-first-order kinetics (k: 0.084 min^{-1}) for an amoxicillin concentration of 25 mg L^{-1}.

3.2.2 Doped metal oxides. According to Klauson *et al.*,[155] TiO_2 doped with C (32 at%) and Fe (2.2 at%) under identical conditions of solar radiation in 2 h of treatment and pH 6.0 TiO_2 showed about 83%, 73% and 75% degradation of amoxicillin, respectively. Mohammadi *et al.*[167] used Sn (1.5 mol%) doped/TiO_2 nanoparticles to carry out the photocatalytic decomposition of amoxicillin trihydrate in aqueous solutions under UV light. It showed high photocatalytic activity during the mineralization of AMX due to hydroxyl radicals and band gap energy. Sol–gel-synthesized Sn,Zn-co-doped TiO_2 showed marked improvement in the photocatalytic degradation of amoxicillin trihydrate due to the synergistic actions of the dopants.[168] According to Wahyuni *et al.*,[169] doping of Cu in TiO_2 shifts the light absorption into the visible region. Furthermore, doping of Cu in TiO_2 increased the degradation of amoxicillin under visible light. Amoxicillin (10 mg L^{-1}) exhibited about 90% photodegradation using 0.40 g L^{-1} of a Cu (4.56 mg g^{-1}) doped TiO_2 photocatalyst in 24 h at pH 6 under visible-light irradiation. In another study, the removal of amoxicillin from aquatic and pharmaceutical wastewater solution was studied using Fe^{3+}-doped TiO_2 under UVA radiation.[170] These findings revealed removal efficiencies of 99.14% and 88.92% under the optimum conditions (pH: 11, initial concertation of amoxicillin: 10 mg L^{-1}, catalyst: 90 mg L^{-1}, contact time: 120 min) for synthetic and pharmaceutical water, respectively.

A Ce^{3+}-doped TiO_2 thin film, prepared using polyethylene glycol as the templating agent, acting as a catalyst succeeded in the removal of amoxicillin under UVA radiation from aqueous solution (pH 6.0).[171] It was noted that the removal of amoxicillin increased from 28% to 67% (2 h) in the presence of Ce^{3+}@TiO_2, corresponding to a decrease in the initial concentration of amoxicillin from 15.0 to 0.5 mg L^{-1}, respectively. The Ce^{3+}@TiO_2 thin film retained its photocatalytic stability more or less unaltered even after 6 cycles. It was suggested that cerium ions trapped the electron and hole pairs in the TiO_2 catalyst to form hydroxyl and peroxy radicals that play a significant role in the degradation of amoxicillin. Mn-doped Cu_2O nanoparticles synthesized using aloe vera leaf extract exhibited 92% degradation of amoxicillin under sunlight irradiation at pH 9, an initial concentration of amoxicillin of 15 mg L^{-1}, and a photocatalyst dosage of 1 g L^{-1}.[172] In all likelihood, Mn doping in Cu_2O delays rapid recombination by trapping the photogenerated electrons, accounting for its enhanced photocatalytic performance in amoxicillin degradation.

3.2.3 Metal dispersed on metal oxides. The photocatalytic degradation of amoxicillin antibiotic was investigated in the presence of La and Ce nanoparticles as co-catalysts dispersed on the surface of TiO_2.[173] These findings showed it had more than twice the activity of pure TiO_2 in the removal of amoxicillin, which was attributed to the synergistic interaction between La and Ce nanoparticles loaded on TiO_2. However, more work still needs to be carried out to explore the effect of different metals on the surface of TiO_2 and ZnO for the photodegradation of antibiotics. UV-visible or visible illuminated TiO_2 nanowire arrays (TNAs), TiO_2 nanowires (TNWs)/TNAs, Au–TNAs and Au–TNWs/TNAs degraded amoxicillin completely in aqueous solution within 20 min due to the surface plasmonic effect and synergistic effects.[174] The photodegradation of amoxicillin (and levofloxacin) was performed using an Ag/ZnO photocatalyst in aqueous solution under A-type ultraviolet irradiation (UVA 365 nm) to study its variation with solution pH, initial concentration of amoxicillin, catalyst dosage, and reaction time.[175] According to this, maximum removal (93.7%) of amoxicillin was achieved under optimum conditions corresponding to Ag/ZnO concentration of 0.15 g L^{-1}, pH 5, amoxicillin concentration of 5 mg L^{-1} and contact time of 120 min.

3.2.4 Metal oxide nanocomposites

3.2.4.1 TiO_2 nanocomposites. Bergamonti *et al.*[176] studied the photocatalytic activity of TiO_2 immobilized on a chitosan scaffold under UV/vis irradiation to examine the degradation of amoxicillin in wastewater under UV-vis irradiation. These findings showed high photodegradation efficiency compared to the direct photolysis of amoxicillin. A TiO_2/PAC (powdered activated carbon) mixture in suspension removed 95%

amoxicillin in 60 min owing to significant synergy.[177] TiO_2/zeolite-photocatalysis also presented a feasible methodology for the degradation of the AMX under UV radiation.[178] It was noted that a material obtained by acid–alkaline pretreatment and calcination (300 °C) showed the best performance due to its favorable surface structure and TiO_2 content.

Pastrana-Martínez and others[179] prepared nanodiamond (ND) composites of pristine TiO_2 (NDDT) to study its oxidative degradation of amoxicillin soluble in water under near-UV/vis irradiation. Their findings clearly revealed the complete degradation of amoxicillin by NDDT, owing to the generation of holes and better charge separation. In addition, specific surface area, functional groups introduced in ND and the porosity of NDDT compared to bare TiO_2 also play an important role in the photocatalytic degradation efficiency of amoxicillin. Li and coworkers[180] investigated the effect of Fe_3O_4 loading in TiO_2–Fe_3O_4 composites, H_2O_2 concentration, different initial pH and light intensity on the degradation of amoxicillin. The separation showed the following trend towards the degradation of amoxicillin in 100 min under optimum conditions (amoxicillin: 30 mg L^{-1}, UV irradiation: 200 W, [H_2O_2]: 4.24 mM, pH: 2.84): TiO_2/15 wt% Fe_3O_4 + H_2O_2 > TiO_2/20 wt% Fe_3O_4 + H_2O_2 > TiO_2/25 wt% Fe_3O_4 + H_2O_2 TiO_2/10 wt% Fe_3O_4 + H_2O_2 > TiO_2 + H_2O_2. It was noted that the presence of H_2O_2 contributed to oxidation in a photo-Fenton process while the choice of the optimum pH of 2.84 is guided by the scrambling of Fe^{3+} between OH and H_2O_2. Furthermore, the reaction rate below 200 W increased remarkably with increasing light intensity due to the generation of electrons and holes. As a consequence, maximum AMX removal efficiency (~88% in 100 min) was achieved for 0.4 g L^{-1} of TiO_2/15 wt% Fe_3O_4/H_2O_2 (6 mM) under optimum conditions corresponding to an initial concentration of amoxicillin of 30 mg L^{-1} and catalyst loading of 0.4 g L^{-1}. The highest performance for amoxicillin in the presence of TiO_2/15 wt% Fe_3O_4 could be ascribed to the generation of more active ·OH. The proposed mechanism involved the rapid transfer of excited electrons from TiO_2 to Fe_3O_4, reducing h^+/e^- pair recombination and providing an additional ·OH generation pathway for amoxicillin degradation.

dela Rosa *et al.*[181] studied the degradation and kinetic profiles of amoxicillin using solar/TiO_2/Fe_2O_3/persulfate and the corresponding findings are displayed in Fig. 8(A) and (B), respectively. It was observed that AMX degradation was reduced from 70% (no scavengers) to 39%, 54% and 64% (50 min) in the presence of methanol (MeOH), *tert*-butanol (*t*-BuOH) and 1,4-benzoquinone, respectively. Based on the overall findings, arrangements of reactive oxygen species (ROS) for AMX degradation by a solar/TiO_2–Fe_2O_3/PS process follows the order: $h^+ > SO_4\cdot^- > HO\cdot > O_2\cdot^-$. The overall amoxicillin degradation can be accounted for by considering the suppression of recombination of charges by the presence of PS as well as the generation of ROS at h^+.

TiO_2 immobilized on activated carbon fabricated by a high-temperature impregnation method degraded amoxicillin, diclofenac and paracetamol by 100% (120 min), 85% (180 min) and 70% (180 min) in aqueous solution under solar irradiation.[182] Li *et al.*[183] reported the photocatalytic degradation of amoxicillin using TiO_2 nanoparticles submerged on a porous ceramic membrane. TiO_2 immobilized on sand has been used as a catalyst in a solar photocatalytic process for the removal of amoxicillin residues from aqueous solution.[184] These findings showed 93.12% degradation of amoxicillin under the optimal conditions of pH 5, 7 5 mg L^{-1} of TiO_2, 400 mg L^{-1} of H_2O_2, and 10 mg L^{-1} of AMX concentration at 150 min irradiation time. Furthermore, the removal of undesirable compounds follows a pseudo-second-order kinetic model. In addition, TiO_2/Mg–Al-layered double hydroxide (LDH),[185] Ag-ion-exchanged zeolite/TiO_2,[186] Fe-8-hydroxyquinoline-7-carboxylic/TiO_2 flowers[187] and TiO_2–SiO_2[188] composites have also been used to remove amoxicillin from aqueous solutions.

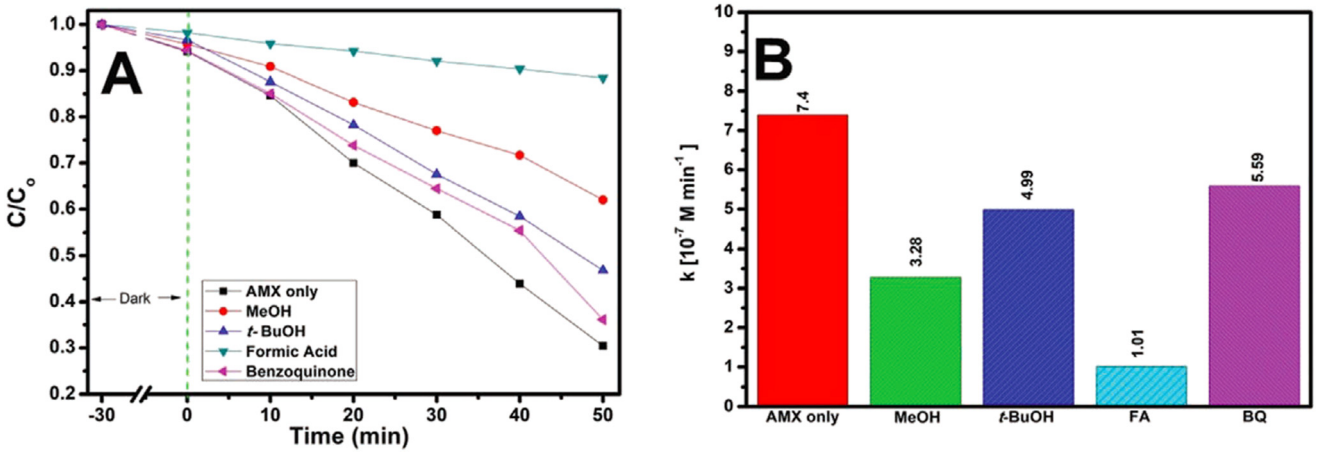

Fig. 8 (A) Photocatalytic degradation of AMX under solar irradiation in the presence of scavengers; and (B) corresponding zero-order rate constants (k_{obs}) (experimental conditions: [AMX] = 50 μm; initial pH = 4; [PS] = 334 μm, treatment time, t = 50 min). Reproduced from ref. 181 with permission from Wiley (2021).

3.2.4.2 ZnO-based nanocomposites. Thi *et al.*[189] observed the enhanced photocatalytic activity of ZnO–TiO_2 (10%) for the ozonation and perozone degradation of amoxicillin in water under visible-light irradiation. The visible-light-driven MIL-53(Al)/ZnO hierarchical photocatalyst produced 100% removal of amoxicillin corresponding to an initial amoxicillin concentration of 10 mg L^{-1}, solution pH 4.5 and catalyst dose of 1.0 g L^{-1}.[190] Recently, Liu and others[191] reported significantly high degradation efficiency of amoxicillin (93.10%) in wastewater using Bi_2WO_6/nano-ZnO (1 : 3) after 120 min in comparison to ZnO and Bi_2WO_6. It is anticipated that the reduction in band gap energy of Bi_2WO_6/nano-ZnO (1 : 3) could prevent the recombination of photogenerated charge carriers.

3.2.5 Graphitic-carbon-based nanocomposites

3.2.5.1 g-C_3N_4-based nanocomposites. Carbon-rich g-C_3N_4 nanosheet samples were prepared by a combination of 20 g of urea and 60 mg, 90 mg and 120 mg of 1,3,5-cyclohexanetriol as starting materials (referred to as C-CN60, C-CN90 and C-CN120, respectively).[192] They included plenty of carbon-rich functionalities and were examined for their photocatalytic activity for amoxicillin degradation under solar and visible light in the aqueous phase and the results are displayed in Fig. 9. The degradation of amoxicillin was found to follow the order: C-CN90 > C-CN60 > C-CN120 > g-C_3N_4. Photocatalyst C-CN90 showed nearly complete photocatalytic degradation of amoxicillin under solar light and visible light after 150 and 300 minutes, respectively. This has been attributed to the interaction between g-C_3N_4 and graphited conjugated construction narrowing the band gap and separating photogenerated electron–hole pairs.

Silva *et al.*[193] synthesized metal-free polymeric carbon nitrides using melamine (CN-M), thiourea (CN-T) and their 1 : 1 mixture (CN-1M : 1T) as precursors in a Teflon reactor comprising 25 mL of deionized water followed by heating of the products at 550 °C for 30 min. Their investigations revealed 100% degradation of AMX for CN-T followed by CN-M (65%) and CN-1M : 1T (56%) after 48 h of visible-light exposure. The superior performance of CN-T was found to be directly related to the greater number of defects present in its structure, that can help in the separation of electron–hole pairs. An Ag/g-C_3N_4/ZnO nanorod (0.08 g L^{-1}) nanocomposite has also acted as an efficient photocatalyst in the photocatalytic degradation of amoxicillin of high concentration (40 mg L^{-1}) irradiated by visible light.[194] V_2O_5-nanodot-decorated laminar C_3N_4 degraded amoxicillin under solar light, exhibiting 91.3% removal efficiency.[195] It is suggested that such a V_2O_5/C_3N_4 S-scheme structure provides an internal electron channel at the interface and maintains the active sites with high potentials for the photodegradation of amoxicillin. Mesoporous g-C_3N_4/persulfate exhibited 99% degradation of AMX under visible-light irradiation within 60 min at pH 7 due to a synergistic effect.[196] Graphitic-carbon–CuO–ZnO nanocomposites exhibited 49% efficiency in the photocatalytic degradation of amoxicillin under direct sunlight and followed pseudo-first-order kinetics.[197] α-Fe_2O_3/g-C_3N_4,[198] mesoporous g-C_3N_4,[199] and CQDs/$K_2Ti_6O_{13}$[200] photocatalysts have also been reported in the photocatalytic degradation of amoxicillin.

3.2.5.2 Graphene-based nanocomposites. Changotra *et al.*[201] prepared nanocomposites of varying FeS_2 to GO weight to study the degradation of amoxicillin as a function of different parameters, such as solution pH value, optimal doses of H_2O_2 and catalyst, stability of the catalyst, and leaching effect of the catalyst, under optimal solar-Fenton treatment. These investigations showed the complete degradation of amoxicillin (~99%) by FeS_2/GO (4 : 3) in 180 min owing to the synergistic coupling of FeS_2 and GO under the optimal conditions of $[amoxicillin]_{init\ conc}$ 25 mg L^{-1}, [FeS/GO] 0.75 g L^{-1}, 12 mM [H_2O_2] and pH 5. Further, HO· acted as dominant reactive species and no toxic secondary products were produced in the amoxicillin degradation. The photocatalytic degradation efficiency for amoxicillin by TiO_2 nanoparticles loaded on graphene oxide under UV light was found to be >99% at pH 6, catalyst dose of 0.4 g L^{-1}, amoxicillin concentration of 50 mg L^{-1} and intensity of 36 W (Fig. 10(a–d)).[202]

According to Song and others,[203] $KBrO_3$ added to graphene–TiO_2 nanotubes achieved 100% photodegradation of amoxicillin under UVA-light irradiation. It is suggested that $KBrO_3$ prevents electron–hole recombination and has a direct role as an oxidant in the degradation of amoxicillin. A

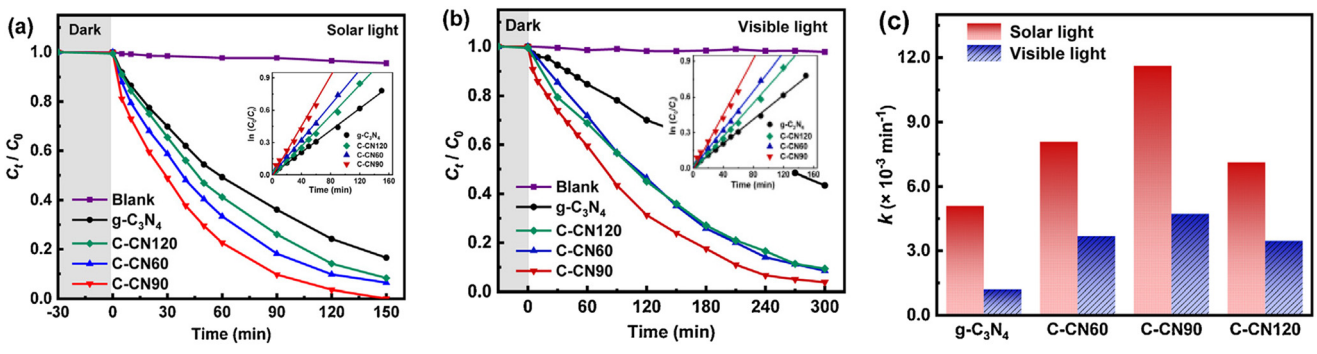

Fig. 9 Photocatalytic degradation kinetics of AMX by the synthesized materials under (a) simulated solar light, (b) visible light, and (c) AMX degradation rate constants under solar and visible light. Reproduced from ref. 192 with permission from Elsevier (2021).

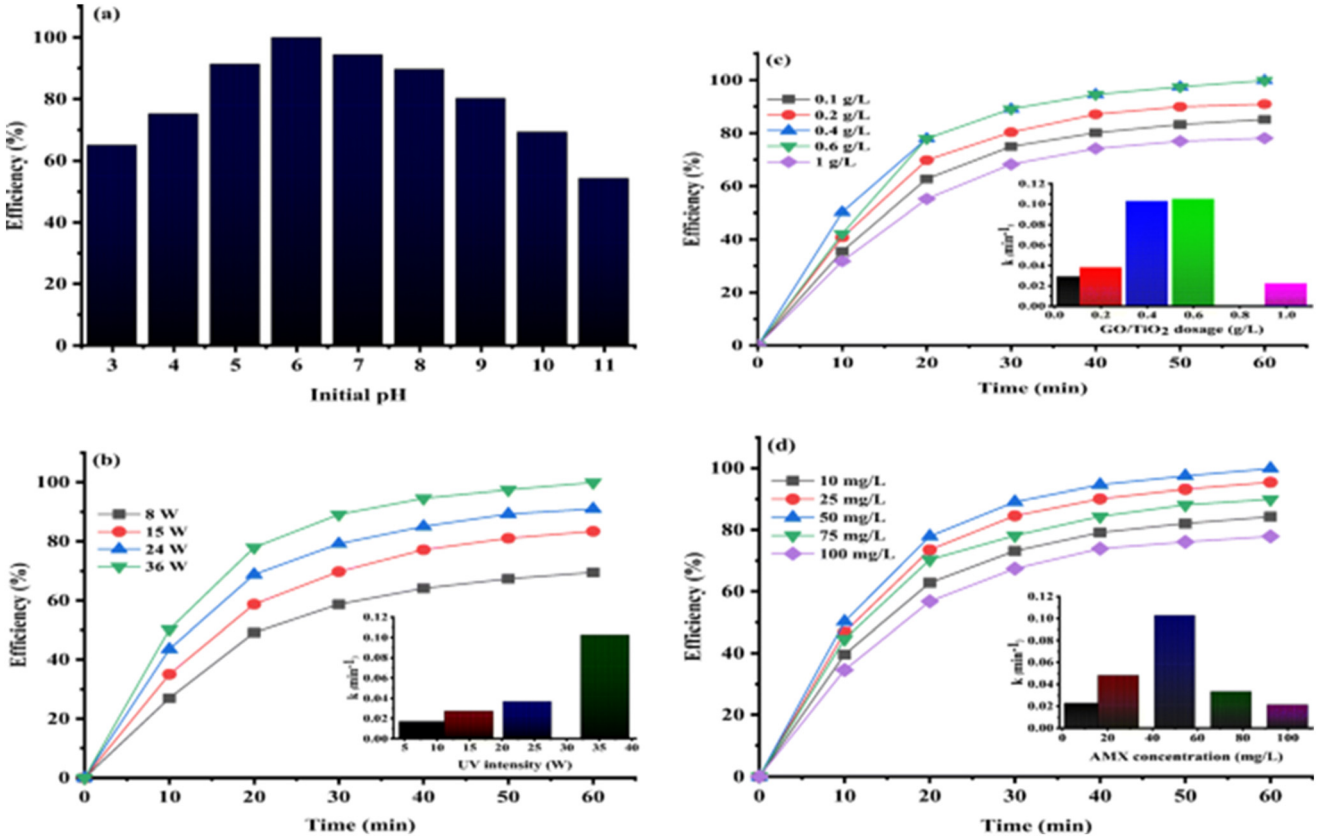

Fig. 10 The effect of different operational factors on AMX photocatalytic degradation and kinetic constant (a–d). Reproduced from ref. 202 with permission from Springer (2021).

visible-light-driven MIL-68(In)–NH_2/graphene oxide (GO) composite photocatalyst (0.6 g L^{-1}) exhibited 93% degradation (120 min) of amoxicillin in aqueous solution of pH 5 compared to pure MIL-68(In)–NH_2.[204] It is suggested that MIL-68(In)–NH_2/GO acted as an electron transporter for suppressing photogenerated carrier recombination and also acted as a sensitizer for enhancing visible-light absorption. The proposed mechanism suggested that h^+ and $\cdot O_2^-$ are active species. In another study, a 2D/3D g-C_3N_4/$BiVO_4$ hybrid photocatalyst decorated with rGO (1.2 wt%) degraded amoxicillin by 91.9% under optimized conditions with visible-light illumination.[205]

3.2.6 Heterostructures, heterojunctions and Z-scheme-based photocatalysts. Thuan *et al.*[206] compared the superior performance of an $InVO_4$@Ag@g-C_3N_4 ternary heterojunction in the photocatalytic degradation of amoxicillin in an aqueous environment at an initial AMX concentration of 10 ppm and catalyst dose of 0.5 g L^{-1} under visible light for 420 min: $InVO_4$@Ag@g-C_3N_4 (~99%) > $InVO_4$@Ag@g-C_3N_4 (~80%) > $InVO_4$@ (~43%) > g-C_3N_4 (~37%). The choice of Ag in this work is mainly guided by its two-fold contribution in the $InVO_4$@Ag@g-C_3N_4 ternary heterojunction. It accounts for the enhanced electron–hole separation of both g-C_3N_4 and $InVO_4$ components. In addition, silver also acts as an electron mediator to improve electron transfer from the $InVO_4$ conduction band to the g-C_3N_4 valence band. A CuI/$FePO_4$ p–n heterojunction nanocomposite showed photodegradation efficiency of 90% for the elimination of amoxicillin under simulated sunlight radiation.[207] A mesoporous SnO_2/g-C_3N_4 nanocomposite exhibited degradation to the extent of 92.1% against amoxicillin and 90.8% for pharmaceutical effluent in 80 min.[208] Such excellent performance is ascribed to the presence of a heterojunction, effective separation, good band structure and good light absorption.

El-Fawal *et al.*[209] observed the better performance of an $AgFeO_2$–graphene/Cu_2(BTC)$_3$ MOF heterojunction compared to $AgFeO_2$/graphene and $AgFeO_2$/Cu_2(BTC)$_3$ binary photocatalysts in achieving about 97% removal of amoxicillin and diclofenac after 150 min under sunlight irradiation, which exhibited excellent stability up to four cycles. Based on these findings, a direct Z-scheme heterojunction mechanism has been proposed for the separation of photo-induced charge carriers at the interface of these photocatalysts. The enhanced photocatalytic activity of the tertiary heterojunction photocatalyst was mainly attributed to its superiority for light absorption (up to 650 nm) with high photostability, accelerated e^-/h^+ pair separation and increased lifetime of photogenerated charges. The heterojunction p-ZnO/CuO (50 : 50 wt%) assisted photocatalytic process removed amoxicillin (initial concentration: 50 mg L^{-1}) from water (pH: 11) almost completely on exposure to solar irradiation for 4 h.[210] The

degradation of amoxicillin followed pseudo-first-order kinetics (k: 9.95×10^{-3} min^{-1}).

Gao *et al.*[211] deposited Ag nanoparticles on the surface of a TiO_2/mesoporous g-C_3N_4 heterojunction and used it in the photocatalytic removal of amoxicillin under visible light. A photocatalyst fabricated in this manner achieved higher degradation efficiency for amoxicillin than a TiO_2/mesoporous-g-C_3N_4 heterojunction, mesoporous-C_3N_4, or bulk-g-C_3N_4. Such photoactivity of an Ag/TiO_2/M–g-C_3N_4 catalyst has been assigned to the synergistic effect accounting for the effective transfer of electrons and inhibition of electron–hole recombination. The effectiveness of this photocatalyst was also tested for the removal of amoxicillin in real situations. A WO_3/Ag_3VO_4 Z-scheme heterojunction with enhanced separation efficiency of electron–hole and surface area was deposited on rGO and used as a photocatalyst in the degradation of amoxicillin under irradiation by visible light.[212] The amoxicillin photocatalytic degradation followed the following order on irradiating it with visible light: Ag_3VO_4/WO_3/r-GO (~96%) > Ag_3VO_4/WO_3 (~37%) > WO_3 > Ag_3VO_4 (~32%). It is suggested that the presence of rGO, by increasing the surface area in Ag_3VO_4/WO_3/rGO, facilitates amoxicillin adsorption and electron transfer for charge separation of Ag_3VO_4/WO_3.

Investigations have also been made on the photodegradation of amoxicillin *via* a magnetic TiO_2–graphene oxide–Fe_3O_4 composite[213] and Pd nanoparticles anchored to anatase TiO_2.[214] Hajipour *et al.*[215] fabricated heterojunctions of TiO_2/CuO, adopting the surface modification of TiO_2 with CuO, and investigated its application in the photocatalytic degradation of amoxicillin in wastewater. It should be noted that TiO_2/CuO (7.5%) showed reduced photo-activity compared to a TiO_2/CuO (10%) photocatalyst, which could be attributed to the partial blockage of the active sites in the TiO_2 nanoparticles, In another study, a novel nanophotocatalyst of CuO nanoparticles and ZnO nanorods anchored on thermally-exfoliated g-C_3N_4 nanosheets established the complete removal of amoxicillin corresponding to a catalytic dosage of 0.9 g L^{-1} and pH 7.0 within 120 min under simulated sunlight illumination.[216] Subsequently, a double Z-scheme mechanism as well as a tentative pathway were proposed in detail.

Table 3 records the performance data of different photocatalysts on the removal of amoxicillin from wastewater.

3.3 Sulfamethoxazole

Sulfamethoxazole is used to treat a wide variety of bacterial infections, including those of the urinary, respiratory, and gastrointestinal tracts.[217] However, it has been frequently detected in wastewater and surface water in aquatic environments due to its extensive consumption, excretion and disposal. Therefore, several investigations have been made by many researchers focusing on the biodegradation of sulfamethoxazole during wastewater treatment following photocatalytic degradation of sulfamethoxazole in water using a variety of photocatalysts.[218–291]

3.3.1 Metal oxides

3.3.1.1 TiO_2. The photodegradation of sulfonamides has been studied in the UV/TiO_2 system to study the effects of pH and salinity on sulfamethoxazole concentration and total organic carbon (TOC) during the removal of sulfonamides in a UV/TiO_2 system.[219] The photodegradation and mineralization rates of sulfonamides in the UV/TiO_2 system satisfied pseudo-first-order kinetics. A TiO_2 suspension has been used as a catalyst in a sunset solar simulator to examine the degradation of sulfamethoxazole in real municipal wastewater treatment plant effluent.[220] It was inferred that hydrogen peroxide can be highly recommended for working with TiO_2 at low concentrations. The photocatalytic degradation of sulfamethoxazole in surface and drinking water in the absence and presence of UV (265 nm) involving TiO_2 nanoparticles after 60 minutes follow the order: UV (~100%) > anatase TiO_2 (~92%) > rutile and commercial TiO_2 (~90%).[221] The effects of different UV-LED (UVA, UVB, and UVC) wavelengths were studied in carrying out the photocatalytic decomposition of sulfamethoxazole by TiO_2.[222] These findings showed complete decomposition within 1 h by TiO_2/UVC under the conditions of TiO_2: 0.5 g L^{-1}, natural pH, and initial concentration of sulfamethoxazole: 20 mg L^{-1}. Sulfamethoxazole in an aqueous suspension of TiO_2 (0.5 g L^{-1}) showed 82% degradation of sulfamethoxazole under UV irradiation.[223] In another study, the removal efficiency for the photocatalytic degradation of sulfamethoxazole (20 mg L^{-1}) in aqueous solution (pH: 3) by TiO_2 (0.08 g L^{-1}) as a photocatalyst was found to be 96.5% in 60 min under UV light.[224] In addition, investigations have also been reported on the degradation of sulfamethoxazole using TiO_2,[225–227] biochar-supported TiO_2[228] and immobilized TiO_2[229–231] as photocatalysts.

3.3.1.2 ZnO. ZnO nanoparticles prepared by a microwave-assisted gel combustion synthesis method showed complete removal of amoxicillin (and sulfamethoxazole) from contaminated water in six hours under UVC irradiation.[162] It was inferred that the photocatalytic removal followed the Langmuir–Hinshelwood model in the range of concentration of 5–20 mg L^{-1}. Mirzaei *et al.*[232] achieved ~97% removal of sulfamethoxazole by a zinc oxide photocatalyst in the presence of fluoride ions (F–ZnO) after 30 min of reaction illuminated by UV irradiation under optimum conditions and followed pseudo-first-order kinetics (k: 0.099 min^{-1}). The hydrothermally synthesized ZnO at 200 °C for 8 h at pH 7.5 reached 84% removal of sulfamethoxazole after 60 min under UVA irradiation.[233] In addition, TiO_2 and WO_3 nanoparticles have also been utilized in the removal of sulfamethoxazole by its photocatalytic degradation.[234]

3.3.2 Metal-modified metal oxide and mixed metal oxides. Tiwari *et al.*[235] studied the removal of sulfamethoxazole aqueous solutions by means of Ag^0(NP)/TiO_2 thin film irradiated under UVA light (λ_{max}: 330 nm) for 2 h by varying

Table 3 The performance data on removal of amoxicillin in water using variety of photocatalysts

Photocatalyst	Method of preparation	AMX	Catalyst dose	pH	Light source details	Degradation (time)	Rate constant
TiO_2 nanoparticles (US3490)[150]	Commercial	15 mg L^{-1}	2 g L^{-1}	5	UV lamp (18 W)	27.6% (15 min)	—
ZnO nanoparticles (US3590)[150]	Commercial	15 mg L^{-1}	2 g L^{-1}	5	UV lamp (18 W)	48.6% (15 min)	—
GO–Fe_3O_4[150]	Ultrasonic mixing followed by reflexing	15 mg L^{-1}	2 g L^{-1}	—	Lamp (UV): 1 8 W	87.1% (15 min)	—
TiO_2 (P25 Degussa)[152]	Commercial	10 mg L^{-1} (20 mL)	0.01 g	—	UV	100% (15 min)	4.33 × 10^{-1} min^{-1}
TiO_2 (P25 Degussa)[152]	Commercial	10 mg L^{-1} (20 mL)	0.01 g	—	Visible	99% (15 min)	—
ZnO (Hoechst)[152]	Commercial	10 mg L^{-1} (20 mL)	0.01 g	—	UV	98% (15 min)	3.03 × 10^{-1} min^{-1}
ZnO (Hoechst)[152]	Commercial	10 mg L^{-1} (20 mL)	0.01 g	—	Visible	99% (15 min)	—
TiO_2 (Fluka)[153]	Commercial	104 mg L^{-1} (500 mL)	1.0 g L^{-1}	11	UV lamp: 6 W (365 nm)	~71% (300 min)	0.007 min^{-1}
TiO_2 (H_2O_2: 100 m L^{-1})[153]	Commercial	104 mg L^{-1} (500 mL)	1.0 g L^{-1}	5	UV lamp: 6 W (365 nm)	100% (20 min)	—
TiO_2 (P25 Degussa)[154]	Commercial	0.01 g	10 mg L^{-1} (20 mL)	—	UV lamp	100% (30 min)	0.433 min^{-1}
TiO_2 (Degussa P25)[155]	Commercial	25 mg L^{-1}	1 g L^{-1}, slurry	6	Solar light (16 mW cm^{-2})	~83% (120 min)	—
Carbon (32%) doped TiO_2 (Degussa P25)[155]	Commercial	25 mg L^{-1}	1 g L^{-1}, slurry	6	Solar light (16 mW cm^{-2})	~73% (120 min)	—
Fe (2.2%) doped TiO_2 (Degussa P25)[155]	Commercial	25 mg L^{-1}	1 g L^{-1}, slurry	6	Solar light (16 mW cm^{-2})	~75% (120 min)	—
TiO_2 (sigma Aldrich)[156]	Commercial	1.5 g L^{-1}	17 mg L^{-1}	9.5	Solar irradiation	84.12% (240 min)	—
ZnO[162]	Microwave assisted gel combustion method	10 mg L^{-1} (200 mL)	0.25 g L^{-1}	10	UVC lamp (30 W)	100% (5 h)	0.014 min^{-1}
WO_3 (sigma Aldrich)[165]	Commercial	1.0 μM	0.104 g L^{-1}	4	Xenon lamp (300 W)	99.99% (180 min)	2.908 × 10^{-2} min^{-1}
NiO[166]	Sol–gel method	25 mg L^{-1}	0.2 g L^{-1}	—	Low mercury lamp (15 W)	~96% (120 min)	0.084 min^{-1}
Cu (4.54 mg g^{-1}) doped TiO_2[169]	Photoreduction method	10 mg L^{-1}	40 mg	6	Wolfram lamp as visible light source	~90% (24 h)	4 × 10^{-4} min^{-1}
Fe^{3+} doped TiO_2[170]	Sol–gel method	10 mg L^{-1}	90 mg L^{-1}	11	UV lamp of C type, 125 W, 247 nm	Synthetic water: 99.14% (120 min), pharmaceutical water: 88.92% (120 min)	—
Mn-doped Cu_2O[172]	Green synthesis	15 mg L^{-1} (100 mL)	1 g L^{-1}	9	Sunlight irradiation (900 W m^{-2})	92% (180 min)	0.073 min^{-1}
La–Ce (1 wt%) TiO_2[173]	Sonochemical-assisted synthesis	10 mg L^{-1} (100 mL)	Appropriate amount	—	Halogen lamp (500 W)	75.7% (?)	—
Ag/ZnO[175]	Conventional method	5 mg L^{-1}	0.15 g L^{-1}	5	UVA, 365 nm	93.76% (120 min)	0.073 min^{-1}
TiO_2/chitosan[176]	3D printing	0.1 mM (40 mL)	15 layers (AMX/TiO_2 molar ratio: 1/100)	6.7	Medium-pressure Hg vapour water jacket lamp (UV-vis), 125 W, 300–800 nm, 3.5 mW cm^{-2}	~95% (2 h)	0.57 × 10^{-2} min^{-1}
TiO_2/PAC[177]	Suspension method	15 mg L^{-1}	TiO_2: 1 g L^{-1}, PAC: 0.1 g L^{-1}	6.5	UV-vis (540 W m^{-2})	90–97% (60 min)	0.034 min^{-1}
TiO_2/zeolite[178]	Modified reported method	30 mg L^{-1} (100 mL)	2 g L^{-1}	4.05	Medium-pressure Hg lamp (47 W) with $\lambda \leq 290$ nm cut-off	88% (240 min)	—
Functionalized nanodiamond-TiO_2[179]	Liquid phase deposition	0.1 mM (7.5 mL)	1 g L^{-1}	—	Medium-pressure hg vapor lamp	100% (60 min)	83.3 × 10^{-3} min^{-1}

Table 3 *(continued)*

Photocatalyst	Method of preparation	AMX	Catalyst dose	pH	Light source details	Degradation (time)	Rate constant
TiO_2-15 wt% Fe_3O_4[180]	Hydrothermal	30 mg L^{-1}, (H_2O_2: 24 mM)	0.4 g L^{-1}	2.84	Low-pressure mercury vapor lamp: 100 W, 1200 mW cm^{-2}	~88% (100 min)	—
TiO_2@α-Fe_2O_3 film (PS: 334 μm)[181]	Spin coating	50 μm	—	4	Xenon lamp (450 W)	70% (50 min)	7.4 × 10^{-7} M min^{-1}
TiO_2 immobilized on activated carbon[182]	High-temperature impregnation method	50 mg L^{-1} (4 L)	1.2 g L^{-1}	10	Solar irradiation	100% (120 min)	0.037 min^{-1}
TiO_2–sand[184]	Sol–gel dip-coating	10 mg L^{-1}, H_2O_2, 400 mg L^{-1}	75 mg L^{-1}	5	Solar irradiation	93.12% (150 min)	0.0175 min^{-1}
TiO_2/Mg–Fe-LDH[185]	Direct co-precipitation method	30 mg L^{-1}	2 g L^{-1}	11	UVA light (λ_{max}: 365 nm)	~100% (240 min)	—
TiO_2/Mg–Al-LDH[185]	Direct co-precipitation method	30 mg L^{-1}	2 g L^{-1}	5.5	UVA light (λ_{max}: 365 nm)	~95% (240 min)	—
Ag/zeolite/TiO_2[186]	Liquid ion-exchange method	One g L^{-1} (15 mL)	0.01 g	6.7	High-pressure Hg lamp (400 W), 120 mW cm^{-2}	~25% (75 min)	—
TiO_2(80%)–SiO_2(20%)[188]	Sol–gel method	20 mg L^{-1} (100 mL)	4 g L^{-1}	5	Hg lamp – UVA (15 W), 365 nm	88% (150 min)	0.0014 min^{-1}
MIL-53 (Al)/ZnO[190]	Hydrothermal/chemical conditions followed	10 mg L^{-1}	1.0 g L^{-1}	4.5	Metal halide lamp: 400 W, 510 nm	100% (60 min)	—
g-C_3N_4[193]	Heating of aq. Thiourea in Teflon reactor	30 mg	50 mg L^{-1} (10 mL)	pH ~ 6	Visible light: 150 W, 16 mW cm^{-2}	100% (48 h)	0.088 h^{-1}
Ag/g-C_3N_4/ZnO nanorods[194]	Dispersion method	40 mg L^{-1}	0.08 g L^{-1} (60 mL)	—	Solar simulator lamp: 300 W ($\lambda \geq 420$ nm)	41.36% (180 min)	0.01017 min^{-1}
V_2O_5/C_3N_4[195]	Heating powdered NH_4VO_3/g-C_3N_4 mixture	20 mg L^{-1}	0.5 g L^{-1}	7	Simulated sunlight	~91% (120 min)	0.0268 min^{-1}
α-Fe_2O_3 (5%)/g-C_3N_4[198]	Solution method	20 mg L^{-1}	0.02 g (60 mL)	Neutral	Solar simulator (300 W) with cut-off filter ($\lambda > 420$ nm)	46% (180 min)	40.20 × 10^{-4} min^{-1}
Mesoporous g-C_3N_4[199]	Template-free method	2 mg L^{-1}	100 g L^{-1} (100 mL)	9	Xenon lamp: 300 W ($\lambda > 420$ nm)	90% (60 min)	0.036 min^{-1}
CQDs modified $K_2Ti_6O_{13}$ nanotubes[200]	Hydrothermal method combined with calcination	1 mg L^{-1} (50 mL)	0.2 g L^{-1}	6	Light-emitting diode, 10 mW cm^{-2}, 365 nm	100% (90 min)	0.0495 min^{-1}
GO/TiO_2[202]	Chemical hydrothermal method	50 mg L^{-1} (100 mL)	0.4 g L^{-1}	6	UV light (36 W)	99.84% (60 min)	0.105 min^{-1}
Graphene@TiO_2 nanotube/$KBrO_3$ (0.20 g L^{-1})[203]	Reaction under autoclave	5 mg L^{-1}	—	—	Light: UVA lamp: 19 W, λ = 369 nm	96.94% (180 min)	0.0186 min^{-1}
MIL-68(In)–NH_2/GrO[204]	Dispersion method	20 ppm (200 mL)	0.6 g L^{-1}	5	Xenon lamp (300 W) with 420 nm cut-off filter	93% (120 min)	0.0187 min^{-1}
1.2 wt% rGO@g-C_3N_4/$BiVO_4$[205]	Wet impregnation method	10 mg L^{-1} (100 mL)	0.1 g (100 mL)	—	Halogen lamp (500 W)	91.9% (180 min)	0.0023 min^{-1}
$InVO_4$/Ag/g-C_3N_4[206]	Hydrothermal	10 ppm	0.5 g L^{-1}	—	Visible light (30 W bulb)	>99% (420 min)	—
CuI/$FePO_4$[207]	Reflux-assisted co-precipitation technique	20 mg L^{-1} (50 mL)	50 mg	—	Visible light (400 W)	90% (120 min)	—
Mesoporous SnO_2/g-C_3N_4[208]	Green modified technique	10 ppm (40 mL)	10 mg	—	Xenon lamp: 300 W with a cut-off filter ($\lambda > 400$ nm)	92.1% (80 min)	—
$AgFeO_2$–graphene/$Cu_2(BTC)_3$ MOF[209]	*In situ* solvothermal impregnation	5 mg L^{-1}	5 g L^{-1} (50 mL)	8	Halogen lamp 500 W, 420–600 nm	97% (150 min)	(6.4–8.7) × 10^{-2} min^{-1}
p-CuO/n-ZnO (50:50 wt%)[210]	Chemical route	50 mg L^{-1}	0.5 g L^{-1}	11	Sunlight (109 mW cm^{-2})	>87% (240 min)	9.95 × 10^{-3} min^{-1}
1.94 wt% Ag/TiO_2/mesoporous g-C_3N_4[211]	Photodeposition means	5 ppm (0.1 L)	0.1 g	—	Xe lamp: 300 W ($\lambda > 420$ nm)	99% (60 min)	0.0614 min^{-1}
WO_3/Ag_3VO_4/rGO[212]	Multiple steps	20 ppm	0.5 g L^{-1}	—	LED lamp (220 V, 30 W)	~96% (420 min)	—

Table 3 *(continued)*

Photocatalyst	Method of preparation	AMX	Catalyst dose	pH	Light source details	Degradation (time)	Rate constant
CuO and ZnO co-anchored on g-C_3N_4[216]	*Via* isoelectric point-mediated annealing	60 mg L^{-1}	0.9 g L^{-1}	7.0	Xenon lamp (250 W) simulated sunlight	100% (120 min)	0.0269 min^{-1}

the solution pH (4.0–8.0) with an initial sulfamethoxazole concentration of 1.0 mg L^{-1}. A decreasing trend in the removal (%) of sulfamethoxazole was noted from 59% to 50% with a variation in pH from 4 to 10. The percentage removal of sulfamethoxazole as a function of pollutant concentration of sulfamethoxazole (0.5 to 15.0 mg L^{-1}) at constant pH of 6.0 under 2 h of UVA light showed a decreasing trend in the degradation of sulfamethoxazole from 57% to 20% with the sulfamethoxazole concentration increasing from 0.5 mg L^{-1} to 15.0 mg L^{-1}. Borowska *et al.*[236] investigated the solar photocatalytic degradation of sulfamethoxazole as a contaminant in water by Pt- and Pd-modified TiO_2. Their findings established significantly enhanced absorption properties from surface modification achieved by 1%Pd/TiO_2 and 1%Pt/TiO_2. As a result, higher removal of sulfamethoxazole is observed compared to unmodified TiO_2 in aqueous solution corresponding to a concentration of catalyst of ~50 mg L^{-1} and a concentration of sulfamethoxazole of 1 mg L^{-1}. This could be explained on the basis of their band gaps (1%Pd/TiO_2: 2.92 eV, 1%Pt/TiO_2: 3.18 eV).

TiO_2 nanotube arrays (TNAs), TiO_2 nanowires on nanotube arrays (TNWs/TNAs), Au-nanoparticle-decorated TNAs, and TNWs/TNAs efficiently degraded sulfamethazine amoxicillin, ampicillin, doxycycline, oxytetracycline, lincomycin, vancomycin and sulfamethoxazole irradiated in water under UV-vis and visible light.[174] Among these, the Au–TNWs/TNAs photocatalyst showed the highest activity towards the degradation of all the antibiotics due to synergistic and surface plasmonic effects. In another study, Cu–TiO_2 (at low mass ratios of 0.016–0.063 wt%) produced nearly complete degradation of sulfamethoxazole by visible light at pH 5.2 for a 4 mg L^{-1} initial concentration of sulfamethoxazole.[237] Further studies revealed the highly stable photoactivity of Cu–TiO_2, as evident from experiments comprising at least 4 cycles. Au, Ag, Cu, Au–Ag and Au–Cu nanoparticles deposited on TiO_2 showed increased photocatalytic activity for the photocatalytic degradation of sulfamethoxazole using UVC light.[238]

3.3.3 Doped metal oxides. Tsiampalis *et al.*[239] used iron-doped TiO_2 (iron/titania ratios: 0–2%) as a photocatalyst to study the photocatalytic degradation of sulfamethoxazole under simulated solar radiation. These findings showed the highest photocatalytic efficiency (95%) for sulfamethoxazole in ultra-pure water with SMX concentration of 234 μg L^{-1}, catalyst loading of 1 g L^{-1} and natural pH. The initial activity of the photocatalyst also retained half of its initial value after 5 consecutive experiments. F,Pd-co-doped TiO_2 nanocomposites prepared by a microwave-assisted hydrothermal synthesis method under direct sunlight irradiation degraded ~94.4% and 98.8% of sulfamethoxazole at 20 and 70 min, respectively.[240] It was suggested that doping of TiO_2 by F and Pd involved multiple processes.

F,Pt-co-doped photocatalysts have also been employed in photocatalytic degradation using direct solar light.[241] Fluoride ions and Pt in the TiO_2 lattice were chosen in order to control the growth of the photocatalytically active anatase phase and to introduce new energy levels between the valence and conductive bands of TiO_2 to narrow its band gap. These findings demonstrated degradation of sulfamethoxazole under direct solar light and a solar simulator corresponding to about >93% (90 min) and 58% (360 min), respectively. An iodine (I)–potassium (K)–C_3N_4 photocatalyst removed nearly 100% of sulfamethoxazole within 45 min under visible-light irradiation.[242] N,Cu-co-doped TiO_2 decorated on SWCNTs demonstrated total removal of sulfamethoxazole under a pH of 6.0, catalyst dosage of 0.8 g L^{-1}, light intensity of 200 W, US power of 200 W, and initial sulfamethoxazole concentration of 60 mg L^{-1} in 60 min.[243]

Ag metal has been used as a co-dopant in P-doped g-C_3N_4 in order to overcome its poor photocatalytic performance.[244] The investigations of Ag (nano)–P-co-doped@g-C_3N_4 (Ag–P@UCN) as a photocatalyst in visible light followed the trend in the removal of sulfamethoxazole in water: Ag(nano)–P@g-C_3N_4 (>99%) > P-doped g-C_3N_4 (68%) > g-C_3N_4 (47%). The presence of silver nanoparticles Ag(nano)–P@g-C_3N_4 enhanced light absorption and also acted as photogenerated electron traps, thereby enabling the effective separation of electron and hole pairs. A mechanism has also been proposed for the degradation of sulfamethoxazole in presence of an Ag–P@UCN photocatalyst. In another study, multi-homojunction gradient-nitrogen-doped TiO_2 exhibited enhanced performance in the removal of sulfamethoxazole from water compared to pristine TiO_2 and non-gradient-doped TiO_2 under simulated solar-light irradiation.[245] Zammit *et al.*[246] examined the removal of sulfamethoxazole using a cerium-doped zinc oxide (Ce–ZnO) photocatalyst and its comparison with ZnO and benchmark TiO_2–P25 in immobilized form on a metallic support and found Ce–ZnO to be most effective under UVA irradiation. In another study,[247] Zn (10 wt%)–TiO_2/pBC (pretreated biochar) was investigated for the photodegradation of sulfamethoxazole under visible-light irradiation and a comparison with TiO_2/pBC and TiO_2 after 3 h took the following order: Zn–TiO_2/pBC (80.81%) > TiO_2/pBC (59.05%) > TiO_2 (50.07%).

3.3.4 Metal oxide–metal oxide based composites. Fernández *et al.*[248] focused on Fe_3O_4/ZnO nanocomposites on the photodegradation performance for sulfamethoxazole, trimethoprim, erythromycin and roxithromycin from surface water under UVA irradiation. Their studies showed complete removal of the antibiotics (100 mg L^{-1}) after 70 min under optimal conditions of pH 7, [H_2O_2] 100 mg L^{-1} and catalyst dose of 100 μg L^{-1}. In addition, a reusability evaluation of Fe_3O_4/ZnO after removing it by applying an external magnetic field showed no significant decrease in its performance even after 8 cycles. Investigations were also made on the solar photocatalytic removal of sulfamethoxazole and other micropollutants (carbamazepine, flumequine, ibuprofen) using TiO_2 and its comparison with TiO_2/Fe_3O_4 applied in a heterogeneous photo-Fenton process.[249] Magnetically separable Fe_2O_3/WO_3 nanocomposites were also successfully used as a peroxymonosulfate activator to efficiently degrade sulfamethoxazole under visible-light irradiation.[250] Wang and others[251] reported that photogenerated holes played an important role in achieving more than 99% photocatalytic degradation efficiency for sulfamethoxazole (initial solution pH: 3) in 30 min by irradiating a Bi_2O_3–TiO_2/PAC (powdered activated carbon) ternary composite with solar light.

A composite comprising titania nanoparticles/activated carbon prepared by calcination at 400 °C exhibited much better performance in the removal of sulfamethoxazole from deionized water and seawater.[252] Clay–TiO_2 nanocomposites prepared *via* biomass-assisted synthesis showed fast degradation of sulfamethoxazole (>90%) in 30 min under sunlight.[253] An LDH–TiO_2 (10%) nanocomposite has been developed, keeping in view its possible reusability and regeneration after subjection to UVA radiation, to carry out the degradation of sulfamethoxazole.[254] These findings established almost complete degradation after 360 min of UVA irradiation, corresponding to initial sulfamethoxazole concentration of 20 mg L^{-1}, pH 10 and LDH–TiO_2 catalyst loading of 50 mg. Recycling and reusability studies were also conducted by dissolving a mass of 50 mg of LDH–TiO_2 in sulfamethoxazole (concentration: 20 mg L^{-1}) and pH 10, irradiated for 8 h under UVA. Further investigations revealed no significant variation in sulfamethoxazole degradation efficiency from the first cycle (100%) to the fifth cycle (90.5%).

According to Długosz *et al.*,[255] a floating TiO_2-expanded perlite (referred to as EP-TiO_2-773: where 773 is the calcination temperature in °C) photocatalyst enhanced the photodegradation of sulfamethoxazole in the aqueous medium over a wide range of pH values on irradiation from the near-UV spectral region. However, the fastest decrease in the concentration of sulfamethoxazole was observed for the system irradiated at pH 10. The degradation of sulfamethoxazole followed pseudo-first-order kinetics in accordance with the Langmuir–Hinshelwood model. Their findings also suggested the key role of hydroxyl radical formation in the degradation of sulfamethoxazole. Noroozi *et al.*[256] synthesized copper doped TiO_2 decorated with carbon quantum dots (CQDs) and observed its excellent performance in the degradation of SMX during 60 minute time under optimum conditions corresponding to initial SMX concentration, catalyst dosage, pH, visible light intensity and CQDs ratio in the composites of 20 mg L^{-1}, 0.8 g L^{-1}, 6, 75 Wm^{-2} and 4 wt% respectively. The photocatalytic degradation of sulfamethoxazole was found to be guided by a pseudo-first-order kinetic model with HO· and $O_2{\cdot}^-$ as active species. Poly(ethylene terephthalate)–TiO_2,[257] $BiVO_4$/$SrTiO_3$,[258] CuO_x–$BiVO_4$[259] and TiO_2@$CuCo_2O_4$[260] were also used for the photocatalytic degradation of sulfamethoxazole.

3.3.5 Graphitic-materials-based composites

3.3.5.1 MWCNT-based composites. WO_3–MWCNT composites with different amounts of functionalized MWCNTs were prepared by a hydrothermal method (named WT-2, WT-4 and WT-8), and SMX degradation was studied under visible-light irradiation.[261] Fig. 11(a) shows the highest efficiency of 73.3% within 3 h for WT-8; however, WT-4 with efficiency of 65.2% was preferred due to its better dispersion in water. Further studies on SMX (10 mg L^{-1}) degradation at different catalyst dosages of WT-4 in Fig. 11(b) showed its maximum efficiency (88.5%) corresponding to a loading of 2.00 g L^{-1}. A possible degradation mechanism highlighting the role of O_2^- and OH· radicals during the photocatalytic process has also been proposed and is displayed in Fig. 11(c). Awfa *et al.*[262] reported ~60% photodegradation of sulfamethoxazole by magnetic carbon nanotube–TiO_2 composites. Martini *et al.*[263] observed almost complete reduction of toxicity using photocatalytic ozonation with H_2O_2 and Fe/CNT.

3.3.5.2 g-C_3N_4-based composites. An Ag (5%)/P–g-C_3N_4 composite synthesized by thermal polymerization combined with a photodeposition method completely degraded sulfamethoxazole within 20 min under visible-light irradiation.[264] This is attributed to the formation of holes and superoxide radicals acting as dominant active species. In addition, the surface plasmon resonance effect (Ag) and the formation of a Schottky barrier on the Ag/P–g-C_3N_4 interface could facilitate the enhanced generation of electrons/holes as well as accounting for the recombination of photogenerated electron–hole pairs. A magnetic ZnO@g-C_3N_4 composite under optimum conditions removed 90.4% of sulfamethoxazole after 60 min.[265] In addition, core–shell g-C_3N_4@ZnO,[266] peroxymonosulfate (PMS)/g-C_3N_4[267] and Ag/g-C_3N_4[268] have also been reported in the photocatalytic degradation of sulfamethoxazole.

3.3.5.3 Graphene-based composites. Visible-light-derived rGO–WO_3 composites showed 98% removal of sulfamethoxazole within 3 hours.[269] In another study, Ag@Ag_2O–graphene nanocomposites comprising variable graphene concentrations (1.7, 2.5, and 3.4 wt%) were prepared to study the degradation of sulfamethoxazole under simulated solar light (λ > 280 nm) and visible-light irradiation (λ > 400 nm), including the stability of the photocatalyst and the mechanism of photocatalytic

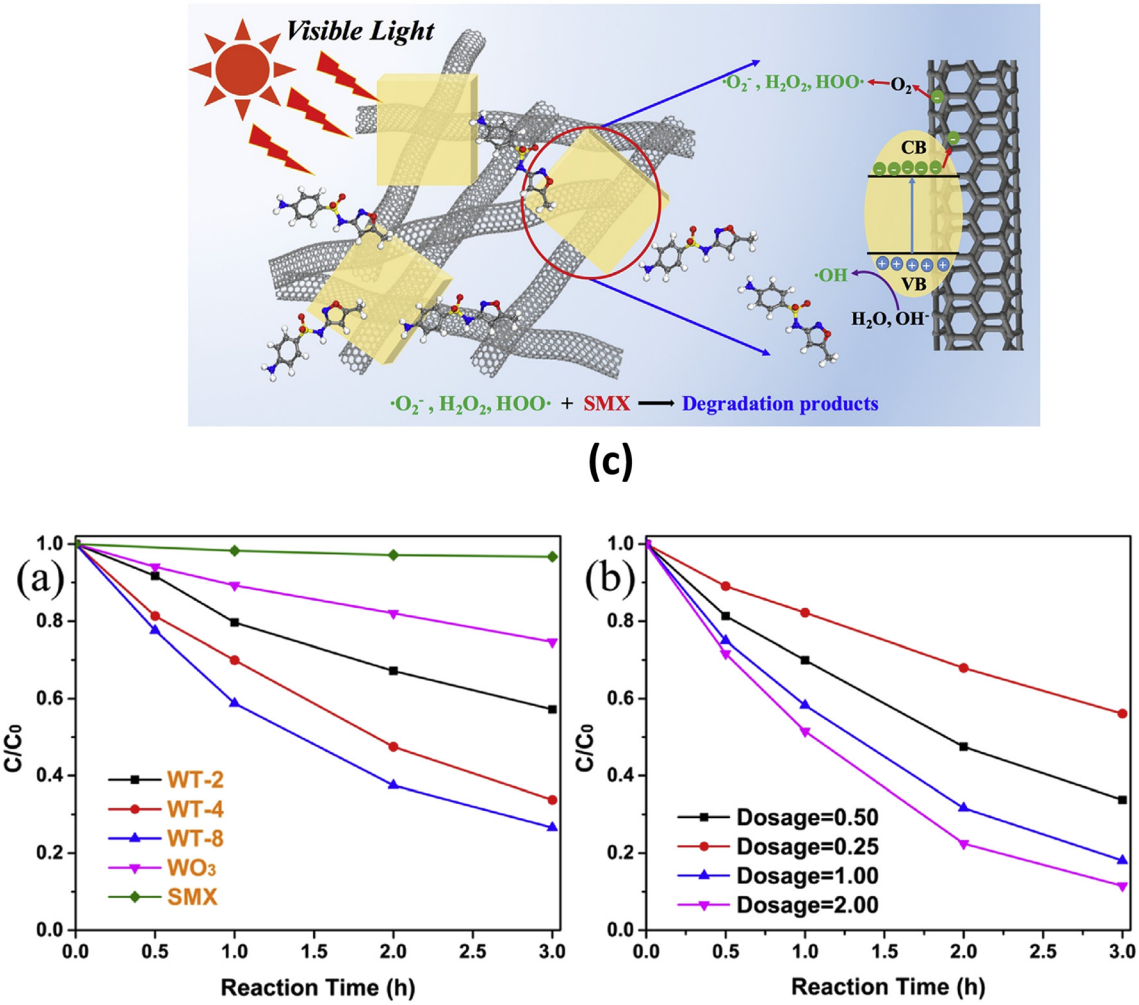

Fig. 11 (a) SMX degradation under visible-light irradiation by WO_3, WT-2, WT-4 and WT-8. Conditions: catalyst: 0.50 g L^{-1}, SM: 10 mg L^{-1}. (b) SMX degradation by WT-4 at different catalyst dosage (0.25, 0.50, 1.00 and 2.00 g L^{-1}). Conditions: SMX: 10 mg L^{-1}. (c) Schematic illustration of the proposed mechanism for the enhanced degradation of SMX by WO_3-CNT composites under visible-light irradiation. Reproduced from ref. 261 with permission from Elsevier (2018).

degradation.[270] These findings indicated higher activity and comparable stability for the first and second cycles in an Ag@Ag_2O–graphene photocatalyst loaded with 2.5 wt% graphene. Possible charge transfer processes were suggested to take place under visible-light irradiation, and holes were major active species for Ag@Ag_2O–graphene photocatalytic degradation while Ag^0 acted as an electron capture center. Lin *et al.*[271] observed 92% degradation of sulfamethoxazole after subjecting an immobilized TiO_2–reduced graphene oxide (rGO) nanocomposite on optical fibers to 180 min of UV irradiation. A visible-light-driven Cu_2O/rGO photocatalyst successfully degraded sulfamethoxazole.[272]

Nawaz *et al.*[273] used graphene oxide and titanium dioxide in combination with sodium alginate to synthesize a reduced graphene oxide–TiO_2/sodium alginate (rGOT/SA) aerogel. They observed more than 99% removal of these contaminants taking place within 45–90 min under UVA light, corresponding to an optimal mass ratio of TiO_2 nanoparticles with respect to graphene oxide of 2 : 1 in an rGOT/sodium alginate aerogel in the presence of 1 wt% sodium alginate solution. Zhou *et al.*[274] investigated the photocatalytic decomposition of SMX by Ag_3PO_4, Ag_3PO_4–graphene and Ag/Ag_3PO_4–graphene under simulated solar-light irradiation. They observed that the photocatalytic activities of Ag_3PO_4–graphene and Ag/Ag_3PO_4–graphene were no better than pure Ag_3PO_4. However, these studies indicated the enhanced structural stability of Ag/Ag_3PO_4–graphene, which would be more practical in real treatment processes.

3.3.6 Heterojunction and Z-scheme-based photocatalysts. WO_3–g-C_3N_4 (WCN) photocatalysts with different g-C_3N_4 amounts (referred to as WCN-4, WCN-6 and WCN-8) were prepared by a hydrothermal method and evaluated for SMX degradation under visible light.[275] In view of this, Fig. 12(a) and (b) show the degradation of SMX by (a) WCN-8 at various pH and (b) WCN-8 at different catalyst dosages under visible light. The optimized WO_3–g-C_3N_4 composite (dosage: 1.0 g L^{-1}) showed 91.7% removal efficiency for SMX as a result of Z-scheme heterojunctions between g-C_3N_4 and

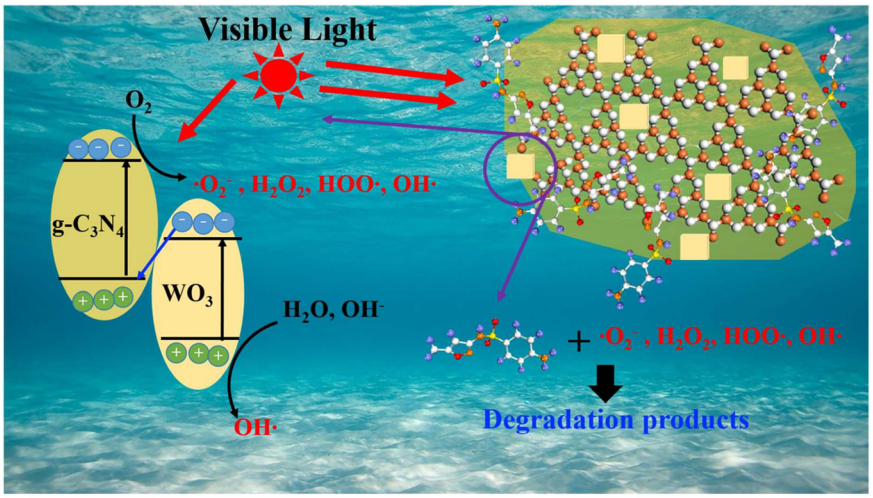

(c)

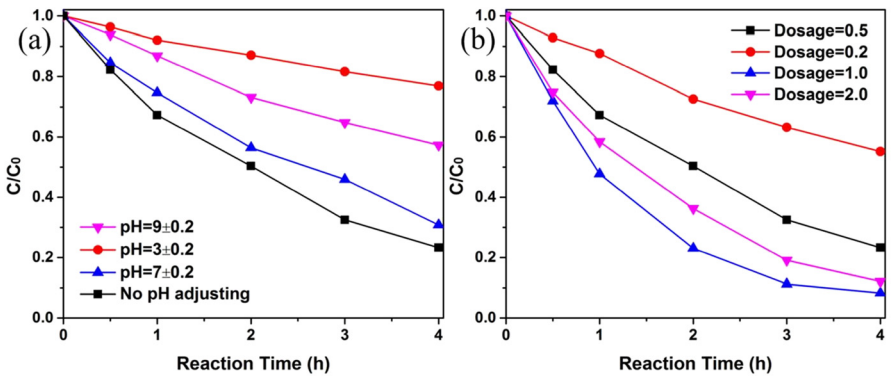

Fig. 12 (a) Degradation of SMX by WCN-8 at various pH values under visible light: Conditions: catalyst = 0.5 g L^{-1}, SMX = 10 mg L^{-1}. (b) Degradation of SMX by WCN-8 at different catalyst dosages under visible light: Conditions: SMX: 10 mg L^{-1}, no pH adjustment. (c) Schematic illustration of SMX photodegradation process over WCN composites under visible-light irradiation. Reproduced from ref. 275 with permission from RSC (2017).

WO_3 to account for the separation between photogenerated electron–hole pairs. Alternatively, the role of the larger surface area and better visible-light absorption capability of the photocatalyst in enhancing the removal efficiency of SMX cannot be ruled out. Fig. 12(c) is a schematic illustration of the SMX photodegradation process over WCN composites under visible-light irradiation. Rodrigues *et al.*[276] observed 97% (120 min) photocatalytic efficiency for sulfamethoxazole using $Ce_{0.8}Gd_{0.2}O_{2-\delta}/TiO_2$ under UV light.

In another study, $Ag_2S/Bi_2S_3/g\text{-}C_3N_4$ heterojunctions exhibited 97.4% degradation of sulfamethoxazole in 90 min in aqueous solution under visible light.[277] The stable hierarchical Fe_2O_3/Co_3O_4 heterojunction on nickel foam exhibited enhanced photocatalytic degradation of sulfamethoxazole.[278] The photocatalyst was also studied to evaluate its effectiveness in surface water, hospital wastewater, and wastewater treatment. A magnetic quaternary $BiOCl/g\text{-}C_3N_4/Cu_2O/Fe_3O_4$ nano-heterojunction exhibited 99.5% photodegradation of sulfamethoxazole (100 μM) in 60 and 120 min under visible and natural sunlight, respectively.[279] Photocatalysts comprising graphene-supported p–n heterojunction $rGO@Cu_2O/BiVO_4$ composites with different Cu_2O loadings (1, 5, 10, 15 and 20 wt%) were prepared to study their photocatalytic degradation activity for sulfamethoxazole oxidation under LED light at neutral pH.[280] All the composites were found to be effective in sulfamethoxazole oxidation owing to the electrical conductivity of rGO and the p–n heterojunction between Cu_2O and $BiVO_4$.

Zhang *et al.*[281] evaluated the performance of a Bi_2WO_6/TiO_2 heterojunction for photocatalytic ozonation degradation of sulfamethoxazole under simulated sunlight. They attained 97.1% removal rate of sulfamethoxazole corresponding to a catalyst dosage of 0.2 g L^{-1}, ozone concentration of 1.5 mg L^{-1}, sulfamethoxazole concentration of 10 mg L^{-1} and pH 5.25. These studies also established excellent recyclability and stability, as evidenced through 5 cycle experiments. They also proposed a new Z-scheme transfer pathway for electrons and a degradation mechanism. A direct Z-scheme MIL-53(Co/Fe)/10 wt% MoS_2 heterojunction composite photocatalyst

displayed 99% removal of sulfamethoxazole (10 mg L^{-1}) in aqueous solution (pH: 6) following visible-light-driven activation of peroxymonosulfate (initial concentration: solution 0.2 g L^{-1}).[282] $Bi_2O_3/C_3N_4/TiO_2$@C quaternary hybrids (fabricated by a hydrothermal and calcination two-step method) exhibited high photocatalytic activity, degrading 100% sulfamethoxazole (SMZ, 5 mg L^{-1}) within 100 min under visible-light irradiation.[283] These investigations further revealed the photocatalytic degradation rates of SMZ by a $Bi_2O_3/C_3N_4/TiO_2$@C junction to be 5.12, 2.87, and 1.35 times higher than those with Bi_2O_3/C_3N_4, C_3N_4/TiO_2@C, and Bi_2O_3/TiO_2@C junctions, respectively.

Ren *et al.*[284] examined Ag (0.5, 1 and 2 wt%) nanoparticles/g-C_3N_4/Bi_3TaO_7 as Z-scheme photocatalysts prepared by combining hydrothermal and photodeposition for visible-light-driven performance in the degradation of sulfamethoxazole. It should be noted that the removal efficiency for sulfamethoxazole by Ag (1 wt%)/g-C_3N_4/Bi_3TaO_7 was found to be about 98% after 25 min and adopted the following order compared to g-C_3N_4, Bi_3TaO_7, g-C_3N_4–Bi_3TaO_7 and other Ag/g-C_3N_4/Bi_3TaO_7 composites: Ag (1 wt%)/g-C_3N_4/Bi_3TaO_7 > Ag (2 wt%)/g-C_3N_4/Bi_3TaO_7 > Ag (0.5 wt%)/g-C_3N_4/Bi_3TaO_7 > g-C_3N_4/Bi_3TaO_7 > g-C_3N_4 > Bi_3TaO_7. Such improved performance of Ag (1 wt%)/g-C_3N_4/Bi_3TaO_7 is attributed to the effective separation/transfer of photo-excited electrons and holes. In another study, an *in situ* prepared $Ag_3PO_4/Bi_4Ti_3O_{12}$-20% heterojunction composite photocatalyst under visible-light irradiation exhibited much better photocatalytic activity in degrading sulfamethoxazole and stability compared to Ag_3PO_4 or pure $Bi_4Ti_3O_{12}$.[285] This is attributed to the formation of a direct Z-scheme improving the stability and activity of the $Ag_3PO_4/Bi_4Ti_3O_{12}$ composite.

An Ag_2O–$KNbO_3$ (0.15Ag–Nb) composite fabricated by an *in situ* deposition method exhibited improved degradation of sulfamethoxazole under visible-light irradiation compared to the corresponding pure $KNbO_3$ and Ag_2O.[286] The apparent rate constant of the composite was found to be 0.40 and 8 times those of $KNbO_3$ and Ag_2O, respectively. According to these studies, a type-I heterojunction formed between $KNbO_3$ and Ag_2O significantly enhanced the separation of photo-induced holes and electrons and accounted for sulfamethoxazole degradation. The rate constant value of the visible-light-driven optimal 0D/1D AgI/MoO_3 (0.13 min^{-1}) Z-scheme heterojunction photocatalyst in sulfamethoxazole degradation was found to be ~22.4 times and 32.5 times those of MoO_3 (0.0058 min^{-1}) and AgI (0.0040 min^{-1}), respectively.[287] In addition, Z-scheme Ag_3PO_4/g-C_3N_4,[288] Fe_3O_4–ZnO@g-C_3N_4,[289] CeO_2/g-C_3N_4 (CeO_2: 5% mass ratio)[290] and S-scheme-based N–$SrTiO_3/NH_4V_4O_{10}$[291] photocatalysts have also been evaluated for the removal of sulfamethoxazole from water.

Table 4 records the performance data of different photocatalysts on the removal of sulfamethoxazole in wastewater.

3.4 Ibuprofen

Ibuprofen (IPF) is a drug belonging to the class of propanoic acid derivatives and is extensively used in the treatment of fever, pain in human beings, inflammatory disorders, muscle problems, including migraines, rheumatoid arthritis, analgesic and painful menstrual periods.[22,292] It is slightly soluble in water, stable, is eliminated from the body through urine and does not undergo biodegradation. As a result, it can be found in water samples of different origins originating from municipal wastewater treatment plant effluents, groundwater through leaching and natural water and cannot be treated through conventional wastewater treatments. The presence of ibuprofen even in low concentration through water affects the reproduction of aquatic animals, including the photosynthesis of aquatic plants. Ibuprofen can leach into ground water and soil in daily life. In view of this, several studies have been made using metal oxide and graphitic material related photocatalysts to make wastewater free from ibuprofen.[293–357]

3.4.1 Metal oxides. The photocatalytic degradation of ibuprofen has been reported in the literature using TiO_2, ZnO and other metal oxides.[294–306] Jallouli *et al.*[294] used a TiO_2/UV-LED system to study the photocatalytic degradation of ibuprofen present in ultrapure water (UP), the secondary treated effluent of a municipal wastewater treatment plant (WWTP) and pharmaceutical industry wastewater (PIWW). They observed the removal of ibuprofen below the detection limit in the case of UP and PIWW compared to municipal water. Their investigations inferred the higher degradation of IBU at near natural pH (5.3) of UP and PIWW compared to acidic (3.0) and alkaline (9.0) pH. In another study, the photocatalytic degradation of ibuprofen in water was carried out using TiO_2 nanoparticles/UV light.[295] The emerging findings established the faster depletion of ibuprofen with TiO_2/UV (pH: 5.05) and followed pseudo-first-order kinetics (k: 1.0 min^{-1}). TiO_2 (0.03 g) resulted in almost 100% (5 min) photodegradation of ibuprofen in aqueous solution (pH: 5.0) on irradiation by a mercury lamp (125 W).[296]

The photodegradation of ibuprofen has been tested as a function of catalyst type (TiO_2 and ZnO), loading (50–500 mg L^{-1}), initial drug concentration (10, 40, 80 mg L^{-1}) and wavelength (200–600 nm) of irradiation.[297] The photocatalytic efficiency was found to be greater than 90% in 15 min under UVA and visible-light irradiation corresponding to an initial concentration of ibuprofen of 10 mg L^{-1} and amount of photocatalysts (TiO_2 and ZnO) of 100 mg L^{-1}. These findings also indicated over 90% conversion of the drug within 8 min with k-values of 0.382 and 0.326 min^{-1} under UVA for TiO_2 and ZnO, respectively, and it correspondingly decreased to 0.199 and 0.144 min^{-1} under visible light. Tanveer and others[298] used UV and solar irradiation to compare the photocatalytic degradation of ibuprofen in water using TiO_2 and ZnO. A much higher rate of degradation was observed in UV for TiO_2 (99%) compared to ZnO (86%) after 15 min compared to solar degradation.

Table 4 Performance data on removal of sulfamethoxazole in water using variety of photocatalysts

Photocatalyst	Preparative method	SMX	Catalyst dose	pH	Light source and other details	Degradation/removal (time)	Rate constant
TiO_2: mainly of anatase (80%), (P25 Degussa)[219]	Commercial	20 mg L^{-1}	1 g L^{-1}	5	Xenon lamp: 400 W (200 nm $< \lambda <$ 700 nm)	96% (180 min)	0.026 min^{-1}
TiO_2, P-25 Degussa[222]	Commercial	20 mg L^{-1}	0.5 g L^{-1}	Natural	UV lamp equipped with UV C (260 nm)	100% (180 min)	—
TiO_2 Degussa P25[223]	Commercial	100 mgL^{-1}	1.0 g L^{-1}	5	Xenon lamp (1000 W) with $\lambda_{cut\text{-}off} <$ 290 nm	88% (360 min)	0.054 min^{-1}
TiO_2 Merck[224]	Commercial	20 mg L^{-1}	0.08 g L^{-1}	3	Low-pressure mercury vapour lamp (15 W)	96.5% (60 min)	—
Biochar supported TiO_2[228]	Sol–gel method	10 mg L^{-1} (0.1 L)	0.5 g	4	UV lamp-UVC (15 W), λ: 254 nm	91% (6 h)	—
TiO_2 immobilized on glass spheres[229]	By dip coating on glass	100 μg L^{-1}	0.335 g L^{-1}	7.82	Solar UV radiation ($\lambda <$ 400 nm)	100% (120 min)	0.030 min^{-1} (first cycle)
F–ZnO[232]	Commercial	1 mM (NH_4F: 2.505 mM)	1.48 g L^{-1}	4.7	UVC lamp: 10 W	97% (30 min)	0.099 min^{-1}
ZnO[233]	Hydrothermal	10 mg L^{-1}	200 mg L^{-1}	7.5	UVA lamp	84% (60 min)	0.030 min^{-1}
TiO_2 nanoparticles (sigma-Aldrich)[234]	Commercial	50 mg L^{-1}	500 mg L^{-1}	4	UV lamp	100% (90 min)	0.0356 min^{-1}
WO_3 commercial (sigma-Aldrich)[234]	Commercial	25 mg L^{-1}	750 mg L^{-1}	3	UV lamp	100% (90 min)	0.0093 min^{-1}
Pd/TiO_2 (1%)[236]	UV-reduction	1 mg L^{-1}	~50 mg L^{-1}	—	Natural sunlight	100% (10 min)	52.1 ± 5.1 × 10^{-2} min^{-1}
Pt/TiO_2 (1%)[236]	UV-reduction	1 mg L^{-1}	~50 mg L^{-1}	—	Natural sunlight	~90% (10 min)	7.6 ± 501 × 10^{-2} min^{-1}
Cu (0.045 wt%)–TiO_2[237]	Microwave assisted impregnation method	4 mg L^{-1} (20 mL)	1 g L^{-1}	5.2	Lamps: 8 W, 77 mW cm^{-2}	100% (120 min)	0.0506 min^{-1}
TiO_2 Evonik P25[238]	Sol–gel procedure	30 mg L^{-1}	0.5 g L^{-1}	—	UVC	100% (90 min)	0.046 min^{-1}
TiO_2 Evonik P25[238]	Sol–gel procedure	30 mg L^{-1}	0.5 g L^{-1}	—	Simulated solar light	100% (240 min)	0.022 min^{-1}
1.5% au/TiO_2[238]	Deposition precipitation method	30 mg L^{-1}	0.5 g L^{-1}	—	UVC light (254 nm)	100% (90 min)	0.071 min^{-1}
1.5% au/TiO_2[238]	Deposition precipitation method	30 mg L^{-1}	0.5 g L^{-1}	—	Simulated solar light	100% (180 min)	0.039 min^{-1}
1.5% Ag/TiO_2[238]	Deposition precipitation method	30 mg L^{-1}	0.5 g L^{-1}	—	UVC light (254 nm) Simulated solar light	100% (45 min) 100% (240 min)	0.201 min^{-1} 0.027 min^{-1}
1.0% Cu/TiO_2[238]	Deposition precipitation method	30 mg L^{-1}	0.5 g L^{-1}	—	UVC light (254 nm) Simulated solar light	100% (90 min) 100% (240 min)	0.186 min^{-1} 0.028 min^{-1}
Au–Ag/TiO_2[238]	Deposition precipitation method	30 mg L^{-1}	0.5 g L^{-1}	—	UVC light (254 nm) Simulated solar light	100% (45 min) 100% (240 min)	0.143 min^{-1} 0.025 min^{-1}
Au–Cu/TiO_2[238]	Deposition precipitation method	30 mg L^{-1}	0.5 g L^{-1}	—	UVC light (254 nm) Simulated solar light	100% (45 min) 100% (240 min)	0.145 min^{-1} 0.026 min^{-1}
Fe-doped Titania (Fe/Ti molar ratio: 0.04%)[239]	Co-precipitation method	234 mg L^{-1}	1 g L^{-1}	Natural pH	Xenon ozone free lamp (100 W)	95% (120 min)	29 × 10^{-3} min^{-1}
F–Pd co-doped TiO_2[240]	Microwave assisted hydrothermal method	30 mg L^{-1}	1 g L^{-1}	—	Sunlight	98.4% (40 min)	—
F–Pd co-doped TiO_2[240]	Microwave assisted hydrothermal method	30 mg L^{-1}	1 g L^{-1}	—	Solar simulator	98.5% (220 min)	—

Table 4 *(continued)*

Photocatalyst	Preparative method	SMX	Catalyst dose	pH	Light source and other details	Degradation/removal (time)	Rate constant
F–Pt co doped TiO_2[241]	Microwave assisted hydrothermal method	20 mg L^{-1} (50 mL)	50 mg	~5.1	Solar light	>93% (90 min)	—
F–Pt co-doped TiO_2[241]	Microwave assisted hydrothermal method	20 mg L^{-1} (50 mL)	50 mg	~5.1	Simulated solar light	~58% (360 min)	—
N–Cu co doped TiO_2@f-SWCNT[243]	Sol–gel method	60 mg L^{-1}	0.8 g L^{-1}	6	Xenon lamp (200 W)	100% (60 min)	0.0512 min^{-1}
Ag,P-co-doped g-C_3N_4[244]	Pyrolysis method	5 mg L^{-1}	1000 mg L^{-1}	9.0	Visible lamps (8 W each), λ: 465 ± 40 nm	>99% (30 min)	2.06×10^{-1} min^{-1}
Ce-doped ZnO[246]	Spray coating	6.332 μg L^{-1}	Catalyst immobilized on 11.5 cm dia discs of area 104 cm^2	6.28	UVA lamp (36 W)	—	1.09×10^{-2} min^{-1}
Zn–TiO_2/pBC[247]	Modified sol–gel method	10 mg L^{-1} (160 mL)	0.2 g	5.03	Xenon lamp (50 W) with 420 nm cut-off filter	80.8% (180 min)	0.0085 min^{-1}
Fe_3O_4/ZnO, (H_2O_2:100 mg L^{-1})[248]	Polyol-mediated preparation	100 μg L^{-1} (20 mL)	200 mg L^{-1}	7	UVA lamp (15 W), λ: 365 nm, 4 mW cm^{-2}	~100% (240 min)	—
Bi_2O_3–TiO_2/PAC[251]	Two-stage calcination method	20 mg L^{-1} (250 mL)	0.05 g	11	Solar light–xenon arc lamp (300 W)	~100% (30 min)	0.159 min^{-1}
LDH–TiO_2[254]	Impregnation process	20 mg L^{-1} (100 mL)	50 mg	10	UVA lamp (λ: 300–400 nm, 300 W)	100% (360 min)	—
Poly(ethylene terephthalate)-10% TiO_2[257]	Solvent casting method	1 mg L^{-1} (100 mL)	50 mg L^{-1}	—	Xenon lamp (simulated solar light): 1.5 kW, 500 W m^{-2}	98% (360 min)	0.015 min^{-1}
$BiVO_4$/$SrTiO_3$ (1%)[258]	Self-template method under hydrothermal condition	10 mg L^{-1} (50 mL)	0.05 g	—	Xenon lamp (500 W)	91% (60 min)	—
0.75 CuO_x–$BiVO_4$[259]	Polyol-reduction method	0.5 mg L^{-1}	500 mg L^{-1} (persulfate: 100 mg L^{-1})	—	Simulated solar light	100% (30 min)	0.0991 min^{-1}
WO_3–MWCNT[261]	Hydrothermal method	10 mg L^{-1}	2.0 g L^{-1}	—	Solar simulator–xenon arc lamp (300 W), 420–630 nm	88.5% (180 min)	—
Magnetic ZnO@g-C_3N_4[265]	*In situ* growth	30 mg L^{-1} (1000 mL)	0.65 g L^{-1}	5.6	UVC lamp (10 W)	90.4% (60 min)	0.0384 min^{-1}
5 wt% Ag/g-C_3N_4[268]	Photo-reduction method	10 μM (100 mL)	5 mg	Natural pH	Xenon lamp (300 W) with a 400 nm cut-off filter	97.5% (60 min)	—
rGO–WO_3[269]	Hydrothermal method	10 mg L^{-1}	1.0 g L^{-1}	No pH adjustment	Xenon arc lamp: 200 W (420–630 nm)	>98% (180 min)	1.607 h^{-1}
Ag@Ag_2O-2.5 wt% graphene[270]	Precipitation method	1 mg L^{-1}	0.05 g L^{-1}	—	Xenon lamp (300 W) with a cut-off filter (λ > 280 nm), 37.7 mW cm^{-2}	~100% (90 min)	0.038 min^{-1}
Immobilized TiO_2-2.7% rGO[271]	Polymer assisted hydrothermal deposition method	5 mg L^{-1}	Bundle of thirty 10 cm photocatalyst-coated SOF (25 mL) placed on a petri disc	6	High-pressure UV mercury vapor lamp (160 W)	92% (180 min)	0.757 h^{-1}

Table 4 *(continued)*

Photocatalyst	Preparative method	SMX	Catalyst dose	pH	Light source and other details	Degradation/removal (time)	Rate constant
Cu_2O/rGO-80 (80 refers amount of GO (mg) used in preparation of rGO)[272]	Wet chemical method	5 mg L^{-1} (80 mL)	20 mg	—	Xe lamp: 300 W (420 nm cut-off filter)	50% (120 min)	0.00525 min^{-1}
rGO–TiO_2/sodium alginate (1 : 3)[273]	Hydrothermal method	10 ppm (200 mL)	0.5 g L^{-1}	Neutral	High-pressure mercury lamp (100 W)	>99% (45–90 min)	0.108 min^{-1}
WO_3–g-C_3N_4 (referred as WCN-8)[275]	Hydrothermal method	10 mg L^{-1}	1.0 g L^{-1}	No pH adjustment	Xenon arc lamp (300 W), 420–630 nm	91.7% (240 min)	—
$Ce_{0.8}Gd_{0.2}O_{2-\delta}/TiO_2$[276]	Modified Pechini method	25 mg L^{-1} (300 mL)	30 mg	—	Mercury lamp (15 W)	97% (120 min)	0.2959 mg^{-1} min^{-1}
Ag_2S/Bi_2S_3/g-C_3N_4[277]	Hydrothermal	20 mg L^{-1}	0.25 mg mL^{-1}	7	Xenon lamp (visible light): 300 W	97.3% (90 min)	0.0642 min^{-1}
BiOCl/g-C_3N_4/Cu_2O/Fe_3O_4[279]	Co-precipitation method	100 μM	0.2 g L^{-1}	6.5	Xenon lamp	99.5% (60 min)	0.0543 min^{-1}
rGO@Cu_2O/$BiVO_4$[280]	Solution method	0.5 mg L^{-1}	100 mg (250 ml)	7	LED light (30 W)	~98.5% (270 min)	—
Bi_2WO_6/TiO_2[281]	Hydrothermal method	10 mg L^{-1}, [ozone]: 1.5 mg L^{-1}	0.2 g L^{-1}	5.25	Simulated sunlight	97.1% (180 min)	1.83×10^{-2} min^{-1}
MIL-53(Co/Fe)/10 wt% MoS_2[282]	Hydrothermal through *in situ* growth	10 mg L^{-1}, (peroxymonosulfate: 0.2 g L^{-1})	0.01 g L^{-1}	6	Visible light	99% (60 min)	—
$Bi_2O_3/C_3N_4/TiO_2$@C[283]	Hydrothermal and calcination	5 mg L^{-1}	1 g L^{-1}	5	Visible light	100% (100 min)	—
Ag (1 wt%)/g-C_3N_4/Bi_3TaO_7[284]	Photo deposition method	5 mg L^{-1}	25 mg (50 mL)	—	Xenon lamp (300 W)	98% (25 min)	0.1499 min^{-1}
$Ag_3PO_4/Bi_4Ti_3O_{12}$-20%[285]	*In situ* growth method	5 ppm (50 mL)	—	—	Xenon lamp: 300 W ($\lambda > 400$ nm)	~77% (40 min)	0.0372 min^{-1}
Ag_2O–$KNbO_3$ (Ag–Nb molar ratio: 0.15/1)[286]	*In situ* growth	5 ppm	0.3 mg mL^{-1}	—	Visible-light irradiation	91% (40 min)	0.0603 min^{-1}
97.9% Ag_3PO_4/2.1% g-C_3N_4[288]	*In situ* precipitation method	1 mg L^{-1} (100 mL)	5 mg	Neutral pH	Xenon lamp (300 W), $\lambda > 400$ nm, 138.7 mW cm^{-2}	~99% (90 min)	0.063 min^{-1}
Fe_3O_4–ZnO@g-C_3N_4[289]	*In situ* growth	30 mg L^{-1}	0.5 g L^{-1}	7	UVC lamp (10 W)	95% (90 min)	0.0351 min^{-1}

The degradation of ibuprofen using a heterogeneous ZnO photocatalyst irradiated with UVC achieved 82.97% removal efficiency within a reaction time of 95 min under optimized conditions (pH: 6.7, ZnO loading: 583 mg L^{-1}, initial IBP concentration: 1.5 mg L^{-1}, humic acid concentration: 54 mg L^{-1}).[299] The reactive species responsible for oxidizing ibuprofen were found to be h^+, $O_2{\cdot}^-$, H_2O_2, and ·OH. In another experiment, ZnO–Ce (0.50 g L^{-1}) showed 60% removal of ibuprofen (20 ppm) under acidic conditions after 120 min under UVC irradiation.[300] Holes played a vital role in the degradation process of ibuprofen and it displayed good degradation activity even after 3 cycles under UV light. Hexagonal α-Fe_2O_3 flakes have removed up to 80% of ibuprofen in a combination of adsorption treatment followed by UV (265 nm) irradiation.[301] TiO_2 immobilized on glass coupled with simulated solar irradiation also eliminated ibuprofen and its derivatives.[302] Investigations on the photocatalytic activity of TiO_2,[303,304] ZnO,[304,305] and ZnO membrane[306] have also been reported in the remediation of water from ibuprofen.

3.4.2 Doped metal oxides. N,S-co-doped TiO_2 exhibited high photocatalytic activity in the degradation of ibuprofen under simulated solar irradiation due to the synergistic effects of N and S co-doping in TiO_2 owing to the separation of photogenerated electrons and holes and higher visible-light adsorption.[307] Reusability tests of the N,S–TiO_2 photocatalyst showed that its catalytic activity was not significantly altered even after 6 cycles. C,N,S-co-doped TiO_2 prepared by thermally treating hydrothermally prepared mesoporous TiO_2 (anatase/brookite) and thiourea in a 1 : 1 wt. ratio demonstrated complete degradation of ibuprofen under visible light within 5 h in contaminated water.[308]

Bi (0.25 wt%) and Ni (0.5 wt%) doped TiO_2 photocatalysts synthesized by a sol–gel method under irradiation of solar light for 6 h achieved degradation of ibuprofen by 89% and 78% repectively.[309] The degradation of ibuprofen followed kinetics in accordance with the Langmuir–Hinshelwood model. In addition, La^{3+}-doped TiO_2 monolith,[310] Cu-doped $LaFeO_3$,[311] Cu_2O-doped TiO_2 nanotube arrays,[312] C,N-co-doped mesoporous TiO_2[313] and TiO_2 co-doping with urea and functionalized CNT[314] photocatalysts also displayed enhanced photocatalytic degradation of ibuprofen in aqueous solution.

3.4.3 Metal oxide–metal oxide composites. Lin *et al.*[315] prepared TiO_2 nanofibers wrapped in BN nanosheets by an electrospinning method, which were examined as a photocatalyst for the removal of ibuprofen from contaminated water under UV irradiation. The ibuprofen was almost completely removed after 2 h owing to wrapping of the BN nanosheets to facilitate improved light absorption and efficient separation of the electron–hole pairs. Investigations were also made on the reusability and regeneration capability of the prepared photocatalyst on the degradation of ibuprofen. Activated carbon (90 wt)% impregnated with TiO_2 showed 92% removal efficiency for ibuprofen solution under UV light within 4 h due to the synergy of adsorption and photodegradation.[316] FeO,[317] Fe_3O_4@MIL-53(Fe),[318] Fe_3O_4/Bi_2WO_6,[319] $BiOBr_{0.9}I_{0.1}/Fe_3O_4@SiO_2$,[320] and Ag/Ag_2O[321] nanocomposites also displayed enhanced removal of ibuprofen under visible-light irradiation.

Ag and Fe_3O_4 co-modified WO_{3-x} ($Ag/Fe_3O_4/WO_{3-x}$) composites were fabricated by hydrothermal and photodeposition processes and showed almost complete photocatalytic-Fenton degradation of ibuprofen (and diclofenac), as evident from (Fig. 13(a) and (b)).[322] This is attributed to the surface plasmon resonance effect of Ag, separation of photogenerated carriers and heterostructures of $Ag/Fe_3O_4/WO_{3-x}$. In addition, the possibility of absorption of light greatly improving the photocatalytic-Fenton degradation efficiency cannot be ruled out. The fabricated $Ag/Fe_3O_4/WO_{3-x}$ also exhibited good photocatalytic-Fenton stability in the photodegradation of ibuprofen (and diclofenac), as indicated by the almost unchanged degradation rate of the antibiotic in (Fig. 13(c) and (d)). The degradation and charge transfer mechanism involved in the removal of the ibuprofen and diclofenac have also been proposed and are displayed in Fig. 13(e).

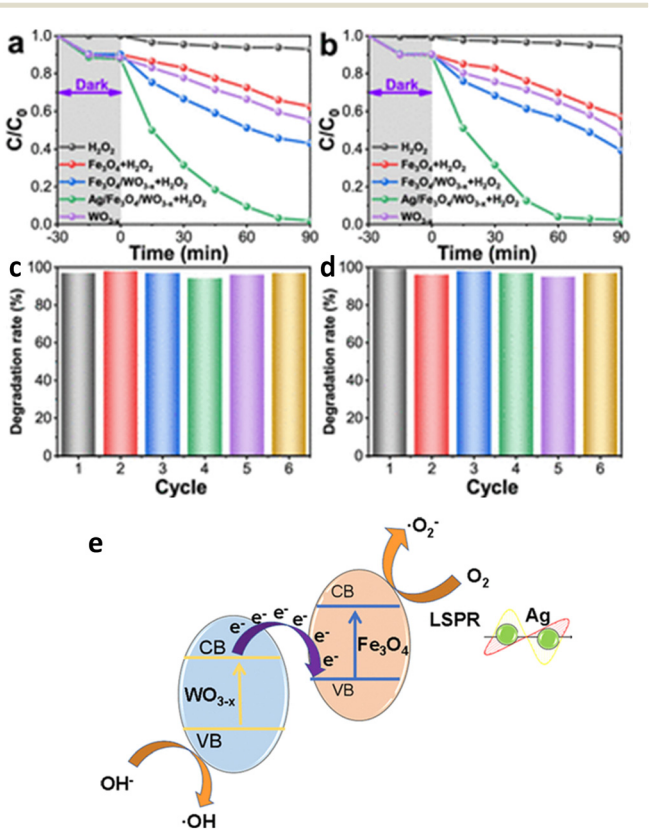

Fig. 13 Photocatalytic-Fenton degradation of (a) ibuprofen and (b) diclofenac by Fe_3O_4, WO_{3-x}, Fe_3O_4/WO_{3-x}, and $Ag/Fe_3O_4/WO_{3-x}$ samples. (c and d) Corresponding recycling study and stability of $Ag/Fe_3O_4/WO_{3-x}$. (e) Schematic illustration of the possible catalytic degradation mechanism and charge transfer of $Ag/Fe_3O_4/WO_{3-x}$ under light irradiation (modified image). Reproduced from ref. 322 with permission from ACS (2021).

Lenzi *et al.*[323] showed that the photocatalytic degradation of ibuprofen (10 ppm) solution (pH: 7) by 0.3 g L^{-1} of Ag/ZnO/$CoFe_2O_4$ (5 wt%) exhibited removal efficiencies of 80% and 47% under artificial and solar radiation, respectively. These studies also confirmed the recovery and reuse of the catalyst after 3 cycles without significant loss of catalytic activity. Visible-light-driven mesoporous hierarchical BiOBr/Fe_3O_4@SiO_2 (dose: 1 g L^{-1}) photocatalyst degraded ibuprofen (initial concentration: 2 mg L^{-1}) almost completely in 60 min.[324] Further studies have shown BiOBr/Fe_3O_4@SiO_2 maintaining its initial photocatalytic activity (~80%) even after five cycles. In another study, a magnetically separable Fe_3O_4–SiO_2-coated TiO_2 composite demonstrated excellent photocatalytic activity.[325] An immobilized TiO_2/ZnO-sensitized copper(II) phthalocyanine heterostructure displayed about 80% degradation of ibuprofen (initial conc.: 5 mg L^{-1}) after 4 h of irradiation under 365 nm UV.[326] The studies revealed a small decline in the IBF degradation (77%) after the 5th cycle. PANI-coated WO_3@TiO_2,[327] polyacrylonitrile (PAN)–MWCNT/TiO_2–NH_2,[328] TiO_2 nanoparticles and C-nanofiber-modified magnetic Fe_3O_4 nanospheres (TiO_2@Fe_3O_4@C-NF),[329] carbon dots/Fe_3O_4@carbon sphere pomegranate-like composites,[330] PVDF–ZnO/Ag_2CO_3/Ag_2O,[331] and PAN–MWCNT nanofiber crosslinked TiO_2–NH_2 nanoparticles[332] have also been examined for their photodegradation performance for ibuprofen.

3.4.4 Graphitic materials. Hernández-Uresti *et al.*[333] observed the following order for the degradation of different pharmaceutical compounds in aqueous solution (pH ~ 5.5) using g-C_3N_4 under UV-vis irradiation: tetracycline (86%) > ciprofloxacin (60%) > ibuprofen (20%). Wang and coworkers[334] undertook investigations on the degradation of pharmaceutical contaminants by bubbling a gas-phase surface discharge plasma combined with g-C_3N_4 photocatalysis. These findings disclosed 82% and 100% removal of ibuprofen and tetracycline hydrochloride after 25 min, corresponding to initial concentrations of 60 and 200 mg L^{-1}, respectively. A photocatalytic study of hydrothermally prepared reduced-graphene-oxide-loaded $HoVO_4$–TiO_2 revealed enhanced photodecomposition efficiency of rGO–$HoVO_4$–TiO_2 (~96%) compared to rGO–$HoVO_4$ (75%), $HoVO_4$ (67%), rGO–TiO_2 (30%) or TiO_2 (10%) in the removal of ibuprofen over 60 min.[335] The findings also showed ibuprofen decomposition to depend mainly on superoxide radicals photogenerated from rGO–$HoVO_4$–TiO_2 under visible-light illumination.

Acidified g-C_3N_4/polyaniline/rGO@biochar (0.5 mg L^{-1}) nano-assemblies degraded ibuprofen (20 mg L^{-1}) to the extent of 98.4% in 50 min under exposure to visible light.[336] Such significant performance is attributed to multiple reasons, such as highly separated charges, enhanced visible absorption and diffusion. The major reactive species in the degradation process for ibuprofen involved hydroxyl and superoxide radical anions. Akbarzadeh *et al.*[337] explored the photodegradation of ibuprofen solution in the presence of a hydrothermally fabricated g-C_3N_4/Ag/AgCl/$BiVO_4$ microflower composite as photocatalyst under visible light and compared its performance with $BiVO_4$, g-C_3N_4/$BiVO_4$ and Ag/AgCl/$BiVO_4$. These findings revealed remarkably enhanced degradation efficiency of g-C_3N_4/Ag/AgCl/$BiVO_4$ (94.7%) compared to g-C_3N_4 (6.5%), $BiVO_4$ (11.4%), g-C_3N_4/$BiVO_4$ (68.6%), or Ag/AgCl/$BiVO_4$ (88.3%) in 1 h corresponding to a photocatalyst dosage of 0.25 g L^{-1} and initial concentration of 2 mg L^{-1}. The reduced band gap energy and recombination rate of the g-C_3N_4/Ag/AgCl/$BiVO_4$ photocatalyst are ascribed to charge transfer along the heterojunction. The photocatalytic degradation performance of IPF increases with the (121)/(040) XRD plane intensity ratio of $BiVO_4$, Ag/AgCl/$BiVO_4$, g-C_3N_4/$BiVO_4$ and g-C_3N_4/Ag/AgCl/$BiVO_4$ and is found to be in good agreement with the photoluminescence findings.

A hierarchical assembly of Ag (7%)/g-C_3N_4/kaolinite composite fabricated following an *in situ* calcination and photodeposition process exhibited 99.9% degradation of ibuprofen (k: 0.01128 min^{-1}) after 5 h under visible-light irradiation compared to g-C_3N_4, g-C_3N_4/kaolinite and Ag/g-C_3N_4.[338] This outcome is due to the stronger adsorption property, efficient separation and transfer of electron–hole pairs. In addition, the presence of monodispersed Ag nanoparticles in the g-C_3N_4/kaolinite sheets led to more active sites, accounting for this. The efficient photocatalytic degradation of ibuprofen has also been reported in aqueous solution using graphene quantum dots/$AgVO_3$ nanoribbons,[339] g-C_3N_4/MIL-68(In)–NH_2 composites,[340] graphene oxide and TiO_2 heterostructures doped with F,[341] reduced-graphene-oxide–TiO_2/sodium alginate 3-dimensional structure aerogel[273] and Fe_3O_4/graphene/S-doped g-C_3N_4[342] also exhibited enhanced visible-light photocatalytic activity for the degradation of ibuprofen.

3.4.5 Heterojunction and Z-scheme-based photocatalysts. A TiO_2/g-C_3N_4 (5%) photocatalyst exhibiting a sea urchin morphology with interface effects was synthesized by a solvothermal method.[343] Its application in the photocatalytic degradation of ibuprofen showed significantly enhanced performance under irradiation by visible light for 60 min. The formed superoxide radicals and holes were assigned as the main active species involved in the photodegradation of ibuprofen. The photocatalytic performance of this catalyst after 5 cyclic experiments indicated its good stability. Wang *et al.*[344] fabricated atomic-scale g-C_3N_4/Bi_2WO_6 comprising ultrathin g-C_3N_4 nanosheets and monolayer Bi_2WO_6 nanosheets (1 : 4 mol ratio) by a hydrothermal reaction. Such an assembly of 2D/2D heterojunctions removed 96.1% ibuprofen under visible-light irradiation within 60 min due to a synergistic effect.

Kumar and others[345] synthesized a magnetically recyclable direct-contact Z-scheme g-C_3N_4/TiO_2/Fe_3O_4@SiO_2 heterojunction nanophotocatalyst and recorded 97% removal of ibuprofen solution (pH: 3) after 15 min under irradiation by visible light (~330 W m^{-2}). Such excellent performance of

a magnetically recyclable direct-contact Z-scheme nanophotocatalyst was attributed to the low recombination rate of photogenerated e^- and h^+. Visible-light-assisted persulfate activation by an SnS_2 (0.5%)/MIL-88B(Fe) Z-scheme heterojunction achieved 100% removal of ibuprofen in 120 min.[346] This was found to be 54 and 4 times higher than SnS_2 and SnS_2 (0.5%)/MIL-88B(Fe), respectively. Such findings could be ascribed to the structure and crystallinity of the photocatalysts. In another reported study, an optimized Z-scheme based 1D/2D FeV_3O_8/g-C_3N_4 composite comprising 10% FeV_3O_8 achieved a maximum degradation rate for ibuprofen of 95% at 85 min under visible-light irradiation.[347] Kinetic studies established that the rate constant is 4 times that of g-C_3N_4 nanosheets. However, the presence of 30% FeV_3O_8 in g-C_3N_4 decreased the degradation efficiency to 52.8%.

Heterostructure g-C_3N_4/Bi_2WO_6/rGO nanocomposites prepared by microwave- assisted treatment for 120 min in a hydrothermal method undertook the maximum photocatalytic degradation of ibuprofen (93.9%) under visible-light illumination.[348] In addition, g-C_3N_4@NiO/Ni@MIl-101,[349] Bi_5O_7I–MoO_3,[350] $AgSCN/Ag_3PO_4/C_3N_4$,[351] N–TiO_2@SiO_2@Fe_3O_4,[352] g-C_3N_4/CQDs/$CdIn_2S_4$,[353] direct Z-scheme Co_3O_4/BiOI,[354] a double Z-scheme system of α-$SnWO_4$/UiO-66(NH_2)/g-C_3N_4,[355] CdS/Fe_3O_4/TiO_2[356] and Ag_2CO_3/Ag_2O/ZnO[357] heterojunctions also exhibited excellent photocatalytic degradation of ibuprofen.

Table 5 records the performance data of different photocatalysts on the removal of ibuprofen from wastewater.

3.5 Norfloxacin

Norfloxacin (NOR) is an effective antibacterial agent of the fluoroquinolone family and is widely used as a drug in clinical treatments for bacterial infections of urinary, biliary, and respiratory tracts, and gastrointestinal and skin infections.[358–360] Norfloxacin has frequently been detected in municipal/wastewater treatment plants, is difficult to biodegrade and is predicted to be a potential risk to human beings and the environment. Therefore, it is considered a potential threat to the water environment and human health.[361–422]

3.5.1 Metal oxides. Reduced TiO_2 (TiO_{2-x}) samples comprising Cat.I-A (anatase), Cat.II-R (rutile) Cat.III-B (brookite) and a series of Cat.IV-A&R (anatase/rutile phases) mixed in different ratios showed about ~100% photocatalytic degradation of norfloxacin in visible light (>400 nm).[361] Such degradation of norfloxacin is guided by the specific surface area, concentration of Ti^{3+} and the density of oxygen vacancies of the photocatalysts. Haque and Muneer[362] reported Degussa P25 (anatase: 75%, rutile: 25%) acting as an efficient photocatalyst for the photodegradation of norfloxacin in aqueous suspensions compared to other TiO_2 powders. Cu_2O particles prepared by a hydrothermal method showed a high degradation rate for norfloxacin (79.8%) with ·OH and $\cdot O_2^-$ species playing major roles.[363] The removal of norfloxacin has also been explored in a broad operating pH range *via* simulated solar-light-mediated bismuth tungstate Bi_2WO_6.[364]

3.5.2 Metal–metal oxides composites. Sayed *et al.*[365] prepared immobilized {001}-faceted TiO_2/Ti film by placing Ti plate water/2-propanol solvent and 0.02 M HF (pH: 2.62) under hydrothermal conditions at 180 °C for 3 h and exhibited the following order for the degradation of norfloxacin (10 mg L^{-1}) under UV irradiation: Milli-Q-water (70.5%, k: 0.0504 min^{-1}) > tapwater (~55.1%, k: 0.03 min^{-1}) > river water (44.9%, k: 0.009 min^{-1}) > synthetic wastewater (39.89%, k: 0.005 min^{-1}). Triangular silver nanoplates (T-Ag)/ZnO nanoflowers significantly enhanced the photocatalytic degradation of norfloxacin under visible light due to synergistic effects in the different water matrices.[366] It was concluded that the degradation efficiency for norfloxacin by T-Ag/ZnO nanoflowers is guided by the choice of water source. In another report, Zhang *et al.*[367] prepared triangular Ag nanoplate coated ZnO nanoflowers by a hydrothermal/dual-reduction method and studied its performance in the photocatalytic degradation of NF in aqueous solutions under visible-light irradiation. It should be noted that the improved photocatalytic degradation of NF activity could be ascribed to the synergetic effect and the unique surface plasmon resonance of triangular silver nanoplates in T-Ag/ZnO. In addition, photogenerated holes are considered to be the main oxidative species that account for the photocatalytic degradation of NF by T-Ag/ZnO composites under visible light. A chemically doped Prussian blue in CeO_2 (doping ratio: 10%) photo-Fenton catalyst showed 88.93% degradation of norfloxacin in 30 min with ·OH acting as the major reactive species.[368]

3.5.3 Doped metal oxides. The effect of ion doping on the properties of photocatalysts has been receiving considerable attention in exploring their better performance for wastewater treatment applications.[369] In this regard, the photocatalytic degradation of norfloxacin has been studied using an N-doped TiO_2 catalyst under visible-light irradiation. Jin *et al.*[370] also fabricated TiO_2 doped with nitrogen to enhance its optical response through reduction in the band gap and carried out the photocatalytic degradation of norfloxacin under visible-light irradiation. These investigations indicated almost complete removal of norfloxacin within 30 min under optimum conditions (pH: 6.37, catalyst dose: 0.54 g L^{-1}, norfloxacin: 6.03 mg L^{-1}). Al-doped TiO_2 achieved 93% norfloxacin removal in 2 h which was found to be ~5 times higher than undoped TiO_2 nanoflakes under visible light.[371] The norfloxacin was completely degraded by visible-light-mediated C-doped TiO_2 in 20 min corresponding to a concentration of 0.0313 mM and catalyst dosage of 2.0 g L^{-1}.[372] It was established that the hydroxyl radical plays an important role in the degradation process.

The photocatalytic degradation of norfloxacin (and ciprofloxacin) was found to be 90–93% under optimized

Table 5 Performance data on removal of ibuprofen in waste in water using variety of photocatalysts

Photocatalyst	Preparation method	IPF	Catalyst dose	pH	Light source	% degradation	Rate constant
TiO_2 Degussa P25 (80% anatase and 20% rutile)[294]	Commercial	213 mg L^{-1}	2.5 g L^{-1}	5.0–5.3	UV-LEDs (10 W), 365 nm, 375 W m^{-2}	100% (5 min)	24×10^{-3} min^{-1}
TiO_2 nanoparticles (Degussa P25)[295]	Commercial	5 μg mL^{-1} (50 mL)	134.5 mg	5.5	UV light: 15 W, 365 nm	100% (10 mi)	1.0 min^{-1}
TiO_2 (Vetec, 98% of purity)[296]	Commercial	10^{-4} M (100 mL)	0.03 g	5	Mercury lamp (125 W)	100% (5 min)	—
TiO_2 P-25 Degussa (75 : 25 w/w mixture of anatase : rutile)[297]	Commercial	10 mg L^{-1}	100 mg L^{-1}	4	UVA	~100% (18 min)	0.382 min^{-1}
ZnO Sigma Aldrich[297]	Commercial	10 mg L^{-1}	100 mg L^{-1}	4	UVA	~100% (18 min)	0.326 min^{-1}
TiO_2 P-25 Degussa (75 : 25 w/w mixture of anatase : rutile)[297]	Commercial	10 mg L^{-1}	100 mg L^{-1}	4	Visible	~94% (18 min)	0.199 min^{-1}
ZnO Sigma Aldrich[297]	Commercial	10 mg L^{-1}	100 mg L^{-1}	4	Visible	~90% (18 min)	0.144 min^{-1}
TiO_2 (Sigma-Aldrich)[298]	Commercial	20 mg L^{-1}	1.5 g L^{-1}	3	UV lamp (40 W)	99% (15 min)	0.54 min^{-1}
ZnO (Sigma-Aldrich)[298]	Commercial	20 mg L^{-1}	1.0 g L^{-1}	7	UV lamp (40 W)	86% (15 min)	0.31 min^{-1}
ZnO (Nano pars Spadana)[299]	Commercial	5 mg L^{-1} (humic acid: 50 mg L^{-1})	500 mg L^{-1}	7	125 W medium-pressure Hg lamp (UVC)	98% (100 min)	—
ZnO–Ce[300]	Precipitation method	20 ppm	0.5 g L^{-1}	3	UV light: 125 W Hg without bulb	60% (120 min)	6.86×10^{-3} min^{-1}
ZnO–Ce; H_2O_2: 0.5 m mole per L[300]	Precipitation method	20 ppm	0.5 g L^{-1}	3	UV light: 125 W Hg without bulb	70% (120 min)	—
TiO_2 (Degussa P25) dispersed powder[302]	Commercial	25 mg L^{-1}	0.2 g L^{-1}	4.5	Solar simulator exposed to xenon lamp irradiation	~95% (150 min)	0.2378 mg L^{-1} min^{-1} (zero order), 0.0251 min^{-1} (first order), 0.0034 L mg^{-1} min^{-1} (second order)
TiO_2 immobilized on the active coated glass[302]	Chemical vapour deposition	25 mg L^{-1}	0.2 g L^{-1}	4.5	Solar simulator and exposed to xenon lamp irradiation	100% (1480 min)	0.0124 mg L^{-1} min^{-1} (zero order), 0.0012 min^{-1} (first order), 0.0001 L mg^{-1} min^{-1} (second order)
TiO_2 Degussa (P-25)[303]	Commercial	4 mg L^{-1}	20 mg L^{-1}	7.8	125 W Hg vapor lamp, 10.75 mW cm^{-2}	>98% (30 min)	—
TiO_2 Degussa P25 (ref. 304)	Commercial	5 mg dm^{-3}	50 mg dm^{-3}	—	Mercury lamp (150 W), $\lambda < 300$ nm	~89% (60 min)	0.0425 min^{-1}
ZnO Degussa P25 (ref. 304)	Commercial	1 mg dm^{-3}	50 mg dm^{-3}	—	Mercury lamp (150 W), $\lambda < 300$ nm	60% (30 min)	0.0328 min^{-1}
ZnO nanoparticles[305]	Chemical method	60 ppm	10 mg L^{-1}	—	Four UV-vis solarium lamps (60 W)	24% (180 min)	0.055 min^{-1}
PVDF- ZnO/Ag_2CO_3/Ag_2O membrane[306]	Casting solution using wet phase inversion method	10 ppm (300 mL)	1.96 wt% (membrane area: 12.56 cm^2)	—	White light-emitting diode lamp ($\lambda > 400$ nm, 100 W)	49.96% (180 min)	—
N,S-co-doped TiO_2 nanoparticles[307]	Sol–gel and hydrothermal methods	5 mg L^{-1} (50 mL)	2.0 g L^{-1}	6	Simulated solar radiation: 350 W xenon lamp	85% (90 min)	0.062 min^{-1}
C–N–S co-doped TiO_2[308]	Thermal treatment method	20 ppm (200 mL)	0.5 g L^{-1}	—	LED lamp (λ_{max}: 420 nm, 1 mW cm^{-2})	~100% (300 min)	0.021 min^{-1}
Bi (0.25 wt%) doped TiO_2[309]	Sol–gel method	25 ppm	2 g L^{-1}	6	UV (36 W, 254 nm)	89% (360 min)	0.0064 min^{-1}
Ni (0.5 wt%) doped TiO_2[309]	Sol–gel method	25 ppm	2 g L^{-1}	6	UV (36 W, 254 nm)	78% (360 min)	0.0046 min^{-1}

Table 5 *(continued)*

Photocatalyst	Preparation method	IPF	Catalyst dose	pH	Light source	% degradation	Rate constant
La^{3+}(2%)-doped TiO_2 monolith[310]	Sol–gel method	50 mg L^{-1} (70 mL)	0.1 g	5	Sunlight	96.9% (150 min)	2.2×10^{-2} min^{-1}
C,N-co-doped mesoporous TiO_2[313]	Hydrothermal method	20 ppm (220 mL)	0.5 g L^{-1}	—	High-pressure Hg lamp (150 W), λ_{max}: 254 nm	98.9% (120 min)	0.0377 min^{-1}
C,N-doped mesoporous TiO_2[313]	Hydrothermal method	20 ppm (220 mL)	0.5 g L^{-1}	—	LED lamp (visible light, λ_{max}: 420 nm, 1 mW cm^{-2})	100% (120 min)	0.0207 min^{-1}
N doped CNT COOH/TiO_2 (anatase/rutile: 20/80)[314]	Hydrothermal	5 mg L^{-1} ppm	400 mg L^{-1}	Natural pH	LED light: 240 W, 40 mW cm^{-2} and 410 nm	85–86% (120 min)	4.45×10^{-3}–1.22×10^{-2} min^{-1}
Activated carbon impregnated with TiO_2[316]	Sol–gel method	25 mg L^{-1} (20 mL)	1.6 g L^{-1}	4.3	UV lamp: 15 W, 254 nm	92% (240 min)	—
Fe_3O_4@MIL-53(Fe)[318]	Calcination (400 °C)	10 mg L^{-1} (50 mL), H_2O_2 (20 mM)	0.4 g L^{-1}	—	Xenon lamp (500 W with 420 nm cut-off filter)	99% (60 min)	4.71×10^{-2} min^{-1}
Fe_3O_4/Bi_2WO_6[319]	Two-step approach	10 mg L^{-1} (70 mL)	70 mg	4.7	Solar light	>80% (120 min)	0.0144 min^{-1}
Ag/Fe_3O_4/WO_{3-x}/H_2O_2 (10 mM)[322]	Simultaneous calcination	10 mg L^{-1} (30 mL)	30 mg	—	Xenon lamp (500 W) with optical filter ($\lambda \geq 420$ nm)	~100% (90 min)	—
Ag/ZnO/$CoFe_2O_4$[323]	Coating $CoFe_2O_4$ with ag/ZnO using Pechini method	10 ppm	0.3 g L^{-1}	7	UV light (125 W medium-pressure Hg lamp)	80% (60 min)	0.03905 min^{-1}
BiOBr/Fe_3O_4@SiO_2[324]	Solvothermal	2 mg L^{-1}	1 g L^{-1} (50 ml)	7	Fluorescent lamp (visible light)	~99% (60 min)	0.08 min^{-1}
TiO_2/ZnO/copper phthalocyanine (CuPc)[326]	Multiple steps	5 mg L^{-1} (50 mL)	Film	6.5	Hg lamp with 365 nm cut-off filter, 1,2 W cm^{-2}	80% (240 min)	0.42 h^{-1}
PAN–MWCNT/TiO_2–NH_2[328]	Electrospinning	5 mg L^{-1} (100 mL)	15 mg L^{-1}	2	UVA lamp (315–400 nm) of 40 W	~100% (120 min)	—
Carbon dots/Fe_3O_4@carbon sphere (in presence of persulfate)[330]	Solvothermal method	50 μmol L^{-1}	0.3 g L^{-1}	—	Xenon lamp (350 W) with a glass filter ($\lambda > 420$ nm)	96% (120 min)	—
PAN–MWCNT/TiO_2–NH_2 composite nanofibers[332]	Multiple steps	5 mg L^{-1} (100 mL)	15 mg	2	Xenon lamp (125 W) with cut-off filter ($\lambda > 400$ nm), 0.1 W cm^{-2}	100% (210 min)	—
g-C_3N_4[333]	Polycondensation	20 mg L^{-1} (200 mL)	200 mg	5.5	Xenon lamp (35 W)	20% (4 h)	—
Reduced graphene oxide–$HoVO_4$–TiO_2[335]	Hydrothermal	10 mg L^{-1}	40 mg L^{-1}	7	Tungsten lamp (150 W), ($\lambda > 4900$ nm)	~96% (60 min)	—
g-C_3N/ag/AgCl/$BiVO_4$[337]	Hydrothermal	2 mg (50 mL)	0.25 g L^{-1}	4	Visible light	94.7% (60 min)	—
Ag (7%)/g-C_3N_4/kaolinite[338]	Two steps	5 ppm (50 mL)	50 mg	—	Xenon lamp (500 W with 400 nm cut-off filter)	99.9% (300 min)	0.01128 min^{-1}
Graphene quantum dots (3 wt%)/$AgVO_3$[339]	Hydrothermal	10 mg L^{-1} (50 mL)	0.01 g	—	Xenon lamp (350 W with $\lambda > 420$ nm)	~100% (180 min)	0.1678 min^{-1}
g-C_3N_4 (10 wt%)/MIL-68(In)–NH_2 composites[340]	*In situ* solvothermal assisted by ultrasonication	20 mg L^{-1}	0.15 g	4	Xenon lamp (300 W with $\lambda > 420$ nm)	93% (120 min)	0.01739 min^{-1}
Graphene oxide/TiO_2 doped with F (BrO_3^- 100 μg L^{-1})[341]	Hydrothermal	100 μg L^{-1}	0.05 g L^{-1}	5.2	Low-pressure Hg lamp (10 W), (26 μW cm^{-2})	~100% (60 min)	0.4504 min^{-1}
rGO–TiO_2/sodium alginate[273]	Hydrothermal	10 ppm (200 mL)	0.5 g L^{-1}	7	High-pressure Hg lamp (100 W), (13.5 W m^{-2})	~100% (90 min)	0.047 min^{-1}
TiO_2/5% g-C_3N_4[343]	Solvothermal	5 mg L^{-1}	50 mg	7	Xenon lamp (259 W)	~90% (60 min)	0.03833 min^{-1}
g-C_3N_4/Bi_2WO_6 (1 : 4 molar ratio)[344]	Hydrothermal	25 μM	0.2 g L^{-1}	—	Xenon lamp (300 W) with 420 nm cut-off filter	~96.1% (60 min)	0.062 min^{-1}
g-C_3N_4/TiO_2/Fe_3O_4@SiO_2[345]	Sol–gel method	2 mg L^{-1} (50 mL)	50 mg	7	Visible light, 330 W m^{-2}	97% (15 min)	—
FeV_3O_8 (10%)/g-C_3N_4[347]	Dispersion, grinding and calcination	10 ppm (30 mL)	10 mg	—	Xenon lamp (300 W) with UV cut-off filter (λ: 420 nm)	95% (85 min)	0.03 min^{-1}

Table 5 *(continued)*

Photocatalyst	Preparation method	IPF	Catalyst dose	pH	Light source	% degradation	Rate constant
g-C_3N_4/Bi_2WO_6/rGO[348]	Microwave assisted hydrothermal preparation	5 mg L^{-1}	1.0 g L^{-1}	4.3	Xenon lamp (300 W), $\lambda > 420$ nm	93% (240 min)	0.011 min^{-1}
g-C_3N_4/Bi_2WO_6/rGO[348]	Microwave assisted hydrothermal preparation	5 mg L^{-1}	1.0 g L^{-1}	4.3	Sunlight	98.6% (240 min)	—
AgSCN/Ag_3PO_4/C_3N_4 (molar % of AgSCN: 11.3)[351]	Precipitation reaction	5 mg L^{-1} (100 mL)	50 mg	—	Sunlight (500 W halide lamp)	91% (6 min)	0.46 min^{-1}
N–TiO_2@SiO_2@Fe_3O_4[352]	Sol–gel method	2 mg L^{-1} (50 mL)	50 mg	—	Fluorescent lamps (9 W), 320 μW cm^{-2}	94% (300 min)	—
g-C_3N_4/CQDs/$CdIn_2S_4$[353]	Hydrothermal	80 mg L^{-1} (100 mL)	0.1 g	—	300 W xenon lamp with 420 nm cut-off filter, 200 mW cm^{-2}	91% (60 min)	—
Co_3O_4/BiOI (1 : 2)[354]	Solvothermal	10 ppm (50 mL)	40 mg	11.3	60 W LED lamp with 420 nm cut-off filter	93.87% (60 min)	0.0945 min^{-1}
α-$SnWO_4$/UiO-66(NH_2)/g-C_3N_4[355]	Solvothermal	10 mg L^{-1} (100 mL)	50 mg	—	Simulated sunlight using high-pressure 300 W xenon lamp	95.5% (120 min)	0.017 min^{-1}

conditions in B and Ce doped TiO_2, irradiated by sunlight.[373] Bi^{3+} and Fe^{2+} ion doped ZnO showed significant photocatalytic degradation of norfloxacin with the addition of HSO_5^- under solar irradiation and followed pseudo-first-order kinetics.[374] The co-doped ZnO exhibited a lower band gap, which accounted for the increased absorption of solar irradiation and reduced electron and hole recombination, which facilitated high norfloxacin degradation compared to undoped ZnO. Fe-doped CeO_2 exhibited about 95% photocatalytic degradation of norfloxacin in aqueous solution (pH: 8.0) within 180 min corresponding to an initial norfloxacin concentration of 2.5 mg L^{-1} and catalyst dose of 0.1 g L^{-1}.[375] An Ag-doped TiO_2/CFA (coal fly ash) photocatalyst has also been used to monitor the photocatalytic degradation of norfloxacin.[376]

3.5.4 Metal oxide–metal oxide composites. A mesoporous Fe_2O_3–TiO_2 photocatalyst showed complete norfloxacin removal from aqueous solution (pH: 7) within 120 min under UV illumination with a stoichiometric amount of H_2O_2.[377] Trang *et al.*[378] used an ordered SBA-15 mesoporous silica support synthesized by a sol–gel method using the triblock copolymer Pluronic P123 and immobilized with different amounts of photocatalyst TiO_2 (TiO_2 : SiO_2 ratios of 0, 0.25, 1.0 and 5.0). Subsequent investigations on the removal of norfloxacin revealed the better photocatalytic activity of 1.0TiO_2/SBA-15 hybrid material in achieving 96.6% degradation of norfloxacin in 150 min under UV-light irradiation. Fe-complex/TiO_2 composites comprising [Fe^{II}(dpbpy)$_2$ (H_2O)$_2$]/TiO_2, [Fe^{II}(dpbpy)(phen)$_2$]/TiO_2 and [Fe^{II}(dpbpy)(bpy)$_2$]/TiO_2 (dpbpy: 2,2′-bipyridine-4,4′-diphosphoric acid, phen: 1,10-phenanthroline, bpy: 2,2-bipyridyl) photocatalysts exhibited 98.5% degradation of norfloxacin in water under visible-light irradiation after 3 h.[379] Further, the photocatalytic performance and cyclic stability of these composites were found to be much better than those of pure TiO_2 or P25. An Ag_2O/TiO_2-zeolite composite fabricated through a modified sol–gel method exhibited high performance in the decomposition of norfloxacin under simulated solar-light illumination.[380] This is a consequence of the narrow band gap of the photocatalyst, its enhanced light absorbance ability in the visible region and high charge separation efficiency.

$FeVO_4$/Fe_2TiO_5 (2 : 1) synthesized *via* a one-pot hydrothermal method exhibited high photocatalytic activity and excellent stability for the removal of norfloxacin in aqueous solution under visible-light irradiation.[381] This is ascribed to the synergistic effect of photogenerated electron–holes with radical OH· and h^+. MIL-101(Fe)–NH_2 immobilized on an α-Al_2O_3 sheet has also been investigated for effective norfloxacin elimination *via* a photo-Fenton process.[382] Ag/AgCl–CeO_2 composite photocatalysts fabricated by *in situ* interspersal of AgCl on CeO_2 and subsequent photoreduction of AgCl to Ag exhibited enhanced photocatalytic activity in the photodegradation of norfloxacin under visible-light irradiation.[383] Fig. 14(a) shows the highest degradation efficiency (91%) for norfloxacin achieved by sample Ag/AgCl–CeO_2 composites with an Ag mass ratio of 13.94 wt% (denoted AC-3) within 90 min under visible-light irradiation. It is also apparent from Fig. 14(b) and (c) that the photodegradation process followed a pseudo-first-order kinetic model with the highest rate constant (0.02279 min^{-1}) for AC-3 compared to CeO_2, Ag/AgCl, Ag/CeO_2 and other AC composites. Fig. 14(d) shows the time-dependent UV-vis spectra of NOF solution for the AC-3 sample. ZnO/ZnS@biochar,[384] $ZnFe_2O_4$/hydroxyapatite–Sn^{2+},[385] $(BiO)_2CO_3$–Bi–TiO_2,[386] and Ag/AgCl/Ag_2MoO_4[387] composites have also been reported as promising photocatalysts in the degradation of norfloxacin in water under UV irradiation.

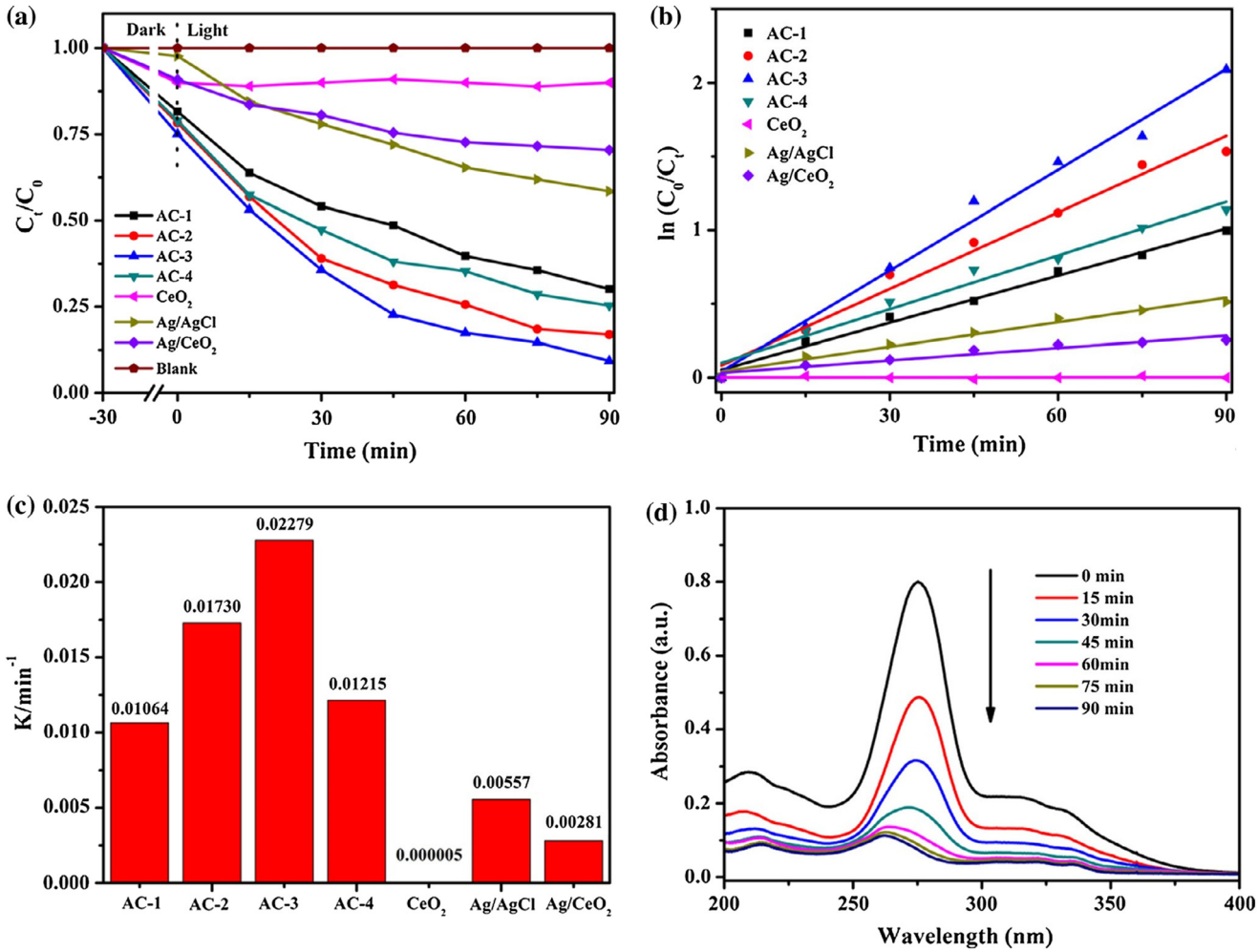

Fig. 14 (a) Photocatalytic degradation NOF curves; (b) kinetic curves of NOF degradation; (c) apparent rate constants for the degradation of NOF; (d) time-dependent UV–vis spectra of NOF solution for AC-3 sample (Ag/AgCl–CeO_2). Reproduced from ref. 383 with permission from Elsevier (2017).

3.5.5 Graphitic composites

3.5.5.1 g-C_3N_4-based composites. Fei *et al.*[388] investigated the photocatalytic degradation of norfloxacin in the presence of a sunlight-driven mesoporous g-C_3N_4. The results showed 90% decomposition of norfloxacin in 1.5 h under simulated sunlight irradiation. Co/g-C_3N_4, Co/g-C_3N_4/H_2O_2 and Co/g-C_3N_4/PMS composite photocatalysts exhibited better performance compared to pure g-C_3N_4 in the photocatalytic degradation of norfloxacin under visible-light irradiation.[389] The optimization and variations of different parameters have been used to study the photocatalytic degradation of norfloxacin in the presence of ZnO/g-C_3N_4/Fe_3O_4 under visible light.[390] These findings indicated a removal rate of norfloxacin greater than 90% in 120 min for a catalyst concentration of 1.43 g L^{-1}, solution pH 7.12 and norfloxacin concentration of <8.61 mg L^{-1}. Shuttle-like CeO_2/g-C_3N_4 combined with persulfate[391] and $NiWO_4$ nanorods anchored on g-C_3N_4 nanosheets[392] also exhibited enhanced degradation of norfloxacin under visible light.

3.5.5.2 Graphene-based composites. A TiO_2/Bi_2WO_6/rGO (0.5%) photocatalyst attained about 87.79% removal of norfloxacin in water under visible-light irradiation after 60 min and was found to be superior to its individual components under optimal conditions.[393] Such enhanced catalytic activity of TiO_2/Bi_2WO_6/rGO arises due to the ligand–metal electron transfer mechanism. According to Zhao *et al.*,[394] an rGO/Bi_2WO_6 composite exhibited outstanding photocatalytic activity for norfloxacin degradation in an aquatic environment under visible-light irradiation, as evident from the time-dependent-UV spectrum and time-dependent-HPLC spectrum displayed in Fig. 15(a) and (b), respectively. Fig. 15(c) and (d) indicate about 87.49% degradation of norfloxacin within 180 min compared to Bi_2WO_6, under visible-light irradiation. Additional investigations revealed ·OH and e^- playing dominant roles in the photocatalytic degradation of norfloxacin. N-doped TiO_2/graphene exhibited enhanced photocatalytic degradation under UV-light irradiation.[395] It is suggested that graphene acts as an efficient "electron pump",

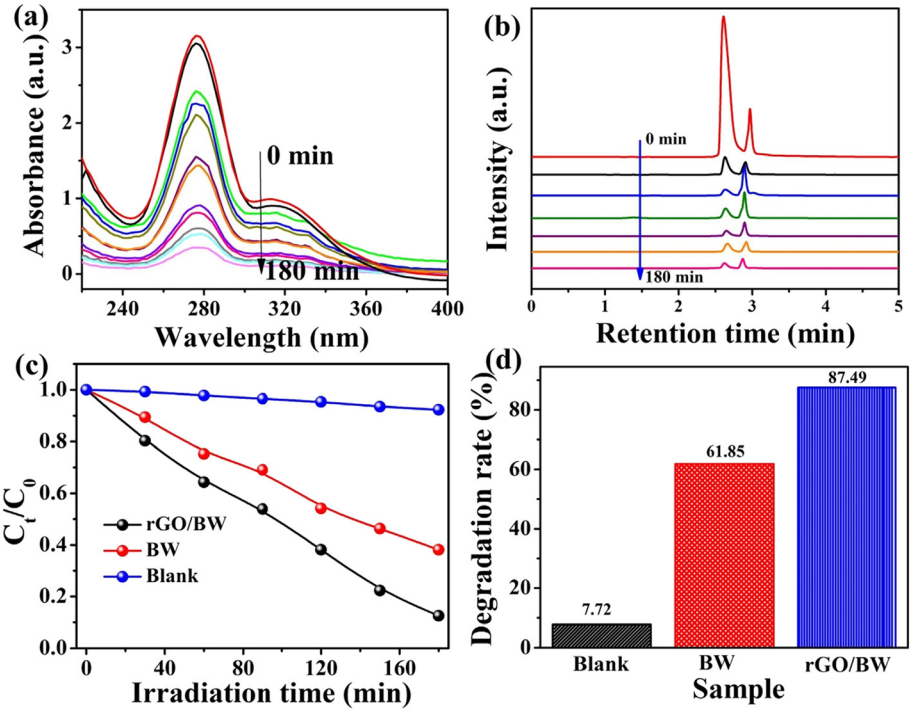

Fig. 15 (a) The time-dependent UV spectrum, (b) the time-dependent-HPLC spectrum, (c) the photodegradation curve, and (d) photocatalytic degradation rate of norfloxacin. Reproduced from ref. 394 with permission from Elsevier (2021).

thereby promoting the separation of carriers to account for the observed photodegradation.

Wu *et al.*[396] reported a UV-assisted nitrogen-doped reduced graphene oxide/Fe_3O_4 composite by a simple hydrothermal–co-precipitation method and investigated the degradation of norfloxacin with activated peroxodisulfate. These findings demonstrated 100% degradation efficiency of norfloxacin (pH: 3.0) within 13 min due to an excellent synergistic effect at m(NGO–Fe_3O_4):m(PDS) of 4:1, and concentrations of NOR and $S_2O_8^{2-}$ of 100 mg L^{-1} and 1 mM, respectively. According to this, *in situ* generated ·OH was considered to be the main active free radical. rGO-coupled manganese oxynitride,[397] immobilized Ag_3PO_4/GO on 3D nickel foam[398] and γ-Fe_2O_3-MIL-53(Fe)–GO[399] photocatalysts also displayed efficient degradation of norfloxacin.

3.5.6 Heterojunction, Z- and S-scheme-based composites. Ni-doped ZnO/MWCNTs were tested for complete degradation of norfloxacin corresponding to initial concentrations in mg L^{-1} (time in min) of 10 (30), 20 (60), 50 (120), 100 (160) and 10 (40), 20 (70), 50 (150), 100 (200) under visible and UV radiation, respectively.[400] The findings also suggested that MWCNTs can act as a charge transfer channel for accelerating electron transfer between Ni and ZnO nanoparticles. This could subsequently effectively decrease the recombination of electron–hole pairs in the Ni-doped ZnO/MWCNTs composite, accounting for the degradation of norfloxacin by the Ni-doped ZnO/MWCNTs photocatalyst. A Bi-containing glass–ceramic defect-rich heterojunction photocatalyst originating from the removal of chloride ions achieved 98%, 73%, and 36% degradation of norfloxacin under UV-vis–NIR, vis–NIR, and NIR irradiation, respectively.[401] Guo *et al.*[402] prepared Co_3O_4/Bi_2MoO_6 p–n heterostructure photocatalysts *via* an *in situ* calcination process and applied them to activate peroxymonosulfate (PMS) in the degradation of norfloxacin under irradiated visible light. These findings indicated 87.68% removal of norfloxacin within 30 min by selecting a 5 wt% Co_3O_4/Bi_2MoO_6/PMS photocatalyst owing to the synergistic effect. A $CoTiO_3$/UiO-66-NH_2 p–n junction mediated heterogeneous photocatalyst showed 90.13% degradation of norfloxacin in 1 h under optimized conditions and followed a type-II p–n heterojunction charge transfer mechanism.[403] An LaOCl/LDH Z-scheme heterojunction catalyst containing oxygen vacancies showed a 82.5% (150 min) removal rate for norfloxacin owing to the synergistic effect of the Z-scheme heterojunction and oxygen vacancies.[404] Further, the degradation of norfloxacin followed pseudo-first-order kinetics with the rate constant of LaOCl/LDH twice that of the individual components.

Z-Scheme ternary heterojunctions comprising phosphate-doped $BiVO_4$/graphene quantum dots/P-doped g-C_3N_4 (BVP/GQDs/PCN) produced an 86.3% degradation rate for norfloxacin under visible light.[405] Such an excellent performance of the photocatalyst is guided by interfacial charge transfer efficiency and a broadened visible-light response range compared to binary type-II heterojunction phosphate-doped $BiVO_4$/PCN. $CoWO_4$ nanoparticles assembled with g-C_3N_4 nanosheets fabricated by a hydrothermal method showed 3.18 and 2.69 times higher photocatalytic degradation of norfloxacin under visible light compared to g-C_3N_4 and $CoWO_4$, respectively.[406] Such

enhanced performance of $CoWO_4$/g-C_3N_4 is attributed to the synergism between $CoWO_4$ and g-C_3N_4 inhibiting the fast recombination of photogenerated electron–hole pairs. Investigations involving radical scavengers suggested that ·OH rather than $O_2^{-\bullet}$ plays a dominant role in the degradation of norfloxacin. Fig. 16 shows the possible mechanism responsible for the photodegradation of norfloxacin by this synthesized $CoWO_4$/g-C_3N_4, a phenomenon driven through a Z-scheme mechanistic pathway.

A $Bi_2Sn_2O_7$/heated perylene diimide (PDIH) Z-scheme heterojunction photocatalyst reached 98.71% degradation of norfloxacin in 90 min under visible light.[407] The apparent rate constant of norfloxacin was found to be 3.65 and 20 times those of PDIH and $Bi_2Sn_2O_7$, respectively. The fabricated $Bi_2Sn_2O_7$/PDIH heterojunction catalyst also facilitated the separation of charge carriers and preserved the redox capability. In another study, piezo-photocatalytic degradation of norfloxacin by the S-scheme heterojunction $BaTiO_3/TiO_2$ was found to be 91.7% (60 min) with a rate constant of 43 × 10^{-3} min^{-1}.[408] Free radical trapping investigations indicated h^+ and ·OH to be the main active species in the degradation process. The heterojunction also showed excellent stability and cyclability, as evident after 5 cycles. An $LaFeO_3$/g-C_3N_4 heterojunction showed 95% photocatalytic degradation of norfloxacin under visible light in 180 min, which was found to 9.32 times higher than pristine g-C_3N_4.[409] Zhang *et al.*[410] prepared an optimized AgBr (3%)/$LaNiO_3$ (30%)/g-C_3N_4 (100%) dual Z-scheme composite system *via* ultrasound-assisted hydrothermal method considering energy band matching and observed 92% photodegradation of norfloxacin within two hours under visible light owing to a synergistic effect. These studies also indicated an almost unaltered photodegradation rate (>90%) even after six cycles.

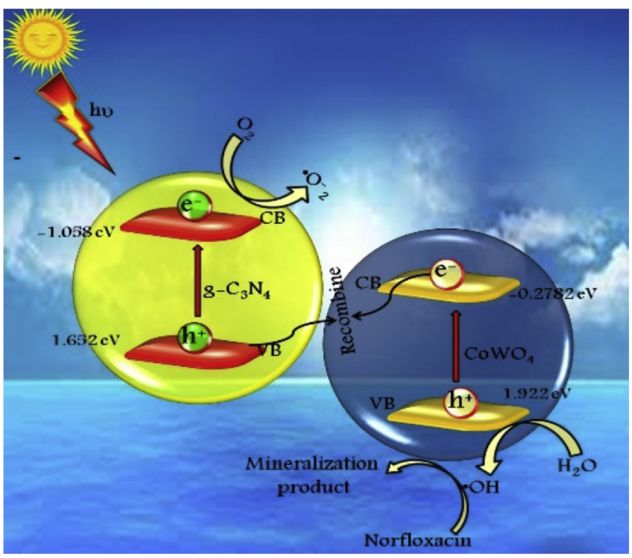

Fig. 16 Schematic illustration of possible Z-scheme photocatalytic mechanism. Reproduced from ref. 406 with permission from Elsevier (2019).

Ag_3PO_4/CNTs exhibited an efficiency of about 93% for the photoelectrocatalytic degradation of NOR within 30 min.[411] This is explained based on the Z-scheme mechanism that significantly promoted the separation of electron–hole pairs. Further, h^+ and $\cdot O_2^-$ made a major contribution to the degradation process to oxidize NOR. An oxygen-vacancy-rich $CuWO_4$/BiOCl composite exhibited excellent photocatalytic degradation of norfloxacin (96.69%) in 120 min under a 300 W xenon lamp due to a Z-scheme structure compared with pure $CuWO_4$ and oxygen-vacancy-rich BiOCl.[412] A dual Z-scheme mechanism has been proposed for Ag (0.3 wt%) @$BiPO_4$/BiOBr/$BiFeO_3$ that enabled 98.1% and 99.1% degradation of norfloxacin (20 mg L^{-1}) in 90 min and in less than 45 min under visible and UV light exposure, respectively.[413] It is suggested that the synergistic effects of ternary nanoheterostructures heterojunctions, electron capture and the surface plasmon resonance effect of Ag lead to such high photocatalytic activity. Immobilized Z-scheme CdS/Au/TiO_2 nanobelts displayed 64.67% (60 min) degradation of norfloxacin under xenon-light-simulated sunlight irradiation which was ascribed to the synergistic effect.[414]

The formation of an S-scheme in the heterojunction of a photocatalyst facilitates the separation of photogenerated electron–hole pairs and reduces the recombination of charge carriers. In view of this, an S-scheme heterojunction comprising N–ZnO/g-C_3N_4 prepared by calcining ZIF-L/g-C_3N_4 in a mass ratio of 15% showed more than 90% degradation of norfloxacin in 90 min under a visible system.[415] The corresponding rate constant was 4.15 times and 4.65 times higher than g-C_3N_4 and N–ZnO, respectively. The effective light capture capacity and migration and separation of carriers accounted for such behavior. Further, holes and superoxide radicals are reported to be the active species in the photodegradation of norfloxacin. The degradation rate of norfloxacin on a 10% g-C_3N_4/$Bi_8(CrO_4)O_{11}$ heterojunction photocatalyst is about 1.38 and 2.33 times higher than that of pure $Bi_8(CrO_4)O_{11}$ and g-C_3N_4, respectively.[416]

Efficient photocatalytic performance for norfloxacin degradation has also been reported in chitosan/TiO_2@g-C_3N_4,[417] AgI/$MFeO_3$/g-C_3N_4 (M: Y, Gd, La),[418] $Bi_2Sn_2O_7$/g-C_3N_4,[419] Ag/graphitic carbon nitride quantum dots (CNQDs)/g-C_3N_4,[420] BiOBr/iron oxides,[421] and CdS QDs/$CaFe_2O_4$@$ZnFe_2O_4$[422] photocatalysts.

Table 6 records the performance data of different photocatalysts on the removal of norfloxacin from wastewater.

3.6 Ciprofloxacin

Ciprofloxacin (CIP) is a synthetic antimicrobial agent of the fluoroquinolone class and considered to be a very promising and efficacious drug for use in the treatment of various community-acquired and nosocomial infections.[360,423,424] It

Table 6 Performance data on removal of norfloxacin in water using various photocatalysts

Photocatalyst	Preparation	NOR	Catalyst dose	pH	Light type	Degradation (time)	Rate constant
TiO_{2-x}[361]	Combustion method	100 μM L^{-1}	0.1 g L^{-1}	7	Xenon lamp: 300 W (>400 nm)	~100% (240 min)	0.0361 min^{-1}
Cu_2O[363]	Hydrothermal	20 mg L^{-1}, (50 mL)	50 mg	—	Xenon lamp (500 W)	79.87% (210 min)	0.0081 min^{-1}
Bi_2WO_6 with $[Fe^{3+}]$: 0.3 mmol L^{-1}[364]	Ultrasonic spray pyrolysis	0.0313 mM L^{-1} (100 mL)	0.5 g L^{-1}	9	Xenon lamp: 300 W	89.7% (20 min)	0.1006 min^{-1}
TiO_2/Ti film with exposed {001} facets (HF: 0.02 M)[365]	Hydrothermal	10 mg L^{-1}	—	2.62	Low-pressure mercury lamp (10 W), λ_{max}: 254 nm	70.5% (90 min)	0.0504 min^{-1}
ZnO nanoflowers[366]	Sol–gel method	10 mg L^{-1}	0.1 g L^{-1}	11	Fluorescent lamp: 8 W (0.55 mW cm^{-2})	~72% (100 min)	3.93 × 10^{-2} min^{-1}
Triangular Ag nanoplates coated ZnO nanoflowers[366]	Sol–gel method	10 mg L^{-1}	1.0 g L^{-1}	11	Fluorescent lamp (8 W), 0.55 mW cm^{-2}	~97% (100 min)	3.93 × 10^{-2} min^{-1}
Triangular Ag nanoplates coated ZnO nanoflowers[367]	Hydrothermal method and dual-reduction method	10 ppm (3 mL)	—	—	Fluorescent lamp (8 W), 0.55 mW cm^{-2}	92.2% (270 min)	9.2 × 10^{-3} min^{-1}
Prussian blue doped CeO_2 (ratio: 10%) with H_2O_2: 9 mM[368]	Physical and chemical loading approaches	16 mg L^{-1} (50 mL)	0.6 g L^{-1}	6	W fluorescent lamp (0.55 mW cm^{-2})	88.93% (30 min)	—
N doped TiO_2[370]	Hydrothermal method	6.03 mg L^{-1}	0.54 g L^{-1}	6.37	Xenon lamp (300 W), 350–780 nm, 150 mW cm^{-2}	99.53% (30 min)	—
Al (1 Mol%)-doped TiO_2 nanoflakes[371]	Solvothermal	2 × 10^{-4} M	15 mg (50 ml)	10.1	Visible light	93% (120 min)	0.0143 min^{-1}
C–TiO_2[372]	Solution phase carbonization method	0.0094 mM	0.2 g L^{-1}	Neutral	Low-pressure mercury lamps (420 nm)	~100% (70 min)	5.44 × 10^{-4} $[NFX]_0$-1 + 0.10 [C–TiO_2] – 1.99 × 10^{-2} min^{-1}
Bi^{3+} and Fe^{2+} doped ZnO[374]	Sol–gel method	10.0 mg L^{-1}	1.0 g L^{-1}	8	Xenon lamp (300 W), 45.2 mW cm^{-2}	80% (120 min)	—
Bi^{3+} and Fe^{2+} doped ZnO (0.2 mM HSO_5^-)[374]	Sol–gel method	10.0 mg L^{-1}	1.0 g L^{-1}	8	Xenon lamp (300 W), 45.2 mW cm^{-2}	99% (120 min)	9.8 × 10^9 M^{-1} s^{-1} (·OH), 9.0 × 10^9 M^{-1} s^{-1} ($SO_4^{\cdot-}$)
[FeII(dpbpy)$(phen)_2$]/TiO_2[379]	Hydrothermal	0.313 mM	1 g L^{-1}	5	Xenon lamp (300 W), λ > 420 nm, 140 mW cm^{-2}	98.5% (180 min)	0.0412 min^{-1}
Ag_2O/TiO_2–zeolite[380]	Sol–gel method	5 mg L^{-1} (100 mL)	50 mg	—	Xenon lamp (35 W), 6.7 mW cm^{-2}	98.7% (60 min)	—
$FeVO_4$/Fe_2TiO_5 (2 : 1)[381]	One-pot hydrothermal method	10 mg L^{-1} (50 mL)	0.05 g	—	500 W Xe lamp	95% (30 min)	—
Ag/AgCl–CeO_2 (Ag mass ratio: 13.94 wt%)[383]	*Via* urea hydrolysis and calcination	10 mg L^{-1} (50 mL)	30 mg	—	Xe lamp: 300 W (equipped with a UV cut-off filter)	91% (90 min)	0.02279 min^{-1}
ZnO/ZnS@biochar ($ZnSO_4$/poplar sawdust ratio: 1 : 1)[384]	Impregnation-roasting method	0.025 g L^{-1} (50 mL)	0.5 g L^{-1}	7	UV-light	95% (180 min)	0.021 min^{-1}
Ag/AgCl/Ag_2MoO_4[387]	*In situ* photoreduction	10 mg L^{-1} (50 mL)	30 mg	—	Xenon lamp: 300 W, (λ > 420 nm)	~65% (90 min)	—
ZnO/g-C_3N_4–Fe_3O_4[390]	Hydrothermal	8.61 mg L^{-1}	1.43 g L^{-1}	7.12	Xenon lamp with 280 nm UV filter	>90% (120) min	0.0117 min^{-1}
CeO_2/g-C_3N_4 (mass ratio of CeO_2 to g-C_3N_4:5 and PS: 5 mM)[391]	Mixing method	10 mg L^{-1} (50 mL)	0.05 g	2	150 W high-pressure xenon lamp with cut-off λ of 420 nm	88.6% (60 min)	0.03573 min^{-1}
$NiWO_4$ nanorods/g-C_3N_4[392]	Hydrothermal followed	10 mg L^{-1}	50 mg	—	W lamp (visible light),	97%	0.0547

Table 6 *(continued)*

Photocatalyst	Preparation	NOR	Catalyst dose	pH	Light type	Degradation (time)	Rate constant
	by sonication		(100 mL)		150 mW cm^{-2}	(60 min)	min^{-1}
rGO/Bi_2WO_6[394]	Hydrothermal	10 mg mL^{-1} (100 mL)	50 mg	—	Xenon lamp (300 W)	87.79% (180 min)	—
N–TiO_2/graphene[395]	Three-step method	30 mg L^{-1} (20 mL)	—	—	Mercury lamp (250 W), 365 nm	50% (160 min)	0.0051 min^{-1}
N-doped rGO/Fe_3O_4 [*m*(N–GO–Fe_3O_4): *m*(peroxodisulfate) = 4 : 1][396]	Hydrothermal-co-precipitation	100 mg L^{-1}, $S_2O_8^{2-}$: 1 mM	1 g L^{-1}	3	UV lamp: 15 W, 254 nm, 44 μW cm^{-2}	100% (13 min)	0.238 min^{-1}
Ni foam supported Ag_3PO_4/GO (16.78 wt%)[398]	Dip-coating	15 mg L^{-1} (120 mL)	—	—	Xenon lamp (250 W) with 400 nm cut-off filter, 100 mW cm^{-2}	83.68% (100 min)	0.426 min^{-1}
γ-Fe_2O_3-MIL-53(Fe)–GO[399]	Multiple steps	10 mg L^{-1}	20 mg	—	500 W Xe lamp (100 mW cm^{-2}), (420 nm cut-off filter)	92.8% (90 min)	—
Ni-doped ZnO/MWCNTs[400]	Dispersion method	100 mgL^{-1} (100 mL)	—	6.8	UV	100% (200 min)	—
					Visible	100% (160 min)	
Bi contained glass–ceramic[401]	Multiple steps	20 mg L^{-1} (20 mL)	20 mg	—	UV-vis–NIR	~53% (180 min)	6.76 × 10^{-3} min^{-1}
Bi contained glass–ceramic[401]	Multiple steps	20 mg L^{-1} (20 mL)	20 mg	—	Visible	~35% (180 min)	2.52 × 10^{-3} min^{-1}
Bi contained glass–ceramic[401]	Multiple steps	20 mg L^{-1} (20 mL)	20 mg	—	UV	~52% (180 min)	4.05 × 10^{-3} min^{-1}
LaOCl/LDH[404]	Precipitation method	10 mg L^{-1} (50 mL)	20 mg	7	Xenon lamp: 300 W	85% (80 min)	0.014 min^{-1}
Phosphate-doped $BiVO_4$/graphene quantum dots/P-doped g-C_3N_4[405]	Hydrothermal	20 mg L^{-1} (50 mL)	50 mg	9.6	Xenon lamp (300 W) with a 420 nm cut-off filter	86.3% (120 min)	0.0148 min^{-1}
$CoWO_4$/g-C_3N_4[406]	Hydrothermal method, followed by ultrasonication	10 mg L^{-1} (100 mL)	50 mg	—	250 W halogen lamps (visible light)	91% (80 min)	0.0283 s^{-1}
$LaFeO_x$/g-C_3N_4[409]	Ultrasound assisted hydrothermal method	20 mg (100 mL)	20 mg L^{-1}	—	Xenon lamp with 420 nm cut-off filter	95% (180 min)	0.01371 min^{-1}
3 wt% AgBr/30 wt% $LaNiO_3$/100% g-C_3N_4[410]	Ultrasound-assisted hydrothermal method	20 mg L^{-1} (100 mL)	20 mg	7	Xenon lamp (500 W) with a 420 nm cut-off filter	92% (120 min)	0.01790 min^{-1}
0.3 wt% ag@$BiPO_4$/BiOBr/$BiFeO_3$[413]	Precipitation-wet impregnation-photo deposition method	20 mg L^{-1}	0.3 g	7.3	Visible	98.1% (90 min)	0.04123 min^{-1}
0.3 wt% ag@$BiPO_4$/BiOBr/$BiFeO_3$[413]	Precipitation-wet impregnation-photo deposition method	20 mg L^{-1}	0.3 g	7.3	UV	99.1% (45 min)	0.07023 min^{-1}
Immobilized CdS/au/TiO_2[414]	Multiple steps	5 mg L^{-1} (35 mL)	4 cm^3	—	Xenon lamp (35 W)	64.67% (60 min)	0.018 min^{-1}
AgI/$LaFeO_3$/g-C_3N_4[418]	Ultrasound-assisted hydrothermal approach	20 mg L^{-1} (100 ml)	0.2 g	—	Xenon lamp (500 W), (40 mW cm^{-2})	95% (180 min)	0.0188 min^{-1}
20% $Bi_2Sn_2O_7$/g-C_3N_4[419]	Ultrasound-assisted hydrothermal method	20 mg L^{-1} (100 mL)	0.02 g	—	500 W xenon lamp with a UV cut-off filter	94% (180 min)	0.01261 min^{-1}
BiOBr/iron oxides[421]	*In situ* co-precipitation method	10 mg L^{-1} (50 mL)	0.5 g	~7	800 W xenon lamp with 420-nm cut-off filter	99.8% (90 min)	~0.076 min^{-1}

is not easily biodegradable and is considered a potential risk to human health. The presence of ciprofloxacin in water acts as pollutant and can be removed by means of a photocatalytic approach.[425–524]

3.6.1 Metal oxides

3.6.1.1 TiO_2. The photocatalytic degradation of ciprofloxacin as a micropollutant in water has been receiving considerable attention in the presence of metal oxides. Zeng *et al.*[424] used carbon-dot-doped TiO_2 to investigate the kinetics, mechanism and pathway following heterogeneous photocatalytic ozonation degradation of ciprofloxacin. It was noted that 1.0 wt% introduction of carbon dots enhanced the degradation of CIP by 91.1% compared to pristine TiO_2 (64%) in 30 min. Several studies have been made on

ciprofloxacin degradation using commercial TiO_2 as a photocatalyst irradiated with simulated solar light,[425,426] artificial sunlight,[426] simulated sunlight[427] and UVA/LED[428] and UVC radiation.[429] TiO_2 nanoparticles irradiated with UVA light demonstrated removal of ciprofloxacin (300 μg L^{-1}) from water in less than 6 minutes.[430] The hydrothermally synthesized mesoporous TiO_2 exhibited 96% photocatalytic degradation of ciprofloxacin hydrochloride (CIP·HCl) under artificial sunlight compared to that prepared by calcination of a titanium glycolate precursor and subsequent hydrothermal-calcination.[431] This is ascribed to the higher electron–hole separation and charge transfer capability.

Li *et al.*[432] fabricated 3D tripyramid TiO_2 (TP-TiO_2) architectures and rod-like morphology of TiO_2 (RL-TiO_2) and studied their application in the photocatalytic degradation of ciprofloxacin hydrochloride under UV-vis-light irradiation. They observed relatively superior removal efficiency (90% within 60 min) for ciprofloxacin and its significantly higher rate constants in the presence of TP-TiO_2 compared to RL-TiO_2. This is ascribed to the key role played by superoxide radicals and photogenic holes in the degradation of ciprofloxacin. Usman *et al.*[433] used TiO_2 nanoparticles (50 mg) in the ~91% degradation of ciprofloxacin aqueous solution (pH: 5.5) on irradiation by a white mercury UV lamp for 5 hours.

3.6.1.2 ZnO and other oxides. ZnO (125 nm) is found to be a very effective photocatalyst in removing 300 μg L^{-1} ciprofloxacin from aqueous solution treated by UVA in less than 6 minutes.[430] ZnO nanoparticles prepared by a chemical precipitation method on irradiation with UV light (365 nm) for 60 min degraded ciprofloxacin (~48%) in aqueous solution (pH: 10) and also followed pseudo-first-order kinetics (~0.00437 min^{-1}).[434] ZnO nanoparticles synthesized by a sol–gel method were used to examine the degradation of ciprofloxacin in contaminated water under UVC light.[435] These findings showed complete photodegradation in 140 minutes corresponding to an initial concentration of ciprofloxacin of 10 mg L^{-1}, pH 5, ZnO loading of 0.15 g L^{-1} and irradiation time of 140 min. According to Ulyankina *et al.*,[436] UVA-irradiated ZnO nanoparticles synthesized by a pulse alternating current electrochemical method reached 93.6% removal efficiency in 30 min under optimal conditions (initial CIP concentration: 5 mg L^{-1}, pH: 6.5, catalyst dosage: 0.5 g L^{-1}, UV light intensity: 2.0 mW cm^{-2}). Such performance of ZnO nanoparticles is attributed to their higher surface area and increased charge carrier separation compared to commercial ZnO. In another study, ZnO nanoparticles prepared by chemical precipitation immobilized on a glass plate showed 69.5% degradation efficiency for an aqueous solution (pH: 6.8) of ciprofloxacin (10 mg L^{-1}) under UVC irradiation (180 min).[437] A ZnO nanostructure prepared by a pyrolysis method achieved 95.5% ciprofloxacin degradation in 60 min under visible light.[438]

A ZnO nanotube photocatalyst on irradiation with the terrestrial solar spectrum showed about 2.9 times faster degradation of ciprofloxacin compared to TiO_2 Degussa P25.[439] The flower-like ZnO architectures assembled with nanorods displayed 96% efficiency (240 min) for the degradation of ciprofloxacin (initial conc.: 0.015 μM) in aqueous solution under a UV lamp as a light source.[440] Finčur *et al.*[441] undertook comparative studies by examining the photocatalytic properties of TiO_2, ZnO and MgO nanopowders prepared by a sol–gel method in the removal of ciprofloxacin from water under UV/simulated sunlight. The corresponding efficiencies of 93.4%, 86.9% and 59.6% suggested TiO_2 to be most efficient nanopowder for this. The photocatalytic activity of CdO nanoparticles synthesized *via* a green route imparted 95% degradation of ciprofloxacin in aqueous media under sunlight (60 minutes).[442] In another work, ZnO nanorod irradiated with UV lamp recorded 92% degradation of ciprofloxacin in 60 minutes.[443]

3.6.2 Metal–metal oxides. A photocatalyst of mesoporous TiO_2 modified with Fe (1.5%) and N (2.5%) degraded nearly 70% of ciprofloxacin under visible light in 6 h.[444] Ag (0.5 to 4%) nanoparticles grown on the surface of TiO_2 exhibited highly enhanced degradation of ciprofloxacin under solar light at low pH.[445] A mechanism has also been proposed based on the formation of intermediates identified during the oxidation of ciprofloxacin. A simple reduction method has been used to prepare Cu@TiO_2 hybrids of varying Cu/TiO_2 wt. ratios (0.1–50) and their photocatalytic performance was examined for ciprofloxacin hydrochloride under sunlight simulated by a 500 W xenon lamp.[446] These findings revealed its complete removal in 3 h, corresponding to a Cu/TiO_2 wt. ratio of 0.1 in Cu@TiO_2 due to the best charge separation and transfer efficiency of photogenerated electrons and holes compared to pure TiO_2.

TiO_2 modified with monometallic and bimetallic nanoparticles comprising 1.5%-Au/TiO_2, 1.5%-Ag/TiO_2, 1.0%-Cu/TiO_2, 1%Au–0.5%Ag/TiO_2 and 1.0%Au–0.5% Cu/TiO_2 were fabricated by a deposition–precipitation method and used as photocatalysts in the degradation of ciprofloxacin in pure water under UVC-light irradiation.[447] These investigations revealed 100% degradation of ciprofloxacin for all these modified TiO_2 catalysts corresponding to 60, 30, 60, 90 and 45 min, respectively. This is ascribed to the lower recombination of the hole–electron pairs arising from the electron trap effect by metal nanoparticles.

3.6.3 Doped metal oxides. The removal of ciprofloxacin from water has been studied in the presence of metals, nonmetals and conducting polymers as dopants in metal-oxide-based photocatalysts. Suwannaruang *et al.*[448] used a hydrothermal method to synthesize nitrogen (12.5%) doped TiO_2 particles by selecting urea as a source of nitrogen. Subsequent investigation of its photocatalytic activity showed maximum degradation of ciprofloxacin (94.29%) after 4 h of UV-light irradiation. This is attributed to the integration of nitrogen into the TiO_2 lattice and the increased formation of OH radicals. Nitrogen-doped TiO_2 (N/Ti wt. ratio: 0.34%) prepared by a sol–gel method and immobilization on glass spheres resulted in 93.5% removal of ciprofloxacin in 90 min under visible-light irradiation.[449] The photodegradation of ciprofloxacin followed first-order-kinetics and the

photocatalyst exhibited excellent stability even after 5 cycles. Visible-light-irradiated P-doped TiO_2 with surface oxygen vacancies (SOVs) exhibited 100% degradation efficiency for ciprofloxacin.[450] This is explained on the basis of the synergistic effect as a result of P doping and SOVs on TiO_2 significantly enhancing the transfer and separation efficiency of photogenerated charge carriers. Polyaniline (PANI)-doped ZrO_2 on UV-light irradiation showed 96.6% photodegradation of ciprofloxacin under optimum conditions (PANI/ZrO_2: 30 mg, ciprofloxacin conc: 4×10^{-5} M) in 120 min.[451]

A ZnO-modified g-C_3N_4 photocatalyst removed 93.8% ciprofloxacin from water, corresponding to an amount of 0.05 g L^{-1} and pH value of 8.[452] Further studies have shown the degradation rate of ciprofloxacin by ZnO-doped g-C_3N_4 to be 4.9 times faster than that of undoped g-C_3N_4. The photocatalyst also exhibited high reusability, as evident from 89.8% efficiency after 3 cycles. Boron-doped TiO_2 and cerium-doped TiO_2 demonstrated about 90–93% photocatalytic degradation of ciprofloxacin and norfloxacin under solar light.[373] Such enhanced photocatalytic activity was explained on the basis of the narrowed band gap and electron–hole separation. In addition, metal-doped metal oxides, such as Fe^0/TiO_2,[453] Fe-doped ZnO[454] Zn-doped Cu_2O,[455] and Cu-doped ZnO,[456] have also been successfully reported in the photodegradation of ciprofloxacin.

Several investigations have also been reported on co-doped metal oxides for their applications as photocatalysts in the removal of ciprofloxacin from water. According to Nguyen and others,[457] the UV-visible-light-driven photocatalytic degradation of ciprofloxacin hydrochloride (30 mg L^{-1}) by N, S-co-doped TiO_2 exhibited a removal efficiency of 78.7% at pH 5.5 for a catalyst dose of 0.05 g. The synthesized N,C-co-doped TiO_2 under optimum conditions demonstrated the highest photocatalytic activity in the removal of ciprofloxacin in water under visible light.[458] It was concluded that photogenerated holes and superoxide radicals play an active role in the degradation of ciprofloxacin. ZnO nanowires doped with copper and cerium oxides displayed 88.9% removal of ciprofloxacin under UV irradiation.[459]

3.6.4 Metal oxide composites. In recent years, several studies have been reported on the photodegradation of ciprofloxacin using a variety of composite materials.[460–471] A graphitized mesoporous carbon–TiO_2 nanocomposite facilitated an almost complete photocatalytic performance in the degradation of ciprofloxacin under UV irradiation.[460] A Co/Mn oxide photocatalyst (1.00 g L^{-1}) prepared by a sol–gel method displayed maximum discoloration (56.3%) of ciprofloxacin (10.00 mg L^{-1}) in water (pH: 4) at about 120 min under sunlight.[461] $TiOF_2/TiO_2$ prepared at 160 °C under hydrothermal conditions exhibited 95.3% degradation of ciprofloxacin hydrochloride under simulated solar light after 90 min.[462] In all likelihood, such a combination of TiO_2 and $TiOF_2$ composites generates more charge carriers, including an improvement in the transmission and separation efficiency of photogenerated electron–hole pairs. TiO_2/Montmorillonite,[463] 3D γ-Fe_2O_3@ZnO core–shell[464] and rGO–$BiVO_4$–ZnO[465] photocatalysts have also shown enhanced degradation of ciprofloxacin.

Teixeira *et al.*[466] made an assessment of the optimization and reusability of $Fe_3O_4/SiO_2/TiO_2$ magnetic photocatalytic particles in the degradation of ciprofloxacin. These studies have shown 95% degradation of ciprofloxacin (pH: 5.5) after 90 min under UV with no significant loss even after five uses. Ternary core–shell $Fe_3O_4/SiO_2/TiO_2$ nanocomposite photocatalysts showed good synergistic properties on the removal efficiency for ciprofloxacin under UVA-light irradiation.[467] The photocatalytic degradation of ciprofloxacin hydrochloride by Ag–$SrTiO_3/TiO_2$ composite nanostructures under simulated sunlight resulted in 97.6% degradation of ciprofloxacin due to an increase in the carriers and separation between electron–hole pairs.[468]

Metal oxide/hydroxyapatite,[469] $CuFe_2O_4$@methyl cellulose,[470] TiO_2-modified Bi_2MoO_6[471] and Ag_2O/Ag_2CO_3/MWNTs[472] have also been examined successfully as composite photocatalysts for the enhancement of ciprofloxacin degradation in water under UV, UVC and visible light, respectively.

3.6.5 Carbonaceous-material-based composites

3.6.5.1 g-C_3N_4 and carbon-dot-based composites. Hernández-Uresti *et al.*[333] used polymeric g-C_3N_4 powder and observed 60% degradation of ciprofloxacin in aqueous solution (pH: 5.5) after 240 min under UV-vis irradiation. Recent studies on exfoliated g-C_3N_4 (2 g L^{-1}) showed 78% degradation of ciprofloxacin (20 ppm) irradiated under solar light for 1 h.[473] In another finding, a 3D g-C_3N_4/TiO_2/kaolinite heterogeneous composite displayed ~92% degradation efficiency for ciprofloxacin in 240 min under visible-light irradiation.[474] This is ascribed to the larger surface area and the availability of more reactive sites, and the efficient separation and longer lifetimes of photogenerated electron–hole pairs. Chuaicham *et al.*[475] observed 98% decomposition of ciprofloxacin (10 mg L^{-1}) within 120 min after irradiation with visible light of a Zn–Cr layered double oxide/fly ash composite photocatalyst in aqueous conditions. The formation of new electronic levels accounted for such enhanced photocatalytic performance. *In situ* synthesized 3D g-C_3N_4/La–N–TiO_2 also showed complete degradation of ciprofloxacin (5 mg L^{-1} starting concentration) at a pH of about 6.5 in about 60 min under exposure to simulated solar light.[476] Carbon dots/$Bi_4O_5Br_2$[477] nanocomposites also displayed improved visible-light photocatalytic degradation of ciprofloxacin.

3.6.5.2 Composites of graphene oxide and graphene. Graphene oxide and reduced graphene have been used to fabricate binary and ternary composites and they have been used as photocatalysts in the removal of ciprofloxacin from water. Sponza *et al.*[478] prepared nano-GO–Fe_3O_4 nanocomposites by adding water-dispersed Fe_3O_4 nanoparticles to an aqueous solution of GO. This irradiated with sunlight produced 80% removal efficiency for ciprofloxacin in water under optimum conditions (initial conc. of ciprofloxacin: 1 mg L^{-1}, original pH: 6.5, nano-GO/M concentration: 2 g L^{-1}, irradiation time: 250 min). ZnO-

particle-coated carboxyl-enriched GO (ZnO@cGO) degraded almost 100% ciprofloxacin in water (pH: 7) within about 5 min under visible irradiation (initial concentration of CIP: 25 μg mL^{-1}, catalyst: 0.5 mg mL^{-1}).[479] It was concluded that degradation of ciprofloxacin depends mainly on O_2^- and h^+. An rGO-supported $BiVO_4/TiO_2$ heterostructure nanocomposite achieved 80.5% degradation rate for ciprofloxacin in acidic ambient (pH: 5) within 150 min, 2.06 times higher than $BiVO_4/TiO_2$.[480] A nanostructured ZnO–CdO incorporated rGO photocatalyst showed degradation of ciprofloxacin of around 99.28% in 75 min under UV light.[481] This is attributed to the effective separation of charge carriers consequential on the production of more reactive oxygen species after incorporation of rGO nanosheets with ZnO–CdO.

The performance of ZnAl mixed metal-oxide (MMO)/rGO_x (x: wt% of rGO) composites was tested and compared with ZnAl MMO and pure ZnAl MMO in the photodegradation of ciprofloxacin hydrochloride in aqueous solution under visible light.[482] It was found to show the following order of photodegradation efficiency at the end of 2 h of irradiation time: ZnAl MMO/rGO20 (~90.58%) > ZnAl LDH/rGO20 (~67.74)% > ZnAl MMO (50.96%) > ZnAl LDH (36.47%). Such enhanced performance of the ZnAl MMO/rGO20 photocatalyst has been ascribed to the synergistic effect of the heterogeneous structure. The degradation mechanism of ciprofloxacin has been clearly explained based on the heterostructure that accounts for efficient charge separation and inhibition of the recombination of photogenerated carriers. It is believed that $O_2\cdot$ radicals and h^+ predominantly contribute to the degradation of ciprofloxacin. TiO_2 (64.3 wt%)-pillared multilayer graphene nanocomposites showed better photodegradation efficiency of 78% than TiO_2 (42%) under light-emitting diode irradiation for 150 min.[483] The photodegradation followed pseudo-first-order kinetics with the rate constant of graphene/TiO_2 composite about 3.89 times that of pristine TiO_2. The graphene/TiO_2 composite also exhibited high stability and reusability even after five consecutive photocatalytic cycles. Urus *et al.*[484] used a GO@Fe_3O_4@TiO_2-type core@shell@shell nanohybrid (10 mg) as a catalyst to remove 91.5% of ciprofloxacin (10 ppm) from water solution (pH: 7) after 240 min. In addition, the photocatalytic removal of ciprofloxacin has also been evaluated using 3D-structured flower-like bismuth tungstate/magnetic graphene nanoplates[485] and Ag_2CrO_4/Ag/$BiFeO_3$@rGO photocatalysts.[486]

Huo *et al.*[487] synthesized an N-doped ZnO/CdS/graphene oxide ternary composite *via* a two-step method and tested its photocatalytic activity in the degradation of ciprofloxacin hydrochloride under visible light and compared it with pure CdS, N–ZnO, and N–ZnO : CdS (2 : 1, 1 : 1, 1 : 2, 1 : 3). The highest degradation rate of about 86% was shown for the 2 : 1 molar ratio of N–ZnO and CdS. This is explained in terms of heterostructure and the contribution from GO in N–ZnO/CdS promoting photogenerated electron transfer and suppressing the recombination of electron–hole pairs. The proposed schematic suggested that charge transfer and holes played a major role in the photocatalytic system.

3.6.6 Heterostructures, heterojunctions and Z-scheme-based photocatalysts. An Ag_3PO_4/TiO_2 heterojunction has been fabricated following the corn-silk-templated synthesis of TiO_2 nanotube arrays with Ag_3PO_4 nanoparticles.[488] Its application as a photocatalyst in the removal of ciprofloxacin showed degradation efficiency of 85.3% within 60 minutes under simulated solar-light irradiation. Deng *et al.*[489] observed 92.6% removal efficiency for ciprofloxacin by Ag-modified P-doped g-$C_3N_4/BiVO_4$ nanocomposites under visible-light irradiation (>420 nm). It was suggested that a synergistic effect could account for such improvements as a result of reduced electron–hole recombination. ZnO–Ag_2O/porous g-C_3N_4 ternary composites achieved 97.4% degradation efficiency for ciprofloxacin compared to ZnO (8.2%), g-C_3N_4 (25.4%), Ag_2O (42.3%), and ZnO–Ag_2O (69.4%) within 48 min under visible-light irradiation.[490]

Magnetic g-$C_3N_4/MnFe_2O_4$/graphene composites have been examined for the photocatalytic degradation of ciprofloxacin in the presence of persulfate as an oxidant under visible-light irradiation.[491] Graphene-layer-anchored TiO_2/g-C_3N_4 showed enhanced photocatalytic performance (degradation rate: 61.7%, k: 0.01675 min^{-1}) under visible light compared to graphene-layer-anchored TiO_2, g-C_3N_4 and g-C_3N_4/TiO_2.[492] This is explained on the basis of accumulation of g-C_3N_4 electrons with high reduction capability and TiO_2 holes with high oxidation capability. Enhanced photocatalytic activity has also been displayed by a visible-light-driven mesoporous TiO_2@g-C_3N_4 hollow core@shell heterojunction in the degradation of ciprofloxacin.[493]

A heterostructure comprising Ag nanoparticles deposited on the surface of ZnO nanoplates and Fe_2O_3 nanorods exhibited superior solar-light-driven photocatalytic activity in ciprofloxacin degradation (76.4%) under optimized conditions (initial ciprofloxacin concentration: 10 mg L^{-1}; pH 4; catalyst loading: 0.3 g L^{-1}).[494] The e^-, h^+, ·OH and $\cdot O_2^-$ played important roles as reactive species in the photocatalytic degradation process. The efficient separation of charge carriers and migration of e^-/h^+ across the heterostructure interface accounted for this. Zhao *et al.*[495] achieved 95.6% removal of ciprofloxacin under visible-light irradiation for 40 min by a ternary $Mn_2O_3/Mn_3O_4/MnO_2$ (molar ratio of 3 : 1 : 2) valence state heterojunction with dual heterostructures under visible light. Such a performance is derived from its enhanced surface area, light absorption and charge separation of the $Mn_2O_3/Mn_3O_4/MnO_2$ heterostructure. Further studies established that holes and superoxide radicals play an important role in the degradation of ciprofloxacin. Other studies comprising a unique 2D/3D/2D rGO (3%)/Fe_2O_3 (4%)/g-C_3N_4 heterojunction showed almost 100% degradation of ciprofloxacin (pH: 7) compared to pristine g-C_3N_4 nanosheets under visible-light irradiation for 40 minutes.[496] Such photocatalytic properties of a heterojunction nanocomposite system are accounted for in terms of enhanced charge migration and separation.

Chen *et al.*[497] noted the enhanced degradation of ciprofloxacin over $Bi_2O_3/(BiO)_2CO_3$ heterojunctions compared to pristine $(BiO)_2CO_3$ and Bi_2O_3 in the presence of simulated solar light. The decay process for ciprofloxacin followed pseudo-first-order kinetics with the rate constant increasing with decreasing concentration of CIP. In addition, CdS/BiOBr,[498] $Cu_2O/Cu_2(PO_4)(OH)$,[499] Sm-doped g-C_3N_4/Ti_3C_2-MXene,[500] $CeO_2/La_2O_3/TiO_2$,[501] g-C_3N_4/NH_2-MIL-88B(Fe)[502] and a polypyrrole-sensitized $ZnFe_2O_4$/g-C_3N_4 n–n heterojunction[503] have also displayed enhanced photocatalytic degradation of ciprofloxacin.

Costa *et al.*[504] observed ~98% photodegradation of ciprofloxacin (initial concentration: 5 ppm) at neutral pH in the presence of a Z-scheme TiO_2/SnO_2 nanostructure photocatalyst. These findings also revealed the active role of oxygen singlets, holes, and superoxide radicals as the main species in the photodegradation of ciprofloxacin. Li *et al.*[505] prepared an oxygen-vacancy-rich TiO_2/Ta_3N_5 composite by a solvothermal method and used it as a direct Z-scheme heterojunction photocatalyst. They observed 95.7% (90 min) degradation rate of ciprofloxacin hydrochloride under visible-light irradiation. It was suggested that oxygen vacancies form an intermediate energy level in TiO_2 that accounts for the separation of photogenerated electrons and holes. In addition, the formation of a Z-scheme energy band structure by oxygen-vacancy-rich TiO_2 and Ta_3N_5 is likely to enable more photogenerated carriers to participate in the photocatalytic reaction. This was also inevitable from the excellent photocatalytic degradation of ciprofloxacin delivered by an oxygen-vacancy-rich TiO_2/Ta_3N_5 composite under visible light. CeO_2/ZnO nanocomposites prepared by a co-precipitation method displayed twice the activity in the photocatalytic degradation of ciprofloxacin compared to undoped ZnO and was ten times more active than pristine CeO_2.[506] Such enhanced formation of a Z-scheme heterojunction is attributed to the migration of photo-excited electrons from the conduction band of ZnO to the valence band of CeO_2.

N-doped carbon quantum dot (NCQD)-decorated $Bi_2O_2CO_3$ heterojunction nanosheets exhibited remarkably enhanced photocatalytic activities for ciprofloxacin photodegradation mediated by radiation in the ultraviolet to near-infrared region.[507] It is suggested that NCQDs act as photosensitizers (hole reservoirs) to harvest solar light and a type-II heterojunction facilitates efficient charge carrier separation to account for this. The mechanisms and pathways of ciprofloxacin degradation mediated by different lights were also discussed. N-doped carbon dots (NCDs) decorated onto a Bi_2MoO_6/g-C_3N_4 (BMCN) nanocomposite photodegraded ciprofloxacin by 98% (30 min) under visible-light irradiation.[508] It is proposed that NCDs play a role as a mediator to transfer electrons from the conduction band to the valence band of Bi_2MoO_6 and g-C_3N_4, respectively. The findings also revealed ·OH and $\cdot O_2^-$ radicals acting as the dominant reactive species. The photocatalyst also displayed good stability and reusability after five consecutive cycles of ciprofloxacin photodegradation.

A Z-scheme involving a TiO_2 nanorod/g-C_3N_4 (30 wt%) nanosheet nanocomposite showed 93.4% degradation of ciprofloxacin (initial concentration: 15 mmol L^{-1}) aqueous solution (pH: 6.3) under simulated sunlight irradiation in 60 min.[509] It was also concluded that h^+ and ·OH played a major role in the degradation of ciprofloxacin. In another study, a biochar@$ZnFe_2O_4$/BiOBr Z-scheme heterojunction photocatalyst prepared by a solvothermal method under visible-light irradiation ($\lambda > 420$ nm) showed no significant degradation efficiency for ciprofloxacin (65.26%).[510] Wen *et al.*[511] fabricated CeO_2–Ag/AgBr composite photocatalysts with a Z-scheme configuration by following the *in situ* interspersal of AgBr on CeO_2 and subsequently studied the photodegradation of ciprofloxacin under visible-light irradiation (Fig. 17(a)). According to this, CeO_2 itself has almost no ability to degrade ciprofloxacin, though it can be partly eliminated in the presence of pristine Ag/AgBr. However, CIP concentration decreased further to some extent for CeO_2 decorated with Ag/AgBr in CeO_2–Ag/AgBr composites with 21.26 wt% of Ag (denoted CAB-21.26) exhibiting the most pronounced photocatalytic activity. This is ascribed to the accelerated interfacial charge transfer process and the improved separation of the photogenerated electron–hole pairs. Furthermore, the kinetic behavior followed pseudo-first-order kinetics and exhibited higher *k*-values for the CeO_2–Ag/AgBr hybrids (Fig. 17(b)). Another Z-scheme-based AgBr/Ag/Bi_2WO_6 heterostructure achieved 57% (5 h) photocatalytic degradation of ciprofloxacin under visible-light irradiation in pure water.[512] Such a performance was ascribed to the synergistic effect of the AgBr/Ag/Bi_2WO_6 heterostructure compared to its single components.

Z-Scheme-guided g-C_3N_4/Bi_2WO_6,[513] Fe_3O_4/Bi_2WO_6,[514] g-C_3N_4/Ti_3C_2/MXene/black phosphorus,[515] g-C_3N_4/Ag_3PO_4/chitosan,[516] $Ag/AgVO_3$/g-C_3N_4,[517] CeO_2/Co_3O_4 p–n hetrojunctions,[518] Bi nanodots/2D Bi_3NbO_7 nanosheets,[519] Bi_2WO_6/Ta_3N_5,[520] g-C_3N_4@$Cs_{0.33}WO_3$,[521] ZnO/SnS_2,[522] g-C_3N_4/rGO/WO_3,[523] and CuS/$BiVO_4$[524] have also displayed enhanced photocatalytic degradation of ciprofloxacin.

Table 7 records the performance data of different photocatalysts on the removal of norfloxacin from wastewater.

3.7 Tetracycline

Tetracycline (TC) is invariably used as an antibiotic against different bacterial infections, such as urinary tract infections, acne, gonorrhea, chlamydia, mycoplasma, rickettsia, cholera, brucellosis, plague and syphilis.[52] It finds extensive application in the medical field, for veterinary purposes, and as a feed additive in the agricultural sector. However, extensive applications of tetracycline mean its presence in surface water, groundwater, wastewater, domestic wastewater and other source-related environments, causing a serious threat to the environment. Therefore, several approaches

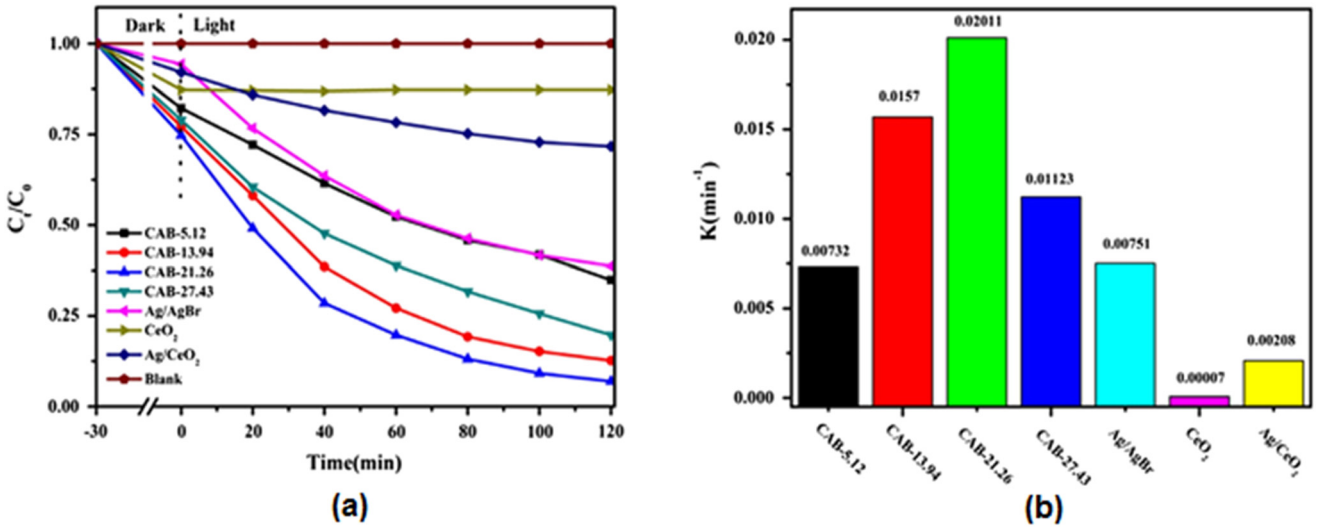

Fig. 17 (a) Photocatalytic degradation CIP curves and (b) apparent rate constants for the degradation of CIP solution for a CAB-21.26 sample. Reproduced from ref. 511 with permission from Elsevier (2018).

have been made to develop a highly efficient approach to remove antibiotics by a photocatalysis approach.[525–662]

3.7.1 Metal oxides

3.7.1.1 TiO_2. Several investigations have been reported using TiO_2 as a photocatalyst in water treatment for the removal of tetracycline. According to Palominos *et al.*,[527] an aqueous suspension of TiO_2 has been used to facilitate the photocatalytic oxidation of tetracycline on irradiation with simulated solar light. Studies indicated the rapid degradation of tetracycline, undergoing 100% completion after 15 min under optimum conditions (tetracycline: 20 mg L^{-1}, TiO_2: 1.5 g L^{-1}, pH: 8.7). The mechanism of photocatalytic tetracycline oxidation involved active roles for holes and OH radicals. The nanosized TiO_2 achieved more than 95% removal of tetracycline within 40 min under UV irradiation for a tetracycline concentration of 40 mg L^{-1} and catalyst dose of 1000 mg L^{-1}.[528] Safari *et al.*[529] also used nanosized TiO_2 (1.0 g L^{-1}) to study the degradation kinetics of a tetracycline hydrochloride (TC·HCl) aqueous solution (55 mg L^{-1}, pH: 5) under ultraviolet irradiation. They observed 100% degradation after 30 min on adding H_2O_2 (100 mg L^{-1}) compared to 91.4% degradation after 90 min for TiO_2/UV. The photocatalytic degradation of tetracycline over commercial TiO_2–P25 showed 94.8% (120 min) removal efficiency under visible light (λ = 700 nm).[530] Recently, a crosslinking method has been followed for immobilizing TiO_2 (P25) nanoparticles in chitosan film, which showed promising photocatalytic activity in the purification of water containing tetracycline hydrochloride under UV irradiation.[531] The stability and reusability of this composite film in four consecutive cycles revealed a significant decrease in removal efficiency after the second run, from 87% to 57%. Tetracycline hydrochloride degradation has also been studied using a green and low-cost approach, involving the preparation of immobilized titania samples by depositing two successive TiO_2 layers on two different commercial supports.[532]

3.7.1.2 ZnO and other oxides. Palominos *et al.*[527] carried out the photocatalytic oxidation of tetracycline in an aqueous suspension containing ZnO and found its performance comparable to TiO_2 (~100% degradation) under simulated solar light. According to the suggested mechanism, the contribution towards photocatalytic tetracycline oxidation on ZnO is mainly guided by hydroxyl radicals. UV-irradiated ZnO/peroxymonosulfate has shown about 95.6% degradation of tetracycline (10 mg L^{-1}, pH: 7) in 90 min compared to UV/ZnO (50.14%), attributed to the formation of $SO_4^{\cdot -}$.[533] In addition, HSO_5^- acts as an electron acceptor and inhibits electron–hole pair recombination, thereby allowing the formation of more ·OH radicals. Iron oxide nanoparticles,[534] nanospherical α-Fe_2O_3 supported on 12-tungstosilicic acid,[535] SnO_2 hollow microspheres,[536] polyaniline coated on magnetic MoO_3[537] and $BiFeO_3$[538] have also been studied in the photocatalytic degradation of tetracycline aqueous solutions.

3.7.2 Metal-loaded metal oxides. A solution casting method has been used to fabricate membranes by mixing previously prepared core–shell Au (0.1, 0.3, 0.5 g)–TiO_2 nanocomposites and PVDF and they were examined for their performance in the degradation of tetracycline under the influence of visible light.[539] It is inferred that an Au (0.3)–TiO_2/PVDF nanocomposite enhanced the photocatalytic degradation rate by 75% within 120 min under visible light. These findings clearly ensured first-order kinetics for Au–TiO_2/PVDF composites, following the order: Au (0.3)–TiO_2/PVDF (0.00599 min^{-1}) > Au (0.1)–TiO_2/PVDF (0.00449 min^{-1}) > Au (0.5)–PVDF (0.01212 min^{-1}). Excellent regeneration stability and its easy separation have also been achieved by this method. Gold-containing zinc–titanium oxide films[540] and Ag/Bi_2O_3[541] have also been reported in the photocatalytic degradation of tetracycline in aqueous media.

Liu *et al.*[542] studied the photoactivity of an Au–ZnO nanomotor system based on vertically aligned ZnO in the photocatalytic degradation of tetracycline as a function of

Table 7 Data on performance data on removal of ciprofloxacin using different photocatalysts

Photocatalyst	Preparative method	CIP[a]/CIP·HCl[b]	Catalyst dose	pH	Light source	Degradation (time)	Rate constant
P25 TiO_2 (anatase : rutile = 80 : 20), [H_2O_2]: 82.5 mg L^{-1} [425]	Commercial	0.030 mmol L^{-1} [a] (500 mL)	0.5 g L^{-1}	6	Simulated solar irradiation, 800 W xenon lamp	~100% (90 min)	0.022 min^{-1}
Degussa P-25 TiO_2 (80:20% w/w anatase-to-rutile)[426]	Commercial	100 mg L^{-1} [b]	1 g L^{-1}	9	Simulated solar irradiation (850 W cm^{-2})	~100% (160 min)	0.108 min^{-1}
Degussa P-25 TiO_2 (80 : 20% w/w anatase-to-rutile)[428]	Commercial	20 mg L^{-1} [a] (100 mL)	100 mg L^{-1}	6.0	UVA/LED lamp (3 W), 10 mW cm^{-2}, $\lambda > 365$ nm	—	0.2217 ± 0.0179 min^{-1}
TiO_2 (80% anatase and 20% rutile) immobilized on glass plates[429]	Multiple steps	60 μmol L^{-1} [a] (500 mL)	TiO_2 (7.5 g L^{-1})	9	UVC lamp: 15 W 254 nm	~98% (120 min)	~25 × 10^{-3} min^{-1}
TiO_2 P25 and ZnO[430]	Commercial	300 μg L^{-1} [a] (50 mL)	1 g L^{-1}	—	UVA (1.6 to 1.7 mW cm^{-2})	100% (6 min)	—
Mesoporous TiO_2 nanoparticles[431]	Hydrothermal	160 mg L^{-1} [b] (40 ml)	0.01 g	—	Xenon lamp (500 W), 200–1000 nm	96.05% (360 min)	0.45 min^{-1}
3D tripyramid TiO_2 architectures[432]	Hydrothermal method	32.6 μM[a] (50 mL)	5 mg	—	UV-vis light	90% (60 min)	4.03 × 10^{-2} min^{-1}
ZnO nanoparticles[434]	Chemical precipitation method	4 mg L^{-1} [a] (3 mL)	20 mg L^{-1}	10	Xenon lamp (365 nm)	~48% (60 min)	0.0043 ± 0.003 min^{-1}
ZnO nanoparticles[435]	Sol–gel method	10 mg L^{-1} [a]	0.15 g L^{-1}	5	Low-pressure mercury-vapour lamps (9 W)	100% (140 min)	0.032 min^{-1}
Nano-ZnO[436]	Pulse electrochemical synthesis	5 mg L^{-1} [a]	0.5 g L^{-1}	6.5	UV light (2.0 mW cm^{-2})	93.6% (30 min)	—
Immobilized ZnO nanoparticles[437]	Heat attachment method	10 mg L^{-1} [a]	14 × 14 × 5 cm^3	6.8	UV lamp (15 W, 42 W m^{-2})	69.5% (180 min)	~0.008 min^{-1}
ZnO nanotubes[439]	Modified published protocol	2 × 10^{-5} mol L^{-1} [a] (0.4 L)	14 mg	8.0	300 W xenon lamp with AM1.5 filter (1000 W m^{-2})	12% (120 min)	9.61 × 10^{-4} min^{-1}
Flower-like ZnO[440]	Thermionic vacuum arc	0.015 μM[a]	ZnO deposited on 2 × 2 cm^2 (Si wafer)	—	UV lamp, 1 W m^{-2}, 253.7 nm	96% (240 min)	14.8 × 10^{-3} min^{-1}
TiO_2[441] $(NH_4)_2S_2O_8$: 0.125 mM	Sol–gel method	0.05 mM[a]	0.5 mg mL^{-1}	—	High-pressure Hg lamp (125 W), 1.4 × 10^{-2} W cm^{-2} in UV region	93.4% (60 min)	—
ZnO[441]	Sol–gel method	0.05 mM[a]	0.5 g L^{-1}	—	High-pressure Hg lamp (125 W) in UV region, 1.4 × 10^{-2} W cm^{-2}	86.9% (60 min)	—
CdO[442]	Green approach	10 ppm[a] (50 mL)	50 mg	—	Sunlight	95% (60 min)	0.04722 min^{-1}
ZnO–Ag-Graphite[443]	Hydrothermal method	5 mg L^{-1} [a] (50 mL)	0.3 g L^{-1}	—	24 W UV lamp, λ: 254 nm	98% (60 min)	0.05983 min^{-1}
2.5% N-1.5% Fe–TiO_2[444]	Hydrothermal method	20 mg L^{-1} [a] (300 mL)	0.3 g	—	LED illumination source	70% (360 min)	5.52 × 10^{-3} min^{-1}
Ag nanoparticles@TiO_2[445]	Sonicating TiO_2 and aq. $AgNO_3$ + aq. Na_2CO_3	1.0 mM[a] (100 mL)	1.0 mg L^{-1}	7	UV light (120 W Hg lamp)	85.21% (14 500 s)	1.53 mM s^{-1}
Ag nanoparticles@TiO_2[445]	Sonicating TiO_2 and aq. $AgNO_3$ + aq. Na_2CO_3	1.0 mM[a] (100 mL)	1.0 mg L^{-1}	7	Sunlight	75.58% (14 500 s)	1.210 mM s^{-1}
Mesoporous Cu (0.1 wt%) @TiO_2[446]	Reduction method	40 mg L^{-1} [b] (40 mL)	0.01 g	—	500 W xenon lamp (sunlight)	~100% (3 h)	1.16 h^{-1}
1.5%-Au/TiO_2[447]	Deposition–precipitation method	30 mg L^{-1} [a] (250 mL)	0.5 g L^{-1}	—	UVC light irradiation (15 W low-pressure	100% (60 min)	0.06 min^{-1}

Table 7 *(continued)*

Photocatalyst	Preparative method	CIP[a]/CIP·HCl[b]	Catalyst dose	pH	Light source	Degradation (time)	Rate constant
					Hg lamp, 254 nm 44 W m^{-2})		
1.5%-Ag/TiO_2[447]	Deposition–precipitation method	30 mg L^{-1} [a] (250 mL)	0.5 g L^{-1}	—	UVC light irradiation (15 W low-pressure Hg lamp, 254 nm 44 W m^{-2})	100% (30 min)	0.117 min^{-1}
1.0%-Cu/TiO_2[447]	Deposition–precipitation method	30 mg L^{-1} [a] (250 mL)	0.5 g L^{-1}	—	UVC light irradiation (15 W low-pressure Hg lamp, 254 nm 44 W m^{-2})	100% (60 min)	0.072 min^{-1}
1% Au–0.5% Ag/TiO_2[447]	Deposition–precipitation method	30 mg L^{-1} [a] (250 mL)	0.5 g L^{-1}	—	UVC light irradiation (15 W low-pressure Hg lamp, 254 nm 44 W m^{-2})	100% (90 min)	0.053 min^{-1}
1.0% Au–0.5% Cu/TiO_2[447]	Deposition–precipitation method	30 mg L^{-1} [a] (250 mL)	0.5 g L^{-1}	—	UVC light irradiation (15 W low-pressure Hg lamp, 254 nm 44 W m^{-2})	100% (45 min)	0.099 min^{-1}
N (12.9%) doped–TiO_2 nanorice particles[448]	Hydrothermal method	20 ppm[a]	0.3 g L^{-1}	5.5	UVA lamps: 20 W, 365 nm, 0.493 mW cm^{-2}	94.29% (240 min)	—
N doped–TiO_2 (N/Ti wt ratio:0.34%) immobilized on glass spheres[449]	Sol–gel method followed by immobilization	20 mg L^{-1} [a] (20 mL)	3 g L^{-1}	—	Xenon lamp: 500 W and $\lambda >$ 420 nm	93.5% (90 min)	0.02859 min^{-1}
P-doped TiO_2 (using 50 mg NaH_2PO_2)[450]	Heat treatment under flowing NH_3	5 ppm[a] (50 mL)	25 mg	—	Visible-light irradiation	100% (60 min)	0.065 min^{-1}
Polyaniline doped ZrO_2[451]	*In situ* oxi. Polym.	4×10^{-5} M[a] (100 mL)	30 mg	—	UV-light irradiation ($\lambda >$ 400 nm)	96.6% (120 min)	—
TiO_2/Fe[0453]	Liquid-phase reduction process	30 mg L^{-1} [a]	1.0 g L^{-1}	3.0	UV-lamp: 10 W, 254 nm, 2.0 W m^{-2}	94.6% (60 min)	—
Fe doped ZnO nanoparticles[454]	Precipitation route	5 mg L^{-1} [b]	150 mg L^{-1}	9	Sunlight, 650 W m^{-2}, 80 000 ± 3000 lux	~80% (210 min)	—
Zn-doped Cu_2O (by adding 0.05 g of $ZnCl_2$)[455]	Solvothermal method	20 mg L^{-1} [a] (50 mL)	30 mg	—	500 W metal halide lamp, $\lambda <$ 400 nm filter	94.6% (240 min)	0.0038 min^{-1}
N-S-doped TiO_2[457]	Sol–gel method	30 ppm[a]	0.05 mg	5.5	Halogen lamp: 500 W (360–780 nm)	78.7% (220 min)	0.0065 min^{-1}
Graphitized mesoporous carbon–TiO_2[460]	Extended resorcinol-formaldehyde method	15 mg L^{-1} [a] (200 mL)	70 mg	—	14 W UV lamp, 254 nm	100% (120 min)	0.102 min^{-1}
Mo/co oxides[461]	Sol–gel method	10 mg L^{-1} [a]	1 g L^{-1}	4	Sunlight	56.3% (180 min)	7.9×10^{-2} min^{-1}
$TiOF_2$/TiO_2[462]	Hydrothermal (160 °C)	20 mg L^{-1} [b] (50 mL)	50 mg	—	Xenon lamp: 300 W with a UV-cut-off filter (420 nm)	~95% (90 min)	0.034 min^{-1}
Core–shell 3D γ-Fe_2O_3@ZnO[464]	Hydrothermal-sintering and atomic layer deposition	10 mg L^{-1} [a] (100 mL)	0.5 g L^{-1}	5.8	Xenon lamp (300 W)	92.5% (60 min)	0.0419 min^{-1}
rGO–$BiVO_4$–ZnO[465]	Hydrothermal method	4×10^{-5} M[a] (100 mL)	30 mg	—	W lamp (150 mW cm^{-2}), ($\lambda <$ 400 nm)	98.4% (60 min)	—
Fe_3O_4/SiO_2/TiO[466]	Sol–gel synthesis (calcined at 600 °C)	5 mg L^{-1} [a]	1 g L^{-1}	5.5	UV irradiation, (365 nm, 1.6 mW cm^{-2})	95% (90 min)	0.032 min^{-1}
Core–shell Fe_3O_4/SiO_2/TiO_2(100 °C)[467]	Microwave-assisted synthesis	10 mg dm^{-3} [a] (100 cm^3)	50 mg	6.5	UVA lamp (365 nm)	94.0% (120 min)	0.0158 min^{-1}

Table 7 *(continued)*

Photocatalyst	Preparative method	CIP[a]/CIP·HCl[b]	Catalyst dose	pH	Light source	Degradation (time)	Rate constant
Ag–$SrTiO_3$/TiO_2[468]	Hydrothermal/photoreduction	20 mg L^{-1} [b] (50 mL)	20 mg	—	300 W xenon lamp	97.6% (60 min)	0.070 min^{-1}
TiO_2/hap (with 40% by wt% of oxide:Hap)[469]	Soft chemical method	20 ppm[a] (100 mL)	2 g L^{-1}	—	HPK 125 W lamp- UV light	100% (15 min)	—
ZnO/HAp (with 40% by wt% of oxide:Hap)[469]	Soft chemical method	20 mg L^{-1} [a]	2 g L^{-1}	—	HPK 125 W lamp-UV light	100% (20 min)	—
$CuFe_2O_4$@methyl cellulose[470]	Microwave-assisted method	3 mg L^{-1} [a]	0.2 g	7	UVC lamps (low pressure, 6 W, Philips)	72.87% (90 min): real sample	0.902 min^{-1}
TiO_2/Bi_2MoO_6 (TiO_2 content: 0.41 wt%)[471]	Solvothermal–calcination process	10 mg L^{-1} [a] (50 mL)	30 mg	—	Xenon lamp 350 W with a UV cut-off filter	88% (150 min)	~8 × 10^{-3} min^{-1}
Ag_2O/Ag_2CO_3/MWNTs[472]	Calcination (10 min)	10 mg L^{-1} [a] (100 mL)	0.05 g	—	Xenon lamp: 300 W (visible light)	76% (60 min)	—
g-C_3N_4[333]	Polycondensation of melamine	10 mg L^{-1} [a]	200 mg (200 mL)	—	Xenon lamp (35 W): UV-vis radiation source	60% (240 min)	4 × 10^{-5} s^{-1}
Exfoliated g-C_3N_4[473]	Green route	20 ppm[a]	1 gL^{-1}	—	Solar-light irradiation	78% (60 min)	23 × 10^{-3} min^{-1}
g-C_3N_4/TiO_2/kaolinite[474]	Sol–gel method/chemical stripping/self-assembly	10 ppm[a] (100 mL)	0.2 g	—	Xenon lamp (90 mW cm^{-2} with 400 nm cut-off filter)	~92% (240 min)	0.00813 min^{-1}
Zn–Cr LDH/fly ash (molar ratio = 2 : 1)[475]	Coprecipitation method followed by dispersion method	10 ppm[a] (50 mL)	1.0 g L^{-1}		Xenon lamp (500 W) with UV cut-off filter	~98% (150 min)	—
g-C_3N_4/La–N–TiO_2[476]	*In situ* synthetic method	10 mg L^{-1} [a]	0.75 g L^{-1}	~6.5	Xenon lamp; (300 W), $\lambda >$ 420 nm	96.8% (60 min)	—
Nano graphene oxide–magnetite[478]	Mixing and dispersion	1 mg L^{-1} [a]	2 g L^{-1}	6.5	Sunlight irradiation at 80 W power	80% (250 min)	—
ZnO–CdO/rGO[481]	Refluxing method	10 mg L^{-1} [a] (50 mL)	10 mg	7	UV light, 800 W xenon lamp with 420-nm cut-off filter	99.28% (75 min)	—
ZnAl mixed metal oxides/rGO[482]	Hydrothermal combined with calcination	10 mg L^{-1} [a] (50 ml)	10 mg	—	800 W xenon lamp with 420 nm cut-off	90.58% (120 min)	0.01893 min^{-1}
TiO_2 (64.3 wt%)-pillared multilayer graphene (35.7 wt%)[483]	Hydrothermal	15 mg L^{-1} [a] (40 mL)	20 mg	5.8	LED lamp (5 W), $\lambda >$ 420 nm	78% (150 min)	0.99111 min^{-1}
GO@Fe_3O_4@TiO_2[484]	*In situ* method	10 ppm[a] (100 mL)	10 mg	7–8	Solar simulator: 300 W	91.5% (240 min)	0.0079 min^{-1}
Ag_2CrO_4/Ag/$BiFeO_3$@8% wt ratio of rGO[486]	Dispersion method	10 mg L^{-1} [a]	0.2 mg mL^{-1}	7	Xenon lamp (300 W) with 400 nm cut-off filter, 450 mW cm^{-2}	96% (60 min)	0.0638 min^{-1}
N–ZnO/CdS/GO[487]	Hydrothermal	15 mg L^{-1} [a] (100 mL)	50 mg	—	Xenon lamp (300 W) with $\lambda >$ 420 nm	86% (60 min)	—
0.6Ag_3PO_4/TiO_2 nanotube arrays (600 °C)[488]	*In situ* growth method	10 mg L^{-1} [a] (40 mL)	40 mg	—	Xenon lamp (300 W), 200 mW cm^{-2}	85.3% (60 min)	0.02499 min^{-1}
P-doped ultrathin g-C_3N_4/$BiVO_4$[489]	Impregnated process	10 mg L^{-1} [a]	1 g L^{-1}	6.72	Visible-light irradiation ($\lambda >$ 420 nm)	92.6% (120 min)	0.0203 min^{-1}
ZnO–Ag_2O/porous g-C_3N_4[490]	Hydrothermal	20 mg L^{-1} [a] (100 mL)	50 mg	—	W lamp (500 W), $\lambda \geq$ 420 nm	97.4% (48 min)	0.057 min^{-1}

Table 7 *(continued)*

Photocatalyst	Preparative method	CIP[a]/CIP·HCl[b]	Catalyst dose	pH	Light source	Degradation (time)	Rate constant
Graphene layers anchored TiO_2/g-C_3N_4[492]	*In situ* calcination method using 40 g of Ti_3C_2	3 mg L^{-1} [a] (100 mL)	60 mg	—	Xenon lamp (300 W), $\lambda >$ 400 nm, 300 mW cm^{-2}	61.7% (60 min)	0.01675 min^{-1}
Ag/Fe_2O_3/ZnO[494]	Ultrasonic-assisted hydrothermal method	10 mg L^{-1} [a] (100 mL)	0.3 g L^{-1}	4	Solar illumination	76.4% (210 min)	0.3036 h^{-1}
Mn_2O_3/Mn_3O_4/MnO_2[495]	Hydrothermal and *in situ* method	10 mg L^{-1} [a] (120 mL)	0.2 g L^{-1}	7	Xenon lamp (300 W), 900 mW cm^{-2}	95.6% (40 min)	—
rGO/Fe_2O_3/g-C_3N_4[496]	Embedding approach	50 mg L^{-1} [a]	100 mg	7	Halogen lamp: 500 W	~100% (40 min)	1.0878 min^{-1}
Bi_2O_3/$(BiO)_2CO_3$[497]	Hydrothermal/calcination	10 mg L^{-1} [a]	0.5 g L^{-1} (100 mL)	7	Xenon lamp: 300 W, 0.641 W cm^{-2}	93.4% (30 min)	0.476 min^{-1}
CdS/BiOBr-1 : 3[498]	Solvothermal route	10 mg L^{-1} [a] (200 mL)	50 mg	7	Sunlight	99.1% (240 min)	0.00692 min^{-1}
Cu_2O/$Cu_2(PO_4)(OH)$[499]	Reflex method	20 mg L^{-1} [a] (100 mL)	100 mg	—	Direct sunlight irradiation	~98% (120 min)	—
CeO_2/La_2O_3/TiO_2[501]	Sol–gel followed by calcination	10 ppm[a] (50 mL)	50 mg	6–7	Visible light using tungsten lamp (300 W cm^{-2})	100% (120 min)	—
TiO_2/SnO_2[504]	Hydrothermal and ion exchange	2.5×10^{-3} g L^{-1} [a]	2.5×10^{-3} g	Neutral	UVC lamps with 35 W each (253 nm)	92.8% (120 min)	22.4 × 10^{-3} min^{-1}
CeO_2/ZnO[506]	Co-precipitation method	15 mg L^{-1} [a] (100 mL)	0.25 g L^{-1}	3.2	200 W mercury-xenon lamp with 365 nm filter	~60% (60 min)	0.0130 min^{-1}
5 wt% N-doped carbon quantum dots decorated $Bi_2O_2CO_3$[507]	Hydrothermal method	10 mg L^{-1} [a] (80 mL)	40 mg	—	UV-vis light Visible	91.1% (60 min) 92.8% (60 min)	~0.0325 min^{-1} ~0.02 min^{-1}
Bi_2MoO_6/g-C_3N_4[508]	Hydrothermal method	5 mg L^{-1} [a]	1.0 g L^{-1}	8	Visible lamps (77 mW cm^{-2})	98% (30 min)	0.12 min^{-1}
TiO_2 nanorod/30 wt% g-C_3N_4 nanosheets[509]	Mixing followed by ultrasonication	15 μmol L^{-1} [a] (50 mL)	10 mg	6.3	Xenon lamp: 500 W	93.4% (60 min)	0.0381 min^{-1}
5 wt% biochar@$ZnFe_2O_4$/BiOBr[510]	Solvothermal/photodeposition/ precipitation	15 mg L^{-1} [a]	50 mg (100 mL)	—	Xenon lamp: 300 W	65.26% (60 min)	—
CeO_2-21.26 wt% Ag/AgBr[511]	*In situ*	10 mg L^{-1} [a] (50 mL)	50 mg	—	Xenon lamp (300 W) with a UV cut-off filter	93.05% (120 min)	0.02011 min^{-1}
Bi_2WO_6/ag/AgBr[512]	Precipitation followed by dispersion	30 mg L^{-1} [a] (250 mL)	125 mg	—	Phillips lamp (50 W), λ = 380–800 nm	57% (5 h)	—
g-C_3N_4/Bi_2WO_6[513]	Solvothermal and grind calcination method	15 mg L^{-1} [a] (100 mL)	0.1 g	—	Xenon lamp:300 W, $\lambda <$ 400 nm	98% (120 min)	—
Fe_3O_4/Bi_2WO_6 (4% iron content)[514]	Hydrothermal method	10 mg L^{-1} [a] (100 mL)	30 mg	—	Visible-light irradiation ($\lambda >$ 420 nm)	~99.7% (15 min)	—
g-C_3N_4/Ti_3C_2 MXene/black P[515]	Calcination process	20 mg L^{-1} [a] (100 mL)	20 mg	—	Xenon lamp: 300 W, $\lambda >$ 420 nm	>99% (60 min)	0.048 min^{-1}
g-C_3N_4/Ag_3PO_4/chitosan[516]	Multiple steps	20 mg L^{-1} [a]	2.0 mg	7	Visible light	90.34% (60 min)	0.01771 min^{-1}
0.5 wt% Ag/$AgVO_3$/g-C_3N_4[517]	Wet-impregnation method	10 ppm[a] (100 mL)	0.1 g	—	Halogen lamp (500 W): visible light	82.6% (120 min)	—
Bi (7%) nanodots/Bi_3NbO_7 nanosheets[519]	Two-step wet chemical reaction	10 mg L^{-1} [a] (100 mL)	50 mg	—	Xenon lamp: 300 W with 400 nm cut-off filter	86% (120 min)	0.01427 min^{-1}
Bi_2WO_6/Ta_3N_5 (1.0/1 mole ratio)[520]	Electrospinning–calcination–solvothermal route	20 mg L^{-1} [a] (100 mL)	40 mg	3	Xenon lamp: 300 W with a cut-off filter ($\lambda >$ 400 nm), 97 mW cm^{-2}	81.1% (120 min)	0.0105 min^{-1}

Table 7 *(continued)*

Photocatalyst	Preparative method	CIP[a]/CIP·HCl[b]	Catalyst dose	pH	Light source	Degradation (time)	Rate constant
g-C_3N_4@$Cs_{0.33}WO_3$[521]	Solvothermal	20 ppm	20 mg (100 mL)	3	Xenon lamp (500 W), λ: 230–2500 nm, 0.25 W cm^{-2}	97% (145 min)	14.9 × 10^{-3} min^{-1}
g-C_3N_4/rGO/WO_3[523]	Photo reduction method	20 mg L^{-1} [a] (50 mL)	10 mg	—	High-pressure xenon arc lamp with 400 nm cut-off filter and 100 mW cm^{-2}	85% (180 min)	—
CuS/$BiVO_4$ (mass ratio: 7%)[524]	*In situ*	10 mg L^{-1} [a] (100 mL)	100 mg	—	Xenon lamp (300 W) with a 420 nm cut-off filter	86.7% (90 min)	0.02151 min^{-1}

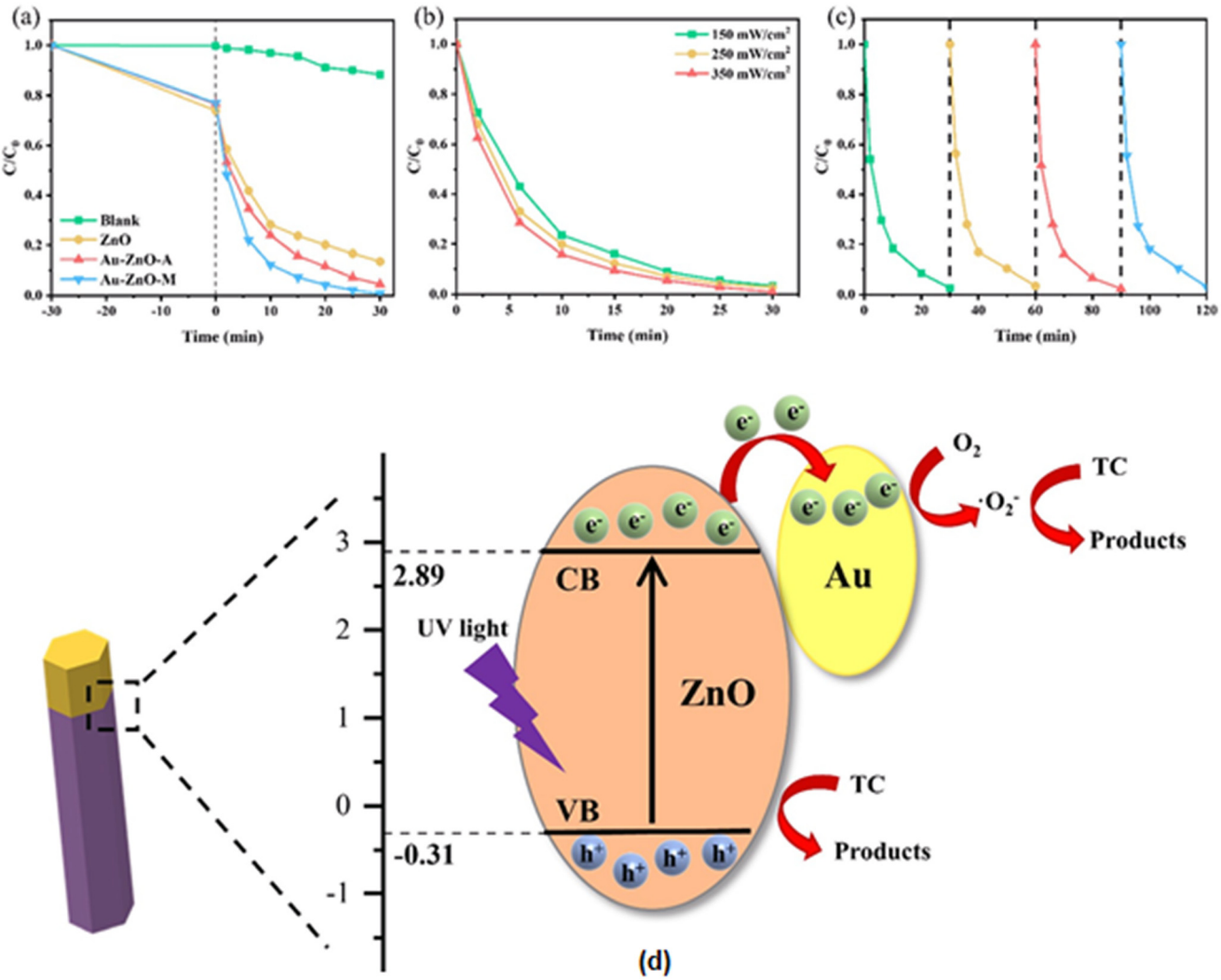

Fig. 18 Photocatalytic degradation of TC. (a) Dynamic curves of different photocatalysts (initial conditions: 40 mg L^{-1}, TC, 0.2 g L^{-1} photocatalyst, and 350 mW cm^{-2} UV light). (b) The impact of UV light intensity (initial conditions: 40 mg L^{-1} TC and 0.2 g L^{-1} Au–ZnO nanomotors). (c) Cycling tests (initial conditions: 30 mg L^{-1} TC: 0.2 g L^{-1}, Au–ZnO nanomotors, and 350 mW cm^{-2} UV light). (d) Proposed photocatalytic mechanism for TC degradation. Reproduced from ref. 542 with permission from RSC (2022).

different photocatalysts, UV light intensity and cycling tests, as presented in Fig. 18(a)–(c), respectively. The findings revealed that the respective degradation rates of tetracycline within 30 min and rate constants corresponding to pseudo-first-order kinetics follow the order: Au–ZnO nanorod motors (Au–ZnO-M): 99.3% > Au–ZnO nanorod array (Au–ZnO-A): 95.5% > ZnO (86.5%), and k 'Au–ZnO nanorod motors (k (Au–ZnO-M): 0.1451 min^{-1} > k (Au–ZnO-A): 0.1120 min^{-1} > k (ZnO): 0.0542 min^{-1}). It was suggested that the Au layer in the Au–ZnO heterojunction nanoarrays acted as an electron reservoir to facilitate charge separation, thereby lowering the possibility of photogenerated carrier recombination. A possible photocatalytic mechanism for the photocatalytic degradation of tetracycline by Au–ZnO nanomotors under UV-light irradiation is displayed in Fig. 18(d). According to this, electrons in Au could react with O_2 to form $\cdot O_2^-$, accounting for the degradation of tetracycline. In contrast, h^+ in the VB of ZnO could directly degrade tetracycline to a stable product.

3.7.3 Doped photocatalysts

3.7.3.1 Doped TiO_2 and ZnO. Several studies have been carried out on the performance of doped TiO_2 and ZnO photocatalysts and subsequently used in the removal of tetracycline from water.[543–546] Red mud and modified red mud originating from industrial solid waste discharged from the aluminum industry have been investigated as low-cost, effective photocatalysts under irradiated visible light.[543] Xu *et al.*[544] developed a C-doped TiO_2–polymethylsilsesquioxane (PMSQ) aerogel followed by thermal treatment at 400 °C in air. They used it to achieve 98% removal of tetracycline hydrochloride from aqueous solution in 180 min and ascribed it to enhanced charge separation. In another study, hydrothermally prepared carbon (3 wt%)-doped TiO_2 with metal (Ni/Co/Cu) nitrate hydroxide was used as a nanocomposite photocatalyst.[545] The photocatalytic activity of this catalyst displayed 97% removal of tetracycline hydrochloride within 60 min. TiO_2 doped with acetylene black,[546] N-doped TiO_2/diatomite,[547] P-doped carbon nitride tubes combined with peroxydisulfate (PDS),[548] N,S-doped TiO_2 and N,S-doped ZnO modified chitosan,[549] and C,N,S-tri-doped TiO_2[550] photocatalysts have also been investigated for the degradation of tetracycline.

Metal-doped photocatalysts have also received a lot of attention for their application in the photocatalytic degradation of tetracycline in aqueous solution. Nb-doped ZnO (Nb : Zn molar ratio: 1 : 1) showed 93.2% degradation efficiency for tetracycline in 180 min under visible light and also possessed superior recyclability and stability.[525] Zhang *et al.*[551] fabricated Ag-doped TiO_2 (Ag^+ : Ti^{4+} mole ratio: 0, 0.5, 1.0, 2.0, 3.0, and 5.0%) hollow microspheres following an applied hydrothermal process by a template-free method. It was noted that Ag-doped TiO_2 (Ag^+ : Ti^{4+} mole ratio: 3.0%) exhibited maximum removal of tetracycline hydrochloride following first-order kinetics with OH· and h^+ playing an active role. Ce (2%)-doped TiO_2/halloysite nanotubes and Ce (2%)–TiO_2/halloysite nanotubes enabled about 78% tetracycline removal within 60 min under visible-light irradiation.[552] TiO_2 composite nanofibers doped with CuO were also studied for the photocatalytic degradation of pharmaceutical wastewater.[553] Bembibre *et al.*[554] used Ca-doped ZnO nanoparticles in the removal of tetracycline under a visible-light-driven sonocatalytic process.

3.7.3.2 Doped graphitic materials. Doped graphitic materials have attracted a lot of attention as photocatalysts in the removal of tetracycline from water.[555] Nitrogen-self-doped g-C_3N_4 nanosheets prepared by a combination of N-self-doping and thermal exfoliation showed higher photocatalytic activity for tetracycline degradation than bulk g-C_3N_4, N-self-doped g-C_3N_4 or g-C_3N_4 nanosheets.[556] This is attributed to the enlarged visible-light absorption ability, reduced recombination and prolonged lifetime of photogenerated charge carriers. Chen *et al.*[557] reported the removal of tetracycline hydrochloride from wastewater (pH: 5) using an S–g-C_3N_4/PTFE membrane under irradiated visible light. These findings indicated 98.1% photocatalytic degradation corresponding to an initial concentration of tetracycline hydrochloride of 10 mg L^{-1}, catalyst dosage of 1 g L^{-1}, and S–g-C_3N_4 loading of 50 mg. Further, the S–g-C_3N_4/PTFE membrane displayed good recovery performance and photocatalytic stability. Ba (2%)-doped g-C_3N_4 demonstrated significant influence on the photocatalytic activity owing to its low band gap and the effective separation of photo-induced e^-–h^+.[558]

Er-doped g-C_3N_4,[559] Cd-doped g-C_3N_4,[560] S-doped carbon quantum dot loaded hollow tubular g-C_3N_4,[561] single-atom Ni,S-co-coped g-C_3N_4,[562] nitrogen defect/boron dopant engineered tubular g-C_3N_4,[563] Ag–g-C_3N_4,[564] Bi-nanoparticle-decorated g-C_3N_4 nanosheets (10 wt%),[565] Co-doped TiO_2-rGO,[566] rGO-doped ZnAlTi-LDH,[567] and graphene oxide/magnetite/cerium-doped titania[568] photocatalysts also acted as efficient photocatalysts in the degradation of tetracycline.

3.7.4 Metal oxide composites. Several studies have been reported on the evacuation removal of tetracycline from water using a combination of metal oxides. Wang *et al.*[526] observed 81% (10 min) photocatalytic degradation of tetracycline by irradiating a 5% carbon quantum dots/TiO_2 composite prepared by a hydrothermal method with visible light. Such performance of the composite is attributed to the improved separation efficiency of photogenerated electrons and holes. According to Liu *et al.*,[569] excellent catalytic performances is observed for 3%-CuO_x/γ-Al_2O_3 in the simultaneous degradation of tetracycline hydrochloride in a wide pH range of 3.10–9.47 under irradiation by a 300 W xenon lamp (190–1100 nm). In another study, a sol–gel-synthesized calcite/TiO_2 photocatalyst accounts for 90% tetracycline removal under UV light in aqueous solution (pH: 7) corresponding to 1.5 g L^{-1} of catalyst and 50 mg L^{-1} of tetracycline.[570] Hunge *et al.*[571] studied the effect of catalyst loading for the MoS_2 (20 wt%)/TiO_2 composite and solution pH, in the degradation of tetracycline under UV-vis irradiation of composites and

observed its superior performance (95%) compared to TiO_2 and MoS_2. ZnO/γ-Fe_2O_3 demonstrated an important role in achieving ~89% degradation efficiency for tetracycline in water under UV-visible light after 150 min.[572]

The degradation of tetracycline in water has been investigated on TiO_2 decorated on magnetically activated carbon as a function of different parameters under ultraviolet and ultrasound irradiation.[573] These findings revealed 93% tetracycline removal at the end of 180 min under optimum conditions corresponding to an optimum intensity of 70 W US power, pH 6.0, catalyst loading of 0.4 g L^{-1}, and initial concentration of tetracycline of 30 mg L^{-1}. ZnO rod-activated carbon fiber,[574] Fe_3O_4/FeP,[575] spatially confined Fe_2O_3 in hierarchical SiO_2@TiO_2 hollow spheres,[576] La-enriched titania–zirconia oxide,[577] $Ni(OH)_2$-decorated TiO_2,[578] IO–TiO_2–CdS,[579] and $WO_{2.72}$/$ZnIn_2S_4$[580] have also been demonstrated as efficient photocatalysts for the removal of tetracycline from water.

Wang *et al.*[581] converted harmful algae into bio-nanohybrid materials by immobilizing *Microcystis aeruginosa* cells onto PAN–TiO_2/Ag hybrid nanofibers. They observed about 96% degradation efficiency for tetracycline hydrochloride under visible light compared to PAN/TiO_2/Ag nanofiber (77%) and *M. aeruginosa* (49%) due to a synergistic effect. It is suggested that enhanced degradation in *M. aeruginosa*/PAN–TiO_2/Ag could be caused by algae facilitating the effective separation of photogenerated electron–holes on TiO_2. The presence of ZnO, carbonaceous layers and Ag nanoparticles improved the optical absorption property in the Ag/ZnO/C structure, resulting in 95.8% (35 min) and 90.6% (280 min) degradation of tetracycline hydrochloride under UV- and visible-light irradiation, respectively.[582] This is ascribed to efficient photogenerated electron separation and transportation and an increase in the active reaction sites. According to Wei *et al.*,[583] an SiO_2–TiO_2–C (n_C : n_{Ti} mol ratio: 3.5) aerogel composite displayed 80.01% degradation efficiency for tetracycline hydrochloride within 180 min under visible light and also retained its high stability and reusability. $\cdot O_2^-$ and ·OH were considered as the active species responsible for the photocatalytic degradation of tetracycline. In addition, ternary chitosan comprising chitosan–TiO_2–ZnO over graphene,[584] palygorskite-supported Cu_2O/TiO_2,[585] CuO/Fe_2O_3,[586] ZnO@zeolitic imidazolate,[587] and bimetallic oxide/carbon[588] have also been tested for the photocatalytic degradation of tetracycline in water.

3.7.5 Graphitic materials

3.7.5.1 g-C_3N_4. Insufficient sunlight usage, low surface area and rapid charge recombination of electron and hole pairs are a major hinderance contributing towards the low photocatalytic performance of g-C_3N_4.[65] As a result, several investigations have been made into the photodegradation of tetracycline using g-C_3N_4 and its composites. Hernández-Uresti *et al.*[333] prepared a graphite-like C_3N_4 photocatalyst by the polycondensation of a melamine precursor and observed the following trend for the photodegradation of four different pharmaceuticals in aqueous solution under UV-vis irradiation: tetracycline > ciprofloxacin > salicylic acid > ibuprofen. The active species responsible for the degradation of tetracycline were considered to be photogenerated holes, OH radicals and H_2O_2. Self-assembly-based g-C_3N_4 nanoflakes showed up to 70% removal efficiency for tetracycline (20 ppm) within 180 min under light irradiation (420 nm).[589]

Shi *et al.*[590] studied the degradation performance of tetracycline in real water systems by metal-free g-C_3N_4 microspheres under various conditions through visible-light catalysis and PMS activation synergy. According to this, the rate constant values for the degradation of tetracycline by photocatalysis, Fenton-like catalysis, and photo-Fenton-like catalysis are 0.013, 0.025, and 0.028 min^{-1}, respectively. The observed superior degradation performance of photo-Fenton-like catalysis is attributed to the synergetic effect between PMS activation and photocatalysis. In another study, Wang and others[591] used graphitic carbon nitride microspheres and recorded 80.54% degradation efficiency for the removal of tetracycline hydrochloride under visible-light irradiation for 2 h, corresponding to a photocatalyst dose of 1.0 g L^{-1}, initial concentration of tetracycline hydrochloride solution of 10 mg L^{-1} and initial pH 7. Porous g-C_3N_4,[592] GQDs/g-C_3N_4,[593] S-doped graphitic carbon nitride,[594] hexagonal BN/g-C_3N_4,[595] poly-*o*-phenylenediamine (POPD)/g-C_3N_4,[596] and N–CNT/mesoporous g-C_3N_4[597] photocatalysts have also been evaluated for the removal of tetracycline.

Jiang *et al.*[598] studied the degradation of tetracycline in aqueous solution using P and S doped g-C_3N_4 under visible light ($\lambda \geq 420$ nm) and showed higher photocatalytic than bare g-C_3N_4 or single-doped g-C_3N_4. According to this, P and S doping in g-C_3N_4 inhibited the recombination of electron–hole pairs and facilitated the efficient separation of photogenerated charges. The h^+ and $\cdot O_2^-$ were the dominant active species responsible for the degradation of tetracycline. Porous g-C_3N_4/TiO_2 (g-C_3N_4 : TiO_2 mass ratio: 12 : 1) photocatalysts removed 88.43% of tetracycline from aqueous solution under a xenon lamp for 90 min, which was ascribed to the synergistic effect.[599] In another study, a ZrO_2-embedded MoS_2/g-C_3N_4 nanocomposite exhibited 94.8% tetracycline degradation in aqueous solution in 90 min under visible light owing to the dual charge-transfer channel between the layers of MoS_2/g-C_3N_4 and ZrO_2 nanoparticles.[600] Poly-*N*-isopropylacrylamide (PNIPAM)/Fe_3O_4/g-C_3N_4 prepared by a hydrothermal method and thermal photoinitiation under visible-light irradiation decomposed tetracycline into harmless small molecules.[601] The catalytic activity remain more or less unaltered even after 5 repeated uses and could be easily separated. In addition, CDs/g-C_3N_4/$BiPO_4$,[602] ZnO/N-doped g-C_3N_4,[603] and g-C_3N_4/$H_3PW_{12}O_{40}$/TiO_2[604] exhibited enhanced photocatalytic degradation performance for tetracycline under visible light.

3.7.5.2 Graphene. Binary and ternary graphitic composite materials have been reported as photocatalysts in the removal of tetracycline from aqueous solution.[605–621] According to Ren *et al.*,[605] a red mud/graphene oxide (mass

ratio: 93 : 7) composite attained the best degradation rate for tetracycline (79.8%) compared to raw red mud under visible light within 80 min owing to its enhanced specific surface area, light absorption and charge separation. Porous hydroxyapatite (Hap) hollow microspheres as a source of cheap and green photocatalysts have been harnessed in fabricating rGO/Hap composites.[606] Investigations revealed significantly enhanced photocatalytic activity of rGO (1.5 wt%)/Hap in tetracycline degradation (92.1%, 30 min) under a xenon lamp (300 W) for full-spectrum irradiation. This is explained on the basis of the photogenerated electrons accumulating at rGO (acting as an electron acceptor) that could interact with O_2 to form $\cdot O_2^-$. In addition, separated positive holes in the VB of porous hollow Hap (acting as an electron donor) microspheres directly participate in the oxidation of tetracycline.

Heteropoly acid ($H_3PMo_8W_4O_{40}$)/graphene oxide nanocomposites based on UiO-66 have been synthesized following an *in situ* growth hydrothermal method and tested as photocatalysts in tetracycline photodegradation under visible-light irradiation.[607] The photocatalytic degradation efficiency for tetracycline was found to be significantly higher (95%: 120 min) compared to GO or heteropoly acid. An Fe_3O_4/GO/ZnO magnetic nanocomposite showed 74% (100 min) degradation of tetracycline hydrochloride under visible-light irradiation.[608] This is explained on the basis of ZnO and Fe_3O_4/GO in Fe_3O_4/GO/ZnO contributing to the generation of the electron–hole pairs under visible light and promoting the transfer of photogenerated electrons, respectively. In another study, graphene quantum dot decorated ZnO–ZnF_2O_4 nanocage ternary composites, prepared by a one-step deposition method exhibited superior performance in the degradation of tetracycline hydrochloride under visible light compared to ZnO or ZnO–$ZnFe_2O_4$.[609] According to Chakraborty *et al.*,[610] an rGO–ZnTe (1 : 1) photocatalyst facilitated the degradation of tetracycline due to a synergistic effect. It is suggested that the 2D wrinkled surface of rGO contributes in minimizing the recombination probabilities of photoinduced electron–hole pairs. N-doped TiO_2 nanoparticles deposited on rGO exhibited more pronounced photodegradation activity for tetracycline hydrochloride than pure TiO_2 or N-doped TiO_2.[611] Subsequent studies on the reusability of N-doped TiO_2/rGO also established the stability of the composite photocatalyst.

Kumar *et al.*[612] fabricated ZnO quantum dots (1.5 wt%)/rGO by a hydrothermal method and observed 68% removal of tetracycline from wastewater (pH: 5) after 120 min under visible light. Fe_3O_4/g-C_3N_4/rGO exhibited 86.7% degradation rate of tetracycline hydrochloride, following pseudo-second-order kinetics.[613] The proposed mechanism suggested $\cdot O_2^-$ and ·OH radicals as the most reactive species in the photocatalytic degradation of tetracycline. Ghoreishian *et al.*[614] reported sonophotocatalytic degradation of tetracycline using a flower-like rGO/$CdWO_4$ composite under simulated visible-light irradiation. These findings under optical conditions (pH: 5.7, initial concentration of tetracycline: 13.54 mg L^{-1}, catalyst dosage: 0.216 g L^{-1}, time: 60 min) revealed its photocatalytic catalytic activity to be 1.5 and 3 times higher than that of commercial nano-ZnO and TiO_2, respectively.

Interfacial growth of a TiO_2–rGO composite by the Pickering emulsion approach showed 94% removal efficiency for tetracycline hydrochloride (10 ppm) after 40 min under the visible light.[615] Such significant enhancement in the photocatalytic efficiency of TiO_2–rGO is ascribed to its 2D sandwich-like structure. Porous hollow hydroxyapatite microspheres decorated with rGO,[616] rGO–CdS,[617] rGO–CdS/ZnS,[72] Ag/TiO_2 nanosheets/rGO,[618] Ag/TiO_2 nanosheets,[619] Ag/TiO_2 nanosheets–rGO,[620] and TiO_2/rGO/activated carbon[621] have also been harnessed as photocatalysts in the degradation of tetracycline in aqueous solution.

3.7.6 Heterojunction-based photocatalysts. Heterojunction photocatalysis have attracted attention for the degradation/removal of tetracycline in aqueous solution by various heterojunctions.[51] In this regard, a core–shell g-C_3N_4@Co–TiO_2 heterostructured nanofibrous membrane exhibited excellent visible-light-driven degradation of tetracycline hydrochloride.[622] Huang *et al.*[623] observed 74.7% degradation efficiency for tetracycline hydrochloride within 30 min by a hierarchical Au (2%)–g-C_3N_4–ZnO heterostructure under xenon lamp irradiation. Mesoporous TiO_2-modified ZnO quantum dots (8%) immobilized on linear low-density polyethylene (LLDPE) under fluorescent light irradiation showed 89.5% removal of tetracycline (initial concentration: 40 mg L^{-1}) from water (pH: 9) within 90 min.[624] g-C_3N_4/CuO (7%)[625] and ZnO globular (15 wt%)/g-C_3N_4[626] showed 55% and 78.4% degradation of tetracyclines in 60 and 50 min under simulated solar light ($\lambda > 365$ nm) and artificial visible sunlight illumination ($\lambda \geq 400$ nm), respectively.

$Ti_{0.7}Sn_{0.3}O_2$/g-C_3N_4 (mass ratio: 10 wt%) achieved 83% degradation of tetracycline hydrochloride in 40 min under irradiated visible light.[627] This is explained on the basis of an S-scheme between $Ti_{0.7}Sn_{0.3}O_2$ and g-C_3N_4 to increase and transport photogenerated charges. The ultrasonic-assisted precipitation method has been used to fabricate a ZnO (20 wt%)/GO (2 wt%)/Ag_3PO_4 heterojunction and it has been used as a photocatalyst in the elimination of tetracycline hydrochloride from wastewater.[628] These findings showed 96.32% (75 min) degradation under visible light corresponding to initial concentration of tetracycline of 30 mg L^{-1} and catalyst dose of 1.0 g L^{-1}.

The degradation rate of tetracycline was found to be about 10 times higher in a g-C_3N_4/C/Fe_3O_4 ternary nanocomposite compared to its individual or binary components under simulated solar light.[629] The degradation process followed a first-order kinetics model with a much higher apparent rate constant for g-C_3N_4/C/Fe_3O_4 (0.0063 min^{-1}) compared to g-C_3N_4 (0.0029 min^{-1}) or carbon (0.0003 min^{-1}). The photoinduced h^+ and $\cdot O_2^-$ free radicals are suggested to act as the main active components in the degradation. The enhanced activity of g-C_3N_4/C/Fe_3O_4 in tetracycline degradation is attributed to heterojunction formation and is

due to the effective separation of the photocarriers. In addition, the introduction of C into g-C_3N_4/C/Fe_3O_4 facilitates an enhancement of the optical response range and effective electron transfer.

Liao *et al.*[630] examined the utility of a core–shell $BiFeO_3$/TiO_2 heterostructure with a p–n heterojunction as a photocatalyst prepared by forming nanospheres of TiO_2 on $BiFeO_3$ (nanocubes) in tetracycline degradation under visible-light irradiation. The findings indicated much higher degradation efficiency of $BiFeO_3$/TiO_2 (72.2%) compared to $BiFeO_3$ (64.9%) and TiO_2 (38.3%) after 180 min of visible illumination. A $BiFeO_3$/TiO_2 p–n heterojunction photocatalyst showed superior degradation efficiency for tetracycline due to its enlarged specific surface area and higher sensitivity to visible light, improved separation and transfer efficiency of photoelectron–hole pairs and a synergistic effect. Fiber-shaped Ag_2O/Ta_3N_5 p–n heterojunctions designed as efficient photocatalysts showed enhanced photocatalytic activity with good stability in photocatalytic activity for tetracycline under visible light ($\lambda > 400$ nm) due to the synergistic effect.[631] It is anticipated that photogenerated holes and superoxide radicals played prominent roles in the photocatalytic process.

Chen and others[632] fabricated an α-Bi_2O_3/g-C_3N_4 heterostructure modified by plasmonic metallic Bi and oxygen vacancies and observed a remarkably high degradation rate for tetracycline (90.2%) under visible light after 180 min. Such enhancement is attributed to the formation of a p–n junction arising from a combination of n-type (g-C_3N_4) and p-type (α-Bi_2O_3) semiconductors, which is beneficial in a ternary photocatalyst. It is suggested that Bi nanoparticles and the presence of oxygen vacancies favor the consumption and separation of the photogenerated electrons and holes in the ternary heterojunction photocatalyst. Several other heterojunction photocatalysts, such as C_3N_4@$MnFe_2O_4$–rGO,[491] $BiVO_4$/TiO_2/rGO,[633] porous g-C_3N_4/AgBr/rGO,[634] C_3N_4-supported WO_3/BiOCl,[635] BiOI/exfoliated C_3N_4,[636] CuO@ZnO,[637] ZnO/SnO_2,[638] Cu_2O–TiO_2,[639] MoS_2/Ag/g-C_3N_4,[640] g-C_3N_4/ZrO_{2-x},[641] and needle SnO_2 nanoparticles anchored on exfoliated g-C_3N_4[642] have also shown enhancement and stability in the degradation of tetracycline.

N-doped ZnO–MoS_2 binary heterojunctions have been fabricated by a hydrothermal method and used to study its photocatalytic activity for the degradation of tetracycline under visible-light irradiation.[643] Fig. 19(a)–(d) show

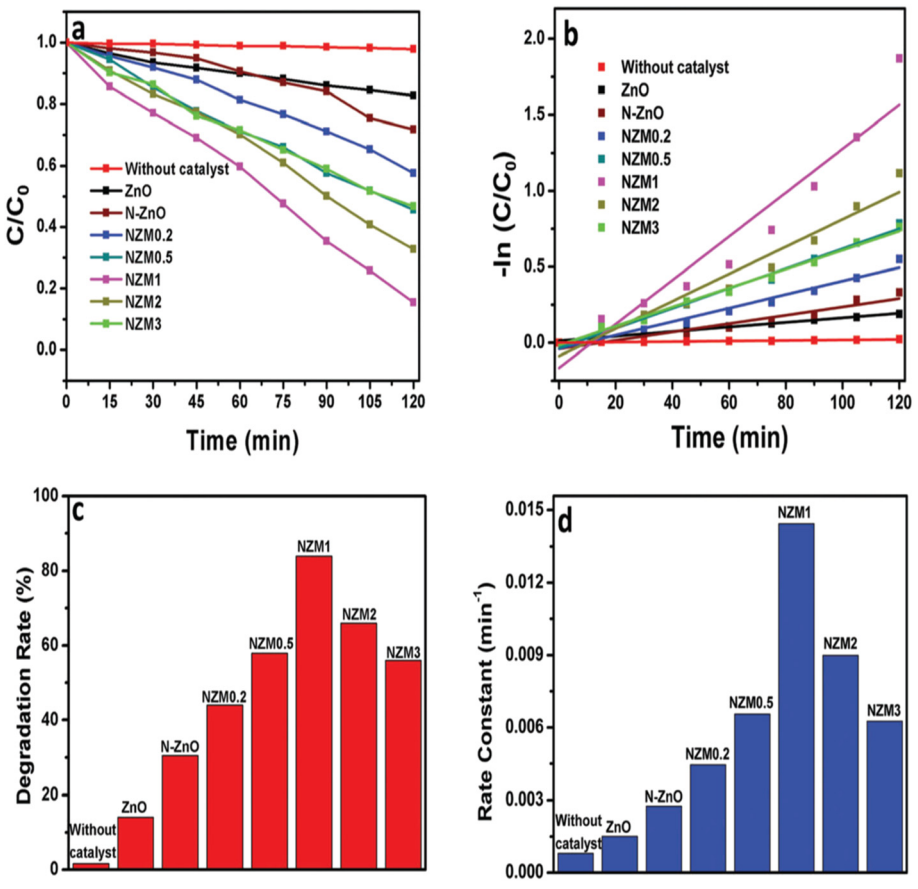

Fig. 19 (a) Kinetic curves for the degradation of TC, (b) ln(C/C_0) *vs.* time curve for the degradation of TC, (c) a histogram showing a comparative degradation rate (%) of TC under visible light illumination and (d) a bar graph showing the values of rate constants for all the photocatalysts (N-doped ZnO nanorods loaded 0.2, 0.5, 1, 2 and 3 wt% of with MoS_2 nanoflowers (MNF) are referred to as NZM0.2, NZM0.5, NZM1, NZM2, and NZM3, respectively). Reproduced from ref. 643 with permission from RSC (2017).

corresponding findings based on variations in the degradation of TC with time, corresponding $\ln(C/C_0)$ *vs.* time plots, a histogram showing a comparative degradation rate (%) of TC under visible light illumination and a bar graph showing the values of rate constants for all the photocatalysts. It should be noted that photocatalytic degradation of tetracycline followed pseudo-first-order kinetics. In addition, fabricated semiconductor heterojunctions demonstrated enhanced performance for the degradation of tetracycline due to the synergistic effect. Furthermore, the enhanced photostability of the photocatalyst over three cycles for a period of 360 min is ascribed to the transfer of holes from the valence band of N-doped ZnO to the valence band of MoS_2.

A novel type-II $Bi_2W_2O_9$/g-C_3N_4 heterojunction has been fabricated and studied for its photocatalytic performance in the removal of tetracycline under simulated solar irradiation and it was compared with $Bi_2W_2O_9$ and g-C_3N_4, as displayed in Fig. 20(a).[72] It is inferred that $Bi_2W_2O_9$/g-C_3N_4 yields high photodegradation (~95%) compared to the degradation observed for pristine g-C_3N_4 (75%) or $Bi_2W_2O_9$ (~60%). This is attributed to the $Bi_2W_2O_9$ semiconductor acting as a trap for photogenerated holes and electrons. A photocatalytic mechanism has also been proposed for the $Bi_2W_2O_9$/g-C_3N_4 system in Fig. 20(b).

Z-scheme WO_3/g-C_3N_4 composite hollow microspheres fabricated by an *in situ* hydrolysis and polymerization process showed an enhanced degradation rate towards tetracycline hydrochloride (82% in 120 min) under visible-light irradiation.[644] The enhanced separation of photoinduced electrons and holes and the synergistic effect of g-C_3N_4 and WO_3 are considered to be a few reasons for this. In addition, the presence of hollow cavities could enable trapping of the incident photons and facilitate availability of more electrons and holes in the photocatalytic process. In another study, a Z-scheme mesoporous Sn_3O_4/g-C_3N_4 heterostructure exhibited superior photocatalytic performance in degrading tetracycline hydrochloride present in water.[645] A possible photocatalytic reaction mechanism has also been examined in detail for this. In another study, BiOI/g-C_3N_4/CeO_2 (3 wt%) photocatalyst possessed the best photocatalytic activity for degradation of tetracycline (91.6%) under visible-light irradiation.[646] It is anticipated that CeO_2/g-C_3N_4 and BiOI/g-C_3N_4 catalysts block the recombination of photoinduced electron–hole pairs through the formation of a heterojunction.

Dai *et al.*[73] *in situ* prepared 3D-20% polyaniline/perylene diimide (PANI/PDI) and found the degradation rate for tetracycline under visible-light irradiation in a static system, by 15.3 times and 17.0 times those of pure PDI and PANI, respectively. The main reactive species in the degradation of tetracycline comprised superoxide radicals, hydrogen peroxide and holes. Fig. 21(a) and (b) schematically show the electron–hole pair separation process and TC degradation mechanism of a 3D 20%-PANI/PDI heterojunction under visible-light irradiation. Scanning electron microscopy images of 3D PANI/PDI in Fig. 21(c and d) indicate a significant decrease in size after the dissolution/assembly process and the PDI are uniformly/orderly dispersed in the 3D network structure of PANI.

In addition, TiO_{2-x}/ultra thin g-C_3N_4/TiO_{2-x},[647] K-doped g-C_3N_4/TiO_2/CdS,[648] γ-Fe_2O_3 nanospheres anchored on g-C_3N_4,[649] CQDs/g-C_3N_4,[650] Ag_3PO_4/MIL-88A(Fe),[651] BiOBr/MoS_2/GO,[652] g-C_3N_4/MnO_2/GO,[653] $BiVO_4$@polypyrrole/g-C_3N_4,[654] AgI/BiOBr/rGO,[655] graphene-bridged Ag_3PO_4/Ag/$BiVO_4$,[656] g-C_3N_4 nanoparticles/WO_3 hollow microspheres,[657] $CuIn_2S_2$/g-C_3N_4,[658] Ag_3PO_4/g-C_3N_4/ZnO,[659] g-C_3N_4 nanosheet/Ag_3PO_4/α-Bi_2O_3,[660] $LaNiO_3$-modified C_3N_4[661] and ultrafine TiO_2 nanoparticle

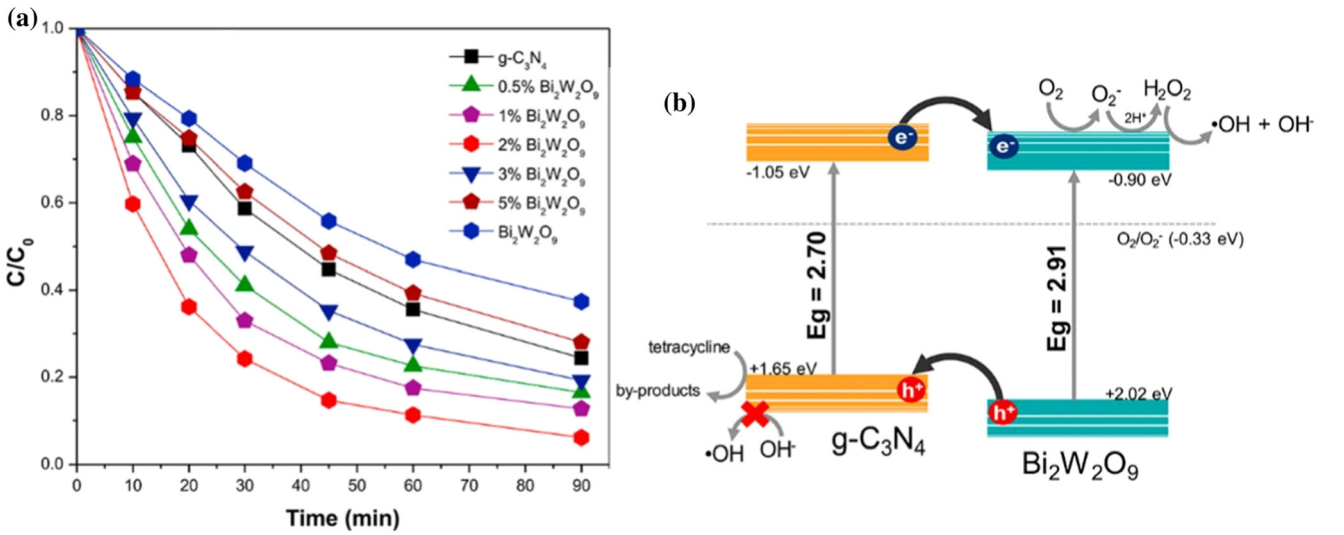

Fig. 20 (a) Photocatalytic degradation of tetracycline antibiotic (C_0 = 10 mg L^{-1}, pH = 4.89) as a function of irradiation time over $Bi_2W_2O_9$, g-C_3N_4 and $Bi_2W_2O_9$/g-C_3N_4 samples. (b) Proposed photocatalytic mechanism for the $Bi_2W_2O_9$/g-C3N4 system under solar-like irradiation. Reproduced from ref. 72 with permission of Elsevier (2020).

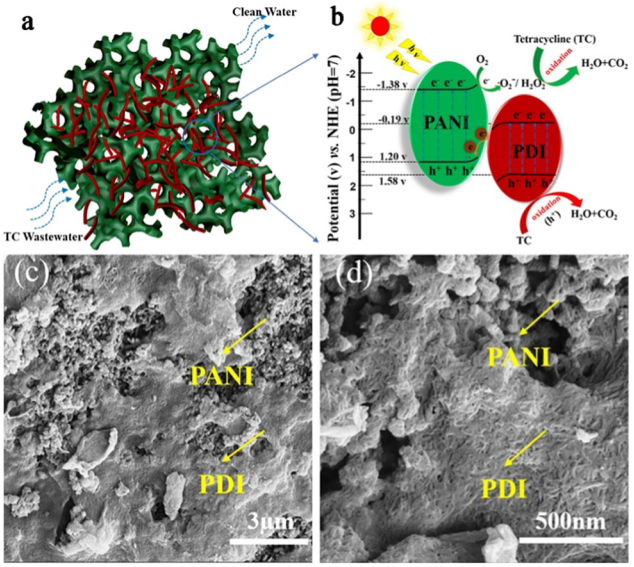

Fig. 21 (a) Morphological structure of PANI/PDI. (b) Photocatalytic mechanism of PANI/PDI heterojunction photocatalysts under visible-light irradiation: direct Z-scheme heterojunction mechanism. (c and d) Scanning electron microscopy images of 3D PANI/PDI. (Modified) Reproduced from ref. 73 with permission of Elsevier (2020).

modified g-C_3N_4[662] heterojunction photocatalysts have also been harnessed in the removal of tetracycline in water.

Table 8 records the performance data of different photocatalysts used in the removal of tetracycline from water.

3.8 Diclofenac

Diclofenac (DCF), an important non-steroidal anti-inflammatory drug, finds multifaceted applications as a painkiller primarily for dysmenorrhea, rheumatoid arthritis and inflammation.[663,664] The intake of diclofenac even at low levels by humans and other living organisms is reported to have an adverse biochemical effect. The solubility and high polarity of diclofenac in water and lower degradability account for its water pollution. Further, it can accumulate in food chains owing to its migration through the aquatic medium (surface water, drinking water, underground water) in food chains. In view of this, the following photocatalytic methods have been used in the removal of diclofenac from water.[665–748]

3.8.1 Metal oxides. Rizza *et al.*[667] studied the degradation of diclofenac sodium by UV/TiO_2 for a wide range of initial DCF concentrations (5–80 mg L^{-1}) and photocatalyst loadings (0.2–1.6 g L^{-1}) in a batch reactor system. These results showed 100% removal of DCF compared to ~3% and 14% for TiO_2 (dark conditions) and photolysis (UV) corresponding to the initial concentration of 5 mg L^{-1} and catalyst dosage of 0.2 g L^{-1}. The photocatalytic degradation of real pharmaceutical wastewater (pH: 9) including diclofenac and other drugs by TiO_2/H_2O_2 was found to be 45.11% under UV-mediated irradiation within 120 minutes.[668] TiO_2 nanofilm membranes fixed on glass panels have also been explored in

Table 8 Performance data of tetracycline on its removal in water using different photocatalysts

Photocatalyst	Preparative method	CIP[a]/CIP·HCl[b]	Catalyst dose	pH	Light source	Degradation and time	Rate constant
TiO_2[526]	Solvothermal	50 mg L^{-1} [a] (100 mL)	30 mg	6.0	Visible light LED 50 W	~25% (12 min)	~0.03 min^{-1}
TiO_2 (P25 Degussa)[527]	Commercial	20 mg L^{-1} [a] (100 L)	1.5 g L^{-1}	8.7	Xenon lamp, 250 Wm^{-2}, 300–800 nm	100% (15 min)	—
ZnO (Sigma Aldrich)[527]	Comme rcial	20 mg L^{-1} [a] (100 mL)	1.0 g L^{-1}	11	Xenon lamp, 250 Wm^{-2}, 300–800 nm	100% (15 min)	—
Nanosized TiO_2 (P25) with 70% anatase and 30% rutile[528]	Commercial	40 mg L^{-1} [b] (40 ml)	1000 mg L^{-1}	9	Medium-pressure mercury lamp (UV), $\lambda < 290$ nm 525 μW cm^{-2}	95% (60 min)	—
Nanosized TiO_2 with 80% anatase and 20% rutile in presence of H_2O_2 (100 mg L^{-1})[529]	Commercial	55 mg L^{-1} [b] (250 mL)	1 g L^{-1}	5	UV lamp: 18 W, λ: 254 nm, 2500 μW cm^{-2}	100% (30 min)	7.25 × 10^{-3} min^{-1}
TiO_2–P25 (80% anatase and 20% rutile) in presence of H_2O_2 (100 mg L^{-1})[530]	Commercial	10 mg L^{-1} [a] (100 mL)	0.2 g L^{-1}	—	Xenon lamp 300 W, 20 mW cm^{-2}, λ: 350 nm	94.8% (120 min)	~3.8 × 10^{-2} min^{-1}
TiO_2 (P25) immobilized in chitosan[531]	Dispersion method	30 mg L^{-1} [b]	0.12 g	4	UV lamp (30 W), λ_{max}: 360 nm	87% (360 min)	0.025 min^{-1}
Nanometric and immobilized TiO_2[532]	Modified sol–gel method (product calcined at 400 °C)	35 ppm[b]	300 mg	—	Jelosil HG500 UV lamp, 30 mW cm^{-2}	90% (35 min)	56 ± 2 × 10^{-3}
ZnO nanoparticles (peroxy monosulfate:2 mM)[533]	Biosynthesis	10 mg L^{-1} [b]	2 g L^{-1}	7.0	Low-pressure UV lamp (6 W), λ: 254–258 nm	95.6% (90 min)	0.018 min^{-1}

Table 8 *(continued)*

Photocatalyst	Preparative method	CIP[a]/CIP·HCl[b]	Catalyst dose	pH	Light source	Degradation and time	Rate constant
Iron oxide nanoparticles[534]	Co-precipitation	83 μM[b] (10 mL)	10 mg	7	Hg quartz lamp (280 W), λ: 180 nm to 623 nm	40% (60 min)	0.0092 min^{-1}
Nanospherical α-Fe_2O_3 supported on 12-tungstosilicic acid (H_2O_2: 0.1 ppm/250 ml)[535]	Solid state dispersion	30 ppm[a]	150 ppm	8	Hg lamp (15 W), λ: 254 nm	97.39% (50 min)	0.0098 min^{-1}
SnO_2 hollow microspheres ($SnCl_2{\cdot}2H_2O$: $Na_3C_6H_5O_7{\cdot}2H_2O$ mole ratio = 1 : 4)[536]	Hydrothermal method	50 mg L^{-1} [b] (40 ml)	50 mg	—	Hg lamp, λ: 365 nm	76% (140 min)	0.00861 min^{-1}
$BiFeO_3$ (in presence of H_2O_2: 9.8 mM)[538]	Calcination of gel formed from bi and Fe nitrates at 600 °C	40 mg L^{-1} [a]	2 g L^{-1}	4	Hg lamp (300 W), λ = 365 nm	100% (210 min)	0.02650 min^{-1}
Nb doped TiO_2 (Nb : Zn molar ratio of 1 : 1)[525]	Green synthesis	150 mg L^{-1} [a] (100 mL)	0.25 g L^{-1}	7	250 W xenon arc lamp with a 420 nm cut-off filter	91. 5% (180 min)	7.3 × 10^{-3} min^{-1}
Au–TiO_2 (0.3 g)/PVDF[539]	Three-step synthesis strategy	20 ml[a] solution	0.1 g	—	Xenon lamp (300 W), λ < 420 nm	75% (120 min)	0.01212 min^{-1}
C-doped TiO_2 (in PMSQ)[544]	Multiple steps	10 mg L^{-1} [b] (50 mL)	0.5 g	7	W halogen lamp (100 W) with filter (λ > 420 nm)	98% (180 min)	—
TiO_2/acetylene black with PS: 3 mM L^{-1}[546]	Mixing method	30 mg L^{-1} [b] (100 mL)	0.5 g L^{-1}	4.1	LED lamp (30 W), λ: 400–780 nm, 50 W m^{-2}	93.3% (120 min)	2.2 × 10^{-2} min^{-1}
N doped TiO_2 diatomite[547]	Mixing followed by calcination	20 mg L^{-1} [b]	5 g L^{-1}	6	Xenon lamp (150 W), λ < 400 nm	91% (300 min)	—
P doped carbon nitride tube (peroxydisulfate: 1.0 g L^{-1})[548]	Hydrothermal calcination	20 mg L^{-1} [a] (100 mL)	0.3 g L^{-1}	4.59	Xenon lamp (300 W) with a cut-off filter of λ: 400 nm, 180 mW cm^{-2}	96.4% (60 min)	0.0492 min^{-1}
Chitosan modified N,S-doped TiO_2[549]	Sol–gel-hydrothermal method	10 mg L^{-1} [a] (100 mL)	0.6 g L^{-1}	8.2	LED lamp: 18 W	91% (20 min)	0.048 min^{-1}
C,N,S-tri-doped TiO_2[550]	Sol–gel method (thiourea-to-Ti molar ratio of 0.05 : 1 and calcined at 450)	5.0 mg L^{-1} [a]	0.5 g L^{-1}	9	Solar stimulator equipped with xenon arc lamp (150 W), λ < 420 nm	98% (180 min)	24.6 × 10^{-3} min^{-1}
Ag-doped TiO_2 (Ag^+ to Ti^{4+}molar ratio: 3.0%)[551]	Template-free route (hydrothermal)	30 mg L^{-1} [b]	100 mg	—	Xenon lamp (300 W) and (λ > 420 nm)	~88% (30 min)	6.77 × 10^{-2} min^{-1}
Ce (2%)–TiO_2/halloysite nanotubes[552]	Modified sol–gel method	20 mg L^{-1} [a] (100 mL)	50 mg	—	Xenon lamp (300 W), λ > 420 nm	78% (60 min)	—
TiO_2 composite nanofibers doped with CuO[553]	Electrospinning technique	100 ppm[a]	1.0 g L^{-1}	Neutral	Xenon lamp (400 W)	71% (60 min)	—
N self-doped g-C_3N_4[556]	Combination of N self-doping and thermal exfoliation process	10 mg L^{-1} [a] (100 mL)	0.5 g L^{-1}	—	Xenon lamp (300 W), λ > 350 nm	89.14% (60 min)	—
S–g-C_3N_4/PTFE membrane[557]	Ultrasonic device method	10 mg L^{-1} [b]	50 mg	5	300 W xenon light irradiation with a 420 nm cut-off filter	98.1% (120 min)	0.03348 min^{-1}
Ba (2%)-doped g-C_3N_4[558]	Facial thermal condensation method	20 mg L^{-1} [a] (50 mL)	50 mg	10	Xenon lamp (150 W) with 400 nm cut-off filter	91.94% (120 min)	0.0175 min^{-1}
Er (0.0035 g)-doped g-C_3N_4[559]	Calcination	25 mg L^{-1} [a] (50 ml)	25 mg	4	Xenon lamp (35 W)	~90% (90 min)	0.0204 min^{-1}
Cd (4.6 wt%) doped g-C_3N_4[560]	Thermal polymerization method	10 mg L^{-1} [a]	0.8 g L^{-1}	5	Xenon lamp (300 W) with λ > 420 nm	98.1% (60 min)	—
S-doped CQDs loaded hollow tubular g-C_3N_4[561]	Ultrasonic assisted synthesis strategy	20 mg L^{-1} [a]	1 g L^{-1}	—	Xenon lamp (300 W), 0.33100 W cm^{-2}	82.67% (60 min)	0.0293 min^{-1}

Table 8 *(continued)*

Photocatalyst	Preparative method	CIP[a]/CIP·HCl[b]	Catalyst dose	pH	Light source	Degradation and time	Rate constant
Ni–S co-coped g-C_3N_4[562]	Thermal polymerization followed by calcination	10 ppm[b] (30 mL)	5 mg	5	Xenon lamp (300 W), 100 W cm^{-2}	91.77% (60 min)	0.031 min^{-1}
Ag doped g-C_3N_4[564]	Heating melamine and urea mixture	20 mg L^{-1} [a] (50 mL)	0.1 g	7	Solar light	96.8% (120 min)	—
Bi nanoparticle-decorated g-C_3N_4 nanosheet (10 wt%)[565]	Ultrasound-assisted electrostatic self-assembly method	10 mg L^{-1} [b]	40 mg	7	Lamp (300 W), λ: 420–780 nm	90.7% (70 min)	—
Co (0.20 wt%) doped TiO_2/rGO[566]	One-pot hydrothermal method	30 mg L^{-1} [b] (100 mL)	100 mg	—	Halogen lamp: 500 W (400 nm cut-off filter)	60% (180 min)	—
Magnetic graphene oxide–Ce (10% mass ratio) doped titania[568]	Dispersion method	25 mg L^{-1} [a] (100 mL)	50 mg	—	Xenon lamp: 300 W, 400 nm cut-off filter	82.92% (180 min)	0.03005 min^{-1}
MoS_2 (20 wt%)/TiO_2[571]	Hydrothermal route	10 mg L^{-1} [a]	100 mg	5.5	Metal halide lamp: 400 W (UV-vis light source)	95% (100 min)	0.0276 min^{-1}
ZnO/γ-Fe_2O_3[572]	Microwave-assisted solution method	30 mg L^{-1} [a] (20 mL)	0.5 mg L^{-1}	6.7	Halogen lamp, 100 mW cm^{-2}	88.52% (150 min)	0.01321 min^{-1}
Magnetic activated C@TiO_2[573]	Impregnation method	10 mg L^{-1} [a]	0.4 g L^{-1}	6	UVC lamp (40 W), (λ: 254 nm)	~100% 180 min	0.19 min^{-1}
ZnO rod-activated carbon fiber (ACF)[574]	Microwave	40 mg L^{-1} [a] (150 mL)	One piece (5.5 cm of ZnO rod-ACF)	8	UV lamp (20 W), λ: 8365 nm	>99% (60 min)	—
Fe_3O_4/FeP (molar ratios of Fe : P at 1 : 6)[575]	Hydrothermal synthesis and partial phosphating annealing method	50 mg L^{-1} [b] (40 mL)	20 mg	—	Xenon lamp (1000 W)	88% (180 min)	0.00984 min^{-1}
Hierarchical hollow SiO_2–Fe_2O_3@TiO_2[576]	Dispersion/*in situ* polymerization/sol–gel approach	10 mg L^{-1} [a] (50 mL)	0.2 mg mL^{-1}	3–7	Simulated solar-light irradiation	100% (140 min)	—
Fe_2O_3 in hierarchical SiO_2@TiO_2 hollow sphere[576]	Dispersion/*in situ* polymerization/sol–gel	10 mg L^{-1} [a] (50 mL)	0.2 mg mL^{-1}	—	Natural sunlight irradiation	100% (80 min)	—
La–TiO_2–ZrO_2[577]	Sol–gel process	10 mg L^{-1} [a] (100 mL)	0.35 mg L^{-1}	5	UV lamp	100% (120 min)	0.0359 min^{-1}
$Ni(OH)_2$ decorated rutile TiO_2[578]	Deposition of $Ni(OH)_2$ on hydrothermally prepared TiO_2 nanorods using 0.2 M $TiCl_4$	100 mg L^{-1} [a] (20 mL)	200 mg	—	200 W Hg xenon lamp, λ < 420 nm (cut-off filter)	76% (150 min)	0.0090 min^{-1}
3D IO–TiO_2–CdS[579]	Hydrothermal synthesis	30 mg L^{-1} [b]	30 mg	—	Xenon lamp (λ < 420 nm)	>99% (20 min)	—
1D/2D $WO_{2.72}$/$ZnIn_2S_4$[580]	Hydrothermal reaction	50 mg L^{-1} [b] (300 mL)	30 mg	—	Xenon lamp: 300 W (λ > 420 nm)	97.3% (60 min)	—
PAN/TiO_2/Ag nanofiber[581]	Immobilizing *M. aeruginosa* cells onto PAN/TiO_2/Ag	20 mg L^{-1} [b] (500 mL)	1 g L^{-1}	6	Halogen lamp: 500 W (λ < 420 nm)	96% (240 min)	5.62 × 10^{-3} min^{-1}
Ag/ZnO/C[582]	Calcination and photodeposition route	20 mg L^{-1} [b] (100 mL)	100 mg	—	Xenon lamp: 500 W, λ > 400 nm	81% (280 min)	—
Ag/ZnO/C[582]	Calcination and photodeposition route	20 mg L^{-1} [b] (100 mL)	100 mg	—	UV lamp: 250 W, λ_{max}: 365 nm	95.8% (35 min)	—
SiO_2–TiO_2–C (n_c : n_{Ti}: 3.5)[583]	Sol–gel method	10 mg L^{-1} [b] (50 mL)	—	—	Visible light (λ > 420 nm)	80.31% (180 min)	0.00831 min^{-1}
Chitosan–TiO_2–ZnO[584]	Sol–gel and ultrasound-assisted method	20 mg L^{-1} [a]	0.5 g L^{-1}	4	UV	97.2% (180 min)	—
Palygorskite-supported Cu_2O/TiO_2[585]	Liquid phase reduction method	30 mg L^{-1} [b] (50 mL)	1.0 mg	8.7	Xenon lamp: 500 W	88.81% (240 min)	0.0129 min^{-1}
CuO/Fe_2O_3[586]	Green synthesis	20 mg L^{-1} [a]	40 mg	7	UV irradiation	88% (80 min)	0.048 min^{-1}
$Zr_{0.3}$Ti/C[588]	Calcination	10 mg L^{-1} [a]	—	—	Xenon lamp (300 W)	98% (30	0.84 L

Table 8 *(continued)*

Photocatalyst	Preparative method	CIP[a]/CIP·HCl[b]	Catalyst dose	pH	Light source	Degradation and time	Rate constant
						min)	Mol^{-1} min^{-1}
Polymeric g-C_3N_4[333]	Polycondensation	20 mg L^{-1} [a] (200 mL)	200 mg	5.5	Xenon lamp (35 W)	86% (240 min)	—
g-C_3N_4 nanoflakes[589]	Thermal condensation followed by heat treatment	20 ppm[a]	—	—	LED (6 W), λ: 365 nm	70% (180 min)	—
Self-assembled g-C_3N_4 microsphere[591]	Supramolecular self-assembly with post-heating treatment	10 mg L^{-1} [b]	1.0 g L^{-1}	7	Xenon lamp: 500 W ($\lambda > 420$ nm)	80.54% (120 min)	—
Porous g-C_3N_4[592]	Calcination of bulk g-C_3N_4	20 mg L^{-1} [b] (50 mL)	30 mg	9	Xenon lamp (300 W) with UV cut-off filter 420 nm	91.8% (60 min)	—
0.5 wt% GQDs/g-C_3N_4[593]	Electrostatic interaction method	20 mg L^{-1} [b]	25 mg	—	300 W xenon arc lamp, $\lambda >$ 400 nm	~67% (120 min)	—
S-doped graphitic carbon nitride[594]	Thermal induction copolymerization	30 mg L^{-1} [a]	0.01 g L^{-1}	4	Solar light	93.8% (60 min)	—
h-BN (2.0 mg)/g-C_3N_4[595]	*In situ* method	10 mg L^{-1} [a] (100 mL)	1.0 g L^{-1}	—	Xenon lamp (300 W, $\lambda > 400$ nm)	79.7% (60 min)	0.02775 min^{-1}
POPD/g-C_3N_4[596]	Suspension polymerization	10 mg L^{-1} [b] (50 mL)	0.5 g L^{-1}	—	Xenon lamp (300 W)	86.0% (120 min)	—
N doped CNT/mpg-C_3N_4[597]	Thermal polycondensation	20 mg L^{-1} [b]	1.0 g L^{-1}	—	Xenon lamp (300 W)	67.1% (240 min)	—
P,S-doped g-C_3N_4 (hexachloro triphosphazene: 50 mg)[598]	*In situ* thermal copolymerization	10 mg L^{-1} [a]	1.0 g L^{-1}	—	300 W xenon lamp, $\lambda > 420$ nm	85.85% (60 min)	0.03823 min^{-1}
Porous g-C_3N_4/TiO_2 nanoparticles[599]	Reaction carried out under autoclave	10 mg L^{-1} [a] (70 mL)	70 mg	5	Xenon lamp irradiation	88.43% (90 min)	—
ZrO_2 nanoparticles@MoS_2/g-C_3N_4[600]	Multiple steps	20 mg L^{-1} [a] (100 mL)	50 mg	3	Xenon lamp (300 W), $\lambda > 420$ nm	94.8% (90 min)	0.0230 min^{-1}
PNIPAM/Fe_3O_4/g-C_3N_4[601]	Thermal photoinitiation technology	20 mg L^{-1} [a] (100 mL)	0. 1 g	—	Xenon lamp (300 W): visible light	~78% (120 min)	—
CDs doped g-C_3N_4//$BiPO_4$[602]	Hydrothermal method	10 mg L^{-1} [b]	1 g L^{-1}	4	Xenon lamp (500 W), under visible light	75.50% (220 min)	0.0005 min^{-1}
20% ZnO/N doped g-C_3N_4[603]	Self-assembled method through electrostatic attraction	20 mgL^{-1} [b] (200 mL)	0.1 mg L^{-1}	—	Xenon lamp (300 W) under visible light	81.3% (15 min)	0.1016 min^{-1}
Red mud modified with graphene oxide (mass ratio: 93 : 7)[605]	Ultrasonic mixing	10 mg L^{-1} [a]	50 mg	6.9	Xenon lamp (300 W), $\lambda > 420$ nm	79.8% (80 min)	0.02011 min^{-1}
rGO (1.5 wt%) hydroxyapatite microsphere[606]	Hydrothermal method	60 mg L^{-1} [a]	1.0 g L^{-1}	5	Xenon lamp (300 W) with full spectrum irradiation	92.1% (30 min)	0.1816 min^{-1}
Heteropoly acid/GO/UiO-66[607]	*In situ* growth hydrothermal method	20 ppm[a] (50 mL)	0.02 g	7	Hg lamp 500 W ($\lambda > 400$ nm)	95% (120 min)	—
Fe_3O_4/GO/ZnO[608]	Dispersion, followed by hydrothermal treatment	50 mg L^{-1} [b]	1 mg L^{-1}	—	Under simulated light irradiation (intensity: 1 kW m^{-2})	74% (100 min)	14×10^{-3} min^{-1}
GQDs (1 mL)/ZnO–$ZrFe_2O_4$[609]	One-step deposition process	20 mg L^{-1} [b]	20 mg (50 mL)	—	Xenon lamp (500 W) coupled with 420 nm cut-off filter	~90% (27 min)	0.08809 min^{-}
rGO/ZnTe (1 : 1)[610]	Single-pot one-step solvothermal process	10 mg L^{-1} [a]	100 mg (50 mL)	—	Solar simulator (AM 1.5, 100 mW cm^{-2})	~70% (40 min)	0.033 min^{-1}
N doped–TiO_2/rGO[611]	Photoreduction method	10 mg L^{-1} [b]	50 mg	—	Xenon arc lamp (300 W) with 400 nm cut-off filter	98% (60 min)	0.05655 min^{-1}
1.5 w% ZnO quantum dots/rGO[612]	Precipitation and hydrothermal methods	20 ppm[a] (50 ml)	50 mg L^{-1}	5	Non halogen lamps (24 V, 250 W)	68% (120 min)	0.00961 min^{-1}

Table 8 *(continued)*

Photocatalyst	Preparative method	CIP[a]/CIP·HCl[b]	Catalyst dose	pH	Light source	Degradation and time	Rate constant
Fe_3O_4/g-C_3N_4/rGO[613]	Ultrasonic dispersion	20 mg L^{-1} [b] (100 ml L^{-1})	0.1 g	7	Xenon lamp (500 W)	86.7% (60 min)	0.0306 min^{-1}
rGO/$CdWO_4$[614]	Heating method	13.54 mg L^{-1} [a]	0.216 g L^{-1}	5.7	Simulated solar light	100% (60 min)	0.0693 min^{-1}
rGO/CdS[617]	Solvothermal	0.08 mmole[a] (40 ml)	40 mg	—	Solar light	83.25% (16 min)	0.13 min^{-1}
Ag/TiO_2/rGO[618]	Ultrasonic impregnation assisted photoreduction strategy	20 mg L^{-1} [a] (50 mL)	1 g L^{-1}	7	Hg lamp (300 W), $\lambda < 400$ nm	~100% (60 min)	0.1578 min^{-1}
TiO_2/rGO/activated carbon[621]	Hydrothermal method	5×10^{-4} M[b]	2.0 g L^{-1}	—	Xenon lamp (solar simulator)	~95% (100 min)	0.0286 min^{-1}
Core–shell g-C_3N_4@Co–TiO_2[622]	Electrospinning approach/thermal polymerization	20 mg L^{-1} [b] (10 mL)	2 × 2 cm^2 membrane	7	Xenon lamp (300 W), $\lambda > 420$ nm, 50 mW cm^{-2}	90.8% (60 min)	0.038 min^{-1}
Hierarchical 2% Au–g-C_3N_4–ZnO[623]	*In situ* preparation of g-C_3N_4 ZnO nanorods on g-C_3N_4 nanosheets and the deposition of Au nanoparticles	50 mg L^{-1} [a] (50 mL)	10 mg	9.3	Xenon lamp	74.7% (30 min)	3.998×10^{-2} min^{-1}
Mesoporous TiO_2-modified ZnO QDs immobilized on LLDPE[624]	Casting method	40 mg L^{-1} [a] (100 mL)	—	9	Fluorescent lamp: 48 W	89.5% (90 min)	0.01312 min^{-1}
7% CuO/g-C_3N_4[625]	Dispersion method	50 mg[b] (1000 mL)	0.2 g	—	Xenon lamp (500 W), $\lambda > 365$ nm	55% (60 min)	0.014 min^{-1}
ZnO globular (15 wt%)/g-C_3N_4[626]	*In situ* growth	20 mg L^{-1} [a] (100 mL)	20 mg	—	PLS-SXE300 (300 W), L.I: 9.6 W m^{-2}, 400–780 nm	78.4% (50 min)	—
ZnO (20 wt%)/GO (2 wt%)/Ag_3PO_4[628]	Ultrasonic-assisted precipitation method	30 mg L^{-1} [b] (50 mL)	1.0 g L^{-1}	6	Visible lamp: 65 W	96.32%	—
g-C_3N_4/C/Fe_3O_4[629]	Sonication and *in situ* precipitation technique	10 mg L^{-1} [a] (40 mL)	10 mg	—	Xenon lamp (500 W)	96.4% (120 min)	0.0292 min^{-1}
Core–shell $BiFeO_3$/TiO_2[630]	Hydrolysis and precipitation method	20 mg L^{-1} [a] (300 mL)	1 g L^{-1}	5	UV light	67.9% (180 min)	—
Core–shell $BiFeO_3$/TiO_2[630]	Hydrolysis and precipitation method	20 mg L^{-1} [a] (300 mL)	1 g L^{-1}	5	Visible light	72.2% (180 min)	—
Fiber-shaped Ag_2O/Ta_3N_5 (molar ratios: 0.3/1)[631]	Electrospinning–calcination–nitridation method, followed by *in situ* anchoring of Ag_2O deposition	10 mg L^{-1} [a] (80 mL)	—	—	Xenon lamp (300 W), $\lambda > 400$ nm	78.3% (60 min)	0.0079 min^{-1}
$BiVO_4$/TiO_2/rGO[633]	Reaction under Teflon reactor	10 μg L^{-1} [a]	—	—	Xenon lamp (1000 W), $\lambda > 420$ nm	96.2% (120 min)	0.02613 min^{-1}
g-C_3N_4/AgBr/rGO[634]	Mixing followed by heating	20 mg L^{-1} [a]	0.05 g (100 mL)	—	Xenon lamp (250 W)	78.4% (90 min)	—
C_3N_4@$MnFe_2O_4$–rGO[491]	Impregnation approach	20 mg L^{-1} [a] (50 mL) + PS	50 mg	—	Xenon lamp (300 W) with 400 nm cut-off filter	94.5% (60 min)	0.0337 min^{-1}
BiOI/exfoliated C_3N_4 (mass ratio: 0.4)[636]	Combination of thermal exfoliation and chemical precipitation	20 mg L^{-1} [a] (50 mL)	1.0 g L^{-1}	6	Xenon lamp (500 W) with 420 nm cut-off filter	86% (30 min)	0.0705 min^{-1}
3.0 wt% CuO@ZnO[637]	One-pot method	20 ppm[a]	1.5 g L^{-1}	—	Xenon lamp (300 W), λ_{cutoff}: 420 nm, 45.2 mW cm^{-2}	100% (45 min)	113.50×10^{-3} min^{-1}
ZnO/5 wt% SnO_2[638]	Solvothermal process	1 g L^{-1} [b] (100 mL)	60 mg	—	Xenon lamp (300 W), λ: 420–780 nm	~90% (60 min)	0.0385 min^{-1}
Cu_2O–TiO_2[639]	Surfactant-free preparation method (TiO_2: Cu_2O = 0.1; 0.2; 0.3)	50 mg[a] (100 mL)	30 mg	—	Xenon lamp (300 W)	91% (60 min)	0.0432 min^{-1}
10 wt% MoS_2/Ag/g-C_3N_4[640]	Ag deposition and MoS_2 coupling is applied co-modify g-C_3N_4 nanosheets	20 mg L^{-1} [a] (50 mL)	10 mg	5.5	Xenon lamp (300 W), $\lambda > 420$ nm	90.1% (30 min)	0.0507 min^{-1}

Table 8 *(continued)*

Photocatalyst	Preparative method	CIP[a]/CIP·HCl[b]	Catalyst dose	pH	Light source	Degradation and time	Rate constant
g-C_3N_4 (7.1 wt%)/ZrO_{2-x}[641]	Anodic oxidation and thermal deposition method (0.06 g melamine taken)	10 ppm[b] (5 mL)	2 mg	—	Xenon lamp (300 W), $\lambda > 420$ nm	90.6% (60 min)	0.0474 min^{-1}
3 wt% needle SnO_2 needle nanoparticles anchored on exfoliated g-C_3N_4[642]	Hydrothermal method	30 mg L^{-1} [a] (100 ml)	50 mg	—	Xenon lamp (250 W) with a cut-of filter of 420 nm	95.90% (120 min)	0.0205 min^{-1}
N-doped ZnO nanorods–MoS_2 nanoflowers (1 wt% MoS_2 loaded in N–ZnO)[643]	Hydrothermal strategy	0.01 g L^{-1} [a]	25 mg (50 mL)	—	CFL lamp (45 W), $\lambda \geq 420$ nm	84% (120 min)	14.43 × 10^{-3} min^{-1}
WO_3/g-C_3N_4[644]	*In situ* hydrolysis and polymerization process	25 mg L^{-1} [b] (100 mL)	50 mg	—	Xenon lamp (300 W) with a 420 nm cut-off filter	82% (120 min)	0.0164 min^{-1}
Sn_3O_4/g-C_3N_4 (with load ratio of 3%)[645]	Two-step hydrothermal process	10 mg L^{-1} [b] (100 mL)	50 mg	—	Xenon lamp (500 W)	72.2% (120 min)	0.0108 min^{-1}
BiOI/g-C_3N_4/CeO_2 (3 wt%)[646]	Calcination and hydrothermal treatment	20 mg L^{-1} [a] (30 mL)	50 mg	—	Xenon lamp (300 W), $\lambda > 420$ nm	91.6% (120 min)	0.0205 min^{-1}
TiO_{2-x}/g-C_3N_4[647]	Grinding and *in situ* reduction	10 mg L^{-1} [b] (50 mL)	50 mg	9	Xeon-lamp (300 W), $\lambda > 420$ nm	87.7% (90 min)	31.7 × 10^{-3} min^{-1}
K doped g-C_3N_4/TiO_2/CdS[648]	Hydrothermal method	20 mg L^{-1} [a] (50 mL)	50 mg	—	Xenon lamp (300 W), $\lambda > 420$ nm	94.2% (30 min)	0.08554 min^{-1}
γ-Fe_2O_3 nanospheres (5%) anchored on g-C_3N_4[649]	Anchoring mesoporous γ-Fe_2O_3 nanospheres on g-C_3N_4 nanosheet surface	10 mg L^{-1} [b] (100 mL)	50 mg	—	Xenon light source (500 W) with 420 nm cut-off filter	73.8% (120 min)	0.0134 min^{-1}
0.50 wt% CQDs/g-C_3N_4[650]	Low-temperature process	10 mg L^{-1} [b] (100 mL)	50 mg	—	Xenon lamp (250 W) with 420 nm UV-cut-off filter	78.6% (210 min)	~0.0065 min^{-1}
BiOBr/MoS_2/graphene oxide[652]	Hydrolysis method	10 mg L^{-1} [b]	25 mg	—	Xenon lamp (300 W) with 380-nm cut-off filter	>98% (40 min)	0.04277 min^{-1}
g-C_3N_4/MnO_2/GO[653]	Wet-chemical method	10 mg L^{-1} [b] (100 mL)	0.5 g L^{-1}	6	Xenon lamp (300 W) with a 420 nm filter	91.4% (90 min)	—
$BiVO_4$@Polypyrrole/g-C_3N_4[654]	Dispersion method	30 mg L^{-1} [a] (50 mL)	30 mg	—	Xenon lamp (300 W), $\lambda > 420$ nm	90% (120 min)	—
AgI/BiOBr/rGO[655]	Solvothermal method followed by *in situ* precipitation	20 mg L^{-1} [a] (100 mL)	50 mg	—	Xenon lamp (5.00 W), simulated sunlight	94.2% (80 min)	0.018 min^{-1}
Ag/Ag_3PO_4/$BiVO_4$/rGO[656]	*In situ* deposition method followed by photo-reduction	10 mg L^{-1} [a]	0.5 g L^{-1}	6.75	Xenon lamp (300 W)	94.96% (60 min)	—
g-C_3N_4/WO_3[657]	Dispersion method	10 mg L^{-1} [b] (100 ml)	40 mg	—	Xenon lamp (500 W), 320–780 nm, 100 mW cm^{-2}	79.8% (180 min)	—
(50%)$CuIn_2S_4$/g-C_3N_4[658]	Synthesis under autoclave	20 mg L^{-1} [a] (100 mL)	0.5 g L^{-1}	—	Xenon lamp (300 W), $\lambda > 420$ nm cut-off filter	83.7% (60 min)	0.02583 min^{-1}
TiO_2/g-C_3N_4[662]	Co-annealing process	20 mg L^{-1} [b] (40 mL)	250 mg	7	Xenon lamp (150 W)	99.40% (120 min)	3.70 × 10^{-4} min^{-1}

the removal of diclofenac sodium from wastewater under UV irradiation.[669] Schulze-Hennings *et al.*[670] studied the durability of the coating containing TiO_2 on glass for the photocatalytic degradation of diclofenac sodium in water using UVA irradiation. The effectiveness of ZnO and V_2O_5 has also been tested in the photocatalytic degradation of diclofenac sodium in water under solar and UV irradiation.[671] The emerging findings indicated 100% photodegradation efficiency for V_2O_5 compared to ZnO under UV and solar irradiation corresponding to the initial DCF concentration of 300 mg L^{-1}, catalyst dosage of 1.0 g L^{-1} and pH 4. The relatively higher rate constant values of V_2O_5 under UV (k: 0.0196 min^{-1}) and solar (k: 0.0141 min^{-1}) irradiation compared to the corresponding values for ZnO in the photodegradation of DCF also supported this. In another report, investigations were made to study the factors affecting diclofenac decomposition in water by UVA/TiO_2 photocatalysis.[672] According to Bagal *et al.*,[673] UV/TiO_2/H_2O_2 fabricated by a hydrodynamic cavitation approach showed 95% degradation of diclofenac sodium under the optimized operating conditions.

ZnO showed highly active photodegradation of diclofenac sodium in aqueous solution under UV lamp irradiation compared to solar radiation.[674] Mimouni *et al.*[675] investigated the effect of heat treatment on the photocatalytic activity of α-Fe_2O_3 nanoparticles towards diclofenac elimination. The findings in Fig. 22(a) and (b) show the highest degradation for α-Fe_2O_3 (calcinated at 300 °C) and the value of the degradation rate constant corresponds to 0.060 min^{-1}. The generation of extremely active OH· radicals is responsible for the total photodegradation of DCF, as schematically described in Fig. 22(c). Meroni *et al.*[676] achieved 70% degradation of diclofenac (25 ppm) by a piezo-enhanced sonophotocatalytic approach based on ZnO (0.1 g L^{-1}) subjected to UV-light irradiation for 360 min. In addition, ZnO modified with

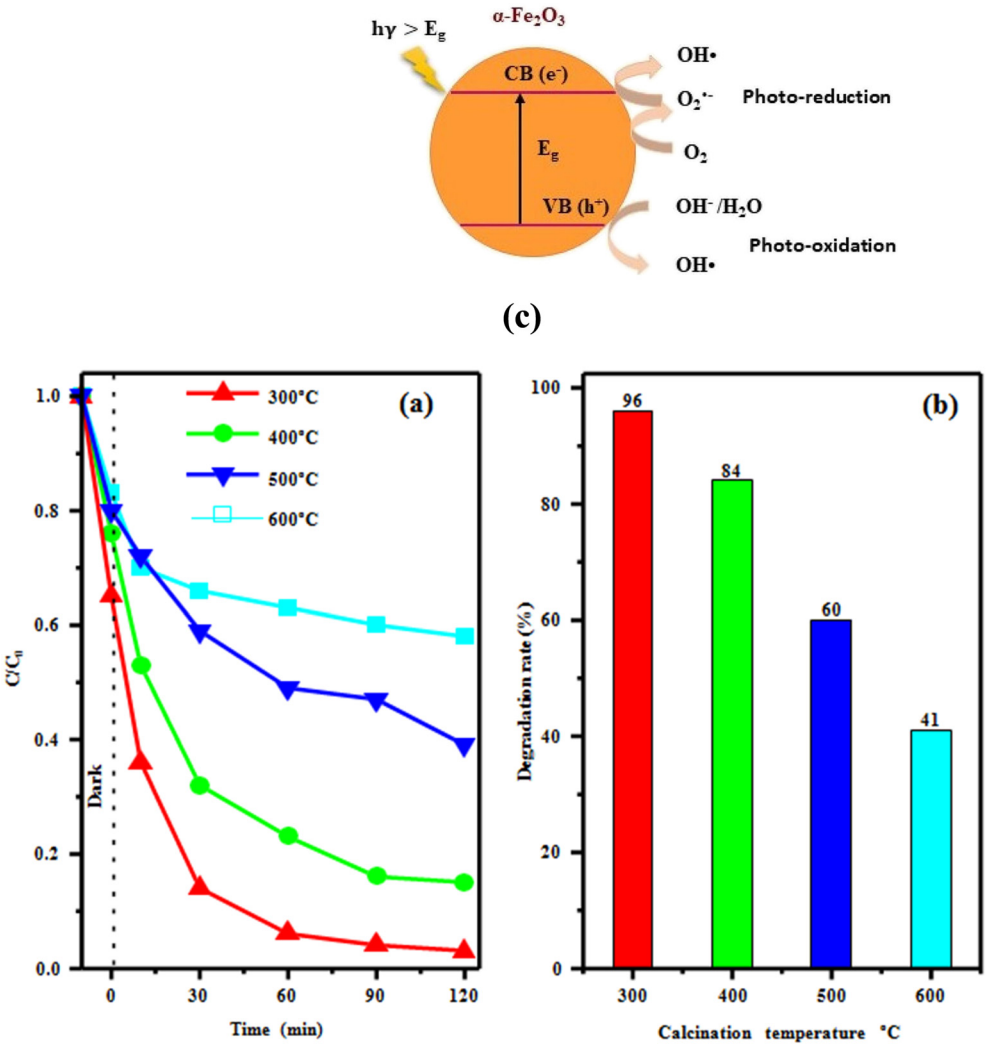

Fig. 22 (a) Conversion plots for photodegradation of DCF in the presence of α-Fe_2O_3 calcinated at different temperatures. (b) The degradation rate of different samples at 120 min. (c) Schematic presentation on the generation of OH· radicals in α-Fe_2O_3. Reproduced from ref. 675 with permission from Springer (2022).

rare earth elements (Ce, Yb) and Fe,[677] Ni_xZn_{1-x} Fe_2O_4 (x = 0, 0.3, 0.7),[678] cobalt ferrite,[679] MgO,[680] and WO_3[681] photocatalysts have also been investigated for the removal of diclofenac from aqueous solution.

3.8.2 Metal–metal oxides. Chakhtouna and coworkers[682] reviewed the role of Ag nanoparticles in enhancing the photocatalytic activity of Ag/TiO_2 in the removal of pharmaceutical pollutants from aqueous solutions under UV and visible light. Espino-Estévez *et al.*[683] synthesized Ag and Pd nanocomposites of TiO_2 (TiO_2–Ag and TiO_2–Pd) by a sol–gel method and observed almost 100% (120 min) photocatalytic degradation of diclofenac sodium salt in water under a UV light source. It was also noted that photocatalytic degradation of DCF follows first-order kinetics. In another study, $Ag@Ag_2O/WO_3$ and $Ag@Ag_2S/WO_3$ were prepared by following a deposition hydrothermal route and used as photocatalysts.[684] Subsequent studies have shown high degradation of DCF (60 mg L^{-1}, pH: 12) in the presence of H_2O_2 (1×10^{-4} M) under visible light ($\lambda > 420$ nm, 160 W) in the presence of $Ag@Ag_2O/WO_3$ ($k = 32.0 \times 10^{-3}$ min^{-1}) and $Ag@Ag_2S/WO_3$ ($k = 7.3 \times 10^{-3}$ min^{-1}) catalysts. Further investigations have also revealed that $\cdot O_2^-$ plays an important role in the degradation of DCF.

3.8.3 Doped metal oxides. Nguyen *et al.*[685] removed diclofenac from wastewater using a submerged photocatalytic membrane reactor comprising immobilized N–TiO_2 under visible irradiation. It was also noted that DCF removal efficiency is enhanced under visible irradiation by coupling H_2O_2 with the photocatalytic process. C-doped TiO_2 synthesized by a microwave digestion method showed almost complete removal of diclofenac after about 160 min under visible light corresponding to diclofenac concentration of 50 mg L^{-1}, catalyst concentration of 250 mg L^{-1} and light intensity of 8000 lx.[686] The doping of titania with 25 wt% Mg resulted in 55% and 48% degradation of diclofenac sodium under UV and visible irradiation, respectively.[95] An Mn (0.6 mol%) and Ag (0.5 mol%) co-doped TiO_2 aerogel exhibited 86% removal of diclofenac under UVA-light irradiation after 4 h.[687] The photodegradation rates followed first-order kinetics with a highest apparent rate constant of 0.0064 min^{-1}.

The photocatalytic performance of a sodium diclofenac solution (pH: 6.5) in F-doped (20 wt%) ZnO under simulated solar radiation indicated the complete degradation of diclofenac sodium of concentration: 10 mg L^{-1} under the optimized experimental conditions (ZnO–F concentration: 1 g L^{-1}).[688] The enhanced photocatalytic activity of F-doped TiO_2 is ascribed to the reduction in the recombination rate of electron–hole pairs. In another similar study, fluorine (0.25, 0.5 and 1 at%)-doped ZnO nano- and meso-crystalline ZnO showed high rates of diclofenac degradation in water compared to bare ZnO.[689] Chaudhari and others[690] used a sol–gel method to prepare Mn/CeO_2, Cu/CeO_2 Ag/CeO_2 (metal semiconductors) and AgI/CeO_2 (an n–p semiconductor–semiconductor) by doping with Mn, Cu, Ag and AgI, respectively. Further investigations have been made to compare their photocatalytic degradation for diclofenac sodium in water under the same optimal conditions (pH: 7, diclofenac concentration: 10 ppm) within 90 min exposure to UV light. It is noted that AgI-doped CeO_2 (1 g L^{-1}) exhibited higher degradation of diclofenac sodium solution (95%) compared to Mn/CeO_2, Cu/CeO_2 or Ag/CeO_2, such enhancement in the photocatalytic activity of AgI/CeO_2 is attributed to its larger surface area and charge separation efficiency.

In addition, $Ce@TiO_2$,[691] granular activated carbon modified with N-doped TiO_2,[692] C,N-co-doped TiO_2,[693] Ce, Mn-co-doped TiO_2,[694] N,S-co-doped carbon quantum dots/TiO_2,[695] TiO_2 doped with B, F, N, P,[696] and S,N,C-tri-doped TiO_2[697] photocatalysts have been investigated for the removal of diclofenac from aqueous solution.

3.8.4 Metal oxide composites. Alalm *et al.*[182] investigated the solar photocatalytic degradation of pharmaceuticals, namely amoxicillin, diclofenac, and paracetamol, using TiO_2 immobilized on powdered activated carbon (TiO_2/AC). According to this, degradation corresponding to the initial concentration of pharmaceuticals of 50 mg L^{-1} and TiO_2/AC dosage of 1.2 g L^{-1} followed the order: amoxicillin (100%: in 120 min) > diclofenac (83% beyond 180 min) > paracetamol (70% in 180 min). TiO_2–WO_3 (molar ratio: 10 : 1) synthesized by a hydrothermal method was the most effective catalyst in the photocatalytic removal of diclofenac under visible-light irradiation compared to pure TiO_2.[698] The composite catalyst successfully degraded diclofenac almost completely in 270 min corresponding to pH 5, initial diclofenac concentration of 25 mg L^{-1} and catalyst concentration of 0.6 g L^{-1}. Subsequent studies showed the catalyst retained 80% catalyst efficiency after four consecutive reaction cycles. N-doped WO_3/TiO_2 synthesized by a sol–gel method enhanced the degradation of diclofenac sodium using simulated solar light owing to the synergistic effect and narrowing of the bandgap.[699] The visible-light-irradiated photocatalytic degradation of diclofenac sodium using ZnO–WO_3 has shown better catalytic activity than bare ZnO.[700] These studies revealed ZnO–WO_3 (Zn : W mole ratio: ≈10 : 1) exhibiting ~76% degradation efficiency at a given pH (6), DCF diclofenac concentration (20 mg L^{-1}) and catalyst loading (0.8 g L^{-1}).

Cordero-García *et al.*[701] studied the effect of carbon doping on WO_3/TiO_2 on the photocatalytic degradation of diclofenac sodium and observed its higher photocatalytic activity compared to WO_3/TiO_2 and TiO_2. Hydroxyapatite/TiO_2 (dose: 4 g L^{-1}) in water degraded DCF (initial concentration: 5 ppm) by 95% in 24 h on irradiating it with simulated solar light.[702] According to Sun *et al.*,[703] the intensity of UV irradiation plays a more significant role in the significant removal of diclofenac by a nano-TiO_2/diatomite composite in a photocatalytic reactor. According to this, diclofenac degraded completely at 30 min under higher UV irradiation intensity at a flux of 3.0 L h^{-1}. A visible-light-responsive TiO_2/Ag_3PO_4 (10 : 1) nanocomposite immobilized in a spherical polymeric matrix showed almost complete removal of diclofenac (k: 0.018 min^{-1}) in 120 min corresponding to

initial drug concentration of 20 mg L^{-1} bead loading of 10 g L^{-1}, and reaction volume of 0.8 L.[704] The ·OH radical and h^+ are reported to be the primary reactive oxygen species in the photodegradation of diclofenac.

An Ag–Ag_2O/reduced TiO_2 nanophotocatalyst demonstrated 99.8% degradation of diclofenac after 50 min of visible irradiation.[705] This is attributed to the effective charge separation, enhanced visible light absorbance and localized SPR of nanocrystalline Ag^0. Silvestri *et al.*[706] synthesized PPy–ZnO (25 : 1) *via* a polymerization method and studied the degradation of DCF under simulated solar light. In this regard, the composite catalyst (1 g L^{-1}) facilitated 81% (60 min) degradation of diclofenac (10 mg L^{-1}) with h^+ the main reactive species involved in the reaction. This performance is ascribed to the mesoporous structure, superior surface area and reduced band gap of PPy–ZnO. According to Das *et al.*,[707] a titania–zirconia (Zr/Ti mass ratio of 11.8 wt%) composite catalyst exhibited a reasonably higher removal of DCF (~92.41%) compared to the anatase form of titania without zirconia.

Attempts have been made to eliminate diclofenac sodium from wastewater through the photocatalytic degradation of hydrothermally prepared TiO_2–SnO_2 (Ti–Sn molar ratio: 1 : 1, 5 : 1, 10 : 1, 20 : 1 and 30 : 1) under various operating conditions.[708] The results indicated the TiO_2–SnO_2 catalyst with a molar ratio of 20 : 1 to be the most effective photocatalyst compared to the other binary composites. The catalyst achieved complete degradation of diclofenac under optimum conditions comprising initial drug concentration of 20 mg L^{-1}, catalyst loading of 0.8 g L^{-1} and pH 5. The photocatalyst also displayed excellent repeatability and better stability over repeated reaction cycles. Fe_3O_4/Ti_xO_y/activated carbon,[709] Fe_3O_4 (nanosphere)/Bi_2S_3 (nanorod)/BiOBr (nanosheet)[710] TiO_2@$ZnFe_2O_4$/Pd,[711] nanotubular titanium

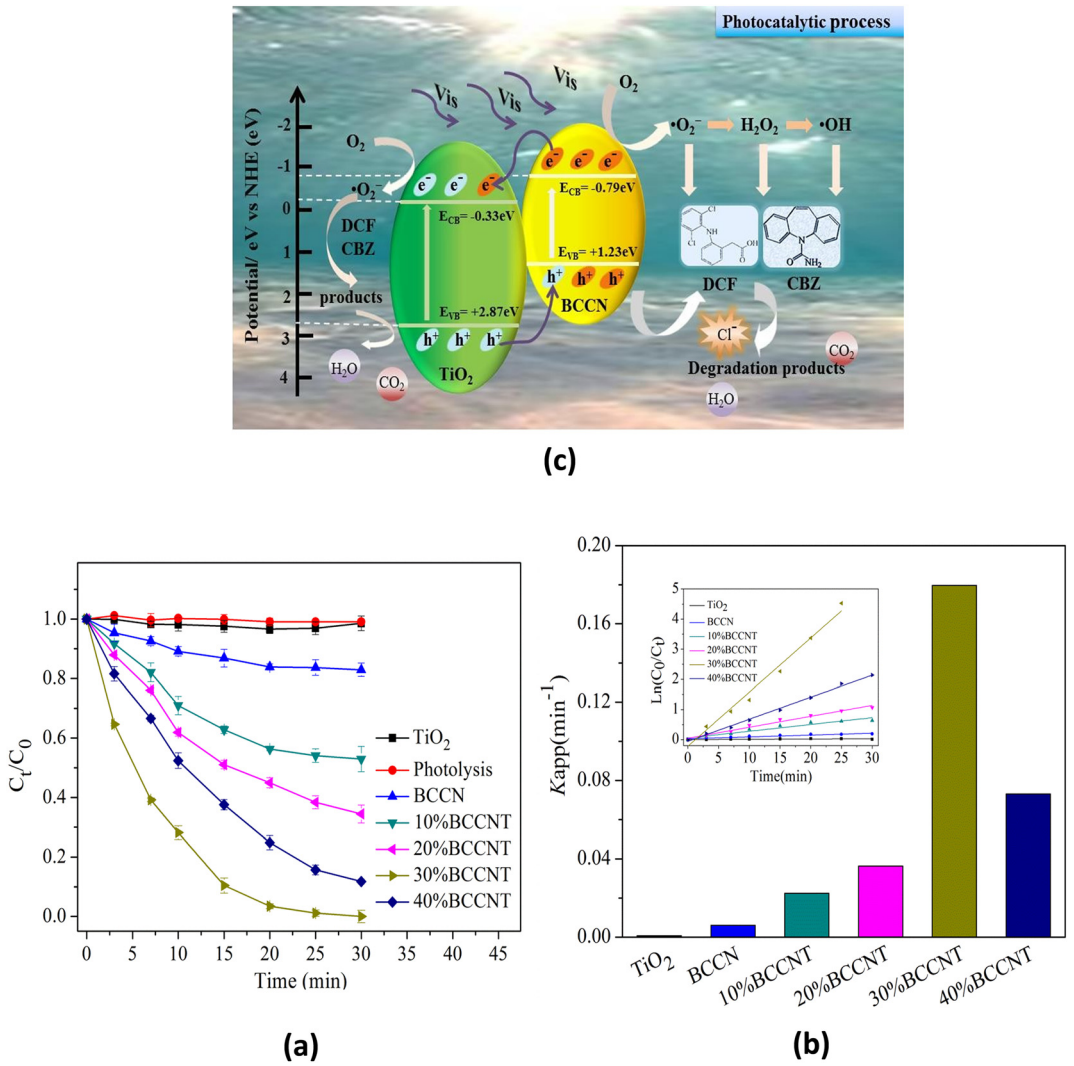

Fig. 23 (a) C_t/C_0 *versus* time plots of different photocatalysts. (b) Respective kinetic curves (inset) and apparent reaction rate constants of diclofenac (conditions: $[DCF]_0$ = 10 mg L^{-1}, [Catal.] =1 g L^{-1}, no pH adjustment and $pH_{initial}$ = 5.05) and (c) possible mechanism for the photodegradation of DCF and CBZ under LED lamp irradiation over 30% BCCNT composites. Reproduced from ref. 719 with permission from Elsevier (2019).

dioxide–polyethersulfone (PES) membrane,[712] Al_2O_3–Nd_2O_3,[713] and TiO_2–zeolite[714] based photocatalysts have also been evaluated for the photocatalytic degradation of diclofenac.

3.8.5 Graphitic materials

3.8.5.1 g-C_3N_4 and its composites. Carbon quantum dot (CQD)-modified porous g-C_3N_4 (dose: 200 mg L^{-1}) synthesized using 20 mL of CQD stock solution showed almost complete degradation of diclofenac solution (pH: 9) of an initial concentration of 10 mg L^{-1} in 12 min under visible light.[715] This is attributed to the tuning of the band structure and enhanced separation of charge carriers. The studies also suggested DCF degradation to be dominated by a photosensitization-like mechanism. The CQD/g-C_3N_4 photocatalyst also exhibited excellent reusability, as evident from studies in the 5th cycle (>90%). Pd quantum dots (1 wt%) deposited on g-C_3N_4 (dose: 0.5 g L^{-1}) achieved 100% removal of diclofenac solution (initial concentration: 1 mg L^{-1}, pH: 7) within 15 min under solar light.[716] The rate constant (0.72 min^{-1}) was found to be 8 times higher than that of g-C_3N_4. Such enhanced photocatalytic activity has been explained based on its narrowed bandgap, reduction in the recombination of photogenerated charge carriers and availability of a photosensitization-like electron transfer pathway.

Graphite-like C_3N_4-modified Ag_3PO_4 nanoparticles exhibited highly enhanced photocatalytic activity under visible-light irradiation owing to the synergistic effect.[717] This is mainly ascribed to the matching band potentials between Ag_3PO_4 and g-C_3N_4, effectively suppressing recombination of electron–hole pairs and promoting their separation efficiency. Diclofenac sodium and ibuprofen (5 mg L^{-1}) achieved complete degradation (180 min) in the presence of carbon microspheres (dia: 0.9–1.9 μm) supported on an anatase phase of TiO_2 (mass ratio TiO_2 to C microspheres: 2) heterostructure photocatalyst under solar light.[718] Further studies revealed the high performance of the photocatalyst even after five successive cycles (80%) as evident from the findings in the first cycle (94%).

Hu *et al.*[719] fabricated eco-friendly 2D heterojunction photocatalyst composites (BCCNT) comprising C-doped supramolecule based g-C_3N_4 (BCCN) layers and TiO_2 nanoparticles and corresponding findings are displayed in Fig. 23(a). It should be noted that degradation of diclofenac solution (10 mg L^{-1}, initial pH: 5.05) by 1 g L^{-1} of 30% C-doped supramolecular based g-C_3N_4 (BCCNT) reached 98.92% within 30 min under LED lamp illumination owing to $\cdot O_2^-$ and h^+ as the main active species. Further investigations established that the degradation kinetics of DCF fitted the pseudo-first-order equation (Fig. 23(b)) with an apparent reaction rate constant (k_{app}: 0.1796 min^{-1}) about 29.4 times higher than BCCN (0.0061 min^{-1}). A possible mechanism for the photodegradation of DCF under LED lamp irradiation is also displayed in Fig. 23(c).

An AgI/g-C_3N_4 (AgI molar mass ratio: 45%) composite photocatalyst exhibited almost complete degradation of diclofenac sodium in 6 min under visible-light irradiation compared to AgI and g-C_3N_4.[720] The reaction rate constant value of AgI/g-C_3N_4 (k: 0.561 min^{-1}) was found to be ~12.5 and 43.2 times higher than those achieved by AgI (0.045 min^{-1}) and g-C_3N_4 (0.013 min^{-1}). The photocatalytic degradation of diclofenac was guided by photogenerated holes and superoxide anion radicals as the main reactive species. Such enhanced photocatalytic activity of AgI/g-C_3N_4 is ascribed to the heterojunction between g-C_3N_4 and AgI that facilitated interfacial charge transfer and prevented the recombination of electron–hole pairs. Ag/g-C_3N_4 (mass ratio of Ag: 54%) heterostructure photocatalysts prepared by photodeposition under ambient conditions showed complete degradation of DCF compared to g-C_3N_4 under visible-light irradiation and followed pseudo-first-order kinetics. The rate constant was k = 0.0429 min^{-1}.[721] The rate constant of diclofenac degradation over Ag/g-C_3N_4 was almost 3.1 times higher than that of pure g-C_3N_4. Further investigations also revealed generated holes as the main reactive species in diclofenac degradation and also established the excellent stability of Ag/g-C_3N_4. CNT–Ni@TiO_2:W nanoparticles[722] and C_3N_4/NH_2-MIL-125 (ref. 723) have also shown remarkable performance in the removal of diclofenac present in water.

3.8.5.2 Graphene composites. The removal of diclofenac (and amoxicillin) has been reported by maltodextrin/reduced graphene and maltodextrin/reduced graphene/copper oxide nanocomposites.[724] Kovacic *et al.*[725] fabricated S-doped TiO_2/rGO by a one-pot solvothermal method to study the removal of diclofenac sodium in aqueous medium (pH 4) under simulated solar irradiation. These findings revealed strong dependence on rGO loading of the photocatalytic performance of S–TiO_2/rGO in the degradation of DCF. Accordingly, 5 wt% rGO in TiO_2 showed improved diclofenac photocatalytic activity compared to bare TiO_2 owing to the effective photogenerated charge separation, as inferred from a photoluminescence study. John *et al.*[726] investigated sunlight-mediated removal of diclofenac sodium from water (25 mg L^{-1}) using TiO_2–reduced graphene oxide (75 mg L^{-1}) and persulfate (20 mg L^{-1}). They achieved an efficiency of more than 98% within 30 min under sunlight illumination. The diclofenac degradation followed the Langmuir–Hinshelwood mechanism and pseudo-first-order kinetics with a pseudo-first-order rate constant (99.4 × 10^3 min^{-1}) about twice that of TiO_2–rGO (50.9 × 10^{-3} min^{-1}). A hydrothermally synthesized BiOCl–GO composite showed 100% and 47.88% removal of DCF from solution (25 mg L^{-1}) under UV light and visible spectrum solar light, respectively.[727] Li *et al.*[728] also used a hydrothermal method to synthesize an Ag–BiOI–rGO nanocomposite. They observed the complete removal of diclofenac (10.0 mg mL^{-1}) by 5 mol% Ag–BiOI–rGO (5 wt%) in 80 min under visible-light irradiation compared to pure BiOI, Ag–BiOI or BiOI–rGO photocatalysts (50 mg in 50 mL). This is attributed to the enhanced charge separation and reduced recombination of photogenerated charge carriers due to Ag and rGO in BiOCl. Other studies reported ~93% decomposition of diclofenac

sodium (25 mg L^{-1}) solution (pH: 6) within 6 min by cubic Ag/AgBr/GO (0.030 g) on illumination with sunlight.[729] It is suggested that the large surface area of the catalyst as well as the superior charge separation and transfer efficiency accounted for this. UV-light-assisted activation of persulfate by rGO–Cu_3BiS_3 (30 mg) reportedly achieved 81% degradation of DCF in 60 min.[730] An $AgFeO_2$–graphene/$Cu_2(BTC)_3$ MOF heterojunction has also been studied under sunlight for the degradation of diclofenac in aqueous solution.[209]

3.8.6 Heterojunctions, S- and Z-scheme-based composites. Co_3O_4/WO_3 nanocomposites were fabricated by dispersing WO_3 in a solution of cobalt acetate (pH: 7) followed by heating at 90 °C.[731] It showed 90.8% degradation of diclofenac sodium salt (15 ppm) solution (pH: 10.7) under visible-light irradiation. According to this, the formation of a monoclinic phase of WO_3 and a p–n heterojunction maximizing the generation of non-selective OH radicals and reducing electron–hole pair combination and the strong absorption of visible light account for such a performance. A solar-active Fe_3O_4@$SrTiO_3/Bi_4O_5I_2$ heterojunction photocatalyst imparted 98.4% diclofenac removal in 90 min under simulated solar-light irradiation.[732] A vis–NIR-driven S-scheme, an WO_{3-x}/S-doped g-C_3N_4 nanocomposite, exhibited ~99.5% degradation rate for diclofenac.[733] g-$C_3N_4/BaBiO_3$ heterojunctions contributed enhanced photocatalysis of diclofenac sodium under visible light through interfacial charge transfer.[734] The photocatalytic activity of g-C_3N_4/$BaBiO_3$ is reported to be 6.5 and 5 times higher than $BaBiO_3$ and g-C_3N_4, respectively. Visible-light-responsive N,S-co-doped TiO_2@MoS_2,[735] S,B-co-doped g-C_3N_4 nanotube@MnO_2,[736] oxygen-doped-g-C_3N_4/ZnO/TiO_2@halloysite nanotubes,[737] and Pt–TiO_2–Nb_2O_5[738] also displayed enhanced photocatalytic degradation of diclofenac.

The optimal BiOCl/$CuBi_2O_4$ exhibited a 90% degradation rate for aqueous DCF in 60 min under visible-light irradiation.[739] The degradation followed pseudo-first-order kinetics (k: 0.03539 min^{-1}), much higher than $CuBi_2O_4$ (k: 0.00139 min^{-1}) or BiOCl (k: 0.00319 min^{-1}). Such enhanced photocatalytic performance of BiOCl/$CuBi_2O_4$ is most likely to be due to the upgraded charge separation and transfer caused by the formation of an S-scheme heterojunction and the presence of oxygen vacancies. Chen *et al.*[740] investigated the photocatalytic performance and mechanism of a Z-scheme $CuBi_2O_4/Ag_3PO_4$ photocatalyst in the degradation of diclofenac sodium under visible-light irradiation. Studies have also been reported on Z-scheme $CuBi_2O_4/Ag_3PO_4$ to study the effects of pH, H_2O_2, and $S_2O_8^{2-}$ on the visible-light-driven degradation of diclofenac sodium.[741]

Visible-light-driven TiO_2/g-C_3N_4 achieved maximum degradation efficiency (93.49%) for the removal of diclofenac sodium from aqueous solution (5 ppm) and the process followed pseudo-first-order kinetics.[742] Such a Z-scheme photocatalyst successfully prevents the fast recombination of electron–hole pairs. Elangovan and others[743] prepared a TiO_2–CdS heterojunction following a two-step hydrothermal treatment. Subsequent use of this as a photocatalyst achieved 86% diclofenac degradation within 4 h under visible-light irradiation. It was suggested that the direct Z-scheme heterojunction structure accounts for the direct charge transfer between heterojunction catalysts. Investigations of a TiO_2–CdS photocatalyst in five successive reaction cycles established its appreciable photochemical stability and reusability. $ZnSnO_3/Bi_2WO_6$,[744] Ag_3PO_4/g-C_3N_4,[745] V_2O_5-B-doped g-C_3N_4,[746] $MoS_2/Cd_{0.9}Zn_{0.1}S$[747] and MoO_3@ZrO_2[748] photocatalysts have also shown enhanced degradation of diclofenac and diclofenac sodium.

Table 9 records the data on the performance of metal oxides and carbonaceous materials based photocatalyst in the removal of diclofenac from water under optimum conditions.

3.9 Atenolol

Atenolol (ATL) belongs to the group of β-blockers and is extensively used in the treatment of cardiovascular diseases, such as hypertension, coronary arterial disease and cardiac arrhythmia.[749] As a result, it has been widely detected in sewage effluent, surface water and wastewater treatment plants on its release into the environment through urban discharges. Atenolol can prevent the growth of human embryonic cells and is toxic to water species. Therefore, it is essential to develop simple and cost-effective technologies for the effective removal of ATL in wastewater before release into natural water.[750–780]

3.9.1 Metal oxides. Several studies have been done into carrying out the degradation of atenolol using commercial as well as synthetic TiO_2 compared to ZnO.[750–752] Hapeshi *et al.*[753] used a variety of commercially available TiO_2 as photocatalysts and found the following relative catalytic activity for the conversion of atenolol: Degussa P25 (67%) > Hombicat UV 100 (39%) > Tronox A-K-1 (30%) > Aldrich (15%) > Tronox TRHP-2 (10%) > Tronox TR (9%) In another study, nano-TiO_2 crystal phase (anatase TiO_2, rutile TiO_2, and mixed phase) coupled with UV-LED was used to study the influence of several parameters on atenolol photodegradation.[754] It was noted that the mixed phase completely degraded atenolol in 60 min under UV-LED (365 nm) corresponding to the ATL concentration of 18.77 μM, catalyst dosage of 2.0 g L^{-1}, light intensity of 774 μW cm^{-2} and pH 7.6. This is in all likelihood due to several contributions originating from the large specific surface area of the catalyst, excellent charge separation efficiency, and the influence of light absorption. The photodegradation of atenolol followed pseudo-first-order kinetics (k: 0.064 min^{-1}).

Among the different commercial TiO_2 catalysts, TiO_2 (Degussa P25) aqueous suspensions (250 mg L^{-1}) delivered 80% photocatalytic conversion of atenolol (10 mg L^{-1}) under irradiation by a 1 kW Xe-OP lamp in 120 min.[755] TiO_2 (Degussa P25) has been tested for the removal by degradation of atenolol, acetaminophen, sulfamethoxazole in hospital wastewater.[756] Rimoldi *et al.*[757] evaluated the degradation of tetracycline hydrochloride, paracetamol, caffeine and

Table 9 Performance data on removal of diclofenac in water presence of various photocatalysts

Photocatalysts	Preparative method	DCF	Catalyst dose	pH	Light source	Degradation and time	Rate constant
TiO_2 [665]	Sol–gel method	5 ppm (100 mL)	50 mg	6	Xenon arc lamp, 300 W, 70 mW cm^{-2}, $\lambda_{cut\text{-}off}$: 420 nm	~80% (120 min)	—
TiO_2 [665]	Sol–gel method	5 ppm (100 mL)	50 mg	6	Natural sunlight	~72% (120 min)	—
TiO_2P25[666]	Commercial	2 mg L^{-1}	200 mg L^{-1}	—	Blacklight Philips TLK05 (40 W), 290–400 nm	100% (60 min)	~0.09 min^{-1}
TiO_2SG[666]	Commercial	2 mg L^{-1}	200 mg L^{-1}	—	Blacklight Philips TLK05 (40 W), 290–400 nm	100% (30 min)	~0.13 min^{-1}
TiO_2 aerogel P25 (Degussa)[667]	Commercial	5 mg L^{-1} (100 mL)	0.2 g L^{-1}	—	125 W black light fluorescent lamp: 300–420 nm	100% (80 min)	4.24 × 10^{-2} min^{-1}
TiO_2 nano thin film on glass slide[669]	Chemical bath deposition	10 ppm	25 × 75 mm deposited film	2	UV lamp	26% (12 min)	—
TiO_2 immobilized on glass[670]	Solution method	0.5 mg L^{-1}	Film of area 144 cm^2	6.2–7.2	UVA lamp: 15 W (300–400 nm)	~100% (26 h)	0.15 h^{-1}
ZnO (Merck)[671]	Commercial	300 mg L^{-1}	1.0 g L^{-1}	4	UV	90.7% (180 min)	0.0144 min^{-1}
ZnO (Merck)[671]	Commercial	300 mg L^{-1}	1.0 g L^{-1}	4	Solar	56.5% (190 min)	0.0044 min^{-1}
V_2O_5 (Merck)[671]	Commercial	300 mg L^{-1}	1.0 g L^{-1}	4	UV	~100% (180 min)	0.0196 min^{-1}
V_2O_5 (Merck)[671]	Commercial	300 mg L^{-1}	1.0 g L^{-1}	4	Solar	~100% (180 min)	0.0141 min^{-1}
TiO_2 immobilized on activated carbon[182]	Temperature impregnation method	50 mg L^{-1} (4 L)	1.2 g L^{-1}	10	Solar irradiation	~85% (180 min)	0.010 min^{-1}
Degussa P25 TiO_2 (75% A:25% R)/H_2O_2: 1.4 mM[672]	Commercial	5 mg L^{-1}	250 mg L^{-1}	—	UVA lamp (9 W lamp)	~99.5% (60 min)	—
TiO_2 (anatase and rutile)[673]	Commercial	20 ppm (5 L)	0.3 g L^{-1}	4	UV lamp: 250 W	80.25% (120 min)	0.0152 min^{-1}
TiO_2 (anatase and rutile)/H_2O_2: 0.3 g L^{-1} [673]	Commercial	20 ppm (5 L)	0.3 g L^{-1}	4	UV lamp: 250 W	95.7% (120 min)	0.0273 min^{-1}
ZnO[674]	Commercial	30 μM	0.25 g L^{-1}	3	UV lamp: 40 W, 254 nm	95% (5 min)	0.403 min^{-1}
α-Fe_2O_3 nanoparticles (calcinated at 300 °C)[675]	Drying followed by heat treatment	15 mg L^{-1} (100 mL)	1 g L^{-1}	—	UVC lamp: 15 W, 254 nm	96% (120 min)	0.04 min^{-1}
MgO nanoparticles[680]	Direct precipitation method	10 mg L^{-1}	0.1 g	6.5	UV light source (254 nm)	100% (60 min)	0.1191 min^{-1}
TiO_2–Pd[683]	Sol–gel method	50 g L^{-1} (0.20 L)	1 g L^{-1}	5	UV light source (15 W), 300–400 nm	100% (120 min)	~0.05 min^{-1}
TiO_2–Ag[683]	Sol–gel method	50 mg L^{-1} (0.20 L)	1 g L^{-1}	5	UV light source (15 W), 300–400 nm	100% (120 min)	~0.04 min^{-1}
Ag/Ag_2O/WO_3 (H_2O_2: 1 × 10^{-4} mM)[684]	Deposition/hydrothermal	0.006 g (100 mL)	0.1 g	12	Mercury lamp (160 W), $\lambda \geq 400$ nm	85% (60 min)	32.0 × 10^{-3} min^{-1}
C-doped TiO_2 (anatase phase)[686]	Microwave digestion method	50 μg L^{-1}	250 mg L^{-1}	7.5	High-pressure W visible lamp (150 W), $\lambda > 400$ nm, 8000 lx	~100% (150 min)	0.0334 min^{-1}
Mg (25 wt%)-doped SiO_2[687]	Mixing of Mg/SiO_2 with $MgCl_2$	20 mg L^{-1} (25 mL)	0.7 g L^{-1}	4.3	UV light	55% (60 min)	—
Mg (25 wt%)-doped SiO_2[687]	Mixing of Mg/SiO_2 with $MgCl_2$	20 mg L^{-1} (25 mL)	0.7 g L^{-1}	4.3	Visible light	48% (60 min)	—
F (0.25)-doped ZnO nano[689]	Hydrothermal approach	10 mg L^{-1} (100 mL)	1.0 g L^{-1}	—	UV-LEDs strip: 10 W, 365 nm	85% (30 min) and ~99% (180 min)	0.06 min^{-1}
Mn doped CeO_2[690]	Sol–gel	10 ppm	1.0 g L^{-1}	7	Mercury vapour lamp (125 W) with cut-off wavelength of 455 nm	48% (60 min)	—
Cu doped CeO_2[690]	Sol–gel	10 ppm	1.0 g L^{-1}	7	Mercury vapour lamp (125 W) with cut-off wavelength of 470 nm	50% (60 min)	—

Table 9 *(continued)*

Photocatalysts	Preparative method	DCF	Catalyst dose	pH	Light source	Degradation and time	Rate constant
Ag doped CeO_2[690]	Sol–gel	10 ppm	1.0 g L^{-1}	7	Mercury vapour lamp (125 W) with cut-off wavelength of 510 nm	57% (60 min)	—
AgI/CeO_2[690]	Sol–gel	10 ppm	1.0 g L^{-1}	—	Mercury vapour lamp (125 W) with cut-off wavelength of 460 nm	88% (60 min)	1.758 × 10^4 L Mol^{-1} min^{-1}
Ce@TiO_2[691]	Precipitation method	5 μM (100 mL)	75 mg	—	UV light	~100% (80 min)	—
1% Ce–0.6% Mn/TiO_2[694]	Sol–gel method	10 mg L^{-1}	50 mg L^{-1}	6	UV lamp: 30 W, λ: 254 nm	94% (240 min)	0.012 min^{-1}
N,S co-doped-CQDs/TiO_2[695]	*Via in situ* phase inversion method	10 ppm (200 mL)	1.5 g (25 cm^2 membrane area)	—	Visible-light irradiation (λ > 400 nm)	62.3% (150 min)	—
					UV light (λ < 380 nm)	~55% (150 min)	—
B (5 wt%) doped TiO_2[696]	Sol–gel method	15 mg dm^{-3}	250 mg dm^{-3}	—	UV lamp	~30% (120 min)	0.0035 min^{-1}
P (5 wt%) doped TiO_2[696]	Sol–gel method	15 mg dm^{-3}	250 mg dm^{-3}	—	UV lamp	~24% (120 min)	0.0019 min^{-1}
F (5 wt%) doped TiO_2[696]	Sol–gel method	15 mg dm^{-3}	250 mg dm^{-3}	—	UV lamp	~27% (120 min)	0.0021 min^{-1}
C–S–N-tri-doped TiO_2 (thiourea/Ti molar ratio: 0.2 : 1)[697]	Sonochemical method	25 mg L^{-1} (50 mL)	0.05 g L^{-1}	Neutral pH	Sunlight	76.48% (90 min)	0.0632 min^{-1}
TiO_2–WO_3 (10 : 1 molar ratio)[698]	Hydrothermal method	25 mg L^{-1} (100 mL)	0.6 g L^{-1}	5	Metal halide lamp, 400 W, visible light	100% (210 min)	—
Hydroxyapatite–TiO_2[702]	Annealing of Ti salt and hydroxyapatite	5 mg L^{-1} (50 mL)	4 g L^{-1}	—	UV lamp, λ: 365 nm, 1.80 mW cm^{-2}	95% (24 h)	—
Nano TiO_2/diatomite[703]	Hydrolysis, precipitation and roasting of diatomite and $TiCl_4$	400 μg L^{-1}	0.5 g L^{-1}	—	UV lamps: 16 W, 254 nm, 1.17 mW cm^{-2}	100% (30 min)	—
Immobilized (12 wt% TiO_2)/Ag_3PO_4 (10 : 1)[704]	Sol–gel method	20 mg L^{-1}	10 g L^{-1} (beads), 0.8 L	—	Visible light source	~90% (120 min)	0.018 min^{-1}
4.25-Ag–Ag_2O/r-TiO_2 -0.130[705]	One-step solution reduction strategy	5 mg·L^{-1} (100 mL)	30 mg	—	Visible light	100% (50 min)	0.04767 min^{-1}
PPy : ZnO (25 : 1)[706]	*Via* polymerization method	10 mg L^{-1} (100 mL)	1 g L^{-1}	6	Xenon lamp (250–800 nm)	81% (60 min)	0.986 min^{-1}
TiO_2–SnO_2 (molar ratio: 20 to 1)[708]	Hydrothermal method	20 mg L^{-1}	0.8 g L^{-1}	5	UV lamp	100% (300 min)	0.0147 min^{-1}
Fe_3O_4/Bi_2S_3/BiOBr (with Bi_2S_3 mass ratio of 4%)[710]	One-pot solvothermal	10 mg L^{-1} (50 mL)	0.03 g L^{-1}	5	LED lamp (50 W), 475 nm	93.81% (40 min)	0.0527 min^{-1}
TiO_2@$ZnFe_2O_4$/Pd[711]	Photodeposition technique	10 mg L^{-1}	0.03 g L^{-1}	4	Solar light	84.87% (120 min)	0.0172 min^{-1}
Nanotubular TiO_2-PES[712]	*Via* anodization of TiO_2 nanotubes on polyethersulfone membrane	5 mg L^{-1}	Circular membranes (Dia: 47 mm)	—	UVA sunlamp (7.6 mW cm^{-2})	~94% (240 min)	9.96 × 10^{-3} min^{-1}
Al_2O_3-(15%) Nd_2O_3[713]	Sol–gel method	80 ppm	200 mg (200 mL)	—	UV lamp, 254 nm, 4400 μW cm^{-2}	>92.0% (40 min)	9.5 × 10^{-2} min^{-1}
CQDs (50 mL) modified g-C_3N_4[715]	Mixing method	10 mg L^{-1} (50 mL)	200 mg L^{-1}	9	Xenon arc lamp (300 W) with UV cut-off filter ($\lambda \geq$ 400 nm), 150 ± 5 mW cm^{-2}	100% (12 min)	0.47 min^{-1}
TiO_2–carbon microspheres (CMS) with Ti : CMS molar ratio = 2[718]	Solvothermal treatment	5 mg L^{-1} (50 mL)	250 mg L^{-1}	6.0	Xenon lamp (500 W m^{-2}). With light correction filter ($\lambda \leq$ 350 nm)	100% (180 min)	—
30% TiO_2-hybridize C-doped based g-C_3N_4[719]	*In situ* method	10 mg L^{-1} (100 mL)	1 g L^{-1}	5.05	LED lamp: 50 W, 380–780 nm	98.92% (30 min)	0.1796 min^{-1}
AgI/g-C_3N_4 (molar ratio of AgI: 45%)[720]	Deposition–precipitation method	1 mg L^{-1} (100 mL)	10 mg	—	Xenon lamp (300 W), $\lambda \geq$ 400 nm, 100 mW cm^{-2}	100% (6 min)	0.561 min^{-1}

Table 9 *(continued)*

Photocatalysts	Preparative method	DCF	Catalyst dose	pH	Light source	Degradation and time	Rate constant
Ag modified g-C_3N_4 (mass ratio of Ag: 54%)[721]	Photodeposition	100 mg L^{-1} (100 mL)	10 mg	—	Xenon lamp: 300 W with cut-off filter ($\lambda \geq 400$ nm), 100 mW cm^{-2}	~100% (120 min)	0.0429 min^{-1}
TiO_2–rGO in presence of persulfate[726]	Solvothermal treatment (using 5 wt% GO)	25 mg L^{-1} (50 mL), (persulfate:20 mg L^{-1})	75 mg L^{-1}	4	Sunlight (1.25×10^6 lx)	>98% (30 min)	99.4 × 10^{-3} min^{-1}
BiOCl–GO[727]	One-pot hydrothermal method	25 mg L^{-1} (100 mL)	1 g L^{-1}	5	Visible spectrum solar light (17.38 mW cm^{-2})	47.88% (180 min)	—
5 Mol% Ag–BiOI–rGO 5 wt%[728]	Hydrothermal strategy	10.0 μg mL^{-1} (50 mL)	50 mg	—	Halogen lamp: 300 W	100% (80 min)	0.026 min^{-1}
Ag/AgBr/GO[729]	Sonochemical route	25 mg L^{-1} (25 mL)	0.030 g	6.2	Sunlight irradiation	~93% (6 min)	—
rGO–Cu_3BiS_3 (15%)/PS (5 mM)[730]	Solvothermal process	10 mg L^{-1} (50 mL)	30 mg	—	UV LED light (15 W)	85% (60 min)	3.8 × 10^{-2} min^{-1}
Co_3O_4/WO_3 (annealed)[731]	Dispersion method	15 ppm (50 ml)	30 mg	6.8	Mercury lamp (80 W) with cut-off of 420 nm	90.8% (180 min)	0.1412 min^{-1}
Fe_3O_4@$SrTiO_3$/$Bi_4O_5I_2$[732]	*In situ* hydrothermal route	10 mg L^{-1}	0.3 mg mL^{-1}	6	Xenon lamp (300 W)	98.4% (90 min)	0.06214 min^{-1}
N,S co-doped TiO_2@MoS_2[735]	Hydrothermal method	0.15 mg L^{-1}	0.98 g L^{-1}	5.5	Visible LED light irradiation	98% (150 min)	0.002 min^{-1}
S–B-co-doped g-C_3N_4 nanotubes–MnO_2 (PMS: 0.06 mM)[736]	Hydrothermal	20 mg L^{-1}	0.5 g L^{-1}	7	Visible light (8 × 8 W), 460 nm	99% (10 min)	—
Pt–TiO_2–Nb_2O_5[738]	Multiple steps	12.5 mg L^{-1} (100 mL)	0.5 g L^{-1}	—	UV-LED	100% (20 min)	0.446 min^{-1}
BiOCl/$CuBi_2O_4$ (mass ratio: 40%)[739]	Solvothermal process	50 mg L^{-1} (40 mL)	1 mg mL^{-1}	—	Xenon lamp (300 W), $\lambda >$ 420 nm	~90% (60 min)	0.03539 min^{-1}
$CuBi_2O_4$/Ag_3PO_4 (1 : 1)[740]	Combination of hydrothermal and *in situ* deposition	10 mg L^{-1} (50 mL)	0.025 g	—	Xenon lamp (300 W) with cut-off filter at $\lambda \geq 400$ nm	~90% (120 min)	0.0143 min^{-1}
$CuBi_2O_4$/Ag_3PO_4 (mass ratio of 3 : 7)[741]	Hydrothermal synthesis and *in situ* deposition method	10 mg L^{-1}	25 mg (50 mL)	4.42	Xenon lamp (300 W), $\lambda >$ 400 nm	82% (60 min)	0.0072 min^{c}
$CuBi_2O_4$/Ag_3PO_4 (mass ratio of 3 : 7)/$S_2O_8^{2-}$: 1–06 mM[741]	Hydrothermal synthesis and *in situ* deposition method	10 mg L^{-1}	25 mg (50 mL)	4.42	Xenon lamp (300 W), $\lambda >$ 400 nm	100% (60 min)	0.0272 min^{-1}
$CuBi_2O_4$/Ag_3PO_4 (mass ratio of 3 : 7)/H_2O_2: 1 mM[741]	Hydrothermal synthesis and *in situ* deposition method	10 mg L^{-1}	25 mg (50 mL)	4.42	Xenon lamp (300 W), $\lambda >$ 400 nm	98.40% (60 min)	0.0162 min^{-1}
TiO_2/g-C_3N_4[742]	Wet impregnation method	5 ppm	0.3 g	5	W halogen lamp (1000 W)	93.49% (90 min)	0.0324 min^{-1}
Ag_3PO_4/g-C_3N_4 (30%)[745]	Deposition–precipitation method	1 mg L^{-1} (100 mL)	0.1 g L^{-1}	—	Xenon lamp (300 W) with filter ($\lambda \geq 400$ nm)	~100% (12 min)	0.453 min^{-1}
50% V_2O_5–g-C_3N_4 (molar ratio: 30%)[746]	Mixing method	10 mg L^{-1}	0.2 mg mL^{-1}	>7	Monochromatic blue lamps (8 W), 465 ± 40 nm	100% (<105 min)	~0.53 min^{-1}
MoS_2/$Cd_{0.9}Zn_{0.1}S$[747]	One-step hydrothermal method	20 μM (50 mL)	25 mg	—	Xenon lamp (300 W) with 420 nm cut-off filter	86% (30 min)	—

atenolol, both as individual pollutants and in mixtures, using UV and simulated-solar-mediated TiO_2. According to Ponkshe and Thakur,[758] degradation of atenolol (2×10^{-4} M) using different commercially available TiO_2 (0.03 g L^{-1}) as photocatalysts in a 100 mL reaction solution (natural pH) under UV light for 120 min followed the order: Aeroxide TiO_2 P25 (94%) > TiO_2 Hombikat UV 100 (68%) > Merck TiO_2 (60%) > TiO_2 Kronoclean 7000 (45%). Rogé *et al.*[759] prepared ZnO nanowires by metal organic chemical vapor deposition and investigated their photocatalytic activity in a solution containing atenolol and sulfadimidine under low-power 365 nm UV light (2.28 mW cm^{-2}). The corresponding pseudo-first-order rate constants in these pollutants were found to be 6.5×10^{-3} and 2.3×10^{-3} min^{-1}. Several other studies also reported the photocatalytic degradation of atenolol in aqueous solution using Degussa TiO_2 P25 suspension,[760] TiO_2,[761] TiO_2/salicylaldehyde–NH_2-MIL-101(Cr)[762] and ZnO.[763]

3.9.2 Metal-doped and metal–metal oxides. Ramasamy *et al.*[104] fabricated an Ag-doped ZnO photocatalyst to study its performance as a photocatalyst in the visible-light region

for the photocatalytic degradation of atenolol (and acetaminophen) in a water medium. The corresponding removal efficiencies were found to be about 70 and 91% for $[ATL]_{int} = [ACT]_{int}$: 5 mg L^{-1}, pH: 8.5, time: 120 min, and Ag–ZnO: 1 g L^{-1}. These findings also confirmed that the removal process takes place through the OH· pathway in the removal of the pollutants. Fe–TiO_2 and Ag–TiO_2 mediated visible-light photocatalysis removed atenolol from aqueous solution under optimum conditions by 75.5% (98 min) and 68.3% (120 min), respectively.[764]

Atenolol has been removed from domestic wastewater effluent using green-synthesized Fe (0–5%)-doped TiO_2 (Fe–TiO_2) under visible-light irradiation.[765] These findings showed 85% removal of atenolol in the presence of Fe (2 wt%)–TiO_2 after 105 min at solution pH 9, initial atenolol concentration of 10 mg L^{-1} and catalyst dose of 1.25 g L^{-1}. The degradation of atenolol by visible-light-activated Fe–TiO_2 was attributed to the cleavage of the ether bond, hydroxylation of the aromatic ring and oxidation of amine moieties. Alternatively, the enhanced photocatalytic activity for atenolol by Fe-doped TiO_2 due to the reduced band gap of TiO_2 cannot be ruled out.

Ag–TiO_2 (Ag/Ti molar ratio: 2%) microtubes showed enhanced degradation of atenolol under UV-light irradiation (λ: 365 nm, power: 0.111 mW cm^{-2}).[766] Further investigations revealed Ag acting as a good photogenerated electron acceptor for photocatalysis. Cobalt-doped TiO_2 nanoparticles (dose: 2.0 g L^{-1}) exhibited about 90% photodegradation (ATL: 15 mg L^{-1}, H_2O_2: 2.0 mL, pH: 2) of atenolol in 40 min under UV irradiation.[767] The photodegradation of atenolol followed first-order kinetics, and the process involved the formation of hydroxyl free radicals and superoxide oxygen anions as active species.

3.9.3 Metal oxide composites. A Bi_2O_3/TiO_2 composite was successfully synthesized by a solvothermal method and its photocatalytic performance was tested for the removal of atenolol removal from aqueous solution under UVC and visible-light irradiation.[768] The investigations revealed the decomposition of atenolol to be better for Bi_2O_3/TiO_2 (68.92%) than Bi_2O_3 (22.58%) after 60 minutes under optimum conditions (pH: 7, catalyst dosage: 400 mg L^{-1} and initial concentration of atenolol: 10 mg L^{-1}). Stojanović *et al.*[769] fabricated a TiO_2/zeolite composite by a solid-state dispersion method and investigated the photocatalytic degradation of atenolol from an aqueous solution (pH ~ 6.5) under simulated solar light. These findings indicated ~94% and 88% degradation of atenolol after 70 min for ZSM-5 combined with P25 TiO_2 and ZSM-5/TiO_2 nanocrystals, respectively. Corchero *et al.*[770] prepared Fe_3O_4@AgCl and Fe_3O_4@TiO_2 nanocatalysts using an ionic liquid. Subsequent evaluation of their effectiveness as photocatalysts under UV light (30 min) showed the degradation of atenolol by 66.0% and 43.7%, respectively. The photocatalytic degradation of atenolol has also been reported using BiOCl@Fe_3O_4[771] and immobilized titania/silica on glass slides.[772]

3.9.4 Graphitic material composite. A hydrothermally prepared graphene oxide–TiO_2 (1.5 g L^{-1}) composite showed 72% degradation of atenolol (25 ppm) solution (pH: 6) under visible-light irradiation after 1 h.[773] The inclusion of graphene oxide in the composite facilitated enhanced electron–hole pair separation. The photocatalytic activities of immobilized graphene–TiO_2[774] and graphene oxide/ZnO composite[775] have also been examined for the photocatalytic degradation of atenolol under UV and solar irradiation, respectively. A metal-free exfoliated g-C_3N_4 photocatalyst

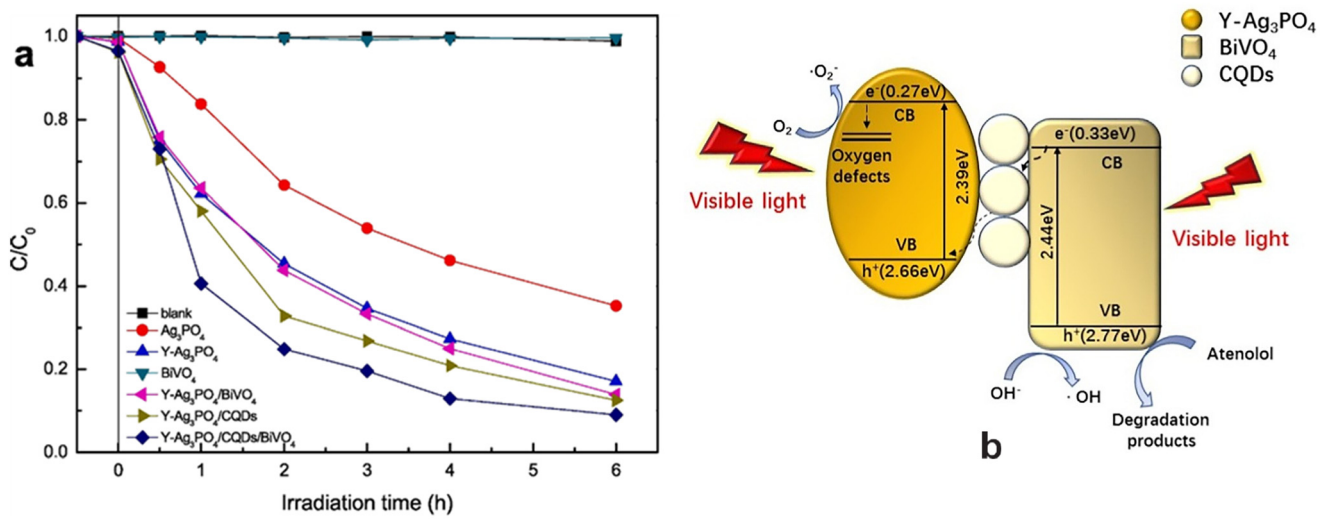

Fig. 24 (a) Photocatalytic activities of photocatalysts for atenolol degradation of Ag_3PO_4, Y–Ag_3PO_4, $BiVO_4$, Y–Ag_3PO_4/$BiVO_4$, Y–Ag_3PO_4/CQDs and Y–Ag_3PO_4/CQDs/$BiVO_4$ for the degradation of atenolol and (b) Z-scheme photocatalysis mechanism for atenolol degradation by Y–Ag_3PO_4/CQDs/$BiVO_4$. Reproduced from ref. 779 with permission from Elsevier (2020).

showed the efficient removal of atenolol from urban wastewater under visible light.[776] In another study, carbon nitride modified by graphene quantum dots exhibited 86% photocatalytic degradation efficiency for atenolol, which still remained above 83% after five cycles.[777]

3.9.5 Heterojunctions and Z-scheme-based photocatalysts. Kumar *et al.*[778] used recycled $LiFePO_4$ from batteries in combination with $B@C_3N_4$ and $CuFe_2O_4$, which were harnessed as sustainable nanojunctions to study xenon-lamp-mediated atenolol degradation and showed 99.5% and 85.3% (60 min) degradation efficiency by $B@C_3N_4/LiFePO_4/CuFe_2O_4$ and $B@C_3N_4/LiFePO_4/CuFe_2O_4$ (30%) photocatalysts. Z-Scheme $Y–Ag_3PO_4/CQDs/BiVO_4$ exhibited 90.9% degradation efficiency for atenolol under visible light (6 h) compared to $Y–Ag_3PO_4$ and $BiVO_4$ (Fig. 24(a)).[779] This could be attributed to an increase in the visible-light absorption and electron mediators as a result of the synergistic effect. The kinetic constant in the photocatalytic degradation of atenolol was found to be ~2.8 times that of pristine Ag_3PO_4 in the presence of $Y–Ag_3PO_4/CQDs/BiVO_4$ and a possible mechanism has also been proposed, as shown in Fig. 24(b). Both $Y–Ag_3PO_4$ and $BiVO_4$ generated photogenerated carriers under visible-light illumination. CQDs not only increase the visible-light absorption of $Y–Ag_3PO_4/CQDs/BiVO_4$ but also act as electron mediators. Simultaneously, oxygen defects caused by the doping of Y^{3+} into Ag_3PO_4 are a capture centre for photogenerated electrons to generate $\cdot O_2^-$, inhibiting the recombination of photogenerated electron–hole pairs. In another study, a double Z-scheme $rGO/CuFe_2O_4/CdS/Bi_2S_3$ QDs nanoheterojunction exhibited ~76.5% degradation of atenolol photo-Fenton-assisted photocatalytic degradation of atenolol in 360 min under visible-light irradiation.[780] The degradation of atenolol was attributed to enhanced surface oxygen vacancies, the formation of OH· and h^+ and the photo-Fenton reaction.

Table 10 records data on the performance of different photocatalysts on removal of diclofenac from water under optimum conditions.

4 Future scope and perspectives

Pharmaceutical pollutants found in water supplies through human and animal consumption of antibiotics, antipyretics, analgesics, *etc.* are considered potential hazards to the environment, humans and aquatic life.[781] However, conventional wastewater treatment methods are ineffective in eliminating them completely. In view of this, the photocatalytic degradation of these pharmaceutical pollutants using semiconducting materials is considered an effective method.

An efficient semiconducting material acting as an efficient photocatalyst is guided by enhanced visible-light absorption, facilitating charge carrier migration and a reduced recombination rate. In view of this, TiO_2, WO_3, ZnO, Fe_2O_3, CdS, MoS_2 *etc.* are widely used photocatalysts for the photodegradation of pharmaceutical pollutants in water.[23–39] However, the large band gaps of photogenerated charge carriers, *i.e.* rapid recombination rate (*i.e.*, short lifetimes) of photogenerated charge carriers, instability in an aqueous medium, reusability of the photocatalyst and poor absorption ability for visible light, are a few drawbacks that limit the practical applications of metal oxide as photocatalysts. Therefore, increasing attention has been focused on achieving the effective separation of photogenerated charge carriers, improvements in the visible-light response and other factors[782] through designing and constructing advanced light energy harvesting assemblies for environmental remediation.[783] This problem has been overcome by modifying semiconducting metal oxides through doping, composite formation, immobilizing semiconducting materials on supports and heterojunction formation for the removal of drugs from contaminated water. In addition, the combination of these semiconducting metal oxides with carbon-based materials, such as activated carbon, biochar, carbon nanotubes, carbon dots, $g\text{-}C_3N_4$ and graphene, has also attracted a lot of attention in the removal of pharmaceutical pollutants present in wastewater. However, there are still several research gaps in the removal of antibiotics by photocatalysts. These future challenges are described below.

The expensive precursors used in the synthesis of metal oxides limit their large-scale application. Therefore, it is desirable to realize the simple, facile, affordable, low-cost synthesis of photocatalysts. The specific surface area,[782] crystallite size,[784] size, shape and overall structure[785] of photocatalysts play important roles in the photocatalytic activity of emerging pollutants. This needs to be correlated with light trapping, charge separation and pollutant adsorption ability parameters under optimized operational conditions.

Carbon-based materials have also attracted significant interest in recent years due to their unique physicochemical, optical and electrical properties following band-gap tuning, composite formation and heterojunction construction, *etc.*[40–50] The enhanced photo-efficiency of the corresponding nanocomposites is ascribed to improvement in visible-range absorption, fast charge carrier migration and reduced recombination rate. However, their choices are limited to batch experiments at the laboratory scale rather than the pilot scale. As a result, there is a gap between on-going research and its application.

The literature revealed considerable interest in investigating the photocatalytic degradation of individual pharmaceutical pollutants in water. However, wastewater could contain complex pollutant mixtures, including other organic and inorganic species originating from heavy metals, dyes, personal care products, pesticides and other sources.[757,786–794] This can affect the degradation process for pharmaceutical pollutants through interference and matrix effects. Therefore, attention also needs to be focused on

Table 10 Performance data on removal of atenolol in water in the presence of different photocatalysts

Photocatalyst	Preparation method	ATL	Catalyst dose	pH	Light source	Degradation (time)	Rate constant
TiO_2: mixed phase (source: Shandong Xiya Chemical Co)[754]	Commercial	18.77 μM	2 g L^{-1}	7.6	UV-lamp (365 nm) and I_0: 774 mW cm^{-2}	100% (60 min)	0.064 min^{-1}
TiO_2 (75% A + 25% R) Degussa P25[755]	Commercial	10 mg L^{-1}	250 mg L^{-1}	8	Xenon-OP lamp (1 kW), I_0: 272.3 W m^{-2}	80% (120 min)	—
Degussa P25[756]	Commercial	10 mg L^{-1}	1.0 g L^{-1}	—	Natural solar irradiation	100% (400 kJ m^{-2})	—
Degussa TiO_2 P25[758]	Commercial	37.6 mM	2.0 g L^{-1} (25 mL)	6.8	High-pressure Hg lamp (125 W), 365 nm, 31.3 mW m^{-2}	~100% (60 min)	0.0570 min^{-1}
Degussa P25 TiO_2 [760]	Commercial	37.6 μM	2.0 g L^{-1}	7	UV light	100% (60 min)	—
TiO_2 immobilized on the clinoptilolite nano particles support[762]	Dispersion method	10 mg L^{-1} (25 mL)	1.5 g L^{-1}	—	UV lamp (80 W)	75% (60 min)	—
TiO_2 immobilized on Salicylaldehyde-NH_2-MIL 101 (Cr) support[762]	Dispersion method	10 mg L^{-1} (25 mL)	1.5 g L^{-1}	—	Xenon lamp (100 W)	82% (60 min)	—
ZnO nanoparticles[763]	Synthetic method	20 mg L^{-1}	10 mg L^{-1}	7	9 W UVC lamp	100% (120 min)	—
Fe–TiO_2 [764]	Green method	5 mg L^{-1} (100 mL)	1005 mg L^{-1}	8	Xenon arc lamp, 300 W, λ: 650 nm	71.2% (98 min)	—
Ag–TiO_2 [764]	Green method	5 mg L^{-1} (100 mL)	1065 mg L^{-1}	8	Xenon arc lamp, 300 W, λ: 650 nm	65.7% (120 min)	—
Ag–ZnO microtubes[104]	Solution method	5 mg L^{-1}	1 g L^{-1}	8.5	W halogen lamp (300 W)	70.2% (120 min)	0.01 min^{-1}
Fe–TiO_2 [765]	Green synthesis	10 mg L^{-1}	1.25 g L^{-1}	9	300 W halogen lamp	85% (105 min)	0.013 min^{-1}
Ag–TiO_2 microtubes (Ag/Ti molar ratio: 2%)/O_3 [766]	Calcination	20 mg L^{-1}	0.2 g	9.11	Medium-pressure Hg lamp: 365 nm and 0.111 mW cm^{-2}	92.23% (9 min)	0.3275 min^{-1}
Co doped-TiO_2 (H_2O_2: 2.0 mL L^{-1})[767]	Mixing followed by calcination	15 mg L^{-1}	2.0 g L^{-1}	2	UV (200 nm)	90% (40 min)	0.059 min^{-1}, 1.75×10^{-4} g mg^{-1} min^{-1}
Bi_2O_3/TiO_2 [768]	Solvothermal method	10 mg L^{-1}	400 mg L^{-1}	7	UVC (visible-light irradiation)	68.92% (60 min)	—
TiO_2/zeolites[769]	Solid-state dispersion method	50 mg L^{-1}	1 g L^{-1} (40 mL)	6.5	Lamp (Osram Vitalux (300 W))	~94% (70 min)	0.132 ± 0.001 min^{-1}
TiO_2@Fe_3O_4 [770]	Mixing method	10 ppm	0.75 g L^{-1}	5.5	Low-pressure Hg vapour lamp (UVC. l: 280 nm)	43.7% (30 min)	—
Fe_3O_4@AgCl[770]	Mixing method	10 ppm	0.75 g L^{-1}	5.5	Low-pressure Hg vapour lamp (UVC. l: 280 nm)	66% (30 min)	—
Fe_3O_4@TiO_2 [770]	Mixing method	10 ppm	0.75 g L^{-1}	5.5	Low-pressure Hg vapour lamp (UVC. l: 280 nm)	66% (30 min)	—
BiOCl@Fe_3O_4 with [PS]: 1.0 mM[771]	Precipitation process	2.5 mg L^{-1}	0.1 g L^{-1}	6.5	Xenon lamp (simulated sunlight): 500 W	~99% (60 min)	(5.34–6.04) × 10^{-2} min^{-1}
Graphene oxide–TiO_2 [773]	Hydrothermal	25 ppm	1.5 g L^{-1} (150 mL)	6	1000 W xenon arc lamp, 750 mW cm^{-2}	72% (60 min)	—
Y–Ag_3PO_4/CQDs/$BiVO_4$ [779]	Mixing method	10 mM (50 mL)	5 mg photocatalyst	—	250 W xenon lamp with UV cut-off filter, $\lambda > 420$ nm	90.9% (6 h)	0.50 h^{-1}

developing photocatalysts capable of simultaneously removing pharmaceuticals even in the presence of other pollutants/interfering substances in the wastewater. Recovery, reusability, and stability remain other issues in the development of high-performing photocatalysts in wastewater treatment. Toxicity assessment is considered to be one of important parameters in the treatment of wastewater by photocatalysis.[795] This could be ascribed to the formation of carcinogenic secondary metabolites due to the incomplete mineralization of targeted contaminants.

Nanomaterial-based photocatalysts have shown great promise due to their superior adsorptive and photocatalytic properties in the removal of pharmaceutical pollutants.[51,57] In this regard, leaching of toxic components could adversely affect the quality of the water environment. This aspect remains a matter of great concern and as a consequence,

extensive investigations are needed to fully understand the role of various photocatalyst nanoparticles and their toxicity risks in aquatic environments.[796,797] Therefore, it remains challenging to recover and separate the nanoparticle-based photocatalysts invariably used in water treatment. Recently, this difficulty has been overcome by immobilizing the photocatalysts on various support materials. Therefore, in the future innovations will be needed for effective, eco-friendly, and sustainable immobilization techniques for the separation/recovery and reuse of photocatalytic materials. Existing research has also invariably focused on laboratory-scale photocatalysis in the degradation of emerging pharmaceutical pollutants without much implementation in real water systems. More studies need to be focused at the pilot and industrial scale levels for its commercialization. The fabrication of economical, environmentally friendly and effective photocatalysts taking into account many of these aspects remains a major challenge in this field.

5 Conclusions

Antibiotics have been invariably used in different fields, such as the medical field, agriculture, and veterinary medicine for the purpose of killing or preventing bacterial growth. However, the presence of these pharmaceutical pollutants on entering surface water and groundwater are a potential threat to human and marine lives and need to be eliminated. Considering this, various conventional processes have been developed for the removal of these pharmaceutical pollutants. However, their choice is limited due to their high cost as well as incomplete elimination of contaminants from the contaminated water.

In view of this, the current review highlights recent advances in the applications of different photocatalysts to the removal of emerging pharmaceutical pollutants in wastewater. As a result, the performance of several metal oxides, carbonaceous materials, composites including surface modification, doping with metals/nonmetals, heterojunction formation, and immobilization using support materials, homo- or hetero-materials composed of two or more inorganic phases, inorganic semiconductors coupled with carbon-based materials, inorganic semiconductors hybridized with 2D materials as excellent photocatalysts have been reviewed to find out the optimum removal efficiency for the pollutants (acetaminophen, amoxicillin, sulfamethoxazole, acetaminophen, norfloxacin, ciprofloxacin, tetracycline, diclofenac and atenolol) in water. However, secondary pollution produced by the formation of by-products during the photocatalytic process, leaching of dopants/active components of the photocatalysts, and the generation of excess CO_2 during the photocatalysis process are additional challenges that need to be addressed in future. Further, most of these findings are reported on the laboratory scale, and real-world and industrial-scale applications have yet to be fully realized. The further development of low-cost, robust photocatalysts utilizing semiconductors and renewable visible/solar light to solve both the world crises of energy supply and environmental pollution remains a pressing demand for industrial application.

Conflicts of interest

There are no conflicts to declare.

Acknowledgements

The author began working on this review article while still a Professor in the Department of Chemistry, Indian Institute of Technology, Kharagpur and thus, remains very appreciative for making this effort possible. Author also expresses his heartfelt thanks to Professor Ashok Kumar Gupta, Department of Civil Engineering, Indian Institute of Technology, Kharagpur and his research scholars Brahma Gupta, Vishal Parida, Adarsh Singh and Akash Rawat for the valuable interactions. The table of content figure was drawn with the help of Biorender and acknowledged. Author also thanks Dr. Kunal Manna and Dr. Ayon Karmakar for their help in arranging copyright permissions and the Figures, respectively.

References

1 https://www.unesco.org/en/articles/imminent-risk-global-water-crisis-warns-un-world-water-development-report-2023.
2 I. Bashir, F. A. Lone, R. A. Bhat, S. A. Mir, Z. A. Dar and S. A. Dar, in *Bioremediation and biotechnology sustainable approaches to pollution degradation*, ed. K. R. Hakeem, R. A. Bhat and H. Qadri, Springer, 2020, pp. 1–26, DOI: 10.1007/978-3-030-35691-0_1.
3 https://reliefweb.int/report/world/wastewater-resource-may-2022.
4 S. Kundu and A. K. Gupta, *Chem. Eng. J.*, 2006, **122**, 93–106.
5 S. Dutta, B. Gupta, S. K. Srivastava and A. K. Gupta, *Mater. Adv.*, 2021, **2**, 4497–4531.
6 S. Dutta, S. K. Srivastava and A. K. Gupta, *Mater. Adv.*, 2021, **2**, 2431.
7 S. Senapati, S. K. Srivastava and S. B. Singh, *Nanoscale*, 2012, **4**, 6604–6612.
8 P. A. Kobielska, A. J. Howarth, O. K. Farha and S. Nayak, *Coord. Chem. Rev.*, 2018, **358**, 92–102.
9 S. Ayoob and A. K. Gupta, *Crit. Rev. Environ. Sci. Technol.*, 2006, **36**, 433–487.
10 A. Singh, D. Saidulu, A. K. Gupta and V. Kubsad, *J. Environ. Chem. Eng.*, 2022, **10**, 109012.
11 B. Gupta, R. S. Ambekar, R. M. Tromer, P. S. Ghosal, R. Sinha, A. Majumder, P. Kumbhakar, P. M. Ajayan, D. S. Galvao, A. K. Gupta and C. S. Tiwary, *RSC Adv.*, 2021, **11**, 19788–19796.
12 B. S. Rathi, P. S. Kumar and D.-V. N. Vo, *Sci. Total Environ.*, 2021, **797**, 149134.
13 M. Hejna, D. Kapuścińska and A. Aksmann, *Int. J. Environ. Res. Public Health*, 2022, **19**, 7717.
14 K. Samal, S. Mahapatra and M. H. Ali, *Energy Nexus*, 2022, **6**, 100076.

15 A. C. Duarte, S. Rodrigues, A. Afonso, A. Nogueira and P. Coutinho, *Pharmaceuticals*, 2022, **15**, 393.
16 T. Zhang, K. Lv, Q. Lu, L. Wang and X. Liu, *J. Environ. Sci.*, 2021, **104**, 415–429.
17 J. O'Neill, Tackling Drug-Resistant Infections Globally: Final Report and Recommendations, 2016, Available online: https://amr-review.org/sites/default/files/160518_Final%20paper_with%20cover.pdf.
18 S. I. Polianciuc, A. E. Gurzău, B. Kiss, M. G. Ştefan and F. Loghin, *Med. Pharm. Rep.*, 2020, **93**, 231–240.
19 V. Vinayagam, S. Murugan, R. Kumaresan, M. Narayanan, M. Sillanpää, D. V. N. Vo, O. S. Kushwaha, P. Jenis, P. Potdar and S. Gadiya, *Chemosphere*, 2022, **300**, 134597.
20 V. K. Parida, S. K. Srivastava, S. Chowdhury and A. K. Gupta, *Chem. Eng. J.*, 2023, **472**, 144969.
21 A. A. Aryee, R. Han and L. Ou, *J. Cleaner Prod.*, 2022, **368**, 133140.
22 B. Sruthi, S. Janani and S. S. Khan, *Sep. Purif. Technol.*, 2021, **279**, 119709.
23 D. Kanakaraju, B. D. Glass and M. Oelgemoller, *Environ. Chem. Lett.*, 2014, **12**, 27–47.
24 M. Minella, D. Fabbri, P. Calza and C. Minero, *Curr. Opin. Green Sustainable Chem.*, 2017, **6**, 11–17.
25 R. Karuppannan, S. Mohan and T.-O. Do, in *Nanostructured materials for environmental applications*, ed. S. Balakumar, V. Keller and M. V. Shankar, Springer Nature Switzerland AG, 2021, pp. 85–112.
26 A. Krishnan, A. Swarnalal, D. Das, M. Krishnan, V. S. Saji and S. M. A. Shibli, *J. Environ. Sci.*, 2024, **139**, 389–417.
27 N. Roy, S. A. Alex, N. Chandrasekaran, A. Mukherjee and K. Kannabiran, *J. Environ. Chem. Eng.*, 2021, **9**, 104796.
28 R. Gusain, K. Gupta, P. Joshi and O. P. Khatri, *Adv. Colloid Interface Sci.*, 2019, **272**, 102009.
29 S. Gautam, H. Agrawal, M. Thakur, A. Akbari, H. Sharda, R. Kaur and M. Amini, *J. Environ. Chem. Eng.*, 2020, **8**, 103726.
30 T. Velempini, E. Prabakaran and K. Pillay, *Mater. Today Chem.*, 2021, **19**, 100380.
31 R. Krakowiak, J. Musial, P. Bakun, M. Spychała, B. Czarczynska-Goslinska, D. T. Mlynarczyk, T. Koczorowski, L. Sobotta, B. Stanisz and T. Goslinski, *Appl. Sci.*, 2021, **11**, 8674.
32 K. P. Gopinath, N. V. Madhav, A. Krishnan, R. Malolan and G. Rangarajan, *J. Environ. Manage.*, 2020, **270**, 110906.
33 D. Chen, Y. Cheng, N. Zhou, P. Chen, Y. Wang, K. Li, S. Huo, P. Cheng, P. Peng, R. Zhang, L. Wang, H. Liu, Y. Liu and R. Ruan, *J. Cleaner Prod.*, 2020, **268**, 121725.
34 A. Mirzaei, Z. Chen, F. Haghighat and L. Yerushalmi, *Sustain. Cities Soc.*, 2016, **27**, 407–418.
35 P. Kar, K. Shukla, P. Jain, G. Sathiyan and R. K. Gupta, *Nano Mater. Sci.*, 2021, **3**, 25–46.
36 K. S. Varma, R. J. Tayade, K. J. Shah, P. A. Joshi, A. D. Shukla and V. G. Gandhi, *Water-Energy Nexus*, 2020, **3**, 46–61.
37 G. Ren, H. Han, Y. Wang, S. Liu, J. Zhao, X. Meng and Z. Li, *Nanomaterials*, 2021, **11**, 1804.
38 R. M. S. Sendão, J. C. G. Esteves da Silva and L. P. da Silva, *Chemosphere*, 2022, **301**, 134731.
39 L. G. Devi and R. Kavitha, *Appl. Surf. Sci.*, 2016, **360**, 601–622.
40 J. Ge, Y. Zhang and S.-J. Park, *Materials*, 2019, **12**, 1916.
41 R. Ma, Y. Xue, Q. Ma, Y. Chen, S. Yuan and J. Fan, *Nanomaterials*, 2022, **12**, 4045.
42 T. H. Pham, N. M. Viet, P. T. T. Hoai, S. H. Jung and T. Y. Kim, *Environ. Res.*, 2023, **231**, 116246.
43 K. K. Gangu, S. Maddila and S. B. Jonnalagadda, *Sci. Total Environ.*, 2019, **646**, 1398–1412.
44 R. B. González-González, A. Sharma, R. Parra-Saldívar, R. A. Ramirez-Mendoza, M. Bilal and H. M. N. Iqbal, *J. Hazard. Mater.*, 2022, **423**, 127145.
45 M. Abdullah, J. Iqbal, M. S. U. Rehman, U. Khalid, F. Mateen, S. N. Arshad, A. G. Al-Sehemi, H. Algarni, O. A. Al-Hartomy and T. Fazal, *Chemosphere*, 2023, **317**, 137834.
46 M.-F. Li, Y.-G. Liu, G.-M. Zeng, N. Liu and S.-B. Liu, *Chemosphere*, 2019, **226**, 360–380.
47 M. Minale, Z. Gu, A. Guadie, D. M. Kabtamu, Y. Li and X. Wang, *J. Environ. Manage.*, 2020, **276**, 111310.
48 O. C. Olatunde and D. C. Onwudiwe, *Int. J. Environ. Res. Public Health*, 2021, **18**, 1529.
49 B. A. Bhanvase, T. P. Shende and S. H. Sonawane, *Environ. Technol. Rev.*, 2017, **6**, 1–14.
50 W. W. Anku, E. M. Kiarii, R. Sharma, G. M. Joshi, S. K. Shukla and P. P. Govender, in *A New Generation Material Graphene: Applications in Water Technology*, ed. M. Naushad, Springer International Publishing AG, part of Springer Nature, 2019, pp. 187–208.
51 V. K. Parida, S. K. Srivastava, A. K. Gupta and A. Rawat, *Mater. Express*, 2023, **13**, 1–38.
52 A. Abbasnia, A. Zarei, M. Yeganeh, H. R. Sobhi, M. Cholami and A. Esrafili, *Inorg. Chem. Commun.*, 2022, **145**, 109959.
53 S. S. Imam, R. Adnan and N. H. M. Kaus, *Toxicol. Environ. Chem.*, 2018, **100**, 518–539.
54 S. Shurbaje, P. T. Huong and T. M. Altahtamounti, *Catalysts*, 2021, **11**, 437.
55 **https://pubchem.ncbi.nlm.nih.gov/**.
56 Z. L. Wang, *J. Phys.: Condens.Matter*, 2004, **16**, R829–R858.
57 A. Pattnaik, J. N. Sahu, A. K. Poonia and P. Ghosh, *Chem. Eng. Res. Des.*, 2023, **190**, 667–686.
58 Z. Wu, Z. Xiong and B. Lai, *Environmental Functional Materials*, 2022, **1**, 298–315.
59 Y. Wang, Z. Lu, Z. Zhu, X. Zhao, N. Gao, D. Wang, Z. Hua, Y. Yan, P. Huoa and M. Song, *RSC Adv.*, 2016, **6**, 51877–51887.
60 S. Heidari, M. Haghighi and M. Shabani, *J. Cleaner Prod.*, 2020, **259**, 120679.
61 P. Wang, B. Huang, Y. Dai and M.-H. Whangbo, *Phys. Chem. Chem. Phys.*, 2012, **14**, 9813–9825.
62 A. Kumar, P. Choudhary, A. Kumar, P. H. C. Camargo and V. Krishnan, *Small*, 2022, **18**, 2101638.
63 E. S. Araújo, M. F. G. Pereira, G. M. G. da Silva, G. F. Tavares, C. Y. B. Oliveira and P. M. Faia, *Toxics*, 2023, **11**, 658.

64 A. Moharana, A. Kumar, A. Thakur, D.-V. N. Vo, A. Sharma and D. Kumar, in *Nanostructured photocatalysts from Fundamental to practical applications*, 2021, pp. 145–167, DOI: 10.1016/B978-0-12-823007-7.00010-9.
65 S. Biswas and A. Pal, *Catalysts*, 2023, **13**, 925.
66 B. Samir, N. Bouazizi, P. N. Fotsing, J. Cosme, V. Marquis, G. L. Dotto, F. L. Derf and J. Vieillard, *Appl. Sci.*, 2023, **13**, 8074.
67 S. Kurwadkar, T. V. Hoang, K. Malwade, S. R. Kanel, W. F. Harper Jr and G. Struckhof, *Nanotechnol. Environ. Eng.*, 2019, **4**, 12.
68 Y. Tang, X. Liu, C. Ma, M. Zhou, P. Huo, L. Yu, J. Pan, W. Shia and Y. Yan, *New J. Chem.*, 2015, **39**, 5150–5160.
69 B. Partoens and F. M. Peeters, *Phys. Rev. B: Condens. Matter Mater. Phys.*, 2006, **74**, 075404.
70 Y. Ren, D. Zeng and W.-J. Ong, *Chin. J. Catal.*, 2019, **40**, 289–319.
71 X. He, T. Kai and P. Ding, *Environ. Chem. Lett.*, 2021, **19**, 4563–4601.
72 S. Obregón, M. A. Ruíz-Gómez, V. Rodríguez-González, A. Vázquez and D. B. Hernández-Uresti, *Mater. Sci. Semicond. Process.*, 2020, **113**, 105056.
73 W. Dai, L. Jiang, J. Wang, Y. Pu, Y. Zhu, Y. Wang and B. Xiao, *Chem. Eng. J.*, 2020, **397**, 125476.
74 M. Miceli, P. Frontera, A. Macario and A. Malara, *Catalysts*, 2021, **11**, 591.
75 V. Wongso, H. K. Chung, N. S. Sambudi, S. Sufian, B. Abdullah, M. D. H. Wirzal and W. L. Ang, *J. Photochem. Photobiol., A*, 2020, **394**, 112436.
76 A. H. Zyoud, A. Zubi, S. Hejjawi, S. H. Zyoud, M. H. Helal, S. H. Zyoud, N. Qamhieh, A. R. Hajamohideen and H. S. Hilal, *J. Environ. Chem. Eng.*, 2020, **8**, 104038.
77 C. A. Aguilar, C. Montalvo, J. G. Ceron and E. Moctezuma, *Int. J. Environ. Res.*, 2011, **5**, 1071–1078.
78 C. A. Aguilar, C. Montalvo, B. B. Zermeño, R. M. Cerón, J. G. Cerón, F. Anguebes and M. A. Ramírez, *Int. J. Environ. Sci. Technol.*, 2019, **16**, 843–852.
79 R. Trujillano, V. Rives and I. García, *Molecules*, 2022, **27**, 2904.
80 A. Marizcal-Barba, J. A. Sanchez-Burgos, V. Zamora-Gasga and A. Perez Larios, *Photochem*, 2022, **2**, 225–236.
81 C. J. Lin, W. T. Yang, C.-Y. Chou and S. Y. H. Liou, *Chemosphere*, 2016, **152**, 490–495.
82 X. Zhang, F. Wu, X. W. Wu, P. Chen and N. Deng, *Materials*, 2008, **157**, 300–307.
83 S. A. Lozano-Morales, G. Morales, M. Á. L. Zavala, A. Arce-Sarria and F. Machuca-Martínez, *Processes*, 2019, **7**, 319.
84 N. Kaneva, A. Bojinova, K. Papazova, D. Dimitrov, K. Zaharieva, Z. Cherkezova-Zheleva and A. Eliyas, *Arch. Pharmacal Res.*, 2016, **39**, 1418–1425.
85 R. Katal, M. H. D. A. Farahani and H. Jiangyong, *Sep. Purif. Technol.*, 2020, **230**, 115859.
86 M. Cantarella, A. D. Mauro, A. Gulino, L. Spitaleri, G. Nicotra, V. Privitera and G. Impellizzeri, *Appl. Catal., B*, 2018, **238**, 509–517.
87 M. Jiménez-Salcedo, M. Monge and M. T. Tena, *Photochem. Photobiol. Sci.*, 2022, **21**, 337–347.
88 O. Nasr, O. Mohamed, A.-S. Al-Shirbini and A.-M. Abdel-Wahab, *J. Photochem. Photobiol., A*, 2019, **374**, 185–193.
89 R. Katal, S. M. Panah, M. Saeedikhani, M. Kosari, C. C. Sheng, O. S. Leong, G. Xiao and H. Jiangyong, *Adv. Mater. Interfaces*, 2018, **5**, 1801440.
90 T. H. Yu, W. Y. Cheng, K.-J. Chao and S. Y. Lu, *Nanoscale*, 2013, **5**, 7356–7360.
91 C. A. Huerta-Aguilar, A. A. Ramírez-Alejandre, P. Thangarasu, J. A. Arenas-Alatorre, I. A. Reyes-Dominguez and M. de la L. Corea, *Catal. Sci. Technol.*, 2019, **9**, 3066.
92 S. Sayegh, F. Tanos, A. Nada, G. Lesage, F. Zaviska, E. Petit, V. Rouessac, I. Iatsunskyi, E. Coy, R. Viter, D. Damberga, M. Weber, A. Razzouk, J. Stephan and M. Bechelany, *Dalton Trans.*, 2022, **51**, 2674–2695.
93 V. Y. Safitri, A. Santoni, D. V. Wellia, K. Khoiriah and S. Safni, *Mol. Ther.*, 2017, **12**, 189–195.
94 Y. A. Shaban and H. M. Fallata, *Res. Chem. Intermed.*, 2019, **45**, 2529–2547.
95 W. L. da Silva, M. A. Lansarin, J. H. Z. dos Santos and F. Silveira, *Water Sci. Technol.*, 2016, **74**, 2370–2383.
96 L. Rimoldi, D. Meroni, E. Falletta, A. M. Ferretti, A. Gervasini, G. Cappelletti and S. Ardizzone, *Appl. Surf. Sci.*, 2017, **424**, 198–205.
97 Z. Khani, D. Schieppati, C. L. Bianchi and D. C. Boffito, *Catalysts*, 2019, **9**, 949.
98 A. M. S. Asadi and M. Malakootian, *J. Mater. Sci.: Mater. Electron.*, 2019, **30**, 14878–14889.
99 M. L. P. Dalida, K. M. S. Amer, C.-C. Su and M.-C. Lu, *Environ. Sci. Pollut. Res.*, 2014, **21**, 1208–1216.
100 M. Abid, E. Makhoul, F. Tanos, I. F. Iatsunskyi, E. Coy, G. Lesage, M. Cretin, D. Cornu, A. B. H. Amara and M. Bechelany, *Membranes*, 2023, **13**, 204.
101 M. D. G. de Luna, J. C.-T. Lin, M. J. N. Gotostos and M.-C. Lu, *Sustainable Environ. Res.*, 2016, **26**, 161–167.
102 A. Alzamly, F. Hamed, T. Ramachandran, M. Bakiro, M. Bakiro, S. H. Ahmed, S. Mansour, S. Salem, K. Abdul al, N. S. Al Kaabi, M. Meetani and A. Khalee, *J. Water Reuse Desalin.*, 2019, **9**, 31–46.
103 H. A. Abbas, R. A. Nasr, R. N. Vannier and T. S. Jamil, *J. Environ. Sci.*, 2022, **112**, 331–342.
104 B. Ramasamy, J. Jeyadharmarajan and P. Chinnaiyan, *Environ. Sci. Pollut. Res.*, 2021, **28**, 39637–39647.
105 V. H.-T. Thi and B.-K. Lee, *Mater. Res. Bull.*, 2017, **96**, 171–182.
106 R. A. Abri, F. A. Marzouqi, A. T. Kuvarega, M. A. Meetani, S. M. Z. Al Kindy, S. Karthikeyan, Y. Kim and R. Selvaraj, *J. Photochem. Photobiol., A*, 2019, **384**, 112065.
107 D. R. Kumar, K. S. Ranjith, Y. Haldorai, A. Kandasami and R. T. R. Kumar, *ACS Omega*, 2019, **4**, 11973–11979.
108 O. F. S. Khasawneh, P. Palaniandy, M. Ahmadipour, H. Mohammadi, M. Razak and B. Hamdan, *J. Environ. Chem. Eng.*, 2021, **9**, 104921.
109 O. F. S. Khasawneh, P. Palaniandy and L. P. Teng, *MethodsX*, 2019, **6**, 2735–2743.

110 H. Shahabi, A. Allahrasani and A. Naghizadeh, *Desalin. Water Treat.*, 2019, **149**, 164–170.
111 P. M. Álvareza, J. Jaramillo, F. López-Piñero and P. K. Plucinski, *Appl. Catal., B*, 2010, **100**, 338–345.
112 B. Czech and K. Tyszczuk-Rotko, *Sep. Purif. Technol.*, 2018, **206**, 343–355.
113 T. A. Fernandes, S. G. Mendo, L. P. Ferreira, N. R. Neng, M. C. Oliveira, A. Gil, M. D. Carvalho, O. C. Monteiro, J. M. F. Nogueira and M. J. Calhorda, *Environ. Sci. Pollut. Res.*, 2021, **28**, 17228–17243.
114 R. Mu, Y. Ao, T. Wu, C. Wang and P. Wang, *J. Hazard. Mater.*, 2020, **382**, 121083.
115 J. H. F. Chau, C. W. Lai, B. F. Leo, J. C. Juan and M. R. Johan, *Catal. Commun.*, 2022, **163**, 106396.
116 S. Basha, D. Keane, K. Nolan, M. Oelgemöller, J. Lawler, J. M. Tobin and A. Morrissey, *Environ. Sci. Pollut. Res.*, 2015, **22**, 2219–2230.
117 A.-M. Abdel-Wahab, A.-S. Al-Shirbini, O. Mohamed and O. Nasr, *J. Photochem. Photobiol., A*, 2017, **347**, 186–198.
118 N. Jallouli, K. Elghniji, H. Trabelsi and M. Ksibi, *Arabian J. Chem.*, 2017, **10**, S3640–S3645.
119 L. Yanyan, T. A. Kurniawan, Z. Ying, A. B. Albadarin and G. Walker, *J. Mol. Liq.*, 2017, **243**, 761–770.
120 C.-T. Chang, J.-J. Wang, T. Ouyang, Q. Zhang and Y.-H. Jing, *Mater. Sci. Eng., B*, 2015, **196**, 53–60.
121 N. Miranda-García, S. Suárez, M. Ignacio Maldonado, S. Malato and B. Sánchez, *Catal. Today*, 2014, **230**, 27–34.
122 V. Vaiano, M. Matarangolo and O. Sacco, *Chem. Eng. J.*, 2018, **350**, 703–713.
123 S. Behravesh, N. Mirghaffari, A. A. Alemrajabi, F. Davar and M. Soleimani, *Environ. Sci. Pollut. Res.*, 2020, **27**, 26929–26942.
124 G. Fan, H. Peng, J. Zhang, X. Zheng, G. Zhu, S. Wang and L. Hong, *Catal. Sci. Technol.*, 2018, **8**, 5906–5919.
125 T. A. Kurniawan, L. Yanyan, T. Ouyang, A. B. Albadarin and G. Walker, *Mater. Sci. Semicond. Process.*, 2018, **73**, 42–50.
126 G. Fan, X. Zheng, J. Luo, H. Peng, H. Lin, M. Bao, L. Hong and J. Zhou, *Chem. Eng. J.*, 2018, **351**, 782–790.
127 F. Al Marzouqi, R. Selvaraj and Y. Kim, *Mater. Res. Express*, 2019, **6**, 125538.
128 A. Smýkalová, B. Sokolová, K. Foniok, V. Matejka and P. Praus, *Nanomaterials*, 2019, **9**, 1194.
129 M. Z. A. Warshagha and M. Muneer, *Int. J. Environ. Anal. Chem.*, 2022, **102**, 6339–6358.
130 M. Kohantorabi, G. Moussavi, P. Oulego and S. Giannakis, *Sep. Purif. Technol.*, 2022, **299**, 121723.
131 R. R. Solís, M. A. Quintana, M. Á. Martín-Lara, A. Pérez, M. Calero and M. J. Muñoz-Batista, *Int. J. Mol. Sci.*, 2022, **23**, 12871.
132 S. Gupta, J. Gandhi, S. Kokate, L. G. Raikar, V. G. Kopuri and H. Prakash, *Heliyon*, 2023, **9**, e16450.
133 A. H. C. Khavar, G. Moussavi and A. R. Mahjoub, *Appl. Surf. Sci.*, 2018, **440**, 963–973.
134 B. Palas, G. Ersöz and S. Atalay, *Chem. Eng. Sci.*, 2021, **242**, 116593.
135 J. Zhu, Z. Zhu, H. Zhang, H. Lu, W. Zhang, Y. Qiu, L. Zhuc and S. Küppers, *Appl. Catal., B*, 2018, **225**, 550–562.
136 H. Tao, X. Liang, Q. Zhang and C.-T. Chang, *Appl. Surf. Sci.*, 2015, **324**, 258–264.
137 E. C. Umejuru, E. Prabakaran and K. Pillay, *ACS Omega*, 2021, **6**, 11155–11172.
138 C. Gomez-Solis, R. Mendoza, J. F. Rios-Orihuela, G. Robledo-Trujillo, L. A. Diaz-Torres, J. Oliva and V. Rodriguez-Gonzalez, *J. Environ. Manage.*, 2021, **290**, 112665.
139 L. Allagui, B. Chouchene, T. Gries, G. Medjahdi, E. Girot, X. Framboisier, A. B. H. Amara, K. Balan and R. Schneider, *Appl. Surf. Sci.*, 2019, **490**, 580–591.
140 S. Sravya, D. R. Devi, N. Belachew, K. Eswara Rao and K. Basavaiah, *RSC Adv.*, 2021, **11**, 12030.
141 Y. L. Wang, M. Penas-Garzon, J. J. Rodriguez, J. Bedia and C. Belver, *Chem. Eng. J.*, 2022, **446**, 137229.
142 L. K. B. Paragas, V. D. Dang, R. S. Sahu, S. Garcia-Segura, M. D. G. de Luna, J. A. I. Pimentel and R.-A. Doong, *Sep. Purif. Technol.*, 2021, **272**, 117567.
143 X. Du, X. Bai, L. Xu, L. Yang and P. Jin, *Chem. Eng. J.*, 2020, **384**, 123245.
144 M. Z. A. Warshagha and M. Muneer, *Environ. Nanotechnol., Monit. Manage.*, 2022, **18**, 100728.
145 Z. Ren, Z. Zhao, Z. Yang, B. Cheng and X. Yang, *Nano*, 2021, **16**, 2150100.
146 M. Noorisepehr, K. Ghadirinejad, B. Kakavandi, A. R. A. Esfahani and A. Asadi, *Chemosphere*, 2019, **232**, 140–151.
147 S. Moradi, A. A. Isari, F. Hayati, R. Rezaei, R. R. Kalantary and B. Kakavandi, *Chem. Eng. J.*, 2021, **414**, 128618.
148 I. Gozlan, A. Rotstein and D. Avisar, *Chemosphere*, 2013, **91**, 985–992.
149 K. D. Radosavljević, A. V. Golubović, M. M. Radišić, A. R. Mladenović, D. Ž. Mijin and S. D. Petrović, *Chem. Ind. Chem. Eng. Q.*, 2017, **23**, 187–195.
150 M. Fazilati, *Desalin. Water Treat.*, 2019, **169**, 222–231.
151 J. H. O. S. Pereira, A. C. Reis, O. C. Nunes, M. T. Borges, V. J. P. Vilar and R. A. R. Boaventura, *Environ. Sci. Pollut. Res.*, 2014, **21**, 1292–1303.
152 B. Ambrosetti, L. Campanella and R. Palmisano, *J. Environ. Sci. Eng. A*, 2015, **4**, 273–281.
153 E. S. Elmolla and M. Chaudhuri, *Desalination*, 2010, **252**, 46–52.
154 R. Palmisano, L. Campanella and B. Ambrosetti, *J. Environ. Anal. Chem.*, 2015, **2**, 1000143.
155 D. Klauson, J. Babkina, K. Stepanova, M. Krichevskaya and S. Preis, *Catal. Today*, 2010, **151**, 39–45.
156 F. S. Moosavi and T. Tavakoli, *Environ. Sci. Pollut. Res.*, 2016, **23**, 23262–23270.
157 D. Dimitrakopoulou, I. Rethemiotaki, Z. Frontistis, N. P. Xekoukoulotakis, D. Venieri and D. Mantzavinos, *Environ. Manage.*, 2012, **98**, 168–174.
158 N. Ellepola and G. Rubasinghege, *Environments*, 2022, **9**, 77.
159 A. F. Alkaim and A. M. Aljobree, *Int. J. Adv. Sci. Technol.*, 2020, **29**, 5480–5487.
160 F. Moosavi, C. Cheng, T. T. Gheinani, M. Traore, A. Kanaev and M. Nikravech, *Chem. Eng. Trans.*, 2019, **73**, 175–180.

161 E. S. Elmolla and M. Chaudhuri, *J. Hazard. Mater.*, 2010, **173**, 445–449.
162 S. Pourmoslemi, A. Mohammadi, F. Kobarfard and N. Assi, *Desalin. Water Treat.*, 2016, **57**, 14774–14784.
163 K. M. M. Al-zobai, A. A. Hassan and N. O. Kariem, *Solid State Technol.*, 2020, **63**, 1–9.
164 B. A. Utami, H. Sutanto, I. Alkian, F. Sa'Adah and E. Hidayanto, *Cogent Eng.*, 2022, **9**, 2119534.
165 T. T. Nguyen, S. N. Nam, J. Son and J. Oh, *Sci. Rep.*, 2019, **9**, 9349.
166 D. Balarak and F. K. Mostafapour, *Indones. J. Chem.*, 2019, **19**, 211–218.
167 R. Mohammadi, B. Massoumi and M. Rabani, *Int. J. Photoenergy*, 2012, 514856, DOI: **10.1155/2012/514856**.
168 R. Mohammadi, B. Massoumi and H. Eskandarloo, *Desalin. Water Treat.*, 2015, **53**, 1995–2004.
169 E. T. Wahyuni, P. Y. Yulikayani and N. H. Aprilita, *J. Mater. Environ. Sci.*, 2020, **11**, 670–683.
170 N. Olama, M. Dehghani and M. Malakootian, *Appl. Water Sci.*, 2018, **8**, 97.
171 Lalliansanga, D. Tiwari, S.-M. Lee and D.-J. Kim, *Environ. Res.*, 2022, **210**, 112914.
172 Y. T. Gaim, S. M. Yimanuh and Z. G. Kidanu, *J. Compos. Sci.*, 2022, **6**, 317.
173 M. F. R. Samsudin, F. Maeght, N. Kamarudin and S. Sufian, *Malays. J. Microsc.*, 2020, **16**, 37–43.
174 T. C. M. V. Do, D. Q. Nguyen, K. T. Nguyen and P. H. Le, *Materials*, 2019, **12**, 2434.
175 M. R. Rezaei, M. H. Sayadi and N. Ravankhah, *Journal of Natural Environment*, 2021, **74**, 331–344.
176 L. Bergamonti, C. Bergonzi, C. Graiff, P. P. Lottici, R. Bettini and L. Elviri, *Water Res.*, 2019, **163**, 114841.
177 S. Moles, J. Berges, M. P. Ormad, M. J. Nieto-Monge, J. Gómez and R. Mosteo, *Environ. Sci. Pollut. Res.*, 2021, **28**, 24167–24179.
178 D. Kanakaraju, J. Kockler, C. A. Motti, B. D. Glass and M. Oelgemöller, *Appl. Catal., B*, 2015, **166–167**, 45–55.
179 L. M. Pastrana-Martínez, S. Morales-Torres, S. A. C. Carabineiro, J. G. Buijnsters, J. L. Figueiredo, A. M. T. Silva and J. L. Faria, *Appl. Surf. Sci.*, 2018, **458**, 839–848.
180 Q. Li, H. Kong, R. Jia, J. Shao and Y. He, *RSC Adv.*, 2019, **9**, 12538.
181 F. M. dela Rosa, J. Papac, S. Garcia-Ballesteros, M. Kovačić, Z. Katančić, H. Kušić and A. L. Božić, *Adv. Sustainable Syst.*, 2021, **5**, 2100119.
182 M. G. Alalm, A. Tawfik and A. Ookawara, *J. Environ. Chem. Eng.*, 2016, **4**, 1929–1937.
183 Q. Li, R. Jia, J. Shao and Y. He, *J. Cleaner Prod.*, 2019, **209**, 755–761.
184 F. A. Sulaiman and A. I. Alwared, *J. Ecol. Eng.*, 2022, **23**, 293–304.
185 A. Aissani, M. Kameche and K. Benabbou, *Inorg. Nano-Met. Chem.*, 2022, **52**, 1197–1207.
186 N. Torkian, A. Bahrami, A. Hosseini-Abari, M. M. Momeni, M. Abdolkarimi Mahabadi, A. Bayat, P. Hajipour, H. A. Rourani, M. S. Abbasi, S. Torkian, Y. Wen, M. Y. Mehr and A. Hojjati-Najafabadi, *Environ. Res.*, 2022, **207**, 112157.
187 Y. Chen, X. Zhang, L. Wang, X. Cheng and Q. Shang, *Chem. Eng. J.*, 2020, **402**, 126260.
188 S. Rani, A. Garg and N. Singh, *Toxicol. Environ. Chem.*, 2021, **103**, 137–153.
189 T. D. N. Thi, L. H. Nguyen, X. H. Nguyen, H. V. Phung, T. H. T. Vinh, P. V. Viet, N. V. Thai, H. N. Le, D. T. Pham, H. T. Van, L. H. T. Thi, T. D. P. Thi, T. L. Minh, H. H. P. Quang, H. P. N. Vu, T. T. Duc and H. M. Nguyen, *Mater. Sci. Semicond. Process.*, 2022, **142**, 106456.
190 A. Fawzy, H. Mahanna and M. Mossad, *Environ. Sci. Pollut. Res.*, 2022, **29**, 68532–68546.
191 H. Liu, L. Wang, S. Wei, Y. Wu, Y. Zheng, F. Yuan and J. Hou, *Opt. Mater.*, 2022, **123**, 111835.
192 D. Huang, X. Sun, Y. Liu, H. Ji, W. Liu, C.-C. Wang, W. Ma and Z. Cai, *Chin. Chem. Lett.*, 2021, **32**, 2787–2791.
193 I. F. Silva, I. F. Teixeira, R. D. F. Rios, G. M. do Nascimento, I. Binatti, H. F. V. Victória, K. Krambrock, L. A. Cury, A. P. C. Teixeira and H. O. Stumpf, *J. Hazard. Mater.*, 2021, **401**, 123713.
194 N. Q. Thang, A. Sabbah, L.-C. Chen, K.-H. Chen, C. M. Thi and P. V. Viet, *Chemosphere*, 2021, **282**, 130971.
195 S. Le, C. Zhu, Y. Cao, P. Wang, Q. Liu, H. Zhou, C. Chen, S. Wang and X. Duan, *Appl. Catal., B*, 2022, **303**, 120903.
196 M. Dou, J. Wang, B. Gao, Z. Ma and X. Huang, *Chem. Eng. J.*, 2020, **394**, 124899.
197 E. G. Shankar, S. Billa, A. B. V. Kiran Kumar and J. S. Yu, *Ceram. Int.*, 2021, **47**, 30572–30583.
198 V. V. Pham, T. K. Truong, L. V. Hai, H. P. P. La, H. T. Nguyen, V. Q. Lam, H. D. Tong, Q. Nguyen, A. Sabbah, K.-H. Chen, S.-J. You and T. M. Cao, *ACS Appl. Nano Mater.*, 2022, **5**, 4506–4514.
199 M. Dou, J. Wang, B. Gao, C. Xu and F. Yang, *Chem. Eng. J.*, 2020, **383**, 123134.
200 Q. Chen, L. Chen, J. Qi, Y. Tong, Y. Lv, C. Xu, J. Ni and W. Liu, *Chin. Chem. Lett.*, 2019, **30**, 1214–1218.
201 R. Changotra, Q. He and A. Dhir, *Chem. Eng. J.*, 2022, **442**, 136201.
202 D. Balarak, N. Mengelizadeh, P. Rajiv and K. Chandrika, *Environ. Sci. Pollut. Res.*, 2021, **28**, 49743–49754.
203 J. Song, Z. Xu, W. Liu and C.-T. Chang, *Mater. Sci. Semicond. Process.*, 2016, **52**, 32–37.
204 C. Yang, X. You, J. Cheng, H. Zheng and Y. Chen, *Appl. Catal., B*, 2017, **200**, 673–680.
205 M. F. R. Samsudin and S. Sufian, *J. Mol. Liq.*, 2020, **314**, 113530.
206 D. V. Thuan, T. L. Nguyen, H. H. P. Thi, N. T. Thanh, S. Ghotekar, A. K. Sharma, M. T. Binh, T. T. Nga, T.-D. Pham and D. P. Cam, *Opt. Mater.*, 2022, **123**, 111885.
207 F. Beshkar, A. Al-Nayili, O. Amiri, M. Salavati-Niasari and M. Mousavi-Kamazani, *J. Alloys Compd.*, 2022, **892**, 162176.
208 M. R. S. Nivetha, J. V. Kumar, J. S. Ajarem, A. A. Allam, V. Manikandan, R. Arulmozhi and N. Abirami, *Environ. Res.*, 2022, **209**, 112809.

209 E. M. El-Fawal, S. A. Younis and T. Zaki, *J. Photochem. Photobiol., A*, 2020, **401**, 112746.
210 Y. Belaissa, D. Nibou, A. A. Assadi, B. Bellal and M. Trari, *J. Taiwan Inst. Chem. Eng.*, 2016, **68**, 254–265.
211 B. Gao, J. Wang, M. Dou, C. Xu and X. Huang, *Environ. Sci. Pollut. Res.*, 2020, **27**, 7025–7039.
212 M. H. T. Tung, T. T. T. Phuong, D. M. N. Tram, D. M. The, N. V. N. Mai, T. T. T. Hien, L. T. C. Nhung, N. T. T. Binh, C. V. Hoang, D. N. Nhiem, T.-D. Pham and N. T. D. Cam, *Diamond Relat. Mater.*, 2022, **121**, 108788.
213 Q. Li, H. Kong, P. Li, J. Shao and Y. He, *J. Hazard. Mater.*, 2019, **373**, 437–446.
214 K. H. Leong, H. Y. Chu, S. Ibrahi and P. Saravanan, *Beilstein J. Nanotechnol.*, 2015, **6**, 428–437.
215 P. Hajipour, A. Eslami, A. Bahrami, A. Hosseini-Abari, F. Y. Saber, R. Mohammadi and M. Y. Mehr, *Ceram. Int.*, 2021, **47**, 33875–33885.
216 M. Moradi, F. Hasanvandian, A. A. Isari, F. Hayati, B. Kakavandi and S. R. Setayesh, *Appl. Catal., B*, 2021, **285**, 119838.
217 G. Prasannamedha and P. S. Kumar, *J. Cleaner Prod.*, 2020, **250**, 119553.
218 J. Musial, D. T. Mlynarczyk and B. J. Stanisz, *Sci. Total Environ.*, 2023, **856**, 159122.
219 C. H. Wu, C. Y. Kuo, C. D. Dong, C. W. Chen and Y. L. Lin, *Water Sci. Technol.*, 2019, **79**, 349–355.
220 L. Prieto-Rodriguez, S. Miralles-Cuevas, I. Oller, P. Fernández-Ibánez, A. Agüera, J. Blanco and S. Malato, *Appl. Catal., B*, 2012, **128**, 119–125.
221 A. Hu, X. Zhang, D. Luong, K. D. Oakes, M. R. Servos, R. Liang, S. Kurdi, P. Peng and Y. Zhou, *Waste Biomass Valorization*, 2012, **3**, 443–449.
222 M. R. Eskandarian, H. Choi, M. Fazli and M. H. Rasoulifard, *Chem. Eng. J.*, 2016, **300**, 414–422.
223 M. N. Abellán, B. Bayarri, J. Giménez and J. Costa, *Appl. Catal., B*, 2007, **74**, 233–241.
224 D. Balarak and H. Azarpira, *Int. J. ChemTech Res.*, 2016, **9**, 731–738.
225 J. Carbajo, M. Jiménez, S. Miralles, S. Malato, M. Faraldos and A. Bahamonde, *Chem. Eng. J.*, 2016, **291**, 64–73.
226 A. Kutuzova, T. Dontsova and W. Kwapinski, *Catalysts*, 2021, **11**, 728.
227 O. Porcar-Santos, A. Cruz-Alcalde, N. López-Vinent, D. Zanganas and C. Sans, *Sci. Total Environ.*, 2020, **736**, 139605.
228 J. R. Kim and E. Kan, *J. Environ. Manage.*, 2016, **180**, 94–101.
229 N. Miranda-Garcia, S. Suarez, B. Sanchez, J. M. Coronado, S. Alato and M. I. Maldonsado, *Appl. Catal., B*, 2011, **103**, 294–301.
230 S. Ramasundaram, M. G. Seid, J. W. Choe, E.-J. Kim, Y. C. Chung, K. Cho, C. Lee and S. W. Hong, *Chem. Eng. J.*, 2016, **306**, 344–351.
231 M. J. Arlos, M. M. Hatat-Fraile, R. Liang, L. M. Bragg, N. Y. Zhou, S. A. Andrews and M. R. Servos, *Water Res.*, 2016, **101**, 351–361.
232 A. Mirzaei, L. Yerushalmi, Z. Chen, F. Haghighat and J. Guo, *Water Res.*, 2018, **132**, 241–251.
233 T. Makropoulou, I. Kortidis, K. Davididou, D. E. Motaung and E. Chatzisymeon, *J. Water Process. Eng.*, 2020, **36**, 101299.
234 F. Beheshti, R. M. A. Tehrani and A. Khadir, *Int. J. Environ. Sci. Technol.*, 2019, **16**, 7987–7996.
235 A. Tiwari, A. Shukla, Lalliansanga, D. Tiwari and S. M. Lee, *J. Environ. Manage.*, 2018, **220**, 96–108.
236 E. Borowska, J. F. Gomes, R. C. Martins, R. M. Quinta-Ferreira, H. Horn and M. Gmurek, *Catalysts*, 2019, **9**, 500.
237 L.-F. Chiang and R. A. Doong, *Sep. Purif. Technol.*, 2015, **156**, 1003–1010.
238 R. Zanella, E. Avella, R. M. Ramírez-Zamora, F. Castillón-Barraza and J. C. D. Álvarez, *Environ. Technol.*, 2018, **39**, 2353–2364.
239 A. Tsiampalis, Z. Frontistis, V. Binas, G. Kiriakidis and D. Mantzavinos, *Catalysts*, 2019, **9**, 612.
240 M. Jahdi, S. B. Mishra, E. N. Nxumalo, S. D. Mhlanga and A. K. Mishra, *Appl. Catal., B*, 2020, **267**, 118716.
241 M. Jahdi, S. B. Mishra, E. N. Nxumalo, S. D. Mhlanga and A. K. Mishra, *RSC Adv.*, 2020, **10**, 27662.
242 L. K. B. Paragas, M. D. G. de Luna and R.-A. Doong, *Chemosphere*, 2018, **210**, 1099–1107.
243 A. A. Isari, F. Hayati, B. Kakavandi, M. Rostami, M. Motevassel and E. Dehghanifard, *Chem. Eng. J.*, 2020, **392**, 123685.
244 T.-B. Nguyena, C. P. Huang, R. Doong, C.-W. Chen and C.-D. Dong, *Chem. Eng. J.*, 2020, **384**, 123383.
245 A. Mirzaei, M. Eddah, S. Roualdès, D. Ma and M. Chaker, *Chem. Eng. J.*, 2021, **422**, 130507.
246 I. Zammit, V. Vaiano, A. R. Ribeiro, A. M. T. Silva, C. M. Manaia and L. Rizzo, *Catalysts*, 2019, **9**, 222.
247 X. Xie, S. Li, H. Zhang, Z. Wang and H. Huang, *Sci. Total Environ.*, 2019, **659**, 529–539.
248 L. Fernández, M. Gamallo, M. A. González-Gómez, C. Vázquez-Vázquez, J. Rivas, M. Pintado and M. T. Moreira, *J. Environ. Manage.*, 2019, **237**, 595–608.
249 V. Polliotto, F. R. Pomilla, V. Maurino, G. Marcì, A. B. Prevot, R. Nisticò, G. Magnacca, M. C. Paganini, L. Ponce Robles, L. Perez and S. Malato, *Catal. Today*, 2019, **328**, 164–171.
250 N. T. T. Nguyen, A. Q. K. Nguyen, M. S. Kim, C. Lee, S. Kim and J. Kim, *Sep. Purif. Technol.*, 2021, **267**, 118610.
251 N. Wang, X. Li, Y. Yang, Z. Zhou, Y. Shang and X. Zhuang, *J. Water Process. Eng.*, 2020, **36**, 101335.
252 N. Rioja, P. Benguria, F. J. Peñas and S. Zorita, *Environ. Sci. Pollut. Res.*, 2014, **21**, 11168–11177.
253 M. O. Alfred, M. O. Omorogie, O. Bodede, R. Moodley, A. Ogunlaja, O. G. Adeyemi, C. Gunter, A. Trubert, H. Eckert, L. D. A. Silva, A. S. S. de Camargo, A. de J. Motheo, S. M. Clarke and E. I. Unuabonah, *Chem. Eng. J.*, 2020, **398**, 125544.
254 E. H. Mourid, E. M. El Mouchtari, L. El Mersly, L. Benaziz, S. Rafqah and M. Lakraimi, *J. Photochem. Photobiol., A*, 2020, **396**, 112530.

255 M. Długosz, P. Zmudzki, A. Kwiecień, K. Szczubiałka and J. Krzek, *J. Hazard. Mater.*, 2015, **298**, 146–153.
256 R. Noroozi, M. Gholami, M. Farzadkia and R. R. Kalantary, *Environ. Sci. Pollut. Res.*, 2022, **29**, 56403–56418.
257 N. Malesic-Eleftheriadou, E. Evgenidou, G. Z. Kyzas, D. N. Bikiaris and D. A. Lambropoulou, *Chemosphere*, 2019, **234**, 746–755.
258 J. Li, F. Wang, L. Meng, M. Han, Y. Guo and C. Sun, *J. Colloid Interface Sci.*, 2017, **485**, 116–122.
259 K. Kouvelis, A. A. Kampioti, A. Petala and Z. Frontistis, *Catalysts*, 2022, **12**, 882.
260 O. Mertah, A. Gomez-Aviles, A. Kherbeche, C. Belver and J. Bedia, *J. Environ. Chem. Eng.*, 2022, **10**, 108438.
261 W. Zhu, Z. Li, C. He, S. Faqian and Y. Zhou, *J. Alloys Compd.*, 2018, **754**, 153–162.
262 D. Awfa, M. Ateia, M. Fujii and C. Yoshimura, *J. Water Process. Eng.*, 2019, **31**, 100836.
263 J. Martini, C. A. Orge, J. L. Faria, M. F. R. Pereira and O. S. G. P. Soares, *Appl. Sci.*, 2019, **9**, 2652.
264 M. Chen, C. Guo, S. Hou, L. Wu, J. Lv, C. Hu, Y. Zhang and J. Xu, *J. Hazard. Mater.*, 2019, **366**, 219–228.
265 A. Mirzaei, L. Yerushalmi, Z. Chen and F. Haghighat, *J. Hazard. Mater.*, 2018, **359**, 516–526.
266 G. K. Teye, J. Huang, Y. Li, K. Li, L. Chen and W. K. Darkwah, *Nanomaterials*, 2021, **11**, 2609.
267 X. Ao, Z. Li and H. Zhang, *J. Cleaner Prod.*, 2022, **356**, 131822.
268 Y. Song, J. Qi, J. Tian, S. Gao and F. Cui, *Chem. Eng. J.*, 2018, **341**, 547–555.
269 W. Zhu, F. Sun, R. Goei and Y. Zhou, *Appl. Catal., B*, 2017, **207**, 93–102.
270 L. Zhou, G. Zou and G. L. Deng, *Catalysts*, 2018, **8**, 272.
271 L. Lin, H. Wang and P. Xu, *Chem. Eng. J.*, 2017, **310**, 389–398.
272 S.-H. Liu, Y.-S. Wei and J. S. Lu, *Chemosphere*, 2016, **154**, 118–123.
273 M. Nawaz, A. A. Khan, A. Hussain, J. Jang, H.-Y. Jung and D. S. Lee, *Chemosphere*, 2020, **261**, 127702.
274 L. Zhou, O. G. Alvarez, C. S. Mazon, L. Chen, H. Deng and M. Sui, *Catal. Sci. Technol.*, 2016, **6**, 5972.
275 W. Zhu, F. Sun, R. Goei and Y. Zhou, *Catal. Sci. Technol.*, 2017, **7**, 2591–2600.
276 M. H. de M. Rodrigues, P. A. R. de Sousa, K. C. M. Borges, L. de M. Coelho, R. F. Gonçalves, M. D. Teodoro, F. da V. Motta, R. M. do Nascimento and M. G. Júnior, *J. Alloys Compd.*, 2019, **808**, 151711.
277 A. Kumar, G. Sharma, M. Naushad, Z. A. Alothman and P. Dhiman, *Earth Syst. Environ.*, 2022, **6**, 141–156.
278 J. Qiu, C. Yue, W. Zheng, F. Liu and J. Zhu, *Chin. Chem. Lett.*, 2021, **32**, 3431–3434.
279 A. Kumar, A. Kumar, G. Sharma, A. H. Al-Muhtaseb, M. Naushad, A. A. Ghfar and F. J. Stadler, *Chem. Eng. J.*, 2018, **334**, 462–478.
280 Z. Huang, X. Dai, Z. Huang, T. Wang, L. Cui, J. Ye and P. Wu, *Chemosphere*, 2019, **221**, 824–833.
281 L. Zhang, G. Meng, B. Liu and X. Ge, *J. Mol. Liq.*, 2022, **360**, 119427.
282 D. Roy, S. Niyogi and S. De, *Process Saf. Environ. Prot.*, 2022, **161**, 723–738.
283 T. Ke, S. Shen, K. Yang and D. Lin, *Appl. Surf. Sci.*, 2022, **580**, 152302.
284 M. Ren, Y. Ao, P. Wang and C. Wang, *Chem. Eng. J.*, 2019, **378**, 122122.
285 C. Liu, J. Xu, J. Niu, M. Chen and Y. Zhou, *Sep. Purif. Technol.*, 2020, **241**, 116622.
286 C. Liu, J. Xu, X. Du, Q. Li, Y. Fu and M. Chen, *Opt. Mater.*, 2021, **112**, 110742.
287 J. Xu, J. Chen, Y. Ao and P. Wang, *Chin. Chem. Lett.*, 2021, **32**, 3226–3230.
288 L. Zhou, W. Zhang, L. Chen and H. Deng, *J. Colloid Interface Sci.*, 2017, **487**, 410–417.
289 A. Mirzaei, Z. Chen, F. Haghighat and L. Yerushalm, *Chemosphere*, 2018, **205**, 463–474.
290 G. Liu, H. Wang, D. Chen, C. Dai, Z. Zhang and Y. Feng, *Sep. Purif. Technol.*, 2020, **237**, 116329.
291 Y. Zhang, Y. Li and Y. Yuan, *J. Colloid Interface Sci.*, 2023, **645**, 860–869.
292 E. Brillas, *Chemosphere*, 2022, **286**, 131849.
293 J. Jan-Roblero and J. A. Cruz-Maya, *Molecules*, 2023, **28**, 2097.
294 N. Jallouli, L. M. Pastrana-Martinez, A. R. Ribeiro, N. F. F. Moreira, J. L. Faria, O. Hentati, A. M. T. Silva and M. Ksibi, *Chem. Eng. J.*, 2018, **334**, 976–984.
295 M. Jiménez-Salcedo, M. Monge and M. T. Tena, *Chemosphere*, 2019, **215**, 605–618.
296 M. O. Miranda, W. E. C. Cavalcanti, F. F. Barbosa, J. A. de Sousa, F. I. da Silva, S. B. C. Pergher and T. P. Braga, *RSC Adv.*, 2021, **11**, 27720.
297 I. Georgaki, E. Vasilaki and N. Katsarakis, *Am. J. Anal. Chem.*, 2014, **5**, 518–534.
298 M. Tanveer, G. T. Guyer and G. Abbas, *Water Environ. Res.*, 2019, **91**, 822–829.
299 N. Rastkari, A. Eslami, S. Nasseri, E. Piroti and A. Asadi, *Pol. J. Environ. Stud.*, 2017, **26**, 785–794.
300 A. S. Sá, R. P. Feitosa, L. Honório, R. Peña-Garcia, L. C. Almeida, J. S. Dias, L. P. Brazuna, T. G. Tabuti, E. R. Triboni, J. A. Osajima and E. C. da Silva-Filho, *Materials*, 2021, **14**, 5891.
301 M. Ulfa, D. Prasetyoko, H. Bahruji and R. E. Nugraha, *Materials*, 2021, **14**, 6779.
302 S. Khalaf, J. H. Shoqeir, F. Lelario, S. A. Bufo, R. Karamanand and L. Scrano, *Catalysts*, 2020, **10**, 560.
303 F. S. Braz, M. R. A. Silva, F. S. Silva, S. J. Andrade, A. L. Fonseca and M. M. Kondo, *J. Environ. Prot.*, 2014, **5**, 620–626.
304 J. Bohdziewicz, E. Kudlek and M. Dudziak, *Desalin. Water Treat.*, 2016, **57**, 1552–1563.
305 J. Choina, A. Bagabas, C. Fisher, G. U. Flechsig, H. Kosslick, A. Alshammari and A. Schulz, *Catal. Today*, 2015, **241**, 47–54.
306 N. Rosman, W. N. W. Salleh, J. Jaafar, Z. Harun, F. Aziz and A. F. Ismail, *Catalysts*, 2022, **12**, 209.

307 A. Eslami, M. M. Amini, A. R. Yazdanbakhsh, A. Mohseni-Bandpei, A. A. Safari and A. Asadi, *J. Chem. Technol. Biotechnol.*, 2016, **91**, 2693–2704.
308 T. M. Khedr, S. M. El-Sheikh, A. Hakki, A. A. Ismail, W. A. Badawy and D. W. Bahnemann, *J. Photochem. Photobiol., A*, 2017, **346**, 530–540.
309 V. Bhatia and A. Dhir, *J. Environ. Chem. Eng.*, 2016, **4**, 1267–1273.
310 A. Jraba, Z. Anna and E. Elaloui, *J. Mater. Sci.: Mater. Electron.*, 2020, **31**, 1072–1083.
311 R. Pelosato, V. Carrara and I. N. Sora, *Chem. Eng. Trans.*, 2019, **73**, 181–186.
312 Q. Sun, Y.-P. Peng, H. Chen, K.-L. Chang, Y.-N. Qiu and S.-W. Lai, *J. Hazard. Mater.*, 2016, **319**, 121–129.
313 S. M. El-Sheikh, T. M. Khedr, A. Hakki, A. A. Ismail, W. A. Badawy and D. W. Bahnemann, *Sep. Purif. Technol.*, 2017, **173**, 258–268.
314 C. Yuan, C.-H. Hung, H.-W. Li and W.-H. Chang, *Chemosphere*, 2016, **155**, 471–478.
315 L. Lin, W. Jiang, M. Bechelany, M. Nasr, J. Jarvis, T. Schaub, R. R. Sapkota, P. Miele, H. Wang and P. Xu, *Chemosphere*, 2019, **220**, 921–929.
316 Y. Gu, J. Yperman, R. Carleer, J. D'Haen, J. Maggen, S. Vanderheyden, K. Vanreppelen and R. M. Garcia, *Chemosphere*, 2019, **217**, 724–731.
317 M. Mohadesi, A. Gouran and K. Seifi, *Environ. Sci. Pollut. Res.*, 2022, **29**, 34338–34348.
318 N. Liu, J. Wang, J. Wu, Z. Li, W. Huang, Y. Zheng, J. Lei, X. Zhang and L. Tang, *Mater. Res. Bull.*, 2020, **132**, 111000.
319 T. R. Bastami, A. Ahmadpour and F. A. Hekmatikar, *J. Ind. Eng. Chem.*, 2017, **51**, 244–254.
320 C. S. L. Fung, M. Khan, A. Kumar and I. M. C. Lo, *Sep. Purif. Technol.*, 2019, **216**, 102–114.
321 M. P. Villavicencio, A. E. Morales, M. de L. R. Peralta, M. Sánchez-Cantú, L. R. Blanco, E. C. Anota, J. H. C. García and F. Tzompantzi, *Catal. Lett.*, 2020, **150**, 2385–2399.
322 J. Liao, Y. Xu, Y. Zhao, C.-C. Wang and C. Ge, *ACS Appl. Nano Mater.*, 2021, **4**, 1898–1905.
323 G. G. Lenzi, M. F. Lopes, D. I. Andrade, J. S. Napoli, A. Parolin, Y. B. Fávaro, M. E. K. Fuziki, L. N. B. de Almeida, T. G. Josué, D. T. Dias and A. M. Tusset, *Water Sci. Technol.*, 2021, **84**, 2158–2179.
324 M. Khan, C. S. L. Fung, A. Kumar and I. M. C. Lo, *J. Hazard. Mater.*, 2019, **365**, 733–743.
325 K. Kang, M. Jang, M. Cui, P. Qiu, B. Park, S. A. Snyder and J. Khim, *J. Mol. Catal. A: Chem.*, 2014, **390**, 178–186.
326 C. B. Anucha, I. Altin, E. Bacaksiz, I. Degirmencioglu, T. Kucukomeroglu, S. Yilmaz and V. N. Stathopoulos, *Separations*, 2021, **8**, 24.
327 S. Sambaza, A. Maity and K. Pillay, *J. Saudi Chem. Soc.*, 2022, **26**, 101563.
328 A. Mohamed, A. Salama, W. S. Nasser and A. Uheida, *Environ. Sci. Eur.*, 2018, **30**, 47.
329 E. Yilmaz, S. Salem, G. Sarp, S. Aydin, K. Sahin, I. R. Korkmaz and D. Yuvali, *Talanta*, 2020, **213**, 120813.
330 B.-T. Zhang, Q. Wang, Y. Zhang, Y. Teng and M. Fan, *Sep. Purif. Technol.*, 2020, **242**, 116820.
331 N. Rosman, W. N. W. Salleh, N. A. M. Razali, S. Z. Ahmad, N. H. Ismail, F. Aziz, Z. Harun, A. F. Ismail and N. Yuso, *Mater. Today: Proc.*, 2021, **42**, 69–74.
332 A. Uheida, A. Mohamed, M. Belaqziz and W. S. Nasser, *Sep. Purif. Technol.*, 2019, **212**, 110–118.
333 D. Hernández-Uresti, A. Vázquez, D. Sanchez-Martinez and S. Obregón, *J. Photochem. Photobiol., A*, 2016, **324**, 47–52.
334 X. Wang, J. Luo, Y. Huang, J. Mei and Y. Chen, *Environ. Sci.: Water Res. Technol.*, 2021, **7**, 610.
335 A. Raja, P. Rajasekaran, K. Selvakumar, M. Arivanandhan, S. A. Bahadur and M. S. Swaminathan, *Appl. Surf. Sci.*, 2020, **513**, 145803.
336 A. Kumar, G. Sharma, M. Naushad, A. H. Al-Muhtaseb, A. Kumar, I. Hira, T. Ahamad, A. A. Ghfar and F. J. Stadler, *J. Environ. Manage.*, 2019, **231**, 1164–1175.
337 R. Akbarzadeh, C. S. L. Fung, R. A. Rather and I. M. C. Lo, *Chem. Eng. J.*, 2018, **341**, 248–261.
338 Z. Sun, X. Zhang, X. Dong, X. Liu, Y. Tan, F. Yuan, S. Zheng and C. Li, *J. Materiomics*, 2020, **6**, 582–592.
339 Z.-D. Lei, J.-J. Wang, L. Wang, X.-Y. Yang, G. Xu and L. Tang, *J. Hazard. Mater.*, 2016, **312**, 298–306.
340 W. Cao, Y. Yuan, C. Yang, S. Wu and J. Cheng, *Chem. Eng. J.*, 2020, **391**, 123608.
341 Y. Zhang, J. Li and H. Liu, *J. Nanomater.*, 2020, 6094984, DOI: **10.1155/2020/6094984**.
342 L. Wang, Q. Sun, Y. Dou, Z. Zhang, T. Yan and Y. Li, *J. Hazard. Mater.*, 2021, **413**, 125288.
343 X. Chen, X. Li, J. Yang, Q. Sun, Y. Yang and X. Wu, *Int. J. Hydrogen Energy*, 2018, **43**, 13284–13293.
344 J. Wang, L. Tang, G. Zeng, Y. Deng, Y. Liu, L. Wang, Y. Zhou, Z. Guo, J. Wang and C. Zhang, *Appl. Catal., B*, 2017, **209**, 285–294.
345 A. Kumar, M. Khan, X. Zeng and I. M. C. Lo, *Chem. Eng. J.*, 2018, **353**, 645–656.
346 N. Liu, F. Fei, W. Dai, J. Lei, F. Bi, B. Wang, G. Quan, X. Zhang and L. Tang, *J. Colloid Interface Sci.*, 2022, **625**, 965–977.
347 S. Mao, C. Liu, M. Xia, F. Wang and X. Ju, *Catal. Sci. Technol.*, 2021, **11**, 3466–3480.
348 S.-H. Liu and W.-T. Tang, *Sci. Total Environ.*, 2020, **731**, 139172.
349 Y. Cong, Y. Li, X. Wang, X. Wei, L. Che and S.-W. Lv, *Sep. Purif. Technol.*, 2022, **297**, 121531.
350 P. J. Mafa, U. S. Swana, D. Liu, J. Gui, B. B. Mamba and A. T. Kuvarega, *Colloids Surf., A*, 2021, **612**, 126004.
351 J. Zhang, L. Xin, L. Qianwen, L. Yuqian, G. Liu and X. Shi, *Ceram. Int.*, 2020, **46**, 106–113.
352 A. Kumar, M. Khan, L. Fang and I. M. C. Lo, *J. Hazard. Mater.*, 2019, **370**, 108–116.
353 M. Liang, Z. Zhang, R. Long, Y. Wang, Y. Yu and Y. Pei, *Environ. Pollut.*, 2020, **259**, 113770.
354 M. E. Malefane, U. Feleni, P. J. Mafa and A. T. Kuvarega, *Appl. Surf. Sci.*, 2020, **514**, 145940.

355 Q. Wei, S. Xiong, W. Li, C. Jin, Y. Chen, L. Hou, Z. Wu, Z. Pan, Q. He, Y. Wang and D. Tang, *J. Alloys Compd.*, 2021, **885**, 160984.
356 A. Zhou, L. Liao, X. Wu, K. Yang, C. Li, W. Chen and P. Xie, *Sep. Purif. Technol.*, 2020, **250**, 117241.
357 N. Rosman, W. N. W. Salleh, M. A. Mohamed, Z. Harun, A. F. Ismail and F. Aziz, *Sep. Purif. Technol.*, 2020, **251**, 117391.
358 L. Chierentin and H. R. N. Salgado, *Crit. Rev. Anal. Chem.*, 2016, **46**, 22–39.
359 B. Holmes, R. N. Brogden and D. M. Richards, *Drugs*, 1985, **30**, 482–513.
360 A. J. Schaeffer, *Eur. Urol.*, 1990, **17**, 19–23.
361 H. Yang, L. Mei, P. Wang, J. Genereux, Y. Wang, B. Yi, C. Au, L. Dang and P. Feng, *RSC Adv.*, 2017, **7**, 45721.
362 M. M. Haque and M. Muneer, *J. Hazard. Mater.*, 2007, **145**, 51–57.
363 Z. Liu, X. Yu, F. Yang, J. Nie, N. Zhao, J. Li and B. Yao, *IOP Conf. Ser. Earth Environ. Sci.*, 2020, **453**, 012084.
364 M. Chen, Y. Huang and W. Chu, *Chin. J. Catal.*, 2019, **40**, 673–680.
365 M. Sayed, L. A. Shah, J. A. Khan, N. S. Shah, J. Nisar, H. M. Khan, P. Zhang and A. R. Khan, *J. Phys. Chem. A*, 2016, **120**, 9916–9931.
366 S.-L. Zhou, S. Zhang, F. Liu, J.-J. Liu, J.-J. Xue, D.-J. Yang and C.-T. Chang, *J. Photochem. Photobiol., A*, 2016, **328**, 97–104.
367 S. Zhang, S.-L. Zhou, J.-J. Liu, D.-J. Yang, J.-J. Xue and C.-T. Chang, *J. Nanosci. Nanotechnol.*, 2018, **18**, 4087–4092.
368 R. Xiao, Y. Zhang, S. Wang, H. Zhu, H. Song, G. Chen, H. Lin, J. Zhang and J. Xiang, *Environ. Sci. Pollut. Res.*, 2021, **28**, 69301–69313.
369 S. S. Mohtar, F. Aziz, A. F. Ismail, N. S. Sambudi, H. Abdullah, A. N. Rosli and B. Ohtani, *Catalysts*, 2021, **11**, 1160.
370 X. Jin, X. Zhou, P. Sun, S. Lin, W. Cao, Z. Li and W. Liu, *Chemosphere*, 2019, **237**, 124433.
371 R. Kaushik, P. K. Samal and A. Halder, *ACS Appl. Nano Mater.*, 2019, **2**, 7898–7909.
372 M. Chen and W. Chu, *J. Hazard. Mater.*, 2012, **219**, 183–189.
373 M. Manasa, P. R. Chandewar and H. Mahalingam, *Catal. Today*, 2021, **375**, 522–536.
374 N. S. Shah, J. A. Khan, M. Sayed, Z. U. H. Khan, A. D. Rizwan, N. Muhammad, G. Boczkaj, B. Murtaza, M. Imran, H. M. Khan and G. Zaman, *Chem. Eng. J.*, 2018, **351**, 841–855.
375 Y. Hsu, J. Thomas, C. T. Chang and C. M. Ma, *J. Nanosci. Nanotechnol.*, 2021, **21**, 3099–3106.
376 B. P. Patil and R. V. Jayaram, *Catal. Green Chem. Eng.*, 2021, **4**, 51–63.
377 P. Garcia-Muñoz, N. P. Zussblatt, G. Pliego, J. A. Zazo, F. Fresno, B. F. Chmelka and J. A. Casas, *J. Environ. Manage.*, 2019, **238**, 243–250.
378 N. T. T. Trang, T. Q. Vinh, H. V. Giang, N. S. Mai, N. T. Dong, P. T. Linh, N. V. Hoang and N. M. Tan, *Vietnam J. Sci. Technol.*, 2020, **58**, 13–19.
379 X. Wang, Y. Sun, L. Yang, Q. Shang, D. Wang, T. Guo and Y. Guo, *Sci. Total Environ.*, 2019, **656**, 1010–1020.
380 J. Gou, Q. Ma, X. Deng, Y. Cui, H. Zhang, X. Cheng, X. Li, M. Xie and Q. Cheng, *Chem. Eng. J.*, 2017, **308**, 818–826.
381 J. Li, M. Han, Y. Guo, F. Wang and C. Sun, *Chem. Eng. J.*, 2016, **298**, 300–308.
382 Q. Zhao, C.-C. Wang and P. Wang, *Chin. Chem. Lett.*, 2022, **33**, 4828–4833.
383 X.-J. Wen, C.-G. Niu, D.-W. Huang, L. Zhang, C. Liang and G.-M. Zeng, *J. Catal.*, 2017, **355**, 73–86.
384 W. Liu, T. He, Y. Wang, G. Ning, Z. Xu and X. Chen, *Sci. Rep.*, 2020, **10**, 11903.
385 L. Bharali, J. Kalita, S. S. Dhar and N. S. Moyon, *ChemistrySelect*, 2022, **7**, e202203487.
386 C.-H. Zhang, X.-B. Zhao, Y.-J. Li and D.-W. Sun, *Yingyong Huaxue*, 2021, **38**, 99–106.
387 Z. Jiao, J. Zhang, Z. Liu and Z. Ma, *J. Photochem. Photobiol., A*, 2019, **371**, 67–75.
388 W. Y. Fei, W. F. Liang, L. J. Hua, X. Z. Jie, S. Y. Han, Z. Q. Xin, Y. Kun, L. W. Ying, L. Jin and L. G. Guang, *Zhongguo Huanjing Kexue*, 2018, **38**, 1346–1355.
389 W. Zhang, Z. Bian, X. Xin, L. Wang, X. Geng and H. Wang, *Chemosphere*, 2021, **262**, 127955.
390 Q. Chen, Y. Hao, Z. Song, M. Liu, D. Chen, B. Zhu, J. Chen and Z. Chen, *Ecotoxicol. Environ. Saf.*, 2021, **225**, 112742.
391 W. Liu, J. Zhou and J. Yao, *Ecotoxicol. Environ. Saf.*, 2020, **190**, 110062.
392 S. L. Prabavathi and V. Muthuraj, *Colloids Surf., A*, 2019, **567**, 43–54.
393 L. Ma, J. Duan, B. Ji, Y. Liu, C. Li, C. Li, W. Zhao and Z. Yang, *J. Alloys Compd.*, 2021, **869**, 158679.
394 Y. Zhao, X. Liang, X. Hu and J. Fan, *J. Colloid Interface Sci.*, 2021, **589**, 336–346.
395 W. Zhao, J. Duan, B. Ji, L. Ma and Z. Yang, *J. Environ. Chem. Eng.*, 2018, **8**, 102206.
396 J. Wu, J. Bai, Z. Wang, Z. Liu, Y. Mao, B. Liu and X. Zhu, *Environ. Technol.*, 2022, **43**, 95–106.
397 H. Mohan, S. Vadivel, P. M. Sathya, M. Fujii, G. H. Ha, G. Kim and T. Shin, *ACS Appl. Energy Mater.*, 2022, **5**, 12851–12859.
398 B. Ji, W. Zhao, J. Duan, L. Fu, L. Ma and Z. Yang, *RSC Adv.*, 2020, **10**, 4427–4435.
399 Q. Wu, Y. Liu, H. Jing, H. Yu, Y. Lu, M. Huo and H. Huo, *Chem. Eng. J.*, 2020, **390**, 124615.
400 S. Wen, M. Chen and H. Cao, *Int. J. Electrochem. Sci.*, 2021, **16**, 210733, DOI: **10.20964/2021.07.63**.
401 G. Li, S. Huang, N. Zhu, H. Yuan, D. Ge and Y. Wei, *Chem. Eng. J.*, 2021, **421**, 127852.
402 J. Guo, C.-H. Shen, J. Sun, X.-J. Xu, X.-Y. Li, Z.-H. Fei, Z.-T. Liu and X.-J. Wen, *Sep. Purif. Technol.*, 2021, **259**, 118109.
403 S. Subudhi, L. Paramanik, S. Sultana, S. Mansingh, P. Mohapatra and K. Parida, *J. Colloid Interface Sci.*, 2020, **568**, 89–105.
404 W. Zhang, Y. Meng, Y. Liu, H. Shen, Z. Ni, S. Xia, W. Han, Y. Li and H. Tang, *J. Environ. Chem. Eng.*, 2022, **10**, 107812.

405 M. Wang, H. Yu, P. Wang, Z. Chi, Z. Zhang, B. Dong, H. Dong, K. Yu and H. Yu, *Sep. Purif. Technol.*, 2021, **274**, 118692.
406 S. L. Prabavathi, K. Govindan, K. Saravanakumar, A. Jang and V. Muthuraj, *J. Ind. Eng. Chem.*, 2019, **80**, 558–567.
407 N. Yin, H. Chen, X. Yuan, Y. Zhang, M. Zhang, J. Guo, Y. Zhang, L. Qiao, M. Liu and K. Song, *J. Hazard. Mater.*, 2022, **436**, 129317.
408 Z. Zhao, Q. Ling, Z. Li, K. Yan, C. Ding, P. Chen, L. Yang, Z. Sun and M. Zhang, *Sep. Purif. Technol.*, 2023, **308**, 122928.
409 J. Jiang and Y. Li, *Crystals*, 2021, **11**, 1173.
410 J. Zhang, Z. Zhu, J. Jiang and H. Li, *Molecules*, 2020, **25**, 3706.
411 Y. Lv, H. Liu, D. Jin, H. Yang, D. He, Z. Zhang, Y. Zhang, J. Qu and Y.-N. Zhang, *Chem. Eng. J.*, 2022, **429**, 132092.
412 L. Chang, Y. Pu, P. Jing, J. Ji, X. Wei, B. Cao, Y. Yu, S. Xu and H. Xie, *Surf. Interfaces*, 2022, **31**, 102010.
413 A. Kumar, S. K. Sharma, G. Sharma, A. H. Al-Muhtaseb, M. Naushad, A. A. Ghfar and F. J. Stadler, *J. Hazard. Mater.*, 2019, **364**, 429–440.
414 J. Li, Z. Xia, D. Ma, G. Liu, N. Song, D. Xiang, Y. Xin, G. Zhang and Q. Chen, *J. Colloid Interface Sci.*, 2021, **586**, 243–256.
415 C. Zhang, M. Jia, Z. Xu, W. Xiong, Z. Yang, J. Cao, H. Peng, H. Xu, Y. Xiang and Y. Jing, *Chem. Eng. J.*, 2022, **430**, 132652.
416 X. Gu, T. Chen, J. Lei, Y. Yang, X. Zheng, S. Zhang, Q. Zhu, X. Fu, S. Meng and S. Chen, *Chin. J. Catal.*, 2022, **43**, 2569–2580.
417 Y. Liu, R. Chen, F. Wu, W. Gan, L. Chen, M. Zhang and Z. Sun, *Sep. Purif. Technol.*, 2023, **324**, 124572.
418 J. Zhang, Z. Zhu, J. Jiang and H. Li, *Catalysts*, 2020, **10**, 373.
419 Z. Zhu, H. Xia, H. Li and S. Han, *Inorganics*, 2022, **10**, 131.
420 C. Li, T. Sun, G. Yi, D. Zhang, Y. Zhang, X. Lin, J. Liu, Z. Shi and Q. Lin, *Colloids Surf., A*, 2023, **662**, 131001.
421 C. Guo, S. Gao, J. Lv, S. Hou, Y. Zhang and J. Xu, *Appl. Catal., B*, 2017, **205**, 68–77.
422 A. Behera, D. Kandi, S. Sahoo and K. Parida, *J. Phys. Chem. C*, 2019, **123**, 17112–17126.
423 P. C. Sharma, A. Jain, S. Jain, R. Pahwa and M. S. Yar, *J. Enzyme Inhib. Med. Chem.*, 2010, **25**, 577–589.
424 Y. Zeng, D. Chen, T. Chen, M. Cai, Q. Zhang, Z. Xie, R. Li, Z. Xiao, G. Liu and W. Lv, *Chemosphere*, 2019, **227**, 198–206.
425 W. Li, C. Guo, B. Su and J. Xu, *J. Chem. Technol. Biotechnol.*, 2012, **87**, 643–650.
426 R. Shetty, G. Kothari, A. Tambe, B. D. Kulkarni and S. P. Kamble, *Indian J. Chem., Sect. A: Inorg., Bio-inorg., Phys., Theor. Anal. Chem.*, 2016, **55**, 16–22.
427 T. A. Gad-Allah, M. E. M. Ali and M. I. Badawy, *J. Hazard. Mater.*, 2011, **186**, 751–755.
428 S. Li and J. Hu, *Water Res.*, 2018, **132**, 320–330.
429 A. Salma, S. Thoröe-Boveleth, T. C. Schmidt and J. Tuerk, *J. Hazard. Mater.*, 2016, **313**, 49–59.
430 A. R. Silva, P. M. Martins, S. Teixeira, S. A. C. Carabineiro, K. Kuehn, G. Cuniberti, M. M. Alves, S. Lanceros-Mendezagh and L. Pereira, *RSC Adv.*, 2016, **6**, 95494–95503.
431 Y. Gan, Y. Wei, J. Xiong and G. Cheng, *Chem. Eng. J.*, 2018, **349**, 1–16.
432 Y. Li, Y. Fu and M. Zhu, *Appl. Catal., B*, 2020, **260**, 118149.
433 M. R. Usman, A. Prasasti, S. Fajriyah, A. W. Marita, S. Islamiah, A. N. Firdaus, A. R. Noviyanti and D. R. Eddy, *Bull. Chem. React. Eng. Catal.*, 2021, **16**, 752–762.
434 M. El-Kemary, H. El-Shamy and I. El-Mehasseb, *J. Lumin.*, 2010, **130**, 2327–2331.
435 M. Eskandari, N. Goudarzi and S. G. Moussavi, *Water Environ. J.*, 2018, **32**, 58–66.
436 A. Ulyankina, T. Molodtsova, M. Gorshenkov, I. Leontyev, D. Zhigunov, E. Konstantinova, T. Lastovina, J. Tolasz, J. Henych, N. Licciardello, G. Cuniberti and N. Smirnova, *J. Water Process. Eng.*, 2021, **40**, 101809.
437 S. Aghdasi and M. Shokri, *Iran. J. Catal.*, 2016, **6**, 481–487.
438 F. Nekouei and S. Nekouei, *Sci. Total Environ.*, 2017, **601–602**, 508–517.
439 C. Bojer, J. Schöbel, T. Martin, M. Ertl, H. Schmalz and J. Breu, *Appl. Catal., B*, 2017, **204**, 561–565.
440 V. Tiron, M. A. Ciolan, G. Bulai, G. Mihalache, F. D. Lipsa and R. Jijie, *Nanomaterials*, 2022, **12**, 2193.
441 N. Finčur, P. Sfîrloagă, P. Putnik, V. Despotović, M. Lazarević, M. Uzelac, B. Abramović, P. Vlazan, C. Ianăș, T. Alapi, M. Náfrádi, I. Maksimović, M. Putnik-Delić and D. Š. Merkulov, *Nanomaterials*, 2021, **11**, 215.
442 M. Mahjoore, A. Aryafar and M. Honarmand, *Journal of Mining and Engineering*, 2022, **13**, 155–164.
443 T. S. Roy, S. Akter, M. R. Fahim, M. A. Gafur and T. Ferdous, *Heliyon*, 2023, **9**, e13130.
444 T. Suwannaruang, J. P. Hildebrand, D. H. Taffa, M. Wark, K. Kamonsuangkasem, P. Chirawatkul and K. Wantala, *J. Photochem. Photobiol., A*, 2020, **391**, 112371.
445 C. A. Huerta-Aguilar, Y. S. García Gutiérrez and P. Thangarasu, *Chem. Eng. J.*, 2020, **394**, 124286.
446 Y. Gan, M. Zhang, J. Xiong, J. Zhu, W. Li, C. Zhang and G. Cheng, *J. Taiwan Inst. Chem. Eng.*, 2019, **96**, 229–242.
447 J. C. Durán-Álvarez, E. Avella, R. M. Ramírez-Zamora and R. Zanella, *Catal. Today*, 2016, **266**, 175–187.
448 T. Suwannaruang, P. Kidkhunthod, N. Chanlek, S. Soontaranon and K. Wantala, *Appl. Surf. Sci.*, 2019, **478**, 1–14.
449 X. Xing, Z. Du, J. Zhuang and D. Wang, *J. Photochem. Photobiol., A*, 2018, **359**, 23–32.
450 X. Feng, P. Wang, J. Hou, J. Qian, Y. Ao and C. Wang, *J. Hazard. Mater.*, 2018, **351**, 196–205.
451 S. Vijayalakshmi, E. Kumar, P. S. Venkatesh and A. Raja, *Ionics*, 2020, **26**, 1507–1513.
452 D. V. Thuan, T. B. H. Nguyen, T. H. Pham, J. Kim, T. T. Hien Chu, M. V. Nguyen, K. D. Nguyen, W. A. Al-onazi and M. S. Elshikh, *Chemosphere*, 2022, **308**, 136408.
453 Z.-H. Diao, X.-R. Xu, D. Jiang, J.-J. Liu, L.-J. Kong, G. Li, L.-Z. Zuo and Q.-H. Wu, *Chem. Eng. J.*, 2017, **315**, 167–176.
454 S. Das, S. Ghosh, A. J. Misra, A. J. Tamhankar, A. Mishra, C. S. Lundborg and S. K. Tripathy, *Int. J. Environ. Res. Public Health*, 2018, **15**, 2440.

455 X. Yu, J. Zhang, J. Zhang, J. Niu, J. Zhao, Y. Wei and B. Yao, *Chem. Eng. J.*, 2019, **374**, 316–327.
456 A. Tofanello, E. Belleti, A. M. M. Brito and I. L. Nantes-Cardoso, *Mater. Res.*, 2021, **24**, DOI: **10.1590/1980-5373-mr-2021-0198**.
457 L. T. Nguyen, H. T. Nguyen, T. D. Pham, T. D. Tran, H. T. Chu, H. T. Dang and B. V. Bruggen, *Top. Catal.*, 2020, **63**, 985–995.
458 X. Huang, W. Yang, G. Zhang, L. Yan, Y. Zhang, A. Jiang, H. Xu, M. Zhou, Z. Liu, H. Tang and D. D. Dionysiou, *Catal. Today*, 2021, **361**, 11–16.
459 M. Mirzai, F. Akhlaghian and F. Rahmani, *Water Environ. J.*, 2020, **34**, 420–431.
460 X. Zheng, S. Xu, Y. Wang, X. Sun, Y. Gao and B. Gao, *J. Colloid Interface Sci.*, 2018, **527**, 202–213.
461 A. Alam, U. Rahman, Z. U. Rahman, S. A. Khan, Z. Shah, K. Shaheen, H. Suo, M. N. Qureshi, S. B. Khan, E. M. Bakhsh and K. Akhtar, *J. Mater. Sci.: Mater. Electron.*, 2022, **33**, 4255–4267.
462 Z. Liu, X. Liu, Q. Lu, Q. Wang and Z. Ma, *J. Taiwan Inst. Chem. Eng.*, 2019, **96**, 214–222.
463 A. Hassani, A. Khataee and S. Karacaa, *J. Mol. Catal. A: Chem.*, 2015, **409**, 149–161.
464 N. Li, J. Zhang, Y. Tian, J. Zhao, J. Zhang and W. Zuo, *Chem. Eng. J.*, 2017, **308**, 377–385.
465 A. Raja, P. Rajasekaran, K. Selvakumar, M. Arunpandian, K. Kaviyarasu, S. Asath Bahadur and M. Swaminathan, *Sep. Purif. Technol.*, 2020, **233**, 115996.
466 S. Teixeira, H. Mora, L.-M. Blasse, P. M. Martins, S. A. C. Carabineiro, S. Lanceros-Méndez, K. Kühn and G. Cuniberti, *J. Photochem. Photobiol., A*, 2017, **345**, 27–35.
467 I. Gabelica, L. Ćurković, V. Mandić, I. Panžić, D. Ljubas and K. Zadro, *Catalysts*, 2021, **11**, 1136.
468 Z. Liu and Z. Ma, *Mater. Res. Bull.*, 2019, **118**, 110492.
469 A. J. Labrag, C. E. Bekkali, I. Es-Saidi, H. Bouyarmane, A. Laghzizil, M. Khamar and D. Robert, *E3S Web Conf.*, 2020, **150**, 02006.
470 F. Tamaddon, A. Nasiri and G. Yazdanpanah, *MethodsX*, 2020, **7**, 100764.
471 Z. Liu, J. Tian, D. Zeng, C. Yu, W. Huang, K. Yang, X. Liu and H. Liu, *Mater. Res. Bull.*, 2019, **112**, 336–345.
472 H. Wang, J. Li, P. Huo, Y. Yan and Q. Guan, *Appl. Surf. Sci.*, 2016, **366**, 1–8.
473 S. P. Pattnaik, A. Behera, S. Martha, R. Acharya and K. Parida, *J. Mater. Sci.*, 2019, **54**, 5726–5742.
474 C. Li, Z. Sun, W. Zhang, C. Yu and S. Zheng, *Appl. Catal., B*, 2018, **220**, 272–282.
475 C. Chuaicham, T. Inoue, V. Balakumar, Q. Tian, B. Ohtani and K. Sasaki, *J. Environ. Chem. Eng.*, 2022, **10**, 10697.
476 Y. Yu, K. Liu, Y. Zhang, X. Xing and H. Li, *Int. J. Environ. Res. Public Health*, 2022, **19**, 4793.
477 Y. Zhang, H. Pan and F. Zhang, *Mater. Lett.*, 2019, **251**, 114–117.
478 D. T. Sponza and P. Koyuncuoglu, *Clin. Microbiol. Infect.*, 2019, **4**, 1–10.
479 Y. He, S. Han, G. Zhao, J. Luo, C. Jia, Y. Chen, Q. Liu, J. Gao, C. Wang and J. Wang, *J. Environ. Chem. Eng.*, 2022, **10**, 107829.
480 M. Shi, W. Li, Q. Wang, H. Xu, Y. Zhao, G. He, Q. Meng and H. Chen, *Opt. Mater.*, 2021, **122**, 111726.
481 S. Kumar, R. D. Kaushik and P. Purohit, *J. Hazard. Mater.*, 2022, **424**, 127332.
482 J. Ni, J. Xue, J. Shen, G. He and H. Chen, *Appl. Surf. Sci.*, 2018, **441**, 599–606.
483 X.-F. Zeng, J.-S. Wang, Y.-N. Zhao, W.-L. Zhang and M.-H. Wang, *Int. J. Miner., Metall. Mater.*, 2021, **28**, 503–510.
484 S. Urus, M. Caylar, H. Eskalen and S. Ozganm, *J. Mater. Sci.: Mater. Electron.*, 2022, **33**, 4314–4329.
485 X. Hou, J. Liu, W. Guo, S. Li, Y. Guo, Y. Shi and C. Zhang, *Catal. Commun.*, 2019, **121**, 27–31.
486 A. Kumar, G. Sharma, M. Naushad, T. Ahamad, R. C. Veses and F. J. Stadler, *Chem. Eng. J.*, 2019, **370**, 148–165.
487 P. Huo, M. Zhou, Y. Tang, X. Liu, C. Ma, L. Yu and Y. Yan, *J. Alloys Compd.*, 2016, **670**, 198–209.
488 J. Du, S. Ma, Y. Yan, K. Li, F. Zhao and J. Zhou, *Colloids Surf., A*, 2019, **572**, 237–249.
489 Y. Deng, L. Tang, C. Feng, G. Zeng, J. Wang, Y. Zhou, Y. Liu, B. Peng and H. Feng, *J. Hazard. Mater.*, 2018, **344**, 758–769.
490 X. Rong, F. Qiu, Z. Jiang, J. Rong, J. Pan, T. Zhang and D. Yang, *Chem. Eng. Res. Des.*, 2016, **111**, 253–261.
491 X. Wang, A. Wang and J. Ma, *J. Hazard. Mater.*, 2017, **336**, 81–92.
492 Z. Wu, Y. Liang, X. Yuan, D. Zou, J. Fang, L. Jiang, J. Zhang, H. Yang and Z. Xiao, *Chem. Eng. J.*, 2020, **394**, 124921.
493 N. Guo, Y. Zeng, H. Li, X. Xu, H. Yu and X. Han, *J. Hazard. Mater.*, 2018, **353**, 80–88.
494 A. Kaur, W. A. Anderson, S. Tanvir and S. K. Kansal, *J. Colloid Interface Sci.*, 2019, **557**, 236–253.
495 J. Zhao, Z. Zhao, N. Li, J. Nan, R. Yu and J. Du, *Chem. Eng. J.*, 2018, **353**, 805–813.
496 S. Shanavas, S. M. Roopan, A. Priyadharsan, D. Devipriya, S. Jayapandi, R. Acevedo and P. M. Anbarasan, *Appl. Catal., B*, 2019, **255**, 117758.
497 M. Chen, J. Yao, Y. Huang, H. Gong and W. Chu, *Chem. Eng. J.*, 2018, **334**, 453–461.
498 T. Senasu, S. Nijpanich, S. Juabrum, N. Chanlek and S. Nanan, *Appl. Surf. Sci.*, 2021, **567**, 150850.
499 F. Beshkar, M. Salavati-Niasari and O. Amiri, *Ind. Eng. Chem. Res.*, 2021, **60**, 9578–9591.
500 M. Yu, H. Liang, R. Zhan, L. Xu and J. Niu, *Chin. Chem. Lett.*, 2021, **32**, 2155–2158.
501 A. S. Prasad, S. N. Kumar, M. A. Maheswari and D. Prabhakaran, *Bull. Mater. Sci.*, 2021, **44**, 99.
502 J. Yi, K. Wu, H. Wu, J. Guo, L. Zhang, H. Li and J. Lim, *Nano*, 2021, **16**, 2150063.
503 K. K. Das, S. Patnaik, S. Mansingh, A. Behera, A. Mohanty, C. Acharya and K. M. Parida, *J. Colloid Interface Sci.*, 2020, **561**, 551–567.
504 L. N. Costa, F. X. Nobre, A. O. Lobo and J. M. E. de Matos, *Environ. Nanotechnol., Monit. Manage.*, 2021, **16**, 100466.
505 M. Li, J. Zhang, L. Wang, X. Cheng, X. Gao, Y. Wang, G. Zhang, Y. Qi, H. Zhai, R. Guan and Z. Zhao, *Appl. Surf. Sci.*, 2022, **583**, 152516.

506 L. Wolski, K. Grzelak, M. Muńko, M. Frankowski, T. Grzyb and G. Nowaczyk, *Appl. Surf. Sci.*, 2021, **563**, 150338.
507 X. Hu, H. Zhao, Y. Liang, F. Chen, J. Li and R. Chen, *Chemosphere*, 2021, **264**, 128434.
508 V. D. Dang, J. A. Jr, T. Annadurai, T. A. N. Bui, H. L. Tran, L.-Y. Lin and R.-A. Doong, *Chem. Eng. J.*, 2021, **422**, 130103.
509 K. Hu, R. Li, C. Ye, A. Wang, W. Wei, D. Hu, R. Qiu and K. Yan, *J. Cleaner Prod.*, 2020, **253**, 120055.
510 M. Chen, Y. Dai, J. Guo, H. Yang, D. Liu and Y. Zhai, *Appl. Surf. Sci.*, 2019, **493**, 1361–1367.
511 X.-J. Wen, C.-G. Niu, L. Zhang, C. Liang, H. Guo and G.-M. Zeng, *J. Catal.*, 2018, **358**, 141–154.
512 J. C. Durán-Álvarez, M. Méndez-Galván, L. Lartundo-Rojas, M. Rodríguez-Varela, D. Ramírez-Ortega, D. Guerrero-Araque and R. Zanella, *Top. Catal.*, 2019, **62**, 1011–1025.
513 J. Mao, B. Hong, J. Wei, J. Xi, Y. Han, H. Jin, D. Jin, X. Peng, J. Li, Y. Yang, J. Gong, H. Ge and X. Wang, *ChemistrySelect*, 2019, **4**, 13716–13723.
514 B. Zhu, D. Song, T. Jia, W. Sun, D. Wang, L. Wang, J. Guo, L. Jin, L. Zhang and H. Tao, *ACS Omega*, 2021, **6**, 1647–1656.
515 Y. Zhou, M. Yu, H. Liang, J. Chen, L. Xu and J. Niu, *Appl. Catal., B*, 2021, **291**, 120105.
516 N. S. Alhokbany, R. Mousa, M. Naushad, S. M. Alshehri and T. Ahamad, *Int. J. Biol. Macromol.*, 2020, **164**, 3864–3872.
517 M. F. R. Samsudin, C. Frebillot, Y. Kaddoury, S. Sufian and W.-J. Ong, *J. Environ. Manage.*, 2020, **270**, 110803.
518 C.-H. Shen, X.-J. Wen, Z.-H. Fei, Z.-T. Liu and Q.-M. Mu, *Chem. Eng. J.*, 2020, **391**, 123612.
519 K. Wang, Y. Li, G. Zhang, J. Li and X. Wu, *Appl. Catal., B*, 2019, **240**, 39–49.
520 S. Li, J. Chen, S. Hu, H. Wang, W. Jiang and X. Chen, *Chem. Eng. J.*, 2020, **402**, 126165.
521 A. A. Tessema, C.-M. Wu and K. G. Motora, *ACS Omega*, 2022, **7**, 38475–38486.
522 A. B. Makama, A. Salmiaton, E. B. Saion, T. S. Y. Choong and N. Abdullah, *J. Nanomater.*, 2015, 108297, DOI: **10.1155/2015/108297**.
523 N. Lu, P. Wang, Y. Su, H. Yu, N. Liu and X. Quan, *Chemosphere*, 2019, **215**, 444–453.
524 C. Lai, M. Zhang, B. Li, D. Huang, G. Zeng, L. Qin, X. Liu, H. Yi, M. Cheng, L. Li, Z. Chen and L. Chen, *Chem. Eng. J.*, 2019, **358**, 891–902.
525 T. H. A. Nguyen, V. T. Le, V.-D. Doan, A. V. Tran, V. C. Nguyen, A.-T. Nguyen and Y. Vasseghian, *Mater. Lett.*, 2022, **308**, 131129.
526 K. Wang, L. Liang, Y. Zheng, H. Li, X. Niu, D. Zhang and H. Fan, *New J. Chem.*, 2021, **45**, 16168–16178.
527 R. A. Palominos, M. A. Mondaca, A. Giraldo, G. Penuela, M. Perez-Moya and H. D. Mansilla, *Catal. Today*, 2009, **144**, 100–105.
528 X.-D. Zhu, Y.-J. Wang, R.-J. Sun and D.-M. Zhou, *Chemosphere*, 2013, **92**, 925–932.
529 G. H. Safari, M. Hoseini, M. Seyedsalehi, H. Kamani, J. Jaafari and A. H. Mahvi, *Int. J. Environ. Sci. Technol.*, 2015, **12**, 603–616.
530 S. Wu, H. Hu, Y. Lin, J. Zhang and Y. H. Hu, *Chem. Eng. J.*, 2020, **382**, 122842.
531 T. Ikhlef-Taguelmimt, A. Hamiche, I. Yahiaoui, T. Bendellali, H. Lebik-Elhadi, H. A. Amar and F. Aissani-Benissad, *Water Sci. Technol.*, 2020, **82**, 1570–1578.
532 L. Rimoldi, D. Meroni, G. Cappelletti and S. Ardizzone, *Catal. Today*, 2017, **281**, 38–44.
533 M. Malakootian, S. N. Asadzadeh, M. Mehdipootarr and D. Kalantar-Neyestanaki, *Desalin. Water Treat.*, 2021, **222**, 302–312.
534 S. J. Olusegun, G. Larrea, M. Osial, K. Jackowska and P. Krysinski, *Catalysts*, 2021, **11**, 1243.
535 M. Saghi and K. Mahanpoor, *Int. J. Ind. Chem.*, 2017, **8**, 297–313.
536 H. Shi, Q. Wu, L. Jiang, L. Wang, M. Huang, B. Han, Z. Yu and Y. Zuo, *Int. J. Electrochem. Sci.*, 2020, **15**, 1539–1547.
537 S. K. Fanourakis, S. Q. Barroga, R. A. Mathew, J. Pena-Bahamonde, S. M. Louie, J. V. D. Perez and D. F. Rodrigues, *J. Environ. Chem. Eng.*, 2022, **10**, 107635.
538 Y. Jiang, C. Xing, Y. Chen, J. Shi and S. Wang, *Environ. Sci. Pollut. Res.*, 2022, **29**, 57656–57668.
539 M. Yan, Y. Wu and X. Liu, *J. Alloys Compd.*, 2021, **855**, 157548.
540 O. Linnik, E. Manuilov, S. Snegir, N. Smirnova and A. Eremenko, *J. Adv. Oxid. Technol.*, 2009, **12**, 265–270.
541 S. Zhao, Y. Yang, R. Lu, Y. Wang, Y. Lu, R. D. Rodriguez, E. Sheremet and J. Chen, *J. Environ. Chem. Eng.*, 2022, **10**, 107107.
542 M. Liu, J. Jiang, H. Tan, B. Chen, J. Ou, H. Wang, J. Sun, L. Liu, F. Wang, J. Gao, C. Liu, F. Peng, Y. Liu and Y. Tu, *Nanoscale*, 2022, **14**, 12804–12813.
543 W. Shi, H. Ren, M. Li, K. Xu, Y. Shu, C. Yan and Y. Tang, *Chem. Eng. J.*, 2020, **382**, 122876.
544 H. Xu, Y. Dingi, S. H. Yang, H. Zhang, X. Wang, J. Yuan, M. Long, Q. Zhao and Y. Liu, *Bull. Mater. Sci.*, 2021, **44**, 226.
545 K. Pandi, M. Preeyanghaa, V. Vinesh, J. Madhavan and B. Neppolian, *Environ. Res.*, 2022, **207**, 112188.
546 T. Zhang, Y. Liu, Y. Rao, X. Li, D. Yuan, S. Tang and Q. Zhao, *Chem. Eng. J.*, 2020, **384**, 123350.
547 Y. Chen and K. Liu, *Chem. Eng. J.*, 2016, **302**, 682–696.
548 K. Zheng, J. Chen, X. Gao, X. Cao, S. Wu and J. Su, *Water Sci. Technol.*, 2021, **84**, 1919–1929.
549 N. Farhadian, R. Akbarzadeh, M. Pirsaheb, T. C. Jen, Y. Fakhri and A. Asadi, *Int. J. Biol. Macromol.*, 2019, **132**, 360–373.
550 P. Wang, P.-S. Yap and T.-T. Lim, *Appl. Catal., A*, 2011, **399**, 252–261.
551 J. Zhang, X. Li, M. Peng, Y. Tang, A. Ke, W. Gan, X. Fu and H. Hao, *Mater. Res. Express*, 2018, **5**, 065008.
552 H. Wang, D. Wu, X. Li and P. Huo, *J. Mater. Sci.: Mater. Electron.*, 2019, **30**, 19126–19136.
553 A. Moradi, F. Rahmani and M. Khamforoush, *Iran. J. Polym. Sci. Technol.*, 2021, **33**, 465–478.
554 A. Bembibre, M. Benamara, M. Hjiri, E. Gómez, H. R. Alamri, R. Dhahri and A. Serrà, *Chem. Eng. J.*, 2022, **427**, 132006.

555 D. S. Pattanayak, D. Pal, J. Mishra, C. Thakur and K. L. Wasewar, *Environ. Sci. Pollut. Res.*, 2023, **30**, 24919–24926.
556 L. Jiang, X. Yuan, G. Zeng, J. Liang, Z. Wu, H. Yu, D. Mo, H. Wang, Z. Xiao and C. Zhou, *J. Colloid Interface Sci.*, 2019, **536**, 17–29.
557 S. Chen, F. Liu, R. Cui, B. Zhu and X. You, *Water Cycle*, 2022, **3**, 8–17.
558 T. S. Bui, P. Bansal, B.-K. Lee, T. Mahvelati-Shamsabadi and T. Soltani, *Appl. Surf. Sci.*, 2019, **506**, 144184.
559 G. Li, B. Wang, J. Zhang, R. Wang and H. Liu, *Chem. Eng. J.*, 2020, **391**, 123500.
560 Y. Zhao, H. Qin, Z. Wang, H. Wang, Y. He, Q. Tian, Q. Luo and P. Xu, *Environ. Sci. Pollut. Res.*, 2022, **29**, 74062–74080.
561 W. Wang, Z. Zeng, G. Zheng, C. Zhang, R. Xiao, C. Zhou, W. Xiong, Y. Yang, L. Lei, Y. Liu, D. Huang, M. C. Y. Cheng, Y. Fu, H. Luo and Y. Zhou, *Chem. Eng. J.*, 2019, **378**, 122132.
562 J. Xu, Y. Chen, M. Chen, J. Wang and L. Wang, *Chem. Eng. J.*, 2022, **442**, 136208.
563 L. Chen, Y. Wang, S. Cheng, X. Zhao, J. Zhang, Z. Ao, C. Zhao, B. Li, S. Wang, S. Wang and H. Sun, *Appl. Catal., B*, 2022, **303**, 120932.
564 N. L. M. Tri, J. Kim, B. L. Giang, T. M. A. Tahtamouni, P. T. Huong, C. Lee, N. M. Viet and D. Q. Trung, *J. Ind. Eng. Chem.*, 2019, **80**, 597–605.
565 D. Jia, Y. Zhang, X. Zhang, P. Feng, L. Yang, R. Ning, H. Pan and Y. Miao, *Environ. Sci.: Nano*, 2021, **8**, 415–431.
566 S. J. Alyani, A. E. Pirbazari, F. E. Khalilsaraei, N. A. Kolur and N. Gilani, *J. Alloys Compd.*, 2019, **799**, 169–182.
567 J. Ye, J. Liu, Z. Huang, S. Wu, X. Dai, L. Zhang and L. Cui, *Chemosphere*, 2019, **227**, 505–513.
568 M. Cao, P. Wang, Y. Ao, C. Wang, J. Hou and J. Qian, *J. Colloid Interface Sci.*, 2016, **467**, 129–139.
569 J. Liu, H. Chen, C. Zhu, S. Han, J. Li, S. She and X. Wu, *J. Colloid Interface Sci.*, 2022, **622**, 526–538.
570 N. Belhoucheta, B. Hamdia, H. Chenchounid and Y. Bessekhoua, *J. Photochem. Photobiol., A*, 2019, **372**, 196–205.
571 Y. M. Hunge, A. A. Yadav, S.-W. Kang and H. Kim, *J. Colloid Interface Sci.*, 2022, **606**, 454–463.
572 P. Semeraro, S. Bettini, S. Sawalha, S. Pal, A. Licciulli, F. Marzo, N. Lovergine, L. Valli and G. Giancane, *Nanomaterials*, 2020, **10**, 1458.
573 B. Kakavandi, N. Bahari, R. R. Kalantary and E. D. Fard, *Ultrason. Sonochem.*, 2019, **55**, 75–85.
574 V. H. T. Thi and B.-K. Lee, *J. Hazard. Mater.*, 2017, **324**, 329–339.
575 H. Shi, Q. Wu, X. Yang, Y. Zuo, H. Yang, R. Zhang, Y. Zhang, Y. Fan, X. Du and L. Jiang, *Int. J. Electrochem. Sci.*, 2021, **16**, 210314, DOI: **10.20964/2021.03.70**.
576 S. Zhang, J. Yi, J. Chen, Z. Yin, T. Tang, W. Wei, S. Cao and H. Xu, *Chem. Eng. J.*, 2020, **380**, 122583.
577 E. Weidner, K. S. Ciesielczyk, D. Moszynsky, T. Jesionowski and F. Ciesielczyk, *Environ. Technol. Innovation*, 2021, **24**, 102016.
578 S. Leong, D. Li, K. Hapgood, X. Zhang and H. Wang, *Appl. Catal., B*, 2016, **198**, 224–233.
579 C. Lv, X. Lan, L. Wang, X. Dai, M. Zhang, J. Cui, S. Yuan, S. Wang and J. Shi, *Environ. Technol.*, 2021, **42**, 377–387.
580 W. Chen, L. Chang, S.-B. Ren, Z.-C. He, G.-B. Huang and X.-H. Liu, *J. Hazard. Mater.*, 2020, **384**, 121308.
581 L. Wang, C. Zhang, R. Cheng, J. Ali, Z. Wang, G. Mailhot and G. Pan, *Catalysts*, 2018, **8**, 628.
582 J. Xue, S. Ma, Y. Zhou, Z. Zhang and P. Jiang, *RSC Adv.*, 2015, **5**, 18832–18840.
583 J. Wei, P. Zhu and P. Chen, *Materials*, 2022, **15**, 1963.
584 H. A. Patehkhor, M. Fattahi and M. R. Khosravi-Nikou, *Sci. Rep.*, 2021, **11**, 24177.
585 Y. Shi, Z. Yang, B. Wang, H. An, Z. Chen and H. Cui, *Appl. Clay Sci.*, 2016, **119**, 311–320.
586 S. Kaushal, A. Kumar, H. Bains and P. P. Singh, *Environ. Sci. Pollut. Res.*, 2023, **30**, 37092–37104.
587 X. Zhang, H. Wang, M. Gao, P. Zhao, W. Xia, R. Yang, Y. Huang, L. Wang, M. Liu, T. Wei, L. Wang, R. Yao, X. Li and Z. Fan, *Chemosphere*, 2022, **294**, 133782.
588 Y. Wang, S. Zhang, Y. Ge, C. Wang, J. Hu and H. Liu, *Acta Phys.-Chim. Sin.*, 2020, **36**, 1905083.
589 C. Hu, Z.-T. Liu, P.-C. Yang, Y.-X. Ding, K.-Y. A. Lin and B.-S. Nguven, *J. Taiwan Inst. Chem. Eng.*, 2021, **123**, 219–227.
590 H. Shi, Y. He, Y. Li, T. He and P. Luo, *Sep. Purif. Technol.*, 2022, **280**, 119864.
591 D. Wang, S. Li and Q. Feng, *J. Mater. Sci.: Mater. Electron.*, 2018, **29**, 9380–9386.
592 J. Zhang and Z. Ma, *Chin. J. Chem. Eng.*, 2018, **26**, 753–760.
593 J. Liu, H. Xu, Y. Xu, Y. Song, J. Lian, Y. Zhao, L. Wang, L. Huang, H. Ji and H. Li, *Appl. Catal., B*, 2017, **207**, 429–437.
594 V. T. Quyen, H. J. Kim, J. T. Kim, L. T. T. Ha, P. T. Huong, D. M. Thanh, N. M. Viet and P. Q. Thang, *Sol. Energy*, 2021, **214**, 288–293.
595 L. Jiang, X. Yuan, G. Zeng, Z. Wu, J. Liang, X. Chen, L. Leng, H. Wang and H. Wang, *Appl. Catal., B*, 2018, **221**, 715–725.
596 X. Chen, L. Liu, Y. Zhao, J. Zhang, D. Li, B. Hu and X. Hai, *ChemistrySelect*, 2017, **2**, 9256–9260.
597 J. Liu, Y. Song, H. Xu, X. Zhu, J. Lian, Y. Xu, Y. Zhao, L. Huang, H. Ji and H. Li, *J. Colloid Interface Sci.*, 2017, **494**, 38–46.
598 L. Jiang, X.-Z. Yuan, G. Zeng, X. Chen, Z. Wu, J. Liang, J. Zhang, H. Wang and H. Wang, *ACS Sustainable Chem. Eng.*, 2017, **5**, 5831–5841.
599 R. Chen, X. Wang and L. Zhu, *Research Square*, 2022, preprint, DOI: **10.21203/rs.3.rs-1172368/v1**.
600 E. Vijayakumar, M. G. Raj, M. G. Narendran, R. Preetha, R. Mohankumar, B. Neppolian and A. J. Bosco, *ACS Omega*, 2022, **7**, 5079–5095.
601 X. Tang, L. Ni, J. Han and Y. Wang, *Chin. J. Catal.*, 2017, **38**, 447–457.
602 W. Qian, W. Hu, Z. Jiang, Y. Wu, Z. Li, Z. Diao and M. Li, *Catalysts*, 2022, **12**, 774.
603 F. Wang, Z. Zhu and J. Guo, *RSC Adv.*, 2021, **11**, 35663–35672.

604 H. Shi, T. Zhao, J. Wang, Y. Wang, Z. Chen, B. Liu, H. Ji, W. Wang, G. Zhang and Y. Li, *J. Alloys Compd.*, 2021, **860**, 157924.
605 H.-J. Ren, Y.-B. Tang, W.-l. Shi, F.-Y. Chen and Y.-S. Xu, *New J. Chem.*, 2019, **43**, 19172–19179.
606 R. Zou, T. Xu, X. Lei, Q. Wu and S. Xue, *Solid State Sci.*, 2020, **99**, 106067.
607 A. Maridiroosi, A. R. Mahjoub and H. Fakhr, *Int. J. Chem. Biomol. Sci.*, 2020, **14**, 31–36, DOI: **10.5281/zenodo.3669194**.
608 D. Qiao, Z. Li, J. Duan and X. He, *Chem. Eng. J.*, 2020, **400**, 125952.
609 B. Li, X. Yu, X. Yu, R. Du, L. Liu and Y. Zhang, *Appl. Surf. Sci.*, 2019, **478**, 991–997.
610 K. Chakraborty, T. Pal and S. Ghosh, *ACS Appl. Nano Mater.*, 2018, **1**, 3137–3144.
611 X. Tang, Z. Wang and Y. Wang, *Chem. Phys. Lett.*, 2018, **691**, 408–414.
612 K. V. A. Kumar, B. Lakshminarayana, D. Suryakala and C. Subrahmanyam, *RSC Adv.*, 2020, **10**, 20494–20503.
613 J. Shan, X. Wu, C. Li, J. Hu, Z. Zhang, H. Liu, P. Xia and X. Huang, *Research Square*, 2022, preprint, DOI: **10.21203/rs.3.rs-1721079/v1**.
614 S. M. Ghoreishian, G. S. R. Raju, E. Pavitra, C. H. Kwak, Y.-K. Han and Y. S. Huh, *Appl. Surf. Sci.*, 2019, **489**, 110–122.
615 S. Zhang, J. Xu, J. Hu, O. Cui and H. Liu, *Langmuir*, 2017, **33**, 5015–5024.
616 R. Zou, T. Xu, X. Lei, Q. Wu and S. Xue, *Solid State Sci.*, 2020, **99**, 106067.
617 S. K. Ibrahim, T. Pal and S. Ghosh, *AIP Conf. Proc.*, 2019, **2115**, 030188, DOI: **10.1063/1.5113027**.
618 Y. Hou, S. Pu, Q. Shi, S. Mandal, H. Ma, S. Xue, G. Cai and Y. Bai, *J. Taiwan Inst. Chem. Eng.*, 2019, **104**, 139–150.
619 F.-S. Tabatabai-Yazdi, A. E. Pirbazari, F. E. Khalilsaraei, N. A. Kolur and N. Gilani, *Water Environ. Res.*, 2020, **92**, 662–676.
620 F.-S. Tabatabai-Yazdi, A. E. Pirbazari, F. E. K. Saraei and N. Gilani, *Phys. B*, 2021, **608**, 412869.
621 L.-L. Qu, N. Wang, Y.-Y. Li, D.-D. Bao, G.-H. Yang and H.-T. Li, *J. Mater. Sci.*, 2017, **52**, 8311–8320.
622 J. Song, X. Wu, M. Zhang, C. Liu, J. Yu, G. Sun, Y. Si and B. Ding, *Chem. Eng. J.*, 2020, **379**, 122269.
623 L. Huang, D. Bao, J. Li and X. Jiang, *Appl. Surf. Sci.*, 2021, **555**, 149696.
624 A. Iqbal, U. Saidu, F. Adam, S. Sreekantan, N. Yahaya, M. N. Ahmad, R. J. Ramalingam and L. D. Wilson, *Molecules*, 2021, **26**, 2509.
625 Y. Zhao, A. Zada, Y. Yang, J. Pan, Y. Wang, Z. Yan, Z. Xu and K. Qi, *Front. Chem.*, 2021, **9**, 797738.
626 H. Jingyu, Y. Ran, L. Zhaohui, S. Yuanqiang, Q. Lingbo and A. N. Kani, *Solid State Sci.*, 2019, **92**, 60–67.
627 B. Guo, B. Liu, C. Wang, Y. Wang, S. Yin, M. S. Javed and W. Han, *J. Environ. Chem. Eng.*, 2022, **10**, 107118.
628 P. Zhu, M. Duan, R. Wang, J. Xu, P. Zou and H. Jia, *Colloids Surf., A*, 2020, **602**, 125118.
629 J. Gu, H. Jia, S. Ma, Z. Ye, J. Pan, R. Dong, Y. Zong and J. Xue, *ACS Omega*, 2020, **5**, 30980–30988.
630 X. Liao, T.-T. Li, H.-T. Ren, Z. Mao, X. Zhang, J.-H. Lin and C.-W. Lou, *Ceram. Int.*, 2021, **47**, 10786–10795.
631 S. Li, S. Hu, K. Xu, W. Jiang, Y. Liu, Z. Leng and J. Liu, *J. Colloid Interface Sci.*, 2017, **504**, 561–569.
632 D. Chen, S. Wu, J. Fang, S. Lu, G. Y. Zhou, W. Feng, F. Yang, Y. Chen and Z. Q. Fang, *Sep. Purif. Technol.*, 2018, **193**, 232–241.
633 W. Wang, Q. Han, Z. Zhu, L. Zhang, S. Zhong and B. Liu, *Adv. Powder Technol.*, 2019, **30**, 1882–1896.
634 Y. Zhou, J. Li, C. Liu, P. Huo and H. Wang, *Appl. Surf. Sci.*, 2018, **458**, 586–596.
635 Z. Liu, A. Zhang, Y. Liu, Y. Fu and Y. Du, *Colloids Surf., A*, 2022, **643**, 128818.
636 H. Liu, W. Huo, T. C. Zhang, L. Ouyang and S. Yuan, *Mater. Today Chem.*, 2022, **23**, 100729.
637 M. Al-Haddad, A. Shawky and I. A. Mkhalid, *J. Taiwan Inst. Chem. Eng.*, 2021, **123**, 284–292.
638 H. M. Lwin, W. Zhan, S. Song, F. Jia and J. Zhou, *Chem. Phys. Lett.*, 2019, **736**, 136806.
639 X. Zhang, D. Han, M. Dai, K. Chen, Z. Han, Y. Fan, Y. He, D. Han and L. Niu, *Catal. Sci. Technol.*, 2021, **11**, 6248.
640 C. Jin, J. Kang, Z. Li, M. Wang, Z. Wu and Y. Xie, *Appl. Surf. Sci.*, 2020, **514**, 146076.
641 Q. Chen, W. Yang, J. Zhu, L. Fu, D. Li and L. Zhou, *J. Hazard. Mater.*, 2020, **384**, 121275.
642 A. O. Oluwole and O. S. Olatunji, *Environ. Sci. Eur.*, 2022, **34**, 5.
643 S. Kumar, V. Sharma, K. Bhattacharyya and V. Krishnan, *Mater. Chem. Front.*, 2017, **1**, 1093–1106.
644 T. Xiao, Z. Tang, Y. Yang, L. Tang, Y. Zhou and Z. Zou, *Appl. Catal., B*, 2018, **220**, 417–428.
645 C. Li, S. Yu, H. Dong, C. Liu, H. Wu, H. Che and G. Chen, *Appl. Catal., B*, 2018, **238**, 284–293.
646 X. Jiang, S. Lai, W. Xu, J. Fang, X. Chen, J. Beiyuan, X. Zhou, K. Lin, J. Liu and G. Guan, *J. Alloys Compd.*, 2019, **809**, 151804.
647 J. Ni, W. Wang, D. Liu, Q. Zhu, J. Jia, J. Tian, Z. Li, X. Wang and Z. Xing, *J. Hazard. Mater.*, 2021, **408**, 124432.
648 Y. Liu, J. Tian, L. Wei, Q. Wang, C. Wang, Z. Xing, X. Li, W. Yang and C. Yang, *Sep. Purif. Technol.*, 2021, **257**, 117976.
649 C. Li, S. Yu, H. Che, X. Zhang, J. Han, Y. Mao, Y. Wang, C. Liu and H. Dong, *ACS Sustainable Chem. Eng.*, 2018, **6**, 16437–16447.
650 Y. Hong, Y. Meng, G. Zhang, B. Yin, Y. Zhao, W. Shi and C. Li, *Sep. Purif. Technol.*, 2016, **171**, 229–237.
651 Z. Yang, X. Xia, L. Shao, L. Wang and Y. Liu, *Chem. Eng. J.*, 2021, **410**, 128454.
652 Y. Li, Z. Lai, Z. Huang, H. Wang, C. Zhao, G. Ruan and F. Du, *Appl. Surf. Sci.*, 2021, **550**, 149342.
653 C. Du, Z. Zhang, S. Tan, G. Yu, H. Chen, L. Zhou, L. Yu, Y. Su, Y. Zhang, F. Deng and S. Wang, *Environ. Res.*, 2021, **200**, 111427.
654 L. Yan, W. Li, Q. Zhao, Z. Zhu, C. Hu and B. Liu, *Colloids Surf., A*, 2021, **524**, 126783.
655 J. Chen, X. Xiao, Y. Wang, M. Lu and X. Zeng, *J. Alloys Compd.*, 2019, **800**, 88–98.

656 F. Chen, Q. Yang, X. Li, G. Zeng, D. Wang, C. Niu, J. Zhao, H. An, T. Xie and Y. Deng, *Appl. Catal., B*, 2017, **200**, 330–342.
657 H. Jing, R. Ou, H. Yu, Y. Zhao, Y. Lu, M. Huo, H. Huo and X. Wang, *Sep. Purif. Technol.*, 2021, **255**, 117646.
658 F. Guo, W. Shi, M. Li, Y. Shi and H. Wen, *Sep. Purif. Technol.*, 2019, **210**, 608–615.
659 P. Zhu, M. Hu, M. Duan, L. Xie and M. Zhao, *J. Alloys Compd.*, 2020, **840**, 155714.
660 Z. Zhang, X. Xue and X. Chen, *Dalton Trans.*, 2022, **51**, 8015–8027.
661 X. Zhou, Y. Chen, C. Li, L. Zhang, X. Zhang, X. Ning, L. Zhan and J. Luo, *Sep. Purif. Technol.*, 2019, **211**, 179–188.
662 B. Zhang, X. He, X. Ma, Q. Chen, G. Liu, Y. Zhou, D. Ma, C. Cui, J. Ma and Y. Xin, *Sep. Purif. Technol.*, 2020, **247**, 116932.
663 L. Lonappan, S. K. Brar, R. K. Das, M. Verma and R. Y. Surampalli, *Environ. Int.*, 2016, **96**, 127–138.
664 A. S. Mestre and A. P. Carvalho, *Molecules*, 2019, **24**, 3702, DOI: **10.3390/molecules24203702**.
665 K. C. Hui, W. L. Ang, W. Z. N. Yahya and N. S. Sambudi, *Chemosphere*, 2022, **290**, 133377.
666 D. Fabbri, M. J. López-Muñoz, A. Daniele, C. Medana and P. Calza, *Photochem. Photobiol. Sci.*, 2019, **18**, 845–852.
667 L. Rizza, S. Meric, D. Kassinos, M. Guida, F. Russo and V. Belgiorno, *Water Res.*, 2009, **43**, 979–988.
668 W. Z. Khan, I. Najeeb, S. Ishtiaque and S. Jabeen, *International Organization of Scientific Research (IOSR) Journal of Engineering*, 2016, **6**, 36–46.
669 A. C. Khraibet, N. J. Imran, H. M. Majeed, M. A. Ehmood, G. S. Hasoon, Z. F. Nathim, A. K. Alwan and A. S. A. Alsada, *J. Genet. Environ. Resour. Conserv.*, 2022, **10**, 41–48.
670 U. Schulze-Hennings, I. Brückner, W. Gebhardt, M. Groteklaes, S. P. Blöß, M. Wett, V. Linnemann, D. Montag and J. Pinnekamp, *Water Environ. J.*, 2017, **31**, 508–514.
671 M. Baniamer, A. Almasi and S. Sharifnia, *Iran. J. Chem. Chem. Eng.*, 2018, **15**, 3–16.
672 A. Achilleos, E. Hapeshi, N. P. Xekoukoulotakis, D. Mantzavinos and D. Fatta-Kassinos, *Chem. Eng. J.*, 2010, **161**, 53–59.
673 M. V. Bagal and P. R. Gogate, *Ultrason. Sonochem.*, 2014, **21**, 1035–1043.
674 M. Tanveer, G. Tezcanli, M. T. Sadiq, S. M. Kazmi, N. Noshad, G. Abbas and A. Ali, *Eng. Proc.*, 2022, **12**, 76.
675 I. Mimouni, A. Bouziani, Y. Naciri, M. Boujnah, M. Alaoui, E. Belghiti and M. E. Azzouzi, *Environ. Sci. Pollut. Res.*, 2022, **29**, 7984–7996.
676 D. Meroni, C. L. Bianchi, D. C. Boffito, G. Cerrato, A. Bruni, M. A. Sartirana and E. Falletta, *Ultrason. Sonochem.*, 2021, **75**, 105615.
677 I. Berruti, N. P. F. Gonçalves, P. Calza, M. C. Paganini, I. Oller and M. I. Polo-López, *Chemosphere*, 2022, **303**, 135017.
678 H. Mohan, P. M. Sathya, S. Vadivel, G. H. Ha, H. S. Oh, G. Kim, K.-K. Seralathan and T. Shin, *Chemosphere*, 2022, **301**, 134699.
679 M. V. Gerbaldo, S. G. Marchetti, V. R. Elías, S. N. Mendieta and M. E. Crivello, *Chem. Eng. Res. Des.*, 2021, **166**, 237–247.
680 M. A. H. Karim and B. K. Aziz, *React. Kinet., Mech. Catal.*, 2022, **135**, 1113–1124.
681 A. Rey, E. Mena, A. M. Chavez, F. J. Beltron and F. Medina, *Chem. Eng. Sci.*, 2015, **126**, 80–90.
682 H. Chakhtouna, H. Benzeid, N. Zari, A. E. K. Qaiss and R. Bouhfid, *Environ. Sci. Pollut. Res.*, 2021, **28**, 44638–44666.
683 M. R. Espino-Estevez, C. Fernandez-Rodríguez, O. M. Gonzalez-Díaz, J. Arana, J. P. Espinos, J. A. Ortega-Mendez and J. M. Dona-Rodríguez, *Chem. Eng. J.*, 2016, **298**, 82–95.
684 E. Torad, E. H. Ismail, M. M. Mohamed and M. M. H. Khalil, *Mater. Res. Bull.*, 2021, **137**, 111193.
685 V.-H. Nguyena, Q. B. Tran, X. C. Nguyen, L. T. Hai, T. T. T. Ho, M. Shokouhimehr, D.-V. N. Vo, S. S. Lami, V.-H. Nguyena, Q. B. Tranc, X. C. Nguyenc, L. T. Hai, T. T. T. Ho, M. Shokouhimehr, D.-V. N. Vo, S. S. Lam, H. P. Nguyenj, C. T. Hoang, Q. V. Ly, W. Peng, S. Y. Kim, T. V. Tunge and Q. V. Lec, *Process Saf. Environ. Prot.*, 2020, **142**, 229–237.
686 A. Surenjan, B. Sambandam, T. Pradeep and L. Philip, *J. Environ. Chem. Eng.*, 2017, **5**, 757–767.
687 I. Tbessi, M. Benito, J. Llorca, E. Molins, S. Sayadi and W. Najjar, *J. Alloys Compd.*, 2019, **779**, 314–325.
688 L. Rueda-Salaya, A. Hernández-Ramírez, L. Hinojosa-Reyes, J. L. Guzmán-Mar, M. Villanueva-Rodríguez and E. Sánchez-Cervantes, *J. Photochem. Photobiol., A*, 2020, **391**, 112364.
689 G. Vitiello, G. Iervolino, C. Imparato, I. Rea, F. Borbone, L. D. Stefano, A. Aronne and V. Vaiano, *Sci. Total Environ.*, 2021, **762**, 143066.
690 S. M. Chaudhari, O. S. Gonsalves and R. Nemade, *Mater. Res. Bull.*, 2021, **143**, 111463.
691 M. Thiruppathi, P. S. Kumar, P. Devendran, C. Ramalingan, M. Swaminathan and E. R. Nagarajan, *J. Alloys Compd.*, 2018, **735**, 728–734.
692 P. Apopei, C. Orha, M. I. Popescu, C. Lazau, F. Manea, C. Catrinescu and C. Teodosiu, *Process Saf. Environ. Prot.*, 2020, **138**, 324–336.
693 W. Buda and B. Czech, *Water Sci. Technol.*, 2013, **68**, 1322.
694 I. Tbessi, M. Benito, E. Molins, J. Liorca, A. Touati, S. Sayadi and W. Najjar, *Solid State Sci.*, 2019, **88**, 20–28.
695 W. S. Koe, W. C. Chong, Y. L. Pang, C. H. Koo, M. Ebrahim and A. W. Mohammad, *J. Water Process. Eng.*, 2020, **33**, 101068.
696 A. Gil, A. M. García, M. Fernández, M. A. Vicente, B. González-Rodríguez, V. Rives and S. A. Korili, *J. Ind. Eng. Chem.*, 2017, **53**, 183–191.
697 S. Ramandi, M. H. Entezari and N. Ghows, *Ultrason. Sonochem.*, 2017, **38**, 234–245.
698 E. Mugunthan, M. B. Saidutta and P. E. Jagadeeshbabu, *Environ. Nanotechnol., Monit. Manage.*, 2018, **10**, 322–330.
699 A. Cordero-García, G. T. Palomino, L. Hinojosa-Reyes, J. L. Guzmán-Mar, L. MayaTeviño and A. Hernández-Ramírez, *Environ. Sci. Pollut. Res.*, 2017, **24**, 4613–4624.
700 E. Mugunthan, M. B. Saidutta and P. E. Jagadeeshbabu, *J. Photochem. Photobiol., A*, 2019, **383**, 111993.
701 A. Cordero-García, J. L. Guzmán-Mar, L. Hinojosa-Reyes, E. Ruiz-Ruiz and A. Hernández-Ramírez, *Ceram. Int.*, 2016, **42**, 9796–9803.

702 S. Murgolo, I. S. Moreira, C. Piccirillo, P. M. L. Castro, G. Ventrella, C. Cocozza and G. Mascolo, *Materials*, 2018, **11**, 1779.
703 W. Sun, H. Chu, B. Dong, D. Cao and S. Zheng, *Int. J. Electrochem. Sci.*, 2014, **9**, 4566–4573.
704 C. T. Mehmood, Z. Zhong, H. Zhou, C. Zhang and Y. Xiao, *RSC Adv.*, 2020, **10**, 36349–36362.
705 Y. Cui, Q. Ma, X. Deng, Q. Meng, X. Cheng, M. Xie, X. Li, Q. Cheng and H. Liu, *Appl. Catal., B*, 2017, **206**, 136–145.
706 S. Silvestri, C. D. Ferreira, V. Oliveira, J. M. T. B. Varejão, J. A. Labrincha and D. M. Tobaldi, *J. Photochem. Photobiol., A*, 2019, **375**, 261–269.
707 L. Das, S. K. Barodia, S. Sengupta and J. K. Basu, *Int. J. Environ. Sci. Technol.*, 2015, **12**, 317–326.
708 E. Mugunthan, M. B. Saidutta and P. E. Jagadeeshbabu, *Environ. Technol.*, 2019, **40**, 929–941.
709 E. I. Moreno-Valencia, S. P. Paredes-Carrera, J. C. Sánchez-Ochoa, S. O. Flores-Valle and J. R. Avendaño-Gómez, *Mater. Res. Express*, 2017, **4**, 115026.
710 S. Li, Z. Wang, X. Zhang, J. Zhao, Z. Hu, Z. Wang and X. Xie, *Chem. Eng. J.*, 2019, **378**, 122169.
711 N. Ahmadpour, M. H. Sayadi, S. Sobhani and M. Hajiani, *J. Environ. Manage.*, 2020, **271**, 110964.
712 K. Fischer, M. Kühnert, R. Gläser and A. Schulze, *RSC Adv.*, 2015, **5**, 16340–16348.
713 J. E. Casillas, J. Campa-Molina, F. Tzompantzi, G. G. C. Arízaga, A. López-Gaona, S. Ulloa-Godínez, M. E. Cano and A. Barrera, *Materials*, 2020, **13**, 1345.
714 S. Salaeh, D. J. Perisic, M. Biosic, H. Kusic, S. Babic, U. Lavrencic Stangar, D. D. Dionysiou and A. L. Bozic, *Chem. Eng. J.*, 2016, **304**, 289–302.
715 W. Liu, Y. Li, F. Liu, W. Jiang, D. Zhang and J. Liang, *Water Res.*, 2019, **151**, 8–19.
716 X. Liu, F. Li, Y. Liu, P. Li, L. Chen, B. Li, T. Qian and W. Liu, *J. Environ. Chem. Eng.*, 2022, **10**, 107545.
717 Z. Xiu, H. Bo, Y. Wu and X. Hao, *Appl. Surf. Sci.*, 2014, **289**, 394–399.
718 M. Penas-Garzon, W. H. M. Abdelraheem, C. Belver, J. J. Rodriguez, J. Bedia and D. D. Dionysiou, *Sep. Purif. Technol.*, 2021, **275**, 119169.
719 Z. Hu, X. Cai, Z. Wang, S. Li, Z. Wang and X. Xie, *J. Hazard. Mater.*, 2019, **380**, 120812.
720 W. Zhang, L. Zhou, J. Shi and H. Deng, *J. Colloid Interface Sci.*, 2017, **496**, 167–176.
721 W. Zhang, L. Zhou and H. Deng, *J. Mol. Catal. A: Chem.*, 2016, **423**, 270–276.
722 E. Valadez-Renteria, R. Perez-Gonzalez, C. Gomez-Solis, L. A. Diaz-Torres, A. Encinas, J. Oliva and V. Rodriguez-Gonzalez, *J. Environ. Sci.*, 2023, **126**, 575–589.
723 V. Muelas-Ramos, M. J. Sampaio, C. G. Silva, J. Bedia, J. J. Rodriguez, J. L. Faria and C. Belver, *J. Hazard. Mater.*, 2021, **416**, 126199.
724 O. Moradi, H. Alizadeh and S. Sedaghat, *Chemosphere*, 2022, **299**, 134435.
725 M. Kovacic, K. Perovic, J. Papac, A. Tomic, L. Matoh, B. Žener, T. Brodar, I. Capan, A. K. Surca, H. Kuši, U. L. Štangar and A. L. Božic, *Materials*, 2020, **13**, 1621.
726 D. John, J. Jose, S. G. Bhat and V. S. Achari, *Heliyon*, 2021, **7**, e07451.
727 J. Rashid, S. Oooim, R. Kumar, M. A. Barakat, B. Akram, N. Hussain, H. B. Bin and M. Xu, *Sci. Rep.*, 2020, **10**, 14191.
728 W. Li, R. Yu, M. Li, N. Guo, H. Yu and Y. Yu, *Chemosphere*, 2019, **218**, 966–973.
729 A. Esmaeili and M. H. Entezari, *RSC Adv.*, 2015, **5**, 97027.
730 O. C. Olatunde and D. C. Onwudiwe, *Results Chem.*, 2022, **4**, 100273.
731 M. E. Malefane, U. Feleni and A. T. Kuvarega, *J. Environ. Chem. Eng.*, 2020, **8**, 103560.
732 A. Kumar, S. K. Sharma, A. Kumar, G. Sharma, N. Almasoud, T. S. Alomar, M. Naushad, Z. A. Alothman and F. J. Stadler, *J. Cleaner Prod.*, 2021, **315**, 128137.
733 L. Zhang, L. Liu, X. Zhang, C. Ge and J. Liao, *Adv. Energy Sustainability Res.*, 2022, **3**, 2200138.
734 D. Kulhary and S. Singh, *ChemistrySelect*, 2022, **7**, e202201964.
735 M. Irandost, R. Akbarzadeh, M. Pirsaheb, A. Asadi, P. Mohammadi and M. Sillanpää, *J. Mol. Liq.*, 2019, **291**, 111342.
736 M. D. Nguyen, T. B. Nguyen, L. H. Tran, T. G. Nguyen, I. Fatimah, E. P. Kuncoro and R.-A. Doong, *Chem. Eng. J.*, 2023, **452**, 139249.
737 N. Aghababaei, M. Abdouss, H. Hosseini-Monfared and F. Ghanbari, *Journal of Water Process Engineering*, 2023, **53**, 103702.
738 O. Sacco, J. J. Murcia, A. E. Lara, M. Hernández-Laverde, H. Rojas, J. A. Navío, M. C. Hidalgo and V. Vaiano, *Mater. Sci. Semicond. Process.*, 2020, **107**, 104839.
739 S. Wu, X. Yu, J. Zhang, Y. Zhang, Y. Zhu and M. Zhu, *Chem. Eng. J.*, 2021, **411**, 128555.
740 X. Chen, C. Yu, R. Zhu, N. Li, J. Chen, S. Li, W. Xia, S. Xu, H. Wang and X. Chen, *Nanomaterials*, 2019, **9**, 959.
741 X. Chen, C. Yu, R. Zhu, N. Li, J. Chen, Q. Lin, S. Xu, X. Chen and H. Wang, *Sci. Total Environ.*, 2020, **711**, 134643.
742 P. John, K. Johari, G. S. Nirmala, A. Appusamy and M. Thanabalan, *Environ. Technol. Innovation*, 2020, **22**, 101412.
743 M. Elangovan, S. M. Bharathaiyengar and J. P. Ettiyappan, *Environ. Sci. Pollut. Res.*, 2021, **28**, 18186–18200.
744 N. Li, W. Fu, G. Sun, M. Shi, M. Wu, W. Shen, Q. Li and J. Ma, *Appl. Organomet. Chem.*, 2023, **37**, e7170.
745 W. Zhang, L. Zhou, J. Shi and H. Deng, *Catalysts*, 2018, **8**, 45.
746 A. N. Oliveros, J. A. I. Pimentel, M. D. G. de Luna, S. Garcia-Segura, R. R. M. Abarca and R.-A. Doong, *Chem. Eng. J.*, 2021, **403**, 126213.
747 M. Cai, R. Li, Z. Xie, J. Huang, Y. Zeng, Q. Zhang, H. Liu, W. Lv and G. Liu, *Appl. Catal., B*, 2019, **259**, 118033.
748 G. A. Ashraf, R. T. Rasool, R. U. Rasool, M. F. Saleem, J. Ali, D. Ghernaout, M. Hassan, A. M. Aljuwayid, M. A. Habila and H. Guo, *J. Water Process Eng.*, 2023, **51**, 103435.
749 M. V. Krishna, G. Madhavi, N. F. Idris, S. A. M. Idris and L. R. K. Chowdary, *Arabian J. Chem.*, 2019, **12**, 1290–1297.

750 F. Pomati, S. Castiglioni, E. Zuccato, R. Fanelli, D. Vigetti, C. Rossetti and D. Calamari, *Environ. Sci. Technol.*, 2006, **40**, 2442.
751 Z. Bensaadi, N. Yeddou-Mezenner, M. Trari and F. Medjene, *J. Environ. Chem. Eng.*, 2014, **2**, 1371–1377.
752 H. Yang, T. An, G. Y. Li, W. Song, W. J. Cooper, H. Luo and X. Guo, *J. Hazard. Mater.*, 2010, **179**, 834–839.
753 E. Hapeshi, A. Achilleos, M. I. Vasquez, C. Michael, N. P. Xekoukoulotakis, D. Mantzavinos and D. Kassinos, *Water Res.*, 2010, **44**, 1737–1746.
754 Z. Ran, L. Wang, Y. Fang, C. Ma and S. Li, *Catalysts*, 2019, **9**, 876.
755 L. A. Ioannou, E. Hapeshi, M. I. Vasquez, D. Mantzavinos and D. Fatta-Kassinos, *Sol. Energy*, 2011, **85**, 1915–1926.
756 D. A. Pino-Sandoval, L. Hinojosa-Reyes, J. L. Guzmán-Mar, J. C. Murillo-Sierra and A. Hernandez-Ramirez, *Water, Air, Soil Pollut.*, 2022, **233**, 17, DOI: **10.1007/s11270-021-05484-7**.
757 L. Rimoldi, D. Meroni, E. Falletta, V. Pifferi, L. Falciola, G. Cappelletti and S. Ardizzone, *Photochem. Photobiol. Sci.*, 2017, **16**, 60.
758 A. Ponkshe and P. Thakur, *Mater. Today: Proc.*, 2019, **18**, 1162–1175.
759 V. Rogé, C. Guignard, G. Lamblin, F. Laporte, I. Fechete, F. Garin, A. Dinia and D. Lenoble, *Catal. Today*, 2018, **306**, 215–222.
760 Y. Ji, L. Zhou, C. Ferronato, X. Yang, A. Salvador, C. Zeng and J.-M. Chovelon, *J. Photochem. Photobiol., A*, 2013, **254**, 35–44.
761 C. Medana, P. Calza, F. Carbone, E. Pelizzetti, H. Hidaka and C. Baiocchi, *Rapid Commun. Mass Spectrom.*, 2009, **23**, 206.
762 Z. Mehrabadi and H. Faghihian, *J. Photochem. Photobiol., A*, 2018, **356**, 102–111.
763 M. Eskandari, N. Goudarzi, M. A. Chamjangali and S. G. Moussavi, *Journal of Sabzevar University of Medical Science*, 2020, **27**, 131–141.
764 B. Ramasamy, J. Jeyanthi and P. Chinnaiyan, *Environ. Nanotechnol., Monit. Manage.*, 2023, **19**, 100779.
765 R. Bhuvaneswari, J. Jeyanthi and S. M. Kumar, *Optik*, 2021, **239**, 166658.
766 Y. Ling, G. Liao, Y. Xie, J. Yin, J. Huang, W. Feng and L. Li, *J. Photochem. Photobiol., A*, 2016, **329**, 280–286.
767 Z. A. Alothman, A. Y. Badjah, O. M. Alharbi and I. Ali, *Environ. Sci. Pollut. Res.*, 2021, **28**, 7423–7430.
768 B. Bina, A. Fatehizadeh, E. Taheri, M. Heydari, M. Darvishmotevalli and A. Bazmeh, *Int. J. Environ. Anal. Chem.*, 2022, 1–12, DOI: **10.1080/03067319.2022.2085045**.
769 S. Stojanović, M. Vranješ, Z. Šaponjić, V. Rac, V. Rakić, L. Ignjatović and L. Damjanović-Vasilić, *Int. J. Environ. Sci. Technol.*, 2023, **20**, 1–16.
770 R. Corchero, R. Rodil, A. Soto and E. Rodil, *Nanomaterials*, 2021, **11**, 411.
771 Y. Shi, H. Chen, Y. Wu and W. Dong, *Environ. Sci. Pollut. Res.*, 2017, **25**, 693–703.
772 V. Pistková, M. Tasbihi, M. Vávrová and U. L. Stangar, *J. Photochem. Photobiol., A*, 2015, **305**, 19–28.
773 V. Bhatia, G. Malekshoar, A. Dhir and A. K. Ray, *J. Photochem. Photobiol., A*, 2017, **332**, 182–187.
774 V. Bhatia, K. Manoli, A. Dhir and A. K. Ray, *Can. J. Chem. Eng.*, 2020, **98**, 1767–1775.
775 V. Bhatia, A. Dhar and A. K. Ray, *J. Photochem. Photobiol., A*, 2021, **409**, 113136.
776 N. F. F. Moreira, M. J. Sampaio, A. R. Ribeiro, C. G. Silva, J. L. Faria and A. M. T. Silva, *Appl. Catal., B*, 2019, **248**, 184–192.
777 Y. Zhang, S. Yang, L. Wei, X. Zhao and X. Lu, *Environ. Technol.*, 2024, **45**, 972–987.
778 A. Kumar, A. Kumar, G. Sharma, M. Naushad, T. Ahamad and F. J. Stadler, *Chemosphere*, 2018, **209**, 457–469.
779 Y. Wang, J. Niu, X. Gao and Y. Zhang, *Appl. Surf. Sci.*, 2020, **533**, 147458.
780 M. R. Rajeshwari, A. Syed, A. H. Bahkali, A. M. Elgorban, M. K. Rahiman, R. S. Varma and S. S. Khan, *J. Ind. Eng. Chem.*, 2022, **115**, 402–415.
781 A. H. Shah and M. A. Rather, *Adv. Nano Res.*, 2021, **10**, 397–414.
782 S. Sun, X. Yu, Q. Yang, Z. Yang and S. Liang, *Nanoscale Adv.*, 2019, **1**, 34–63.
783 *Photocatalytic Functional Materials for Environmental Remediation*, ed. A. Pandikumar and K. Jothivenkatachalam, 2019, Wiley.
784 A. B. D. Nandiyanto, R. Zaen and R. Oktiani, *Arabian J. Chem.*, 2020, **13**, 1283–1296.
785 Z. Cui, L. Zhang, Y. Xue, Y. Feng, M. Wang, J. Chen, B. Ji, C. Wang and Y. Xue, *Int. J. Miner., Metall. Mater.*, 2022, **29**, 2221–2231.
786 Z.-H. Diao, J.-C. Jin, M.-Y. Zou, H. Liu, J.-Q. Qin, X.-H. Zhou, W. Qian, P.-R. Guo, L.-J. Kong and W. Chu, *Sep. Purif. Technol.*, 2021, **278**, 119620.
787 L. Han, B. Li, H. Wen, Y. Guo and Z. Lin, *J. Mater. Sci. Technol.*, 2021, **70**, 176–184.
788 E. Omrani, A. Ahmadpour, M. Heravi and T. R. Bastami, *J. Water Process Eng.*, 2022, **47**, 102581.
789 A. Majumder, A. K. Gupta and M. Sillanpää, *Colloids Surf., A*, 2022, **648**, 129250.
790 S. Das, M. Sanjay, S. Kumar, S. Sarkar, C. S. Tiwary and S. Chowdhury, *Chem. Eng. J.*, 2023, **476**, 146719.
791 T. Zhu, J. Yang, Y. Shen, T. Liang, S. Fan, S. Zhang, Z. Yu, S. Wang and Y. Hou, *Colloids Surf., A*, 2024, **681**, 132802.
792 M. Wang, B. Liang, S. Lin, Z. Zhao, H. He, X. Li and S. Liang, *Appl. Surf. Sci.*, 2024, **657**, 15979.
793 C. Yang, X. Zhang, Z. Li, Z. Wang, J. Shi, H. Xie, T. Li and Y. Zhou, *Mater. Res. Bull.*, 2024, **174**, 112709.
794 Y. Xia, H. Liu, F. Sun, B. Yue, X. Wang, F. Guo, Y. Zhu, H. Yu, G. Liu, W. Yu and X. Dong, *J. Cleaner Prod.*, 2024, **434**, 140445.
795 J. J. Rueda-Marquez, I. Levchuk, P. F. Ibañez and M. Sillanpää, *J. Cleaner Prod.*, 2020, **258**, 120694.
796 C. Blaise, F. Gagné, J. F. Férard and P. Eullaffroy, *Environ. Toxicol.*, 2008, **23**, 591–598.
797 N. B. Turan, H. S. Erkan, G. O. Engin and M. S. Bilgili, *Process Saf. Environ. Prot.*, 2019, **130**, 238–249.